2018

Catalytic Olefin Polymerization and Metathesis: Molecular Structure-Activity Relationships

Anisha Chakrabarti
Lehigh University

Catalytic Olefin Polymerization and Metathesis: Molecular Structure-Activity Relationships

by

Anisha Chakrabarti

A Dissertation
Presented to the Graduate and Research Committee
of Lehigh University
in Candidacy for the Degree of
Doctor of Philosophy

in

Chemical Engineering

Lehigh University
January 2018

Certificate of Approval

Approved and recommended for acceptance as a dissertation in partial fulfillment of the requirements for the degree of Doctor of Philosophy.

_____
Date

Dissertation Director:

_____   _____
        Dr. Israel E. Wachs, Ph.D.   Date
      Advisor and Committee Chair
        G. Whitney Snyder Professor of
          Chemical Engineering
           Lehigh University

_____
Accepted Date

Committee Members:

_____   _____
     Dr. Jonas Baltrusaitis, Ph.D.   Date
Assistant Professor of Chemical Engineering
           Lehigh University

_____   _____
       Dr. Xingtao Gao, Ph.D.   Date
           Senior Chemist
             BASF

_____   _____
       Dr. James T. Hsu, Ph.D.   Date
  Professor of Chemical Engineering
           Lehigh University

_____   _____
      Dr. Mark A. Snyder, Ph.D.   Date
Associate Professor of Chemical Engineering
           Lehigh University

iii

Acknowledgements

My years as a Ph.D. student at Lehigh have been very enriching, and I am grateful for my time here and to have met many wonderful people without whom my time in the Lehigh Valley would not have been the same.

I am fortunate to have been able to work with Professor Israel E. Wachs as my Ph.D. advisor and am grateful to him for the opportunity to join the Wachs research group. Working with Prof. Wachs was an enriching experience, and he was an incredible guide and mentor. He has demonstrated a great deal of patience in teaching me how to conduct research, and his enthusiasm for and incredibly vast knowledge of catalysis research is inspiring. I would like to thank him for the many opportunities I had to attend many conferences in the past and present our research.

The past five years have generally been a very positive experience, filled with joyous experiences, but they have not been without their trials and tribulations. During my first year as a Ph.D. student, in 2013, I was diagnosed with kidney disease resulting from a hidden autoimmune condition. I remember when I was in the hospital for my kidney biopsy, I was concerned about my research falling behind. However, Prof. Wachs made sure to let me know that my health was a priority. In 2015, my grandmother who lived in India became very sick with a respiratory illness and passed away. In this instance, too, I had support from Prof. Wachs and was given the time I needed to travel to India and attend her funeral and be with my family. On a more positive note, in 2016, I got married in Indianapolis, IN. My family and I are very honored that Prof. Wachs and his wife took the time to travel and attend the wedding. These experiences allowed me to see another side of Prof. Wachs and showed me the significance of having an advisor who genuinely cares

about both research and his students. I am grateful for not only his guidance, but also his understanding throughout my years in the Wachs group.

I would like to thank my other committee members, Dr. Jonas Baltrusaitis of Lehigh University, Chemical Engineering, Dr. Xingtao Gao of BASF, Dr. James Hsu of Lehigh University, Chemical Engineering, and Dr. Mark Snyder of Lehigh University, Chemical Engineering. I am grateful to them for taking time out of their busy schedules to be on my Ph.D. committee.

I would like to also thank and acknowledge our collaborators. Dr. Anatoly Frenkel provided us with the beamtime we needed at Brookhaven National Laboratory to collect *in situ* XAS data. He was also an invaluable resource in helping us to analyze the XANES and EXAFS data we collected for the ethylene polymerization project. Dr. Zili Wu and Dr. Si Luo collected the *in situ* Raman spectra of the supported CrO_x/SiO_2 using a moving stage, leading to a very important conclusion concerning the structure of the initial oxidized catalysts. The DFT studies were done by Dr. Jaroslaw Handzlik and Maciej Gierada of Cracow University of Technology, who were instrumental in corroborating our experimental evidence for the active intermediates and initiation mechanism for ethylene polymerization by the supported CrO_x/SiO_2 catalyst.

Of course, I have enjoyed working with my fellow Wachs lab group members. I would like to especially thank Dr. Mike Ford, Dr. Chris Keturakis, and Dr. Soe Lwin. Mike is always available for discussions, whether about research or not. Chris and Soe were always available to help with experiments or data analysis and provide mentorship. I am grateful to Soe for the groundbreaking work in olefin metathesis by supported ReO_x/Al_2O_3 catalysts, which formed a good basis for our present work in olefin metathesis by supported

Most importantly, I am so, so lucky to have my family, who are my biggest fans. My numerous aunts, uncles, and cousins, in India and especially in California and New Jersey, have shown me how wonderful it is to be close to extended family. My uncle, aunt, and cousins in California from my father's side, Sreejit, Aruna, Ayush, and Suhail Chakravarty, my uncle, aunt, and cousins in New Jersey from my father's side, Paritosh, Sharmistha, Srishti, and Noyonika Nath, as well as my aunt and cousins in California on my mother's side of the family, Reena, Nikhil, and Sonia Dutta, have always shown their love and support. My grandmother, Mrs. Maya Sikdar, and my late grandmother, Mrs. Maya Chakrabarti, have also shown their immense support and let me know how proud they are of me. My parents are symbols of strength, courage, and perseverance and have always supported me in my endeavors for higher education. My father moved from India to the U.S. for his Ph.D. and is an accomplished Professor of Economics. I can only imagine how difficult it must have been to move to a new country to pursue a Ph.D., thousands of miles away from home, in a time when travel and long-distance communication was not so accessible. He has always impressed in me the importance of a good education and hard work. My mother is an engineer in a man's world who has always been strong, but this was especially true this past summer during her diagnosis and battle with Stage I breast cancer; we are fortunate that the cancer was caught relatively early. My two younger sisters, Devika and Mithu, have always stood by my side. I am extremely proud to be your older sister and of all that you have accomplished. Devika, I am so thrilled to see the wonderful doctor that I am sure you will become. Mithu, you have always been beyond your years, but you have especially shown your maturity in the last couple of years while at UCSD, and I am incredibly excited to see what the future holds for you.

My husband Reid Erekson, moved to Bethlehem a couple of years ago so we could be in the same place. I am so lucky that I met you at Purdue and have had you as my best friend and companion. Words cannot express the love and gratitude that I have for you, and I could not have done this without all your love and encouragement. I cannot wait to see what the future holds for us.

Graduate school at Lehigh has been a unique and wonderful experience for me, providing an education that would not have been possible elsewhere. I thank all of you for your role in my years here.

Dedicated in loving memory to my late grandparents Dr. Dhirendra N. Sikdar, Mr. Sunil K. Chakrabarti, and Mrs. Maya Chakrabarti.

Table of Contents

Preface

Chapter 3 | *Operando* Molecular Spectroscopy During Ethylene Polymerization by

Supported CrO_x/SiO_2 Catalysts: Active Sites, Surface Intermediates, and Structure-

List of Tables

List of Figures in Chapters

List of Figures in Supporting Information

List of Schemes

Abstract

Olefin chemistry has a long and significant history in the catalysis literature. The polymerization and metathesis reactions were discovered around the same time in the early 1950s. The polyolefin industry has now grown to a multibillion dollar industry. The three main classes of olefin polymerization catalysts are (i) Phillips-type catalysts (CrO_x/SiO_2); (ii) Ziegler-Natta catalysts (transition metal compound with an activator); and (iii) single-site homogeneous catalysts or supported homogeneous catalysts (i.e. metallocene).

The Phillips-type heterogeneous supported CrO_x/SiO_2 catalysts are one of the most widely studied catalysts. It was discovered in the early 1950s at Phillips Petroleum Company, when J.P. Hogan and R.L. Banks determined that ethylene could be converted to high-density polyethylene (HDPE) by supported Cr/SiO_2. This catalyst is now responsible for over half of the production of HDPE sold globally. The reason for the widespread use of the Phillips catalyst lies in its ability to synthesize over 50 different types of HDPE and linear low-density polyethylene (LLDPE), without the use of additional activators, which simplifies the catalyst preparation and production process. The process is also important because HDPE is produced at lower temperatures (65-180 °C) and atmospheric pressure.

A supported CrO_x/SiO_2 catalyst was synthesized and characterized using time-resolved *operando* and *in situ* molecular spectroscopy both before and during ethylene polymerization reaction conditions to investigate the structure-activity relationships for this important industrial catalytic reaction. Metal oxides (AlO_x, TiO_x, and ZrO_x) were used as promoter oxides. A combination of spectroscopic techniques (Raman, UV-vis, XAS, DRIFTS, and TPSR) during ethylene polymerization allows for the first time to monitor

the molecular events taking place during activation of supported $CrO_x/MO_x/SiO_2$ catalysts by ethylene to establish the structure-activity relationships for this reaction. During reaction, the initial surface $Cr^{+6}O_x$ sites reduce to Cr^{+3} sites to form $Cr-(CH_2)_2CH=CH_2$ and $Cr-CH=CH_2$ reaction intermediates, whose activities depend on the promoter oxide ($ZrO_x \sim TiO_x \gg CrO_x \sim AlO_x$).

Olefin metathesis is also quite significant in industry and was commercialized in the late 1960s to produce ethylene and 2-butene from propylene in the Phillips Triolefin Process. There is a current global propylene shortage caused by the shift to lighter feedstocks derived from shale gas fracking, and due to the complete reversibility of the metathesis reaction, the reverse reaction can be used to counteract the propylene shortage. Heterogeneous supported MoO_x/Al_2O_3 catalysts are one type of commercial catalyst employed, used in industrial processes such as the Shell Higher Olefin Process (SHOP) and operate between room temperature and ~200 °C.

Supported MoO_x/Al_2O_3 catalysts were synthesized and characterized with *in situ* Raman, UV-vis, DRIFTS, and TPSR, both before and during propylene metathesis reaction conditions. Three distinct MoO_x species on the Al_2O_3 support were identified: isolated surface dioxo $(O=)_2MoO_2$, anchored to the basic $HO-\mu_1-Al_{IV}$ sites (<1 Mo atom/nm^2), oligomeric surface mono-oxo $O=MoO_{4/5}$ anchored to more acidic $HO-\mu_1-Al_{V/VI}$ sites (1-4.6 Mo atoms/nm^2), and crystalline MoO_3 nanoparticles also present above monolayer coverage (>4.6 Mo atoms/nm^2). The surface oligomeric mono-oxo $O=MoO_{4/5}$ species easily activate at mild temperatures 25-200 °C while the isolated surface dioxo $(O=)_2MoO_2$ species require very high temperatures for activation (>400 °C). The crystalline MoO_3 nanoparticles decrease the number of accessible activated surface MoO_x sites by their

2

physical blocking. For the first time, the structure-reactivity relationship is established for olefin metathesis by supported MoO_x/Al_2O_3 catalysts and demonstrates the significant role that the anchoring surface hydroxyl sites on alumina have on the reactivity of surface MoO_x species.

Chapter 1 | Literature Review of Ethylene Polymerization by Supported CrO$_x$/SiO$_2$ Catalysts

Abstract

This chapter critically reviews the catalysis literature on the ethylene polymerization reaction by the supported CrO$_x$/SiO$_2$ catalysts. Despite the extensive research studies that have been performed about the supported CrO$_x$/SiO$_2$ catalyst system over the past six decades, the same fundamental structural and mechanistic questions are still being debated. From this literature review, it appears that ethylene polymerization by supported CrO$_x$/SiO$_2$ catalysts requires further fundamental understanding. The molecular structures and oxidation states of the chromia sites during ethylene polymerization, surface reaction intermediates, and reaction mechanism are still heavily debated in the literature. The focus on the standard CrO$_x$/SiO$_2$ has hampered progress in the determination of fundamental details and the role of the promoter oxides in the promoted CrO$_x$/SiO$_2$ catalysts.

1.1 Introduction

In the early 1950s, Hogan and Banks of Phillips Petroleum Company made the discovery that ethylene can be converted to polyethylene by a chromium oxide-silica-alumina catalyst[1] that was subsequently commercialized. The Phillips-type catalyst system, CrOx supported on an amorphous support, such as silica, is one of three types of catalysts currently used for olefin polymerization. The other two types are Ziegler-Natta and single-site homogeneous catalysts or supported homogeneous catalysts, both of which require an activator. The appeal of the Phillips catalyst lies in its many advantages: (i) yielding over 50 different types of polyethylene, (ii) functioning without activators, and (iii) operating at low temperatures and pressures.[1-4]

The original catalyst system has since been fine-tuned and ethylene polymerization by silica-supported CrO_x catalysts is now responsible for ~40 to 50% of all high-density polyethylene produced[3]. Despite the extensive research studies that have been performed about the supported CrO_x/SiO_2 catalyst system over the past six decades, many of the same fundamental structural and mechanistic questions are still being debated[1-3,5], although the recent application of *in situ* spectroscopic techniques that directly monitor the surface chromia sites on silica in different environments has significantly improved fundamental understanding of supported CrO_x/SiO_2 catalysts. For example, the initial molecular structure of the oxidized surface $Cr^{+6}O_x$ site has been proposed to be present as isolated surface dioxo CrO_4, isolated surface mono-oxo CrO_5, and dimeric surface Cr_2O_7, while the chromia oxidation state during ethylene polymerization has been proposed to be reduced Cr^{+2} and Cr^{+3}.[4]

To improve the catalytic activity, multiple promoters have been examined over the years, most notably TiO_x and AlO_x, and ZrO_x has also been found to exhibit a similar effect.[3] Other elements such as SnO_x and GaO_x have also been examined[3,6,7], although the focus has primarily been on the former three metal oxide promoters. The addition of a few percent of oxide promoters alters both the catalyst activity and resulting polyethylene (e.g., broadening the molecular weight distribution and enhancing the melt index).[3,8-18]

In contrast with the prolific literature on the standard supported CrO_x/SiO_2 catalyst, there have been few studies of promoted supported CrO_x/SiO_2 catalysts. Like the standard silica-supported chromia catalyst, there is debate concerning the structural and mechanistic details of promoted CrO_x/SiO_2 catalysts questions and more work is needed to elucidate the fundamental aspects of these catalysts. As may be expected, some debate about the

promoted silica-supported chromia catalysts for ethylene polymerization stems from the still disputed details of the standard chromia on silica catalyst, so the fundamental questions are similar: structure of the catalytic active chromia site (monomer or dimer) and oxidation state (Cr^{+2} or Cr^{+3}).[14,15] A considerable amount of disagreement in the promoted catalyst literature is derived from the different environmental conditions used to study the catalysts (ambient, vacuum, or dehydrated conditions, or activation with CO, H_2, or C_2H_4).

1.2   The Nature of Surface CrO_x Sites on SiO_2 in Different Environments

The supported CrO_x on silica catalyst system is prepared by the incipient-wetness impregnation method employing a chromia precursor that is soluble in the solvent being employed. The impregnated catalyst is initially dried overnight at room temperature in air, further dried in air at ~100 °C and then calcined at elevated temperatures (~400-800 °C) in an oxidizing environment.[3,4]

1.2.1   Supported CrO_x/SiO_2 under Ambient Conditions

Upon exposure to ambient air, the oxidized catalyst becomes hydrated by adsorption of moisture, which affects the molecular structures of the oxidized surface CrO_x species on SiO_2[19,20]. The lack of appreciation that the surface CrO_x sites in silica are hydrated under ambient conditions and limited application of characterization techniques capable of discriminating between multiple chromia states has also led to much confusion about the nature of the hydrated surface CrO_x sites on silica. Raman spectroscopy, however, readily discriminates between different chromia molecular structures since each molecular structure gives rise to a unique vibrational spectrum[21].[4]

The first application of Raman spectroscopy to the examination of hydrated supported CrO_x/SiO_2 catalysts was reported by Hardcastle and Wachs[19]. The hydrated surface CrO_x

phase on silica was found to consist of monomers (CrO_4), dimers (Cr_2O_7), trimers (Cr_3O_{10}), and tetramers (Cr_4O_{13}), with the extent of oligomerization increasing with chromia loading. The oligomerization of the surface CrO_x sites on SiO_2 with increasing chromia loading is a consequence of the decreasing pH at point of zero charge (PZC) of the thin aqueous film present on the supported CrO_x/SiO_2 catalyst[22].[4]

Weckhuysen *et al.*[23] investigated supported chromia catalysts on silica under ambient conditions as a function of Cr loading (0.2-8% Cr)[23]. The UV-vis DRS spectra for the lowest Cr loading exhibited two bands dominating at 348 and 240 nm with a shoulder at 429 nm, and the corresponding Raman spectra contained just one band at 895 cm^{-1}. These spectral features indicate hydrated surface dichromate species[21,24]. As the Cr loading was further increased, the UV-vis bands broadened and shifted from 348 to 370 nm, and the shoulder at 429 nm became more pronounced. With increasing Cr loading, the Raman spectra contained bands at 380, 850, 900, and 960 cm^{-1} that are representative of hydrated trichromate and tetrachromate species[21]. The XANES spectra of the hydrated catalyst exhibited a sharp pre-edge at about 5992 eV, which is a dipole-forbidden transition $1s \rightarrow 3d$ characteristic of 3d metal oxides not possessing an inversion center such as tetrahedral coordinated CrO_4. The corresponding EXAFS spectra of the hydrated catalyst possessed one FT peak at ~1.3 Å with an out-of-phase shift correction. After curve-fitting of the EXAFS spectra, the Cr-O distance and coordination number for the first shell were determined to be 1.58 Å and 3.7, respectively, which are similar to those of the CrO_4 unit in the K_2CrO_4 reference compound (R = 1.62 Å and N = 3.9). The combination of the spectroscopic techniques allowed for a full picture of the hydrated chromia species on silica. It was determined that the nature of the hydrated surface CrO_x species only depends

on the pH at the point of zero charge (PZC), which leads to dichromates at low Cr loading and trichromates and tetrachromates at high Cr loading. Crystalline Cr_2O_3 nanoparticles also form at higher Cr loading.[4] The molecular structures of the hydrated surface CrO_x sites on SiO_2 are schematically shown in Figure 1.1.
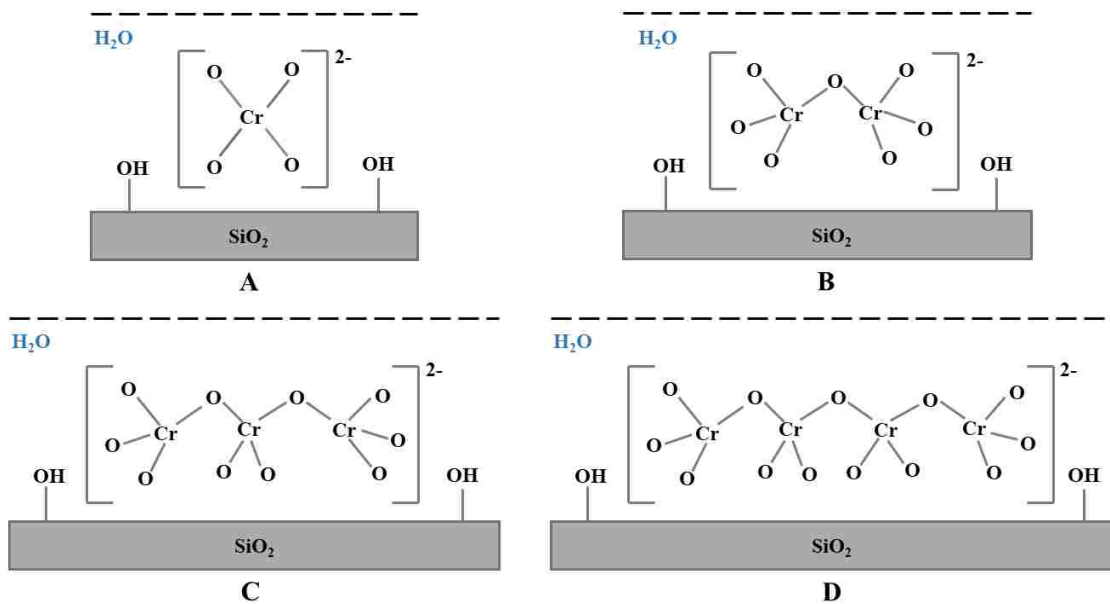
Figure 1.1. Schematic of molecular structures of "hydrated" CrO_x sites on the SiO_2 support: (A) monomer CrO_4^{2-}, (B) dimer $Cr_2O_7^{2-}$, (C) trimer $Cr_3O_{10}^{2-}$, and (D) tetramer $Cr_4O_{13}^{2-}$.[4]

1.2.2 Supported CrO_x/SiO_2 in Initial Oxidized Catalyst under Dehydrated Conditions

The hydrated surface CrO_x species on SiO_2 become dehydrated and change their molecular structures upon heating to elevated temperatures[19]. Early thermogravimetric analysis (TGA) by Hogan examined the loss of water by silica upon adsorption of chromia on dehydrated SiO_2 and led to the conclusion that surface CrO_x on silica is mainly present as isolated CrO_4 sites, although at high temperatures dimeric Cr_2O_7 sites cannot be excluded[25]. This conclusion was based on the model that only isolated surface CrO_4 and dimeric Cr_2O_7 sites are present and anchor to the silica support by titrating surface Si-OH hydroxyls. Each chromia structure was assumed to consume two surface Si-OH hydroxyls with a ratio of 2 Si-OH/Cr for the isolated CrO_4 and 1 Si-OH/Cr for the dimeric Cr_2O_7. This model also assumes that (i) the supported chromia phase is 100% dispersed (crystalline Cr_2O_3 nanoparticles are not present), (ii) the chromia only possesses CrO_4 coordination, and (iii) the SiO_2 surface is not altered by anchoring of the surface chromia species (e.g., siloxane Si-O-Si bonds do not participate). Despite the absence of direct spectroscopic evidence about the nature of the surface CrO_x sites on SiO_2, this early publication introduced the concept that the surface CrO_x sites on SiO_2 are only present as isolated CrO_4 and dimeric $O_3Cr-O-CrO_3$ structures[25].[4]

Zecchina *et al*. were the first group to apply *in vacuo* IR and UV-vis spectroscopy to examine the dehydrated supported CrO_x/SiO_2 catalysts[24]. The IR spectra exhibited a broad band at 925 cm^{-1} that was assigned to surface dichromate sites on silica. Recent DFT and Raman analysis, to be presented below, demonstrate that this IR band is the vibration from the bridging Cr-O-Si bond and does not provide any information about the structure of the

dehydrated surface CrO_x sites on silica. In the silanol stretching region (~3700 cm^{-1}), the intensity of the Si-OH band linearly decreased with increasing chromia loading up to $\sim5\%$ Cr, and the silanol concentration did not further decrease with increasing Cr loading. The leveling of the consumption of the surface silanols coincides with the formation of crystalline α-Cr_2O_3 nanoparticles. The ratio of surface Cr to Si-OH consumed was determined to be ~1, which suggested surface dichromate sites since isolated surface chromate sites would be expected to be ~0.5 according to Hogan's model. The UV-vis spectra contained $O \rightarrow Cr^{+6}$ ligand-to-metal charge transfer (LMCT) bands below 556 nm that were assigned to surface dichromate and isolated surface chromate sites, with relative intensities suggesting that the surface dichromate dominates. The broad nature of these UV-vis bands at 256 and 351 nm with the shoulder at 385 nm, however, can be assigned to both isolated surface chromate and surface dichromate since clear distinction between both structures is complicated by their broad and overlapping UV-vis bands as shown in Figure 1.2. The band at 461 nm was assigned to dichromates, but this band is also present for Cr_2O_3 nanoparticles. A small d-d band above 556 nm at 714 nm was attributed to chromia in an oxidation state lower than Cr^{+6} and was thought to be from surface $Cr^{+5}O_4$ sites on silica. This pioneering characterization study, however, could not clearly provide spectroscopic identification of the nature of the dehydrated surface CrO_x sites on SiO_2 since the UV-vis bands for the dehydrated supported CrO_x/SiO_2 catalyst and the CrO_4 and Cr_2O_7 reference compounds are too broad to allow assignment as shown in Figure 1.2.[4]
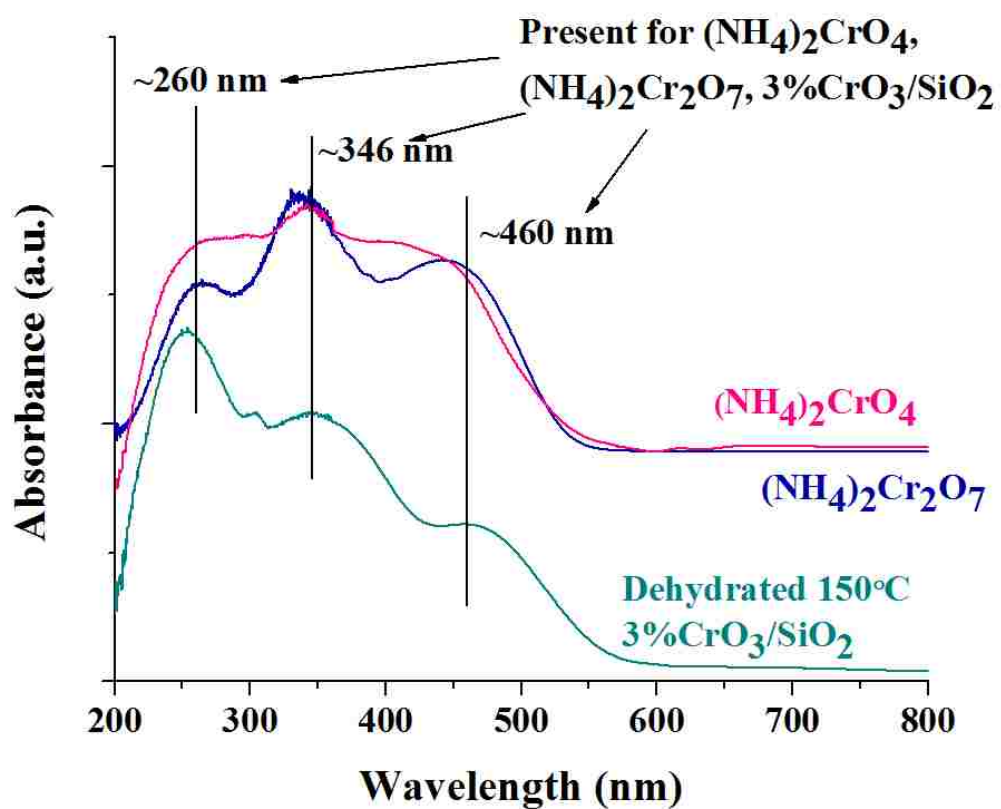
Figure 1.2. UV-vis spectra of reference compounds under ambient conditions.[4]

Fubini *et al.*[26] also reported *in vacuo* UV-vis-NIR spectra of dehydrated supported CrO_x/SiO_2 catalysts and detected LMCT bands at 476, 345, and 238 nm from surface $Cr^{+6}O_x$ sites. These bands were very close to those observed by Zecchina *et al.* apart from an additional shoulder at ~385 nm. Comparison with K_2CrO_4, containing isolated CrO_4 units, and $K_2Cr_2O_7$, consisting of dimeric Cr_2O_7 units, suggested that surface dichromate sites were the dominant surface chromia sites on silica. This group came to the same conclusions as Zecchina *et al.*[4]

In the past two decades, there has been a growing emphasis on investigations with *in situ* characterization techniques that provide direct observation of the dehydrated surface CrO_x sites on silica. Weckhuysen *et al.* examined the structure of the dehydrated surface CrO_x sites on SiO_2 as a function of Cr loading with *in vacuo* XANES/EXAFS, *in situ* Raman, and *in situ* UV-vis spectroscopy[23,27]. The XANES pre-edge intensity possessed a strong feature at 5992 eV indicative of $Cr^{+6}O_4$ coordination. The corresponding *in situ* EXAFS spectra contained 2 Cr-O distances at 1.53 Å and 2.05 Å with coordination numbers of 2.2 and 2.1, respectively. An additional Cr-Cr peak was present at ~3.1 Å with a coordination number of ~0.5. Two possible explanations were given. In the first interpretation, polychromate species are present with Cr=O at 1.53 Å and bridging Cr-O-Si at 2.05 Å. Alternatively, the 1.53 Å distance could be related to surface polychromate sites and the 2.05 Å peak is from the presence of Cr^{+3} oxide species. The Cr-Cr peak at ~3.1 Å is also consistent with Cr_2O_3 nanoparticles. Weckhuysen *et al.* favored the latter interpretation because it was more in line with the corresponding UV-vis spectra that detected Cr^{+3}.[23] The *in situ* UV-vis bands for the supported CrO_x/SiO_2 catalysts gave bands at 645, 455, 328, and 247 nm, with a weak shoulder at 370 nm. These UV-vis spectra were

deconvoluted into 11 bands[27]: 3 weak bands (645, 465, and 295 nm) assigned to $Cr^{+3}O_6$, 4 bands assigned to isolated $Cr^{+6}O_4$ (476, 370, 294, and 268 nm), and 4 bands assigned to dimeric $Cr^{+6}_2O_7$ (455, 323, 282, and 246 nm). The intensity ratio of the 370 nm band for isolated CrO_4 and the 323 nm band for dimeric Cr_2O_7 was employed to estimate the ratio of isolated/dimeric surface chromia species, which was found to be ~0.62 for 0.2% Cr loading. *In situ* Raman spectra of the dehydrated catalysts, unfortunately, could not be collected with the 514.5 nm laser due to strong sample fluorescence.[4] More recent successful Raman analysis of dehydrated supported CrO_x/SiO_2 catalysts confirmed the presence of Cr_2O_3 nanoparticles at loadings of 4% Cr and greater[28]. It was concluded that under dehydrated conditions and very high Cr loading on silica, surface polychromates and Cr_2O_3 nanoparticles dominate[23]. The *in situ* XANES/EXAFS studies by Groppo *et al.* agree with the earlier findings of Weckhuysen *et al.* and demonstrated that the XANES spectra of the dehydrated supported CrO_x/SiO_2 catalysts matched with that of bulk CrO_3, consisting of polymeric dioxo CrO_4 units that are compatible with both dioxo isolated CrO_4 and dimeric Cr_2O_7 structures[29]. Groppo *et al.*'s earlier UV-vis spectra of the dehydrated catalyst showed three main components (250, 333, and 463 nm) assigned to O → Cr^{+6} LMCT transitions, which were quite similar to those previously reported by others[30]. Groppo *et al.* pointed out the limitations of applying UV-vis to identify surface chromate species because of their very broad and overlapping bands and employed Raman spectroscopy to determine the structure of the surface chromia species. *In situ* Raman spectroscopy with the 442 nm laser, as opposed to the 514.5 nm laser previously available, allowed for the first time the elimination of sample fluorescence for the supported CrO_x/SiO_2 catalysts. The Raman spectra gave well-resolved bands at 394 (m), 987 (s), and 1014 (m) cm^{-1} with the 394 and

1014 cm^{-1} bands previously not observed due to strong sample fluorescence with lasers using 514 and 532 nm excitation. The band at 987 cm^{-1} was assigned to the ν_s(O=Cr=O) stretching, the band at 394 cm^{-1} to δ(O=Cr=O) bending, and the band at 1014 cm^{-1} to ν_{as}(O=Cr=O) stretching, as suggested by the DFT calculations of Dines *et al.*[31] Groppo *et al.*[30], however, had some concern about the assignment of the 1014 cm^{-1} band because it was stronger than expected and suggested that there may be some heterogeneity of the surface sites. The Raman spectra also showed an absence of chromia bands at 200-300 and 400-700 cm^{-1} indicating the lack of any surface polymeric chromia species at low Cr loadings. Comparison of DFT calculations and Raman spectra revealed that the presence of surface $Cr^{+6}O_x$ could also modify the pure silica vibrations and the IR band at 908 cm^{-1} band previously reported by Zecchina is related to a Si-O vibration affected by anchoring of the surface chromate species to the silica support (e.g., bridging Cr-O-Si bonds). The combination of *in situ* Raman, IR, and UV-vis spectra of the dehydrated supported CrO_x/SiO_2 catalysts at low chromia loadings on silica led Groppo *et al.* to conclude that surface $Cr^{+6}O_x$ on SiO_2 is anchored as isolated dioxo surface $(O=)_2CrO_2$ species.[30]

The more recent *in situ* UV-vis and Raman studies by Lee and Wachs finally provided the fundamental insights about the molecular structures of the dehydrated surface CrO_x sites on SiO_2.[28,28,32,33] The *in situ* UV–vis absorption bands at ~250, 340, and 460 nm reflect the presence of $Cr^{+6}O_x$ species on silica[28]. The exclusive presence of isolated surface CrO_x species on silica was demonstrated by the high UV-vis edge energy (E_g) value that is consistent with isolated CrO_x reference compounds. The corresponding Raman spectrum, with 442 nm laser excitation, exhibited bands at 987 (s) and 1014 (m) cm^{-1}, and the selective reduction of the 987 cm^{-1} band by H_2 showed that both bands originate from two

distinct surface CrO_x sites on silica[28]. Corresponding isotopic ^{18}O-^{16}O exchange studies of the surface CrO_x species on silica exhibited splitting of the 987 cm^{-1} band into three bands (^{16}O=Cr=^{16}O, ^{16}O=Cr=^{18}O, and ^{18}O=Cr=^{18}O) consistent with the dioxo nature of the 987 cm^{-1} band (($O=)_2CrO_2$). The band at 1014 cm^{-1} was assigned to mono-oxo $O=CrO_4$ sites by comparison with chromium oxide reference compounds, but also contains a small contribution from the v_{as}(O=Cr=O) stretch of the isolated surface dioxo ($O=)_2CrO_2$ species[33]. These molecular assignments to isolated surface dioxo ($O=)_2CrO_2$ and isolated mono-oxo $O=CrO_4$ sites on SiO_2 were further supported by rigorous DFT calculations that also predicted the greater stability of the dioxo CrO_4 species over the mono-oxo CrO_5 surface species on SiO_2[34]. This suggests that the surface dioxo CrO_4 species should have a higher concentration than the surface mono-oxo CrO_5 species on the silica support. The confusion surrounding the dehydrated molecular structures of surface CrO_x sites on SiO_2 required the application of multiple *in situ* spectroscopic approaches and techniques (Raman, H_2 reduction, isotopic ^{18}O-^{16}O exchange, XAS, IR, UV-vis, and DFT calculations) for its final resolution. The proposed molecular structures of the dehydrated surface CrO_x sites on SiO_2 are depicted in Figure 1.3.[4]

Gierada *et al.*[35] very recently conducted periodic and cluster DFT calculations of variously located Cr^{+4} and Cr^{+2} oxide species on silica. It was determined through DFT that the dimeric Cr^{+6} species are less stable than the monomeric Cr^{+6} species, and thus, at low chromia loadings, monomers are expected to dominate. The correlating *in situ* UV-vis DRS results demonstrated the appearance of three O → Cr^{+6} charge transfer bands at ~270, 360, and 450 nm. From literature, the band at ~450 nm could be assigned to either isolated or dimeric species. The authors compared the experimental bands with the calculated UV-vis

16

band maxima of monochromate and dichromate Cr^{+6} species and found that the experimental bands best matched those calculated for the monochromate Cr^{+6}.
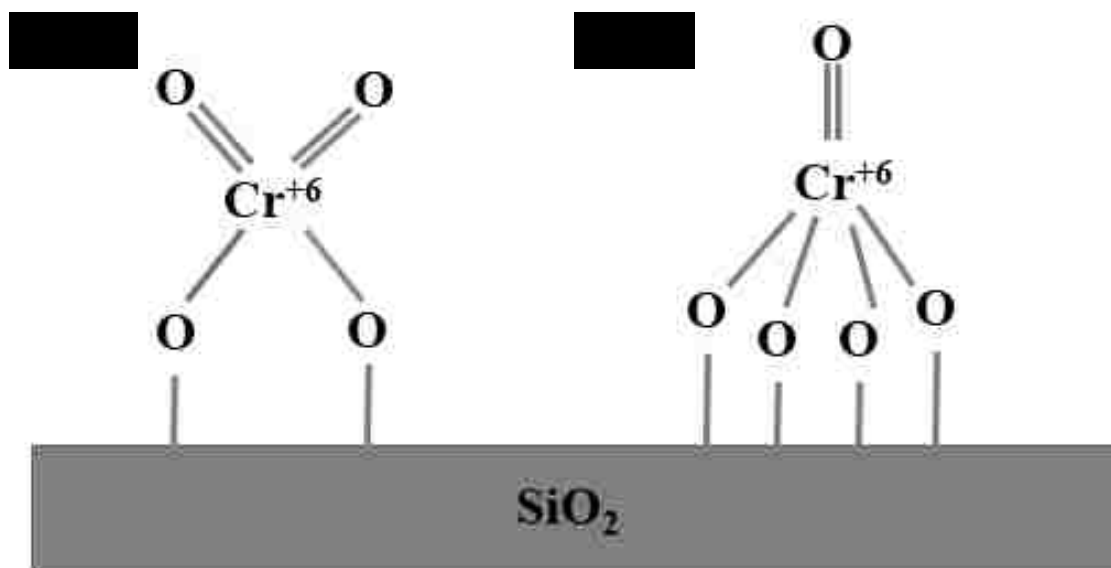
Figure 1.3. Schematic of the proposed molecular structures of the dehydrated isolated surface CrO_x sites on SiO_2 support (A) dioxo $((O=)_2CrO_2$ and (B) mono-oxo $O=CrO_4$.

1.2.3 Activated Supported CrO_x/SiO_2 Catalysts under Reduction Conditions

In industrial ethylene polymerization processes, the supported CrO_x/SiO_2 catalysts are activated with the ethylene reactant[2]. This results in an induction period during which the surface CrO_x catalytic sites are activated by partial reduction to a sub-oxide for ethylene polymerization. Hogan found during his early studies that reduction in CO could basically eliminate the induction period observed with ethylene, after which activity was immediately observed. It became customary in academic studies to initially activate the supported CrO_x/SiO_2 catalyst by reduction with CO and occasionally H_2. Additionally, pretreating with CO or H_2 affects the polyethylene (PE) yields. Pretreatment with CO modestly increases the PE yield while pretreatment with H_2 can significantly suppress the PE yield, and the difference may be related to the presence of moisture produced with the latter[36]. The application of different reducing agents in the literature has caused some confusion since the final activated state may depend on the specific reducing agent being employed.[4]

1.2.3.1 Activation of CrO_x with CO

Reduction with CO is a preferred activation method by academic researchers since it does not generate water as a reaction product that may coordinate with the surface CrO_x sites, and the findings from different groups are listed in Table 1.1. Early studies employed CO-TPR to determine how much oxygen was removed from the supported CrO_x/SiO_2 catalysts and found that ~2.05-2.15 O/Cr were consumed indicating that the average oxidation state was Cr^{+2}.[23,27] This agreed with EPR spectra that showed no Cr signal since Cr^{+2} is EPR silent, although it is d^4 and paramagnetic in most chemical environments[37]. Chemical probing of the reduced surface sites with CO-IR studies suggested that two

surface Cr^{+2} sites and one surface Cr^{+3} site may be present after CO reduction[24]. Other studies concluded that even more reduced surface Cr sites may be present[23,26,27,38-40]. The more recent definitive work of Groppo *et al.* with *in situ* Cr K-edge XANES/EXAFS demonstrated with direct monitoring of the surface chromia species on silica that surface Cr^{+2} sites are present after CO reduction. These studies, however, are somewhat complicated by the presence of 40% Cr_2O_3 nanoparticles in their supported CrO_x/SiO_2 catalyst.[29,30] The UV-vis band at 833 nm was assigned to Cr^{+2}, but is quite close to the UV-vis band of bulk Cr_2O_3 at 810 nm.[4]

Gierada *et al.*[35] recently conducted periodic and cluster DFT calculations of variously located Cr^{+4} and Cr^{+2} oxide species on silica. DFT calculations of the reduction process $Cr^{+6} \rightarrow Cr^{+4} \rightarrow Cr^{+2}$ by CO show that while the reduction of Cr^{+6} to Cr^{+4} is expected to be very exergonic, the thermodynamic driving force of the Cr^{+4} to Cr^{+2} reduction step is much weaker. The DFT calculations were complemented by experimental *in situ* UV-vis-NIR DRS studies on a 1wt% Cr/SBA-15 catalyst synthesized via incipient wetness impregnation of an aqueous Cr (III) nitrate solution. During reduction with dry CO at 600 °C, UV-vis $O \rightarrow Cr^{+6}$ CT bands at ~270, 360, and 455 nm reduced while a broad d-d transition band appeared at ~800 nm, indicating that reduction of chromia by CO yields only Cr^{+2}. The authors also investigated the possible role that water may have during reduction since hydrolysis of the Cr-O-Si bonds is an alternative pathway to reduction. To experimentally investigate, the $CrO_x/SBA-15$ catalyst was subjected to five redox cycles under dry conditions (reduction (dry CO)/oxidation (dry air)) at 600 °C. During each CO-reduction step, the same d-d transition band appeared at ~810 nm assigned to pseudo-O_h Cr^{+2} species. During the re-oxidation steps, the LMCT bands were completely restored,

demonstrating that the reduction of the Cr^{+6} sites by CO is completely reversible. After five

dry cycles, the catalyst was exposed to five wet cycles (reduction ($CO+H_2O$)/re-oxidation

(dry air)) at 600 °C. The broad d-d transition band blue-shifted down to ~720 nm, while a

weak new band appeared at ~460 nm. The repression of the deeper reduction to Cr^{+2} sites

as exhibited in the case of the dry CO reduction indicates the adverse effect of water. A

band did not appear at ~620 nm assigned to $\alpha\text{-}Cr_2O_3$ particles, indicating that hydrolysis is

not favorable during CO reduction. The combination of DFT and *in situ* UV-vis allowed

for confirmation that reduction by CO leads to primarily Cr^{+2} sites.

Most researchers agree that multiple surface Cr^{+2} sites are present on silica after

activation with CO at elevated temperatures (see Table 1.1). The molecular structure of the

Cr^{+2} site(s) still needs to be addressed and is complicated by possible presence of two

distinct surface Cr^{+2} sites from the initial isolated dioxo and mono-oxo surface chromates

on silica.[4]

Table 1.1. Summary of CO-Activation Studies[4]			
Group	**Year**	**Methods**	**Conclusions**
Przhevalskaya et al.[37]	1975	*in vacuo* EPR, UV-vis	CO reduction shows Cr^{+2}
Zecchina et al.[24]	1975	*in vacuo* IR (CO), UV-vis	2 types of Cr^{+2} 1 type of Cr^{+3}
Fubini et al.[26]	1980	*in vacuo* UV-vis	Up to 4 types Cr^{+2} (2 active, 2 inactive)
Rebenstorf et al.[38-40]	~1981 -1991	*in vacuo* IR (CO)	3 dinuclear Cr^{+2} (possibly 4) 2 dinuclear Cr^{+3} (only Cr^{+2} is said to be active)
Gaspar et al.[41]	2001	*in vacuo* IR (CO)	3 types of Cr^{+2}
Weckhuysen et al.[23,27]	1995	*in situ* UV-vis, XANES/EXAFS, CO-TPR	Cr^{+2} and Cr^{+3}; Cr^{+2}: Cr^{+3} ratio increases with decreasing Cr loading
Groppo et al.[29,30]	2005	*in situ* Raman, IR (CO), UV-vis, XANES/EXAFS	Cr^{+2}
Handzlik et al.[35]	2016	*in situ* UV-vis DRS	Cr^{+2} and Cr^{+3}

1.2.3.2 *Activation of CrO$_x$ with H$_2$*

Activation studies involving H$_2$ are relatively rare and none of the studies applied spectroscopic methods to directly monitor the nature of the reduced surface CrO$_x$ sites on silica. All the reported H$_2$ activation studies employed H$_2$-TPR, with or without TGA, to investigate the reduction features of the supported CrO$_x$ sites on silica. Hogan found with TGA that oxygen consumption from the supported CrO$_x$/SiO$_2$ was greater with CO than H$_2$[25]. This was also confirmed by the final colors of the activated CrO$_x$/SiO$_2$ catalysts that showed a gray-green color with H$_2$ reduction and a blue color with CO reduction that are characteristic of Cr^{+3} and Cr^{+2}, respectively. Gaspar *et al.* also applied H$_2$-TPR spectroscopy to investigate the reduction of supported CrO$_x$/SiO$_2$ catalysts[41]. The H$_2$-TPR reduction peak(s) were found to depend on the Cr loading (~479 °C for 0.5% Cr, ~496 °C for ~1% Cr, and ~376 °C and ~470 °C for ~3% Cr). The H$_2$-TPR peaks at the higher temperatures were ascribed to reduction of surface Cr$^{+6} \rightarrow$ Cr^{+3}, and the peak at 376 °C for the higher Cr loading was assigned to reduction of large Cr^{+6}O$_3$ particles $\rightarrow$ Cr^{+3} that formed because the number of hydroxyls was not sufficient to stabilize all the chromium on the silica surface. The CrO$_3$ particles, however, would have thermally decomposed to Cr$_2$O$_3$ particles during the 500 °C calcination and would not be present. Although UV-vis spectra were collected before H$_2$-TPR, the broad nature of the UV-vis bands prevented clear structural assignments of the surface chromia species on silica as already discussed above. After H$_2$-TPR, all the reduced supported CrO$_x$/SiO$_2$ catalysts possessed UV-vis bands at 272, 355, 467, and 610 nm that were assigned to Cr^{+3}. In agreement with Hogan, the final oxidation state resulting from H$_2$ reduction was concluded to be Cr^{+3}.[25]

Very recent studies by Gierada *et al.*[35] combining DFT and *in situ* UV-vis DRS demonstrated that reduction by H_2 may result in a combination of Cr^{+3} and Cr^{+2}. DFT calculations showed that the thermodynamics of the two-step reduction scheme $Cr^{+6} \rightarrow Cr^{+4} \rightarrow Cr^{+2}$ by H_2 versus CO were compared and found to be more thermodynamically favorable for H_2. *In situ* UV-vis during H_2-reduction at 600 °C determined that the $O \rightarrow Cr^{+6}$ CT bands at ~270, 360, and 455 nm for isolated Cr^{+6} species reduced while a broad band at ~780 nm appeared. The latter band was assigned to a superposition of characteristic d-d transition bands of pseudo-T_d Cr^{+2} and pseudo-O_h Cr^{+3}/Cr^{+2}. The authors also investigated the possible role that water may have during reduction since hydrolysis of Cr-O-Si bonds with the H_2O that forms during the first reduction step is an alternative phenomenon to full reduction. This would cause the Cr species to lose its anchoring to the silica surface, forming various reduced chromia species, such as clusters of Cr_2O_3. To experimentally investigate, the CrO_x/SBA-15 catalyst was subjected to five redox cycles under dry conditions (reduction (dry H_2)/oxidation (dry air)) at 600 °C. During each H_2-reduction step, the same d-d transition band appeared at ~780 nm. During the re-oxidation steps, the LMCT bands only partially re-oxidized, demonstrating that the reduction of the Cr^{+6} sites is not completely reversible, contrary to re-oxidation after CO reduction. After the five dry cycles, the catalyst was exposed to five wet cycles (reduction (H_2+H_2O)/re-oxidation (dry air)) at 600 °C. The broad d-d transition band blue-shifted down to ~620 nm, while new bands appeared at ~290 and 460 nm, which were assigned to a combination of pseudo-O_h Cr^{+3} and α-Cr_2O_3 particles. The re-oxidation step after each the wet reduction step confirmed the irreversibility of the chromia reduction and the hindering effect of the presence of water since the LMCT bands were partially re-

oxidized to an even lesser degree than during the dry cycles. Using a combination of theoretical and experimental techniques, these studies showed the possibility of two surface phenomena occurring during H_2 reduction: reduction to Cr^{+3}/Cr^{+2} or hydrolysis of the Cr-O-Si bonds to create α-Cr_2O_3 particles.

1.2.3.3 *Activation of CrO$_x$ with C$_2$H$_4$*

Activation studies with C_2H_4 are also limited because of complications associated with the presence of multiple hydrocarbons and possibly the H_2O reaction product that can interact with the surface CrO_x sites on silica[25]. A recent detailed in situ XANES/EXAFS study by Groppo *et al.*[30] monitored ethylene activation of supported CrO_x/SiO_2 catalysts and found that the catalyst exhibits features different than the CO-activated catalyst, which exhibits an oxidation state of Cr^{+2}. The C_2H_4-reduced CrO_x/SiO_2 catalyst yields a XANES spectrum with a higher intensity of the white line, reflecting an increased average Cr coordination, and the Cr^{+2} fingerprint is not present, which suggests that all surface isolated CrO_x sites are involved. Additionally, as seen in the corresponding EXAFS, these surface sites are not Cr^{+2} dimers because there is no signal for Cr-Cr in the second coordination shell. The fraction of surface Cr sites interacting with ethylene has previously been proposed to vary from 10 to 55% depending on the probe method[8,42,43], but these claims were based on indirect measurements and are not supported by this new direct XAS measurement indicating that all the dispersed Cr sites are involved[30]. The difference in the states of the surface CrO_x sites on silica upon CO reduction and C_2H_4 reduction were further demonstrated by adsorbing ethylene on a catalyst that had been pre-reduced with CO. Adsorption of ethylene on the Cr^{+2} sites increased the white line intensity (slight increase in coordination of Cr^{+2}) and completely removed the Cr^{+2} finger print in the

pre-edge region. These results clearly demonstrate that the surface Cr^{+2} sites formed with CO reduction are not involved in ethylene polymerization reaction at room temperature (and low ethylene pressure) and that all the reduced surface Cr^{+2} sites are oxidized upon exposure to ethylene. This work nicely demonstrates that reduction in different environments leads to different activated surface CrO_x states on SiO_2, and that it is important not to confuse results from one reducing agent with another.[4]

Very recent results[44,45] have provided new insights into the coordination sphere of the reduced CrO_x sites.

Potter *et al.*[44] used TGA, differential scanning calorimetry (DSC), and MS to monitor the adsorption, reaction and desorption of ethylene at 200 °C for 1 and 3wt% Cr/SiO_2 catalysts synthesized via incipient wetness impregnation of CrO_3. TGA and DSC of ethylene pulses (6 pulses of 60% C_2H_4/Ar for 1 min) over the 3% Cr/SiO_2 catalyst showed mass changes in a step shape, indicating the occurrence of an irreversible adsorption, passing through a maximum. The corresponding mass spectra taken indicated the evolution of m/z = 41, then m/z = 56, 55, and 42, then m/z = 43, 50, 51, 53, and 54 during each pulse. Weak MS signals were also observed at m/z = 49, 69, 52, and 57. The amounts of the MS signals corresponded to the size of the mass change, the largest occurring during the second pulse of ethylene. The products observed with the MS were attributed to dimerization and trimerization products, although there was a lack of oxygenated products detected by the MS. During reaction with olefins, the high heat of reaction (~300-465 kJ/mol during the first ethylene pulse) indicated a redox reaction. The redox products were then studied by TPD under Ar and monitored with an online MS. In all cases, two CO_2 (m/z = 44) evolution peaks were seen at ~260-285 °C and 390-435 °C corresponding to ~40% and ~60% of the

mass loss, respectively. HCHO (reported as a major oxidation product in the literature[2,3,46,47]) and ethylene oxide were not detected and excluded as major products of oxidation during ethylene polymerization. Simultaneous to the low and high temperature evolution of CO_2, H_2 (m/z = 2) and CH_4 (m/z = 15) were also detected as respective co-products, which correspond to the decomposition of surface formate and surface acetate, respectively. The relatively high temperatures of the oxidation products (>250 °C) as compared to industrial ethylene polymerization conditions (85-110 °C) suggest that the oxygenates may remain attached to the Cr sites.[44]

In a more recent study inspired by those of Potter *et al.*, Barzan *et al.*[45] employed a combination of *operando* techniques (*operando* Cr K-edge XANES-MS, UV-vis-NIR DRS-MS, and FT-IR-MS) to determine the exact oxygenated ligands present in the coordination sphere. *Operando* XANES-MS demonstrated the reduction of chromates with a decrease in the intense XANES pre-edge at ~5994 eV characteristic of pseudo-T_d chromates into two weak bands at ~5990 and ~5993 eV, a progressive shift down of the edge from ~6007 to ~6002 eV, and an increase in the white line intensity at ~6011 eV. *Operando* UV-vis-NIR DRS-MS corroborated the chromate reduction. The band at ~465 nm assigned to the O → Cr LMCT decreased while bands for d-d transitions assigned to reduced chromia species appeared at ~599 nm and ~1053 nm with a shoulder at ~667 nm simultaneously. After an induction period, bands also appeared at ~2273-2469 nm that were assigned to the combination of $\nu(CH_2)$ and $\delta(CH_2)$ vibrational modes of polyethylene that showed the occurrence of ethylene polymerization. The authors assigned the reduced chromates to pseudo-O_h Cr^{+2} sites primarily based on their own previous results in which

the bands resulting from reduction of Cr/SiO_2 by cyclohexene were assigned to primarily Cr^{+2}, although these conclusions were not corroborated by any other work.[48]

It was concluded that during the reduction step Cr^{+6} sites are converted to both Cr^{+2} sites in interaction with oxygenated byproducts, thought to be primarily methylformate, and a reduced spectator chromia species. Then, ethylene polymerization begins on Cr^{+2} sites in the presence of un-reduced Cr^{+6} sites that are slowly reduced in successive time.

Although this study used multiple *operando*-MS methods, no MS traces were presented, which would have been able to track the gaseous intermediates, providing more direct evidence and corroborating the authors' claims. Additionally, in other recent work[35,49], the band at ~599 nm overlaps with bands that were assigned to Cr^{+3} [49] or a mixture of Cr^{+2} and Cr^{+3}.[35] XANES simulations were used to verify the assignment of the reduced chromate to only Cr^{+2}; however, using XANES, even simulations, may be problematic since this is a technique that is an average of all the sites present.

1.2.3.4 *Activation of Well-Defined Catalysts with C₂H₄*

Recent studies by Copéret *et al*. have examined the polymerization activities of well-defined model catalysts, dinuclear Cr^{+2} and Cr^{+3} model compounds and mononuclear Cr^{+3} model compounds, anchored on SiO_2.[50,51] The grafted dinuclear model $(\equiv SiO)_4Cr^{+2}_2$ and $(\equiv SiO)_6Cr^{+3}_2$ compounds were characterized by *in situ* IR, Cr K-edge XAS, and EPR spectroscopy before and after ethylene polymerization. The IR spectrum of $(\equiv SiO)_4Cr^{+2}_2$ only contained new silanol vibrations and no C-H stretches before exposure to ethylene. X-ray crystallographic analysis of a molecular model closely related to $(\equiv SiO)_6Cr_2$ revealed two five-coordinate Cr^{+3} centers (distorted trigonal bipyramidal and square-pyramidal geometry). The IR spectrum of $(\equiv SiO)_6Cr^{+3}_2$ after exposure to ethylene

possessed C-H stretches and a white film formed on the pellet indicating polyethylene formation. The XANES spectrum of $(\equiv SiO)_4Cr^{+2}_2$ did not undergo any changes during the synthesis procedure. The initial ethylene polymerization activity of $(\equiv SiO)_6Cr^{+3}_2$ was an order of magnitude higher than $(\equiv SiO)_4Cr^{+2}_2$ suggesting that Cr^{+3} is the catalytic active site for this reaction. The EPR spectrum of $(\equiv SiO)_4Cr^{+2}_2$ taken before exposure to ethylene showed a weak signal for Cr^{+3}, suggesting that the minor amount of Cr^{+3} is most probably responsible for the polymerization activity[50]. Similar high initial polyethylene polymerization activity was also found for the mononuclear $(\equiv SiO)_3Cr^{+3}$ model compound consistent with the role of Cr^{+3} sites for ethylene polymerization[42]. Furthermore, the same initial ethylene polymerization rate was also obtained with a traditional CO-activated supported CrO_x/SiO_2 catalyst consistent with the role of surface Cr^{+3} sites for ethylene polymerization[52]. These new findings further support the role of Cr^{+3} sites on silica as the active sites, but may not necessarily be identical to the traditional catalyst.[4]

1.3 Structure-Activity Relationships for Supported CrO_x/SiO_2 Catalysts

Developing fundamental structure–activity relationships requires knowing the molecular structure of the catalytic active site(s). This is rather complicated for traditional supported CrO_x/SiO_2 catalysts since it is likely that the initial dioxo $(O=)_2CrO_2$ sites cause formation of multiple activated chromia sites. The reported studies to date have assumed that only one surface activated CrO_x site is present on SiO_2 and only focused on the average oxidation state, which appears to primarily be surface Cr^{+3} during ethylene polymerization from the above review of activation of supported CrO_x sites by ethylene. Therefore, the establishment of fundamental molecular structure-activity relationships for ethylene

polymerization on each surface chromia site present in supported CrO_x/SiO_2 catalysts still awaits resolution with future studies.[4]

1.4 Proposed Reaction Mechanisms

The development of modern spectroscopy methods for catalysis research has allowed for studies in the past decade to examine the initiation, propagation, and termination mechanisms of ethylene polymerization[50-59] Despite these new studies, researchers have yet to come to a consensus concerning the structure(s) of the initial active sites and the ethylene polymerization initiation mechanism as indicated by the summary of the findings in Table 1.2 below.[50-57,59-61] Most literature research studies begin the ethylene polymerization reaction with a catalyst that contains the Cr^{+2} oxidation state because the supported CrO_x/SiO_2 catalysts have been activated by reduction with CO at elevated temperatures.[53-57,59] This activation procedure, however, eliminates the induction period and is atypical for the industrial reaction conditions that employ the ethylene reactant as the reducing agent.[3,10] Furthermore, the CO activation also results in a lower Cr oxidation state than when activated with ethylene that forms Cr^{+3} sites. Thus, it is important to be conscious of the specific activation procedure employed in any given study since the initiation mechanisms appear to be dependent on the activation procedure.[4,62]

Multiple reaction intermediates have been proposed for ethylene polymerization for CO-reduced supported chromia/silica catalysts and are summarized in Table 1.2: vinyl Cr-hydride formed by C-H activation of ethylene[63], carbene Cr=CH2 created by breaking the C=C bond of ethylene[63], Cr-vinyl produced by C-H activation of ethylene over an O-H bond in the catalyst to make a Cr-C bond[50-52,60,61], Cr=CH-CH3 Cr-alkylidene[42,64-66], and Cr-metallacycles formed from the addition or two or three ethylene molecules[52-57]. Only a

limited number of studies investigated the structure(s) and oxidation state(s) of the surface Cr sites of supported chromia/silica catalysts activated with CO at elevated temperatures. The oxidation state of the Cr after CO activation at 350 °C was found to be Cr^{+2} from *in situ* UV-vis, XANES, and HF-EPR spectroscopy[59]. It was concluded that the Cr^{+2} site reacts with ethylene to form an organo-Cr^{+3} intermediate, but the molecular structure of the organo-Cr^{+3} complex was not discussed. It was also proposed from computational modeling and EXAFS[67] analysis that two surface $Cr^{+2}O_x$ structures (x = 3 with trigonal pyramidal coordination and x = 4 square pyramidal coordination) are formed with the former more dominant and active than the latter. Model organometallic catalysts have also been investigated in an effort to elucidate the initiation mechanism.[50-52,60,61] Using a variety of spectroscopy techniques (IR, UV-vis, EPR, XAS) as well as DFT, it was concluded that the formation of the first Cr-C bond occurs via the heterolytic C-H activation of ethylene on a surface Cr-O bond. Poisoning with CO revealed that two different surface Cr^{+3} sites were present. The model catalysts were prepared by grafting Cr^{+3} onto silica that was partially dehydroxylated at 700 °C and an impregnated CrO_x/SiO_2 catalyst that was activated with CO was also investigated for comparison, and they were found to give rise to the same IR bands at 3692 and 3643 cm^{-1} assigned to silanols interacting with the polymer, and at 3605 cm^{-1} which was due to the C-H overtone of the PE chain.[62]

In recent DFT studies, Gierada *et al*.[68] determined the feasibility of proposed initiation species and mechanisms in the literature and proposed some new initiation mechanisms under more realistic conditions of 100 °C. Cr^{+2}, Cr^{+3}, Cr^{+3}-OH, and Cr^{+5} oxide species were considered as possible active site precursors. Coordination of the first and second ethylene molecules to the bare Cr^{+2} species is thermodynamically preferred, although the binding of

the second ethylene molecule is less exergonic than that of the first. Concerning the possible initiation mechanisms beginning with Cr^{+2} oxide, one feasible mechanism is the oxachromacycle ring expansion over Cr^{+2}, in which ethylene molecules keep inserting into a Cr-O bond, creating progressively bigger rings, since there is a relatively low activation barrier (140 kJ/mol) and propagation steps are faster and more kinetically preferred than termination pathways. Another possible pathway is the formation of either Cr^{+3}/SiO_2 or Cr^{+3}-CH=CH_2/SiO_2 from Cr^{+2}/SiO_2 and surface defect sites, $\equiv$Si-O•, near the Cr^{+2} site. Silica is known to contain defects, particularly after high temperature treatment, and it has been shown that using a higher calcination temperature (which causes dihydroxylation and thus more defects) has higher activity for ethylene polymerization.[28,68-74] There are two possible pathways involving surface defects: addition of a nearby surface $\equiv$Si-O• defect to a Cr^{+2} site, resulting in a Cr^{+3} site and nearby $\equiv$Si• defect or hydrogen transfer reaction from π-bonded ethylene to $\equiv$Si-O•, forming a Cr^{+3}-CH=CH_2 site and a new silanol that would interact with the chromia.[68] Addition of a first ethylene molecule to a bare Cr^{+3} site is less favorable than that to a Cr^{+2} site, and coordination of a second ethylene molecule is predicted to be endergonic. Of the initiation mechanisms already proposed in the literature, for Cr^{+3} oxide sites, oxachromacycle ring expansion seems to be the most plausible. This mechanism was examined with Cr^{+3} since it was the best option for Cr^{+2} sites. Although a viable pathway since it has a moderate overall Gibbs energy of 149 kJ/mol, the oxachromacycle ring expansion mechanism is more preferred over Cr^{+2} sites, having an overall Gibbs energy of 140 kJ/mol. Additionally, the mechanism becomes more favorable for more strained Cr^{+3} sites. In this publication, Gierada *et al.* also expand on a newer mechanism involving Cr^{+3}-OH/SiO_2 sites that was originally proposed in an earlier

publication[62] and will be discussed in a later chapter. In these DFT studies, pathways for ethylene polymerization over Cr^{+5} oxide species were theoretically examined for the first time. The first ethylene molecule inserts into the oxo ligand and creates a radical species which then reacts via terminal C atoms with the silanolate oxygen to form a dioxachromacyclopentane complex. Upon coordination of a second ethylene molecule, proton transfer from the ethylene ligand occurs and forms a Cr^{+3}-CH=CH$_2$ site and surface -OCH$_2$CH$_2$OH ligand. The overall activation barrier is 139 kJ/mol. Further ethylene coordination results in a Cr^{+3} butenyl complex. Further propagation can occur through insertion of ethylene molecules into the Cr-C bond, if the oxygenate ligand de-coordinates and leaves a vacant site. With a predicted overall Gibbs energy of 147 kJ/mol, this mechanism is slower than that starting from a Cr^{+3}-OH site. These very comprehensive DFT studies nicely demonstrated the likelihood of the various reaction mechanisms proposed in literature by determining pathways for the overall reaction (initiation, propagation, and termination), even presenting a newer and viable model.

Table 1.2. Summary of the proposed active sites and surface reaction intermediates reported in literature for catalysts activated with CO except for studies reported in references[50-52] that employed model organometallic compounds.[62]

Research Group	Experimental Conditions	Band Positions	Assignments	Active Sites
Zielinski et al.[63]	*In vacuo* IR	1446 cm^{-1}	$\delta(=CH_2)$ of adsorbed ethylene	Carbene Cr=CH$_2$ or Cr vinyl hydride H-Cr-HC=CH$_2$
		1472 cm^{-1}	$\delta(-CH_2-)$ of PE + $\delta(=CH_2)$ of adsorbed ethylene	
		2850, 2920 cm^{-1}	$\nu_s(CH_2)$, $\nu_{as}(CH_2)$	
Zecchina et al.[42,65]	*In vacuo* IR	3700 cm^{-1}	Silica hydroxy groups weakly interacting with polymer chains	Alkylidene Cr=CH-CH$_3$
		2750 cm^{-1}	Methylene	
		2855, 2926 cm^{-1}	Bulk PE	
Szymura et al.[64]	*In vacuo* IR	2997, 1548, 1448 cm^{-1}	$\nu_s(CH_2)$, $\nu(C=C)$, $\delta(CH_2)$ of ethylene π-adsorbed on Cr^{+2} sites	Alkylidene Cr=CH-CH$_3$
		3016 cm^{-1}	$\nu(CH)$ of =CH-	
		2855, 2927 cm^{-1}	$\nu_s(CH_2)$, $\nu_{as}(CH_2)$	
		2960 cm^{-1}	methyl CH$_3$	
Zecchina et al.[53-57]	*In situ* IR ~100K – RT	3004, 3084, 3104 cm^{-1}	Cr^{+2}…(C$_2$H$_4$)$_n$ π-bonded complexes	Metallacycle (ring structure)
		2750 cm^{-1}	ethylene molecules interacting with the silanol groups	
		3650 cm^{-1}	Perturbed silanol groups	
		2861, 2893, 2915, 2931, 2965 cm^{-1}	"anomalous bands" (metallacycle structure)	
		2850, 2920 cm^{-1}	$\nu_s(CH_2)$, $\nu_{as}(CH_2)$	

Copéret et al.[50-52,60,61]	*In situ* IR 70 °C	3692, 3643, 3605 cm^{-1}	Silanols interacting with PE; silanols interacting with adjacent Cr^{+3} sites to form Si-(μ-OH)-Cr	Cr-vinyl formed by C-H activation over O-H band
Scott et al.[67]	*In situ* EXAFS	Curve Fitting of Spectra		Trigonal pyramidal and four-coordinate square pyramidal
	Computational modeling	NA		
Scott et al.[59]	*In situ* UV-vis C$_2$H$_4$ 80 °C	463 and 676 nm	Cr^{+3}	organo-Cr^{+3}
	In situ EPR C$_2$H$_4$ 80 °C	g = ~2 T	Cr^{+3}	
	In situ XANES C$_2$H$_4$ 80 °C	Cr^{+3}	Cr^{+3}	
Handzlik et al.[68]	DFT studies			Oxachromacycle over Cr^{+2} or Cr^{+3} or Cr^{+3}-vinyl formed from Cr^{+2} and silica surface defect or Cr^{+3}-vinyl formed from Cr^{+3}-OH

1.5 Promoted CrO$_x$/SiO$_2$ Catalysts for Ethylene Polymerization

Many of the early studies on the promoted silica-supported chromia catalysts were conducted at Phillips Petroleum, and focused mostly on the reducibility or activation of the catalysts by H$_2$ consumption.[75,76] The reduction profiles were used to interpret corresponding variations in the yield of ethylene, and it was found that incorporating alumina into the silica- support chromia catalysts decreased the reduction rate compared to the standard catalyst.[75,76] Assumptions, however, were made about the structure of the catalytic active chromia sites and reaction mechanisms since the catalyst surface could not be directly observed.

Subsequent studies with co-precipitated TiO$_2$-promoted CrO$_3$/SiO$_2$ catalyst, employed IR spectroscopy with NO as a chemical probe.[14-16] In these experiments, the catalyst was pretreated with CO and C$_2$H$_4$ and subsequently exposed to NO. The adsorbed NO IR bands were assigned to a combination of both monochromate and dichromate Cr^{+2} and Cr^{+3} sites, but there was no direct evidence for the chromia oxidation state and structure. Furthermore, the measurements were performed *in vacuo* that can change the surface structure and oxidation state.

Other studies applied H$_2$-TPR, UV-vis, and secondary ion mass spectrometry (SIMS) to study titanium-modified silica-supported chromia catalysts.[77,78] These studies attempted to assign the nature of the catalytic active chromia sites, but the experimental conditions of these studies were far removed from ethylene polymerization reaction conditions and the findings are, thus, ambiguous.

An initial density functional theory (DFT) study focusing on the effects of surface doping by titania on the structure and stability of the chromia species suggested that the

charge transfer process between Ti and Cr may explain the increase in reactivity of the Ti-promoted catalyst.[79] Models of the dioxo bridging chromia species were created containing zero, one, or two bridging Cr-O-Ti bonds. The bond distances (1.60 Å) and the bond angles (109°) were unchanged with respect to the nature of the support, while the Bader charges were 2.39e (no Cr-O-Ti), 2.41e (1 Cr-O-Ti), and 2.39e (2 Cr-O-Ti), respectively. The non-monotonic increase in the Bader charge was attributed to the asymmetric structure in the model with only one Cr-O-Ti bond. This structure would lead to a much higher charge on the Cr site, indicating an increase in the electron deficiency, which would aid reduction of the chromia sites and result in a shorter induction period. Vibrational frequency calculations indicated a blue shift when there is a Cr-O-Ti bond.

Later studies combined theoretical studies using DFT with high-resolution x-ray photoelectron spectroscopy (HR XPS) and ^{1}H magic-angle-spin solid-state nuclear magnetic resonance (^{1}H MAS solid-state NMR) to study promoted catalysts.[80,81] In two sets of experiments, Ti-[80] and Al[81]-modified supported CrO_x/SiO_2 catalysts were studied in an effort to explain the shorter induction period and higher polymerization activity. Unfortunately, these experimental measurements were also far removed from ethylene polymerization conditions. DFT calculations suggested that the promotional effect of modification with titanium stems primarily from the increased electron-deficiency as observed with XPS.[80] For the Al-promoted supported CrO_x/SiO_2 catalyst, the opposite effect was found with the XPS binding energy decreasing with Al loading. This suggests that there was no increase in electron-deficiency, as seen with the Ti-modified catalyst. This would not explain, however, the increase in ethylene polymerization activity, and additionally, the XPS measurements were conducted *in vacuo*.[81]

Recently, new types of catalysts have been developed to try to achieve a fundamental understanding of the promotional effects of adding TiO_x to the catalyst. The Zecchina group demonstrated the potential of using H_2-reduced TiO_2 to convert ethylene to HDPE without an activator. UV-vis and IR spectroscopy showed the appearance of a very broad absorption over the entire visible, NIR, and MIR regions attributed to shallow-trap defect sites. It was thus concluded that the active site is a Ti^{4-n} defect site located in the band gap. The idea of the H_2-reduced catalyst was derived from the $TiCl_x$-based heterogeneous Ziegler-Natta catalyst for ethylene polymerization in which the active sites are reduced Ti sites in interaction with an aluminum-alkyl activator; however, the H_2-reduced TiO_2 catalyst creates polyethylene without the use of an activator, like the traditional CrO_x/SiO_2 catalysts. The Weckhuysen group developed a triethylaluminum(TEAl)-modified $Cr/Ti/SiO_2$ catalyst made using a commercially available Cr/SiO_2 pre-catalyst.[49,82] The pre-catalyst was surface titanated creating an outer shell then contacted with triethylealuminum (TEAl) co-catalyst in heptanes to create the ethylene oligomerization sites. A combination of spectroscopic methods was used (DRIFTS, EPR, UV-vis-NIR DRS, STXM, SEM-EDX, and GPC-IR) to directly monitoring the catalyst and demonstrate that there are two distinct active regions that produce two different polymers. It was determined that the Ti-scarce active sites inside the core caused branching of the polyethylene chain, while the Ti-rich active sites located in the shell are responsible for more linear types of polyethylene.

The limitation of many of the above studies is that they were not performed on dehydrated initially oxidized catalysts, activated catalysts or during the ethylene

polymerization reaction. Furthermore, in most cases only indirect information was provided about the catalytic active chromia sites (e.g., NO chemisorption, ^{1}H NMR, or H$_2$-TPR).

Very recent and comprehensive DFT studies concerning chromia sites on an Al-modified silica support predicted that the surface modification can influence both geometry and relative stabilities of the chromia sites.[83] The Al-modified silica support was created by substituting one or two Al sites for Si atoms in the amorphous support structure near the Cr center, with either one or two Cr-O-Al bridges, respectively. Additionally, possible locations were considered for the additional proton that compensates the framework charge and Si-(OH)-Al Brönsted acid sites. Results for just one Cr-O-Al bridge resembled those of the standard CrO$_x$/SiO$_2$ catalyst since the geometries of the dioxo and mono-oxo were still determined to be pseudo-tetrahedral and square pyramidal, respectively. The dioxo site was found to be more thermodynamically preferred than the mono-oxo site, as for the standard catalyst. Although at high temperatures and under low water vapor pressure, formation of the mono-oxo site is preferable with direct transformation, other dehydration reactions resulted in the formation of the most stable dioxo species that is even more preferred than the mono-oxo. With two Cr-O-Al bridges near the Cr center, the most stable sites contain two Brönsted acid sites near each Cr center, and this allows for even deeper dehydration than for either the case of zero or one Cr-O-Al bridge. This further dehydration causes the mono-oxo sites to be 3-fold bonded to the support and exhibit pseudo-tetrahedral geometry, like the dioxo species, rather than the previously seen square pyramidal geometry. The alteration in geometry allows the mono-oxo site to have increased stability

relative to the dioxo site, in contrast to the other cases of zero or one Al site near the Cr center, in which the dioxo site is more thermodynamically preferred.

Thus, the structure of the catalytic active chromia sites, surface reaction intermediates and of the silica-supported chromia catalysts promoted with TiO_x, ZrO_x, or AlO_x are needed to allow for the development of a molecular level model of ethylene polymerization by oxide promoted silica-supported chromia catalysts.

1.6 Summary and Conclusions

The nature of the surface CrO_x sites strongly depends on the environment to which the supported CrO_x/SiO_2 catalysts are exposed. Under ambient conditions, hydrated surface chromia species are present (CrO_4, Cr_2O_7, Cr_3O_{10}, and Cr_4O_{13}), and the extent of oligomerization increases with decreasing surface pH values at point of zero charge. Under dehydrated and oxidizing conditions, the surface chromia sites are present as isolated surface dioxo $(O=)_2CrO_2$ on silica. Crystalline Cr_2O_3 nanoparticles are also present above the maximum dispersion limit, which depends on the Cr precursor, solvent, and surface properties of the SiO_2 support. Many of the early studies applied UV-vis spectroscopy to determine the nature of the surface CrO_x sites on silica, but the broad and overlapping UV-vis bands prevented clear cut structural assignments. The supported CrO_x/SiO_2 catalysts are activated for ethylene polymerization by exposure to reducing environments. Activation with CO leads to Cr^{+2} sites, but activation with H_2 and C_2H_4 results in Cr^{+3} sites.

Less is known concerning the fundamental details of the Ti-, Zr-, and Al-promoted CrO_x/SiO_2 catalysts since most studies in the literature have focused on the standard CrO_x/SiO_2 catalyst. Most publications concerning the promoted catalysts did not study the promoted CrO_x/SiO_2 catalysts under relevant ethylene polymerization reaction conditions,

reducing first with H_2 or CO or applying indirect methods such as NO chemisorption. The role of promoters for ethylene polymerization needs to be examined using a combination of modern *in situ* spectroscopy techniques that can directly probe the catalyst structure during relevant reaction conditions.

1.7 Thesis Outline – Ethylene Polymerization

The above literature review indicates the need for elucidation of fundamental details of ethylene polymerization by heterogeneous supported CrO_x/SiO_2 catalysts. This will be achieved by combining multiple *in situ* spectroscopic techniques capable of directly characterizing the catalyst under relevant ethylene polymerization conditions. The chapters pertaining to ethylene polymerization are outlined below.

Chapter 2: Catalyst Synthesis and Experimental Techniques

Details of the experimental techniques and procedures will be provided in this chapter.

Chapter 3: Ethylene Polymerization by Supported CrO_x/SiO_2 Catalysts: Active Sites, Surface Intermediates, and Structure-Activity Relationships

The standard CrO_x/SiO_2 catalyst will be characterized before and during ethylene polymerization reaction conditions. Using time-resolved *in situ* Raman spectroscopy, TPSR-MS, *operando* DRIFTS, and *in situ* UV-vis DRS, the molecular structure, electronic transitions, and surface intermediates will be elucidated to allow development of the structure-activity relationships of the supported CrO_x/SiO_2 catalyst.

Chapter 4: Operando Ethylene Polymerization by Supported CrO_x/SiO_2 Catalysts: Role of Promoters

Multilayered CrO_x/SiO_2 catalysts will be synthesized and characterized. The silica support will first be impregnated with promoter metal oxides (AlO_x, TiO_x, and ZrO_x), and

the resulting modified support, subsequently impregnated with CrO_x. Following the methods used in Chapter 3 (*operando* DRIFTS, *in situ* Raman spectroscopy, TPSR-MS, and *in situ* UV-vis DRS), the role of promoters will be determined.

Acknowledgements

Chapter 1 References

1. Hogan, J. P. Catalysis of the Phillips Petroleum Company Polyethylene Process. In *Applied Industrial Catalysis*; Leach, B. E., Ed.; Academic Press, Inc.: New York, 1983; Vol. 1, pp 149-176.

2. Groppo, E.; Lamberti, C.; Bordiga, S.; Spoto, G.; Zecchina, Z. The Structure of Active Centers and the Ethylene Polymerization Mechanism on the Cr/SiO_2 Catalyst: A Frontier for the Characterization Methods. *Chem. Rev.* 2005*, 105*, 115-183.

3. McDaniel, M. P. A Review of the Phillips Supported Chromium Catalyst and Its Commercial Use for Ethylene Polymerization. *Advances in Catalysis* 2010*, 53*, 123-606.

4. Chakrabarti, A.; Wachs, I. E. The Nature of CrO_x Sites in Different Environments. *Catal. Lett.* 2015*, 145*, 985-994.

5. Hogan, J. P.; Banks, R. L. Polymers and Production Thereof. 2825721. March 4, 1958.

6. Horvath, B. Polymerization Catalyst. US3622522.

7. Horvath, B. Polymerization Using a Supported Chromia Activated with a Tin on Gallium Compound. US3676417.

8. McDaniel, M. P. Supported Chromium Catalysts for Ethylene Polymerization. *Advances in Catalysis* 1985*, 33*, 47-98.

9. Horvath, B. Polymerization Catalyst System Additives. US3625864.

10. McDaniel, M. P.; Welch, M. B.; Dreiling, M. J. The Activation of the Phillips Petroleum Catalyst. *Journal of Catalysis* 1983*, 82*, 118-126.

11. Pullukat, T. J.; Hoff, R. E.; Shida, M. A Chemical Study of Thermally Activated Chromic Titanate on Silica Ethylene Polymerization Catalysts. *Journal of Polymer Science: Polymer Chemistry Edition* 1980*, 18*, 2857-2866.

12. Hogan, J. P.; Witt, D. R. Olefin Polymerization with Chromium and Titanium-Containing Compounds. US3622521.

13. Deitz, R. E. Polymerization Catalyst. US3887494.

14. Conway, S. J.; Falconer, J. W.; Rochester, C. H. Chromia/Silica-Titania Cogel Catalysts for Ethene Polymerisation Kinetics. *Journal of Chemical Society, Faraday Transactions 1* 1989*, 85*, 71-78.

15. Conway, S. J.; Falconer, J. W.; Rochester, C. H. Chromia/Silica-Titania Cogel Catalysts for Ethene Polymerisation IR Study. *Journal of Chemical Society, Faraday Transactions 1* 1989*, 85*, 79-90.

16. Conway, S. J.; Falconer, J. W.; Rochester, C. H. Chromia/Silica-Titania Cogel Catalysts for Ethene Polymerisation Polymer Characteristics. *Journal of Chemical Society, Faraday Transactions 1* 1989*, 85*, 1841-1851.

17. Hogan, J. P.; Norwood, D. D. Spray Dried Titanium-Containing Catalyst for Stress Crack Resistant Polymer. US4053436.

18. Hogan, J. P.; Norwood, D. D. Polymerization Process Using Spray Dried Titanium-Containing Catalyst. US4101722.

19. Hardcastle, F. D.; Wachs, I. E. Raman Spectroscopy of Chromium Oxide Supported on Al_2O_3, TiO_2 and SiO_2: A Comparative Study. *J. Mol. Catal.* 1988*, 46*, 173-186.

20. Vuurman, M.; Wachs, I. E.; Stufkens, D. J.; Oskam, A. Characterization of chromium oxide supported on Al_2O_3, ZrO_2, TiO_2, and SiO_2 under dehydrated conditions. *J. Mol. Catal.* 1993*, 80*, 209-227.

21. Michel, G.; Cahay, R. Raman spectroscopic investigations on the chromium(VI) equilibriu. Part 2-Species present, influence of ionic strength and chromate-dichromate (CrO42-Cr2O72-) equilibrium constant. *J. Raman Spectrosc.* 1986*, 17*, 79-82.

22. Deo, G.; Wachs, I. E. Predicting Molecular Structures of Surface Metal Oxide Species on Oxide Supports under Ambient Conditions. *J. Phys. Chem.* 1991*, 95*, 5889-5895.

23. Weckhuysen, B. M.; Schoonheydt, R. A.; Jehng, J. M.; Wachs, I. E.; Cho, S. J.; Ryoo, R.; Kljlstra, S.; Poels, E. Combined DRS-RS-EXAFS-XANES-TPR Study of Supported Chromium Catalysts. *J. Chem. Soc. Far. Trans.* 1995*, 91*, 3245-3253.

24. Zecchina, A.; Garrone, E.; Ghiotti, G.; Morterra, C.; Borello, E. *J. Phys. Chem.* 1975*, 79*, 966-972.

25. Hogan, J. P. Ethylene Polymerization Catalysis over Chromium Oxide. *J. Polym. Sci. , Part A: Polym. Chem.* 1970*, 8*, 2637-2652.

26. Fubini, B.; Ghiotti, G.; Stradella, L.; Garrone, E.; Morterra, C. *J. Catal.* 1980*, 66*, 200-213.

27. Weckhuysen, B. M.; De Ridder, L. M.; Schoonheydt, R. A. *J. Phys. Chem.* 1993*, 97*, 4756-4763.

28. Lee, E. L.; Wachs, I. E. In Situ Spectroscopic Investigation of the Molecular and Electronic Structures of SiO_2 Supported Surface Metal Oxides. *J. Phys. Chem. C* 2007*, 111*, 14410-14425.

29. Groppo, E.; Prestipino, C.; Cesano, F.; Bonino, F.; Bordiga, S.; Lamberti, C.; Thune, P. C.; Niemantsverdriet, J. W.; Zecchina, A. In situ, Cr *K*-edge XAS study on the Phillips catalyst: activation and ethylene polymerization. *J. Catal.* 2005*, 230*, 98-108.

30. Groppo, E.; Damin, A.; Bonino, F.; Zecchina, A.; Bordiga, S.; Lamberti, C. New Strategies in the Raman Study of the Cr/SiO_2 Phillips Catalyst: Observation of Molecular Adducts on Cr(II) Sites. *Chem. Mater.* 2005*, 17*, 2019-2027.

31. Dines, T. J.; Inglis, S. *Phys. Chem. Chem. Phys.* 2003*, 5*, 1320-1328.

32. Lee, E. L.; Wachs, I. E. Molecular Design and In Situ Spectroscopic Investigation of Multilayered Supported $M_1O_x/M_2Ox/SiO_2$ Catalysts. *J. Phys. Chem. C* 2008*, 112*, 20418-20428.

33. Lee, E. L.; Wachs, I. E. *J. Phys. Chem. C* 2008*, 112*, 6487-6498.

34. Handzlik, J.; Grybos, R.; Tielens, F. Structure of Monomeric Chromium(VI) Oxide Species Supported on Silica: Periodic and Cluster DFT Studies. *J. Phys. Chem. C* 2013*, 117*, 8138-8149.

35. Gierada, M.; Michorczyk, P.; Tielens, F.; Handzlik, J. Reduction of chromia-silica catalysts: A molecular picture. *J. Catal.* 2016*, 340*, 122-135.

36. Hogan, J. P. Method of Treating Supported Chromium Oxide Catalyst and Polymerization Therewith. US3362946.

37. Przhevalskaya, L. K.; Shvets, V. A.; Kazansky, V. B. The Study of Active Centers of Ethylene Polymerization over Chromium Catalysts Prepared from Tri- and Bivalent Chromium Compounds. *J. Catal.* 1975*, 39*, 363-368.

38. Rebenstorf, B.; Larsson, R. CO Complexes of Chromium(II) and Chromium(III). *Z. Anorg. Allg. Chem.* 1981*, 478*, 119-138.

39. Rebenstorf, B.; Larsson, R. Why do Homogeneous Analogs of Philliips (CrO_3/SiO_2) and Union Carbide (Chromocene/SiO_2) Polyethylene Catalysts Fail? Some Answers from IR Investigations. *J. Mol. Catal.* 1981*, 11*, 247-256.

40. Rebenstorf, B.; Sheng, T. C. Influence of Chromium Concentration and Addition of Fluorine, Titanium, or Boron on the Chromium Species of the Phillips Catalyst: A Quantitative Evaluation. *Langmuir* 1991*, 7*, 2160-2165.

41. Gaspar, A. B.; Martins, R. L.; Schmal, M.; Diguez, L. C. Characterization of Cr^{2+} and ethylene polymerization on Cr/SiO_2 catalysts. *J. Mol. Catal. A: Chem.* 2001*, 169*, 105-112.

42. Ghiotti, G.; Garrone, E.; Zecchina, A. IR Investigation of Polymerization Centres of the Phillips Catalyst. *J. Mol. Catal.* 1988*, 46*, 61-77.

43. Groppo, E.; Lamberti, C.; Cesano, F.; Zecchina, A. On the fraction of Cr^{II} sites involved in the C_2H_4 polymerization on the Cr/SiO_2 Phillips catalyst: a quantification by FTIR spectroscopy. *Phys. Chem. Chem. Phys.* 2006*, 8*, 2453-2456.

44. Potter, K. C.; Beckerle, C. W.; Jentoft, F. C.; Schwerdtfeger, E.; McDaniel, M. P. Reduction of the Phillips catalyst by various olefins: Stoichiometry, thermochemistry, reaction products and polymerization activity. *J. Catal.* 2017*, 344*, 657-668.

45. Barzan, C.; Piovano, A.; Braglia, L.; Martino, G. A.; Lamberti, C.; Bordiga, S.; Groppo, E. Ligands Make the Difference! Molecular Insights into Cr^{VI}/SiO_2 Phillips Catalyst during Ethylene Polymerization. *J. Am. Chem. Soc.* 2017, Ahead of Print.

46. Baker, L. M.; Carrick, W. L. Oxidation of Olefins by Supported Chromium Oxide. *J. Org. Chem.* 1968*, 33*, 616-618.

47. Liu, B.; Nakatani, H.; Terano, M. New aspects of the induction period of ethene polymerization using Phillips CrOx/SiO$_2$ catalyst probed by XPS, TPD and EPMA. *J. Mol. Catal. A: Chem.* 2002*, 184*, 387-398.

48. Barzan, C.; Damin, A. A.; Budnyk, A.; Zecchina, A.; Bordiga, S.; Groppo, E. Pre-reduction of the Phillips Cr^{VI}/SiO$_2$ catalyst by cyclohexene: A model for the induction period of ethylene polymerization. *J. Catal.* 2016*, 337*, 45-51.

49. Cicmil, D.; van Ravenhorst, I. K.; Meeuwissen, J.; Vantomme, A.; Weckhuysen, B. M. Structure-performance relationships of Cr/Ti/SiO$_2$ catalysts modified with TEAl for oligomerisation of ethylene: tuning the selectivity towards 1-hexene. *Catal. Sci. Tech.* 2016*, 6*, 731-743.

50. Conley, M. P.; Delley, M. F.; Siddiqi, G.; Lapadula, G.; Norsic, S.; Monteil, V.; Safonova, O. V.; Coperet, C. Polymerization of Ethylene by Silica-Supported Dinuclear Cr^{III} Sites through an Initiation Step Involving C-H Bond Activation. *Angew. Chem. Int. Ed.* 2014*, 53*, 1872-1876.

51. Delley, M. F.; Nunez-Zarur, F.; Conley, M. P.; Comas-Vives, A.; Siddiqi, G.; Norsic, S.; Monteil, V.; Safonova, O. V.; Coperet, C. Proton transfers are key elementary steps in ethylene polymerization on isolated chromium(III) silicates. *PNAS* 2014*, 111*, 11624-11629.

52. Delley, M. F.; Conley, M. P.; Coperet, C. Polymerization on CO-Reduced Phillips Catalyst initiates through the C-H bond Activation of Ethylene on Cr-O Sites. *Catal. Lett.* 2014*, 144*, 805-808.

53. Bordiga, S.; Bertarione, S.; Damin, A.; Prestipino, C.; Spoto, G.; Lamberti, C.; Zecchina, A. On the first stages of the ethylene polymerization on Cr^{2+}/SiO$_2$ Phillips

catalyst: time and temperature resolved IR studies. *J. Mol. Catal. A: Chem.* 2003*, 204-205*, 527-534.

54. Groppo, E.; Lamberti, C.; Bordiga, S.; Spoto, G.; Damin, A.; Zecchina, A. FTIR Investigation of the H_2, N_2, and C_2H_4 Molecular Complexes Formed on the Cr(II) Sites in the Phillips Catalyst: a Preliminary Step in the understanding of a Complex System. *J. Phys. Chem. B* 2005*, 109*, 15024-15031.

55. Groppo, E.; Lamberti, C.; Bordiga, S.; Spoto, G.; Zecchina, A. In situ FTIR spectroscopy of key intermediates in the first stages of ethylene polymerizaton on the Cr/SiO_2 Phillips catalyst: Solving the puzzle of the initiation mechanism? *J. Catal.* 2006*, 240*, 172-181.

56. Groppo, E.; Estephane, J.; Lamberti, C.; Spoto, G.; Zecchina, A. Ethylene, propylene and ethylene oxide in situ polymerization on the $Cr(II)/SiO_2$ system: A temperature- and pressure-dependent investigation. *Catal. Today* 2007*, 126*, 228-234.

57. Barzan, C.; Groppo, E.; Quadrelli, E. A.; Monteil, V.; Bordiga, S. Ethylene polymerization on a SiH_4-modified Phillips catalyst: detection of *in situ* produced a-olefins by operando FT-IR spectroscopy. *Phys. Chem. Chem. Phys.* 2012*, 14*, 2239-2245.

58. McGuinness, D. S.; Davies, N. W.; Horne, J.; Ivanov, I. Unraveling the Mechanism of Polymerization with the Phillips Catalyst. *Organometallics* 2010*, 29*, 6111-6116.

59. Brown, C.; Krzystek, J.; Achey, R.; Lita, A.; Fu, R.; Meulenberg, R. W.; Polinski, M.; Peek, N.; Wang, Y.; van de Burgt, L. J.; Profeta, J., S.; Stiegman, A. E.; Scott, S. L. Mechanism of Initiation in the Phillips Ethylene Polymerization Catalyst: Redox Processes Leading to the Active Site. *ACS Catal.* 2015*, 5*, 5574-5583.

60. Conley, M. P.; Delley, M. F.; Siddiqi, G.; Lapadula, G.; Norsic, S.; Monteil, V.; Safonova, O. V.; Coperet, C. Corrections ACIE - Polymerization of Ethylene by Silica-Supported Dinuclear Cr^{III} Sites through an Initiation Step Involving C-H Bond Activation. *Angew. Chem. Int. Ed.* 2015*, 53*, 6657-6671.

61. Delley, M. F.; Nunez-Zarur, F.; Conley, M. P.; Comas-Vives, A.; Siddiqi, G.; Coperet, C. Corrections. *PNAS* 2015*, 112*, E4505.

62. Chakrabarti, A.; Gierada, M.; Handzlik, J.; Wachs, I. E. Operando Molecular Spectroscopy During Ethylene Polymerization by Supported CrO$_x$/SiO$_2$ Catalysts: Active Sites, Reaction Intermediates, and Structure-Activity Relationship. *Top. Catal.* 2016*, 59*, 725-739.

63. Zielinski, P.; Dalla Lana, I. G. An FTIR Spectroscopic View of the Initiation of Ethylene Polymerization on Cr/SiO$_2$ Catalyst. *J. Catal.* 1992*, 137*, 368-376.

64. Kantcheva, M.; Dalla Lana, I. G.; Szymura, J. A. FTIR Spectroscopic Investigation of the Initiation of Ethylene Polymerization on Cr/Silica. *J. Catal.* 1995*, 154*, 329-334.

65. Ghiotti, G.; Garrone, E.; Coluccia, S.; Morterra, C.; Zecchina, A. Evidence for Alkylidenic Configuration of Polymethylene Chains on the Phillips Catalyst. *J. C. S. Chem. Comm.* 1979, 1032-1033.

66. Espelid, O.; Borve, K. J. *J. Catal.* 2002*, 206*, 331-338.

67. Zhong, L.; Lee, M. Y.; Liu, Z.; Wanglee, Y. J.; Liu, B.; Scott, S. L. Spectroscopic and structural characterization of Cr(II)/SiO$_2$ active site precursors in model Phillips polymerization catalysts. *J. Catal.* 2012*, 293*, 1-12.

68. Gierada, M.; Handzlik, J. Active sites formation and their transformations during ethylene polymerization by the Phillips CrO$_x$/SiO$_2$ catalyst. *J. Catal.* 2017, *352*, 314-328.

69. Rimola, A.; Costa, D.; Sodupe, M.; Lambert, J. F.; Ugliengo, P. Silica Surface Features and Their Role in the Adsorption of Biomolecules: Computational Modeling and Experiments. *Chem. Rev.* 2013, *113*, 4216-4313.

70. Gao, X.; Bare, S. R.; Fierro, J. L. G.; Banares, M. A.; Wachs, I. E. Preparation of in-Situ Spectroscopic Characterization of Molecularly Dispersed Titanium Oxide on Silica. *J. Phys. Chem. B* 1998, *102*, 5653-5666.

71. Inaki, Y.; Yoshida, H.; Yoshida, T.; Hattori, T. Active Sites on Mesoporous and Amorphous Silica Materials and Their Photocatalytic Activity: An Investigation by FTIR, ESR, VUV-UV and Photoluminescence Spectroscopies. *J. Phys. Chem. B* 2002, *106*, 9098-9106.

72. Antonietti, J. M.; Michalski, M.; Heiz, U.; Jones, H.; Lim, K. H.; Rosch, N.; Del Vitto, A.; Pacchioni, G. Optical Absorption Spectrum of Gold Atoms Deposited on SiO$_2$ from Cavity Ringdown Spectroscopy. *Phys. Rev. Lett.* 2005, *94*, 213402-1-213402-4.

73. Musso, F.; Ugliengo, P.; Solans-Monfort, X.; Sodupe, M. Periodic DFT Study of Radical Species on Crystalline Silica Surfaces. *J. Phys. Chem. C* 2010, *114*, 16430-16438.

74. Zelenak, V.; Zelenakova, A.; Kovac, J. Insight into surface heterogeneity of SBA-15 silica: Oxygen related defects and magnetic properties. *Colloids Surf. A* 2010, *357*, 97-104.

75. Finch, J. N. Reduction Studies on Supported Chromic Anhydride Catalysts. *Journal of Catalysis* 1976*, 43*, 111-121.

76. Holm, V. C. F.; Clark, A. Reduction Studies on Supported Metal Oxide Catalysts. *Journal of Catalysis* 1968*, 11*, 305-316.

77. Ellison, A.; Overton, T. L. Characterisation of Cr/Silica Catalysts. *Journal of Chemical Society Faraday Transactions* 1993*, 89*, 4393-4395.

78. Ellison, A.; Overton, T. L. Characterisation of modified Cr-silica catalysts. *Journal of Molecular Catalysis* 1994*, 90*, 81-86.

79. Guesmi, H.; Tielens, F. Chromium Oxide Species Supported on Silica: A Representative Periodic DFT Model. *J. Phys. Chem. C* 2012*, 116*, 994-1001.

80. Cheng, R.; Xu, C.; Liu, Z.; Dong, Q.; He, X.; Fang, Y.; Terano, M.; Hu, Y.; Pullukat, T. J.; Liu, B. High-resolution spectroscopy (XPS, ^{1}H MAS solid-state NMR) and DFT investigations into Ti-modified Phillips CrO_x/SiO_2 catalysts. *Journal of Catalysis* 2010*, 273*, 103-115.

81. Ma, Y.; Wang, L.; Liu, Z.; Cheng, R.; Zhong, L.; Yang, Y.; He, X.; Fang, Y.; Terano, M.; Liu, B. High-resolution XPS and DFT investigations into Al-modified Phillips CrO_x/SiO_2. *J. Mol. Catal. A: Chem.* 2015*, 401*, 1-12.

82. Cicmil, D.; Meeuwissen, J.; Vantomme, A.; Wang, J.; van Ravenhorst, I. K.; van der Bij, H. E.; Munoz-Murillo, A.; Weckhuysen, B. M. Polyethylene with Reverse Co-monomer Incorporation: From an Industrial Serendipitous Discovery to Fundamental Understanding. *Angew. Chem. Int. Ed.* 2015*, 54*, 13073-13079.

83. Handzlik, J.; Grybos, R.; Tielens, F. Isolated Chromium(VI) Oxide Species Supported on Al-Modified Silica: A Molecular Description. *J. Phys. Chem. C* 2016*, 120*, 17594-17603.

Chapter 2 | Catalyst Synthesis and Experimental Techniques

2.1 Introduction

This chapter will describe all relevant experimental procedures used in the content of this dissertation. There will be no experimental details present in subsequent chapters.

2.2 Catalyst Synthesis and Experimental Techniques for Ethylene Polymerization

2.2.1 Synthesis of Supported CrO$_x$/SiO$_2$ Catalysts

The silica support material used was amorphous SiO$_2$ (Cabot, Cab-O-Sil fumed silica EH-5, S.A. = 332 m^2/g). Following previous methods[1], the Cab-O-Sil was found to be more easily handled by an initial water pretreatment without changing material properties. The highly dispersed silica-supported metal oxide catalyst was prepared under ambient conditions via the incipient wetness impregnation method of an aqueous solution of the chromium (III) nitrate precursor (Cr(NO$_3$)$_3$9H$_2$O, Alfa Aesar, 98.5 %). The samples were then dried overnight. In a programmable furnace (Thermolyne, Model 48000), the samples were dried in a second step in air by holding the samples at 120 °C for 2 h, and the final step was calcination of the catalyst by ramping the temperature at 1 °C/min under flowing air (Airgas, Zero grade) to 500 °C and holding for 6 h. The final synthesized catalyst was then denoted as 3% CrO$_x$/SiO$_2$.

2.2.2 Synthesis of Supported CrO$_x$/MO$_x$/SiO$_2$ Catalysts (M = Al, Ti, Zr)

The dispersed silica-supported metal oxide catalysts were prepared via a 2-step incipient wetness impregnation method. The silica support material used was amorphous SiO$_2$ (Cabot, Cab-O-Sil fumed silica EH-5, S.A. = 332 m^2/g). Using previous methods[1], the Cab-O-Sil was found to be more easily handled using an initial water pretreatment process that did not change material properties of the silica. In the first step after the initial

water pretreatment, the SiO_2 surface was modified by dispersing 5wt% of the metal oxide promoters using non-aqueous (toluene $C_6H_5CH_3$, Alfa Aesar, HPLC grade) solutions corresponding to the precursors aluminum sec-butoxide ($Al[O(CH_3)CHC_2H_5]_3$, Alfa Aesar, 95%), titanium (IV) isopropoxide ($Ti[OCH(CH_3)_2]_4$, Sigma-Aldrich), or zirconium (IV) n-propoxide ($Zr[O(CH_2)_2CH_3]_4$, Alfa Aesar, 70%). The non-aqueous IWI preparations were performed inside a glovebox (Vacuum Atmospheres, Omni-Laboratory VAC 101965) under a nitrogen atmosphere and kept inside overnight after impregnation. The samples were then transferred to a programmable furnace (Thermolyne, Model 48000), in which the samples were first dried in a second step in flowing nitrogen (Airgas, UHP) at 120 °C for 5 h, and then finally calcined by ramping the temperature at 1 °C/min under flowing nitrogen to 500 °C and holding for 6 h. The second impregnation step was of the modified SiO_2 supports with dispersion of 3wt% CrO_3 using methods as outlined above. The final synthesized catalysts were denoted as 3% CrO_x/5% MO_x/SiO_2 (M = Al, Ti, or Zr).

2.2.3 *In situ* X-ray Absorption Spectroscopy (XAS): X-ray Absorption Near-Edge Spectroscopy (XANES) and Extended X-ray Absorption Fine Structure (EXAFS)

Cr K-edge XAS experiments were carried out at Brookhaven National Lab at the X19A beamline. The catalyst was first pressed into a thin pellet, and then loaded into a Nashner-Adler cell to allow for *in situ* treatment of the catalyst. The protocol for obtaining *in situ* XAS spectra was as follows: (1) under flowing 20% O_2/He (Airgas, certified, 20.00% O_2/He balance, 25 mL/min), initially heat the sample to 500 °C, hold for ~30 min, and cool to 100 °C, (2) switch the gas flow to He (Airgas, UHP, 25 mL/min). The dehydrated

spectrum was obtained at 100 °C under flowing He. Data processing and analysis were performed using the Athena software package.[2]

2.2.4 *In situ* **Raman Spectroscopy**

In situ Raman spectra of the dehydrated catalysts were obtained at Oak Ridge National Laboratory. The catalyst was loaded into an environmental cell to allow for *in situ* treatment. The protocol for obtaining *in situ* Raman spectra was as follows: (1) under flowing 5% O_2/He, initially heat the sample to 500 °C, hold for ~1 h, and cool to 100 °C. The *in situ* Raman spectra were obtained using a moving stage to constantly move the sample to minimize laser-induced reduction. The dehydrated spectra were obtained at 100 °C under flowing 5% O_2/He with a 442 nm wavelength laser at 20% laser power.

In situ Raman spectra of the silica-supported catalyst during ethylene polymerization were taken using a high-resolution, dispersive Raman spectrometer system (Horiba-Jobin Yvon LabRam HR), which is equipped with three lasers (532, 442, and 325 nm). The laser employed in these studies was the visible laser at 442 nm (blue), generated by a He–Cd laser (Kimmon, model IK5751I-G; 441.6 nm; output power of 110 mW). The laser was focused on the samples using a confocal microscope equipped with a 50x long working distance objective (Olympus BX-30-LWD) for the visible laser. A 900 grooves/nm grating (Horiba-Jobin Yvon 51093140HR) was used to optimize the LabRam HR spectrometer for obtaining the best spectral resolution (~1 cm^{-1}). The laser was calibrated before experiments, using a silicon standard with its peak at 520.7 cm^{-1}. The Raman spectra were

collected with a 200 µm size hole. Raman vibrations from the SiO_2 support were used as internal standards to normalize signal intensities of the spectra.

The gas flow rates were monitored using mass flow controllers (Brooks, Model 5850E). For each experiment, catalyst sample was loaded as loose powder (~20 mg) into an *in situ* environmental cell (Harrick, HVC-DR2 with a CaF_2 window). The protocol for obtaining the *in situ* Raman spectra was as follows: (1) under flowing 10% O_2/Ar (Airgas, certified, 9.926% O_2/Ar balance, 25 mL/min), initially heat the sample at 10 °C/ min from room temperature to 500 °C, hold for 1 h, and cool to 100 °C at a rate of 10 °C/min, (2) switch the gas flow to Ar (or He for the $CrO_x/MO_x/SiO_2$ catalysts) (Airgas, UHP, 25 mL/min) for ~20 min, and (3) introduce 1% C_2H_4/Ar (Praxair, certified, 1.00% C_2H_4/Ar balance, 25 mL/min) for ~3 h.

2.2.5 C_2H_4-Temperature Programmed Surface Reaction (TPSR)

The temperature programmed surface reaction (TPSR) experiment was performed with an AMI-200 equipped with a Dycor ProLine Process Mass Spectrometer (MS).

The gas flow rates were monitored using mass flow controllers as indicated above. The catalyst sample was loaded as loose powder (~20 mg) into a U-shaped reactor packed with quartz wool. The protocol for obtaining the C_2H_4-TPSR data was as follows: (1) under flowing 10% O_2/Ar (Airgas, certified, 9.926 %O_2/Ar balance, 25 mL/min), initially heat the catalyst bed to 500 °C at 10 °C/min, hold for 1 h, and cool to 100 °C, (2) switch the gas flow to Ar (or He for the $CrO_x/MO_x/SiO_2$ catalysts) (Airgas, UHP, 25 mL/min) for ~30 min, (3) introduce 1% C_2H_4/Ar (Praxair, certified 1.00% C_2H_4/Ar balance, 25 mL/min) and

ramp the temperature to 800 °C at 10 °C/min. An online mass spectrometer (AMI 200) turned on before the C_2H_4 flow was started and was used to monitor gaseous products.

2.2.6 *In situ* Ultra Violet-Visible (UV-vis) Diffuse Reflectance Spectroscopy (DRS)

In situ UV-vis spectra of the standard supported CrO_x/SiO_2 catalyst were obtained with a Varian Cary 5E UV-vis-NIR spectrophotometer employing the integration sphere diffuse reflectance attachment (Harrick Praying Mantis Attachment, DRA-2).

The *in situ* UV-vis spectra of the promoted $CrO_x/MO_x/SiO_2$ catalysts were obtained using an Agilent Cary Series 5000 UV-vis-NIR spectrophotometer employing the integration sphere diffuse reflectance attachment (Harrick Praying Mantis Attachment, DRA-2). The flow rates were monitored with mass flow controllers as indicated above. The catalyst was loaded as a loose powder (~20 mg) into an *in situ* environmental cell (Harrick, HVC-DR2 with a CaF_2 window). Each spectrum was taken from 200 to 1500 nm. MgO was used as a standard for background absorbance, and the edge energies (E_g) were calculated using a Microsoft Excel Macro spreadsheet.

For each experiment, the catalyst sample was loaded as loose powder (~20 mg) into an *in situ* environmental cell (Harrick, HVC-DR2 with a CaF_2 window). The experimental protocol was the same as that used during the *in situ* Raman experiments. Each spectrum was taken for ~10 min from 200 to 800 nm. UV-vis spectra of the promoted supported $CrO_x/MO_x/SiO_2$ catalysts were obtained with an Agilent Cary Series 5000 UV-vis-NIR spectrophotometer. Each spectrum was taken for ~1-2 min from 200-1500 nm. MgO was

used as a standard for background absorbance, and the edge energies (E_g) were calculated using a Microsoft Excel Macro spreadsheet.

2.2.7   *In situ* and *Operando* Diffuse Reflectance Infrared Spectroscopy (DRIFTS)

In situ DRIFT spectra of the supported chromia catalysts were obtained using a Thermo Scientific Nicolet 8700 spectrometer equipped with a Harrick Praying Mantis attachment (Model DRA-2). IR vibrations from the bulk of the SiO_2 support were used as an internal standard to normalize signal intensities of the IR spectra.

The gas flow rates were monitored using mass flow controllers as indicated above. For each experiment, catalyst sample was loaded as loose powder (~20 mg) into an *in situ* environmental cell as indicated above. The experimental protocol was the same as that used during the *in situ* Raman experiments. Spectra were collected using an MCT detector (cooled with liquid N_2) with a resolution of ~4 cm^{-1} and an accumulation of 72 scans (total of ~1 min per spectrum) in the range of 650-4000 cm^{-1}.

2.2.8   Computational Models and Methods

Cluster models of Cr^{+3} surface species have been developed based on the β-cristobalite structure[3,4], often used to represent amorphous silica[4-10]. They contain 9 or 7 Si atoms and are larger or comparable to other proposed models of the supported CrOx/SiO2 catalyst, that have been applied in theoretical studies of the ethylene polymerization mechanism[11-17]. The dangling bonds have been saturated with hydrogen atoms replacing the removed Si atoms. The structures have been fully relaxed to allow for the amorphous nature of the support. The geometry optimization has been performed using the PBE0 functional[18] combined with the def2-SVP basis set[19]. To confirm the potential energy minimum for each intermediate or the transition state, and to compute Gibbs energy corrections, the

harmonic vibrational frequencies have been calculated. The transition state structures have been additionally verified by the IRC analysis[20,21]. Single point energy calculations have been performed for each optimized structure using the PBE0 functional and the def2-TZVPP basis set[19]. The reaction pathways are discussed in terms of Gibbs energies estimated by adding the Gibbs energy corrections and DFT-D3(BJ) dispersion corrections[22,23] to the PBE0/def2-TZVPP single point energies. Spin unrestricted calculations for the Cr^{+3} species have been performed. In each case, the verified ground state is quartet. All calculations have been done with the Gaussian 09 package[24]. For the graphic presentation of the models, the GaussView 5.0 program[25] has been used.

2.3 Catalyst Synthesis and Experimental Techniques for Olefin Metathesis

2.3.1 Synthesis of Supported MoO_x/Al_2O_3 Catalysts

A series of supported MoO_x/Al_2O_3 catalysts (1-25wt% MoO_3) were prepared via incipient-wetness impregnation of an aqueous solution of ammonium molybdate (para) tetrahydrate (($NH_4)_6Mo_7O_{24} \cdot 4H_2O$, Alfa Aesar, 99%, Lot No. 10120802) onto two different Al_2O_3 supports (Harshaw, AI-4126E 1/8", BET S.A. = 180 m^2/g and Sasol, Catalox Lot No. C2939, BET S.A. = 218 m^2/g). The Harshaw Al_2O_3 (hereon referred to as H-Al_2O_3) supported MoO_x catalysts were used for the *in situ* Raman studies because of its lower fluorescence that allowed for better quality Raman spectra. The *in situ* UV-vis DRS, DRIFTS, and TPSR studies were performed with the Sasol Catalox Al_2O_3 (hereon referred to as S-Al_2O_3) since only a limited quantity of the H-Al_2O_3 support was available.

Prior to impregnation, the alumina supports were calcined at 500°C for 16 h under flowing air. The impregnation step was performed under ambient conditions, and the mixtures were stirred for ~30 min to maximize MoO_x dispersion. Using a programmable

furnace (Thermolyne, Model 48000), the samples were further dried at 120°C for 2 h, then calcined by ramping the temperature at 1°C/min under flowing air (Airgas, Dry) to 500°C and holding for 4 h. The final synthesized catalysts are denoted as x% MoO_x/H- or S-Al_2O_3, where x is the weight percent of MoO_3 impregnated on the alumina supports. The 18 and 20% MoO_x/H-Al_2O_3 catalysts and 13, 18, and 20% MoO_x/S-Al_2O_3 catalysts were impregnated with the molybdena in two separate impregnation steps.

2.3.2   *In situ* UV-vis DRS

The *in situ* UV-vis spectra were obtained using an Agilent Cary Series 5000 UV-vis-NIR spectrophotometer employing the integration sphere diffuse reflectance attachment (Harrick Praying Mantis Attachment, DRA-2). The flow rates were monitored with mass flow controllers as indicated above. The catalyst was loaded as a loose powder (~20 mg) into an *in situ* environmental cell (Harrick, HVC-DR2 with a CaF_2 window). Each spectrum was taken from 200 to 800 nm. MgO was used as a standard for background absorbance, and the edge energies (E_g) were calculated using a Microsoft Excel Macro spreadsheet. The protocol for obtaining the *in situ* UV-vis DRS spectra was as follows: (1) under flowing 10% O_2/Ar (Praxair, certified 10.00% O_2/balance Ar, 30 mL/min), initially heat the sample at 10 °C/min from room temperature to 500 °C and hold for 1 h, (2) switch the gas flow was to Ar (Airgas, certified UHP, 30 mL/min) and cool at 10 °C/min to 30°C, (3) introduce 5% C_3H_6/Ar (Praxair, certified 5.00%, 30 mL/min) for 1 h, (4) flush with

UHP Ar for 1 h and heat to 200 °C at 10°C/min, and (5) flow 5% C_3H_6/Ar at 200 °C for 1 h (30 mL/min).

2.3.3 *In situ* **Raman Spectroscopy**

The *in situ* Raman spectra of the alumina-supported MoO_x catalysts were taken using a high-resolution, dispersive Raman spectrometer system (Horiba-Jobin Yvon LabRam High Resolution (HR)), equipped with three lasers (532, 442, and 325 nm). The laser employed in these studies was the visible laser at 442 nm (blue), generated by a He-Cd laser (Kimmon, model IK5751I-G; 441.6 nm; output power of 110 mW). The laser was focused on the catalysts using a confocal microscope equipped with an objective lens with 50x long working distance (Olympus BX-30-LWD). A 900 grooves/nm grating (Horiba-Jobin Yvon 51093140HR) was used to optimize the LabRam HR spectrometer for obtaining the best spectral resolution (~1 cm^{-1}). The laser was calibrated before experiments, using a silicon standard with its peak at 520.7 cm^{-1}. The Raman spectra were collected with a 200 µm size hole.

The gas flow rates were monitored using mass flow controllers (Brooks, Model 5850E). For each experiment, the catalyst was loaded as a loose powder (~20 mg) into an *in situ* environmental cell (Harrick, HVC-DR2 with a CaF_2 window). The protocol for obtaining the *in situ* Raman spectra was as follows: (1) under flowing 10% O_2/Ar (Praxair, certified 10.00% O_2/balance Ar, 30 mL/min), initially heat the sample at 10°C/min from room temperature to 500°C and hold for 1 h, (2) switch the gas flow was to Ar (Airgas, certified UHP, 30 mL/min) and cool at 10 °C/min to 30 °C, (3) introduce 5% C_3H_6/Ar (Praxair,

certified 5.00%, 30 mL/min) for 1 h, (4) flush with UHP Ar for 1 h and heat to 200 °C at 10 °C/min, and (5) flow 5% C_3H_6/Ar at 200 °C for 1 h (30 mL/min).

2.3.4 *In situ* DRIFTS

In situ DRIFTS spectra were obtained using a Thermo Scientific Nicolet 8700 spectrometer equipped with a Harrick Praying Mantis attachment (model DRA-2). The flow rates were monitored with mass flow controllers as indicated above. IR vibrations from the bulk Sasol Catalox Al_2O_3 support were used as an internal standard to normalize signal intensities of the IR spectra. Spectra were collected using an MCT detector (cooled with liquid N_2) with a resolution of 4 cm^{-1} and an accumulation of 96 scans (total of ~1 min per spectrum) in the range of 650-4000 cm^{-1}.

2.3.4.1 *Dehydration Pretreatment*

The experimental protocol was as follows: (1) under flowing 10% O_2/Ar (Praxair, certified 10.2% O_2/balance Ar, 30 mL/min), initially heat the sample at 10 °C/min from room temperature to 500 °C and hold for 1 h, and switch the gas flow to Ar (Airgas, UHP, 30 mL/min) and cool at 10 °C/min to 30 °C or 120 °C.

2.3.4.2 *Adsorption of C_4H_8 and Titration with C_2H_4*

After the initial dehydration treatment as outlined above, the experimental protocol was as follows: (2) adsorb 1% C_4H_8/Ar (Praxair, certified 1.00% C_2H_4/balance Ar, 30 mL/min) for 60 min at 120 °C, (3) flush with Ar for 45 min (Airgas, UHP, 30 mL/min), (4) switch to 1% C_2H_4/Ar (Praxair, certified, 1.00% C_2H_4/balance Ar, 30 mL/min) for 45 min at

120 °C, and (5) ramp the temperature at 10 °C/min to 510 °C under flowing ethylene (30 mL/min).

2.3.4.3 Adsorption and TP of C_3H_6

After the initial dehydration treatment as outlined above, the experimental protocol was as follows: (2) adsorb 1% C_3H_6/He (Praxair, certified, 1.00% C_3H_6/balance He, 30 mL/min) for 45 min at 120 °C, (3) flush with Ar for 45 min (Airgas, UHP, 30 mL/min), (4) switch to 1% C_2H_4/Ar (Praxair, certified, 1.00% C_2H_4/balance Ar, 30 mL/min) for 45 min at 120 °C, and (5) ramp the temperature at 10 °C/min to 510 °C under flowing ethylene (30 mL/min).

2.3.4.4 Adsorption of C_3D_6 and Titration with C_3H_6

After the initial dehydration as outlined above, the experimental protocol was as follows: (3) adsorb 10% C_3D_6/Ar (C/D/N Isotopes, certified, >98% C_3D_6) (30 mL/min) for 30 min at 120 °C, (4) switch to 1% C_3H_6/He (Praxair, certified, 1.00% C_3H_6/balance He, 30 mL/min) for 45 min at 120 °C, and (5) ramp the temperature at 10 °C/min to 510 °C under flowing propylene (30 mL/min).

2.3.4.5 Adsorption of C_3H_8O and TP with C_3H_6

After the initial dehydration procedure as outlined above, the experimental procedure was as follows: (3) adsorb C_3H_8O/Ar (30 mL/min) for 30 min at 30 °C, and (4) switch to 1% C_3H_6/He (Praxair, certified, 1.00% C_3H_6/balance He, 30 mL/min) and ramp the temperature at 10 °C/min to 510 °C under flowing propylene.

2.3.4.6 Adsorption of C_3H_6O and TP with C_3H_6

After the initial dehydration procedure as outlined above, the experimental procedure was as follows: (3) adsorb C_3H_6O/Ar (30 mL/min) for 30 min at 30 °C, and (4) switch to

1% C$_3$H$_6$/He (Praxair, certified, 1.00% C$_3$H$_6$/balance He, 30 mL/min) and ramp the temperature at 10 °C/min to 510 °C under flowing propylene.

2.3.5 Temperature-Programmed Surface Reaction (TPSR)

TPSR results were obtained with an Altamira Instruments system (AMI-200) equipped with an online quadrupole mass spectrometer (MS) (Dycor Dymaxion DME200MS). Flow rates were monitored with mass flow controllers (Brooks, Model 5850E).

For each experiment, the catalyst was loaded as loose powder (~200 mg) into a U-shaped reactor and packed with quartz wool. The MS m/z values that were used for detection of the reactants and products are: propylene (m/z 42), ethylene (m/z 27), butene (m/z 56), water (m/z 18), methane (m/z 16), carbon monoxide (m/z 28), oxygen (m/z 32), carbon dioxide (m/z 44), formaldehyde (m/z 30), acetaldehyde (m/z 43), and acetone (m/z 58). The cracking pattern of propylene gives rise to ethylene (m/z 27), formaldehyde (m/z 30), carbon monoxide (m/z 28), and acetaldehyde (m/z 43), so these were subtracted from the MS signals obtained during TPSR.

2.3.5.1 Dehydration Pretreatment

The experimental protocol was as follows: (1) under flowing 10% O$_2$/Ar (Praxair, certified 10.3% O$_2$/balance Ar, 30 mL/min), heat the sample at 10 °C/min from room temperature to 500 °C and hold for 1 h, and (2) switch the gas flow to Ar (Airgas, UHP, 30 mL/min) and cool to 35 °C.

2.3.5.2 C$_3$H$_6$-TPSR

After the initial dehydration outlined above, the experimental protocol was as follows: (3) hold the temperature at 35 °C in flowing Ar for 30 min and turn on the MS to allow it to stabilize, (4) adsorb propylene at 35 °C for 45 min (Praxair, certified 5.00%

C$_3$H$_6$/balance Ar, 30 mL/min), and (5) ramp the temperature at 10 °C/min under flowing propylene (30 mL/min) to 600 °C.

Acknowledgements

Chapter 2 References

1. Lee, E. L.; Wachs, I. E. In Situ Spectroscopic Investigation of the Molecular and Electronic Structures of SiO$_2$ Supported Surface Metal Oxides. *J. Phys. Chem. C* **2007**, *111*, 14410-14425.

2. Ravel, B. ATHENA XAS Data Processing. **2006-2016**.

3. Wright, A. F.; Leadbetter, A. J. *Philos. Mag.* **1975**, *31*, 1391-1401.

4. Handzlik, J. *J. Phys. Chem. C* **2007**, *111*, 9337-9348.

5. Zhong, L.; Lee, M. Y.; Liu, Z.; Wanglee, Y. J.; Liu, B.; Scott, S. L. Spectroscopic and structural characterization of Cr(II)/SiO$_2$ active site precursors in model Phillips polymerization catalysts. *J. Catal.* **2012**, *293*, 1-12.

6. Mortensen, J. J.; Parrinello, M. *J. Phys. Chem. B* **2000**, *104*, 2901-2907.

7. Solans-Monfort, X.; Filhol, J. S.; Copéret, C.; Eisenstein, O. *New J. Chem.* **2006**, *30*, 842-850.

8. Mian, S. A.; Saha, L. C.; Jang, J.; Wang, L.; Gao, X.; Nagase, S. *J. Phys. Chem. C* **2010**, *114*, 20793-20800.

9. Handzlik, J. *Chem. Phys. Lett.* **2009**, *469*, 140-144.

10. Handzlik, J.; Kurleto, K. *Chem. Phys. Lett.* **2013**, *561-562*, 87-91.

11. Delley, M. F.; Nunez-Zarur, F.; Conley, M. P.; Comas-Vives, A.; Siddiqi, G.; Norsic, S.; Monteil, V.; Safonova, O. V.; Coperet, C. Proton transfers are key elementary steps in ethylene polymerization on isolated chromium(III) silicates. *PNAS* **2014**, *111*, 11624-11629.

12. Espelid, O.; Borve, K. J. *J. Catal.* **2000**, *195*, 125-139.

13. Espelid, O.; Borve, K. J. Molecular-Level Insight into Cr/Silica Phillips-Type Catalysts: Polymerization-Active Mononuclear Chromium Sites. *J. Catal.* **2002***, 205*, 366-374.

14. Espelid, O.; Borve, K. J. *J. Catal.* **2002***, 206*, 331-338.

15. Zhong, L.; Liu, Z.; Cheng, R.; Tang, S.; Qiu, P.; He, X.; Terano, M.; Liu, B. *ChemCatChem* **2012***, 4*, 872-881.

16. Conley, M. P.; Delley, M. F.; Núñez-Zarur, F.; Comas-Vives, A.; Copéret, C. *Inorg. Chem.* **2015***, 54*, 5065-5078.

17. Fong, A.; Yuan, Y.; Ivry, S. L.; Scott, S. L.; Peters, B. Computational Kinetic Discrimination of Ethylene Polymerization Mechanisms for the Phillips (Cr/SiO_2) Catalyst. *ACS Catal.* **2015***, 5*, 3360-3374.

18. Adamo, C.; Barone, V. J. *J. Chem. Phys.* **1999***, 110*, 6158-6170.

19. Weigand, F.; Ahlrichs, R. *Phys. Chem. Chem. Phys.* **2005***, 7*, 3297-3305.

20. Gonzalez, C.; Schlegel, H. B. *J. Chem. Phys.* **1989***, 90*, 2154-2161.

21. Gonzalez, C.; Schlegel, H. B. *J. Phys. Chem.* **1990***, 94*, 5523-5527.

22. Grimme, S.; Antony, J.; Ehrlich, S.; Krieg, H. *J. Chem. Phys.* **2010***, 132*, 154104–1-154104-19.

23. Grimme, S.; Ehrlich, S.; Goerigk, L. *J. Comput. Chem.* **2011***, 32*, 1456-1465.

24. Frisch, M. J.; Trucks, G. W.; Schlegel, H. B.; Scuseria, G. E.; Robb, M. A.; Cheeseman, J. R.; Scalmani, G.; Barone, V.; Mennucci, B.; Petersson, G. A.; Nakatsuji, H.; Caricato, M.; Li, X.; Hratchian, H. P.; Izmaylov, A. F.; Bloino, J.; Zheng, G.; Sonnenberg, J. L.; Hada, M.; Ehara, M.; Toyota, K.; Fukuda, R.; Hasegawa, J.; Ishida, M.; Nakajima, T.; Honda, Y.; Kitao, O.; Nakai, H.; Vreven, T.; Montgomery Jr, J. A.;

Peralta, J. E.; Ogliaro, F.; Bearpark, M.; Heyd, J. J.; Brothers, E.; Kudin, K. N.; Staroverov, V. N.; Kobayashi, R.; Normand, J.; Raghavachari, K.; Rendell, A.; Burant, J. C.; Iyengar, S. S.; Tomasi, J.; Cossi, M.; Rega, N.; Millam, J. M.; Klene, M.; Knox, J. E.; Cross, J. B.; Bakken, V.; Adamo, C.; Jaramillo, J.; Gomperts, R.; Stratmann, R. E.; Yazyev, O.; Austin, A. J.; Cammi, R.; Pomelli, C.; Ochterski, J. W.; Martin, R. L.; Morokuma, K.; Zakrzewski, V. G.; Voth, G. A.; Salvador, P.; Dannenberg, J. J.; Dapprich, S.; Daniels, A. D.; Farkas, O.; Foresman, J. B.; Ortiz, J. V.; Cioslowski, J.; Fox, D. J. Gaussian 09. **2013**.

25. Dennington, R.; Keith, T.; Millam, J. M. GaussView. **2009**, *Version 5*.

Chapter 3 | *Operando* **Molecular Spectroscopy During Ethylene Polymerization**

    by Supported CrO$_x$/SiO$_2$ Catalysts: Active Sites, Surface Intermediates, and

    Structure-Activity Relationships

Abstract

Time-resolved *operando* molecular spectroscopy was applied during ethylene polymerization by supported CrO$_x$/SiO$_2$ catalysts to investigate the structure-activity relationships for this important industrial catalytic reaction. A combination of spectroscopic techniques (Raman, UV-vis, XAS, DRIFTS, and TPSR) during ethylene polymerization allows for the first time to monitor the molecular events taking place during activation of supported CrO$_x$/SiO$_2$ catalysts by ethylene and establishment of the structure-activity relationships for this reaction. Based on complementary DFT computational studies, a new initiation mechanism for ethylene polymerization is proposed. During reaction, the initial surface Cr^{+6}O$_x$ sites reduce to Cr^{+3} sites to form Cr-(CH$_2$)$_2$CH=CH$_2$ and Cr-CH=CH$_2$ reaction intermediates with the latter representing the catalytic active site.

3.1   Introduction

Ethylene polymerization by silica-supported CrO$_x$ catalysts is now responsible for ~40 to 50% of all high-density polyethylene produced[1]. Despite the extensive research studies that have been performed about the supported CrO$_x$/SiO$_2$ catalyst system over the past six decades, many of the same fundamental structural and mechanistic questions are still being debated.[1-4] There has been extensive debate on studies about the initial chromia structures in the initial dehydrated catalyst, particularly due to interpretations of UV-vis results.

The aim of the present study is to elucidate the roles of the initial surface chromia sites on silica for the ethylene polymerization reaction through application of *in situ* and

operando molecular spectroscopy before and during the initial stages of ethylene polymerization by supported CrO_x/SiO_2 catalysts. Using a combination of spectroscopic techniques (Raman, UV-vis, XAS, DRIFTS, and TPSR) during ethylene polymerization allows for the first time to monitor the molecular events taking place during activation of supported CrO_x/SiO_2 catalysts by ethylene and establishment of the structure-activity relationships for this reaction. Based on complementary DFT computational studies, a new initiation mechanism for ethylene polymerization is proposed.[5]

3.2 Results

3.2.1 *In situ* XANES/EXAFS of the Oxidized Supported CrO_x/SiO_2 Catalyst

The normalized *in situ* XANES of the reference compounds CrO_3 (consisting of poorly ordered polymeric $Cr^{+6}O_4$ units due to its low temperature synthesis), Cr_2O_3 (containing linked $Cr^{+3}O_6$ units in the bulk lattice), and dehydrated supported 3% CrO_x/SiO_2 catalyst are presented in Figure 3.1. The XANES spectrum for Cr_2O_3 does not give rise to a pre-edge feature because this transition is not allowed for structures with inverse symmetry such as CrO_6. In contrast, the XANES spectrum of CrO_3 exhibits a strong pre-edge feature (~5994 eV) because it is composed of $Cr^{+6}O_4$ site that do not possess inverse symmetry.[6,7] The similar leading edge energy from ~6000 to 6010 eV for the supported 3% CrO_x/SiO_2 catalyst and CrO_3, Cr^{+6} reference, indicates that the surface CrO_x sites are present as Cr^{+6}. The strong pre-edge feature at ~5994 eV in the XANES spectrum of the dehydrated 3% CrO_x/SiO_2 catalyst shows that CrO_4 coordinated sites are dominant in this catalyst. The slightly stronger XANES pre-edge for the supported 3% CrO_x/SiO_2 catalyst than CrO_3 reflects the greater symmetry of the $Cr^{+6}O_4$ sites in the catalyst. The corresponding *in situ* k^2-weighted, phase-uncorrected Fourier Transform (FT) EXAFS provides information

about the radial distribution of the atoms surrounding Cr and is presented in Figure S 3.1. The phase-uncorrected EXAFS of the dehydrated catalyst shows a strong peak at ~1.2 Å from Cr=O and a weak peak at ~1.8 Å from longer Cr-O. The absence of a peak at ~3 Å for Cr-Cr [6,7] is consistent with the presence of isolated chromia sites on the silica support.[5]
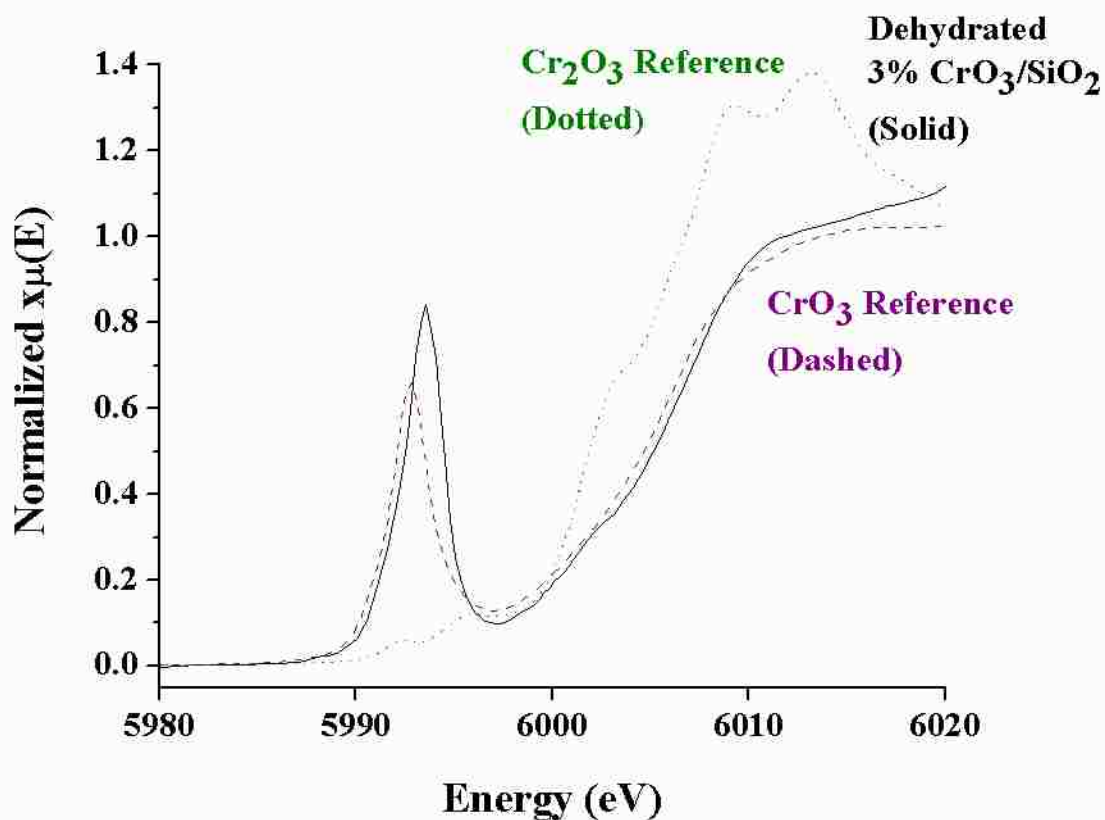
Figure 3.1. *In situ* normalized XANES of the dehydrated supported 3% CrO_x/SiO_2 catalyst. The XANES spectrum of the dehydrated catalyst was taken at 100 °C in flowing He (solid black), and the reference compounds CrO_3 (Cr^{+6}) (dashed purple) and Cr_2O_3 (Cr^{+3}) (dotted green) were collected under ambient conditions.[5]

3.2.2 *In situ* Raman Spectroscopy of the Initial Oxidized Catalyst

The *in situ* dehydrated spectrum of the initial oxidized supported CrO_x/SiO_2 catalyst is shown in Figure 3.2. Strong symmetric and asymmetric stretching vibrations of the surface dioxo $\nu_s((O=)_2CrO_2)$ site are present at ~992 and ~1015 cm^{-1}, respectively.[8-11] The band at ~1015 cm^{-1} has been previously assigned to the $\nu_s(O=CrO_4)$ of an isolated mono-oxo site in a distorted square pyramidal coordination[8,9]. More recent results have shown that the "mono-oxo" site is most likely a combination of laser-induced reduction and the weak asymmetric stretching mode of the isolated dioxo site. The strong 442 nm laser is known to burn and cause laser-induced reduction of the catalytic surface sites[5], even with the employment of a laser filter to only use a small percentage of the laser power. In the recent results (see Figure S 3.2), a moving stage was used to constantly move the sample during spectrum acquisition, thereby avoiding the laser staying focused on one spot. Even so, and in oxidizing conditions, the band at ~1015 cm^{-1} grew over time. These results demonstrate that the band at ~1015 cm^{-1} is an experimental artifact that primarily appears due to laser-induced reduction, although there is a small contribution from the $\nu_{as}((O=)_2CrO_2)$.

The corresponding bending mode $\delta(O=Cr=O)$ appears at ~398 cm^{-1}.[8,11] The absence of Raman bands in the ~200-300 cm^{-1} region demonstrates that bridging Cr-O-Cr bonds are not present, and indicates that the surface CrO_x sites are isolated on the silica support.[8] The *in situ* Raman spectrum also indicates the lack of crystalline Cr_2O_3 NPs present in the initial oxidized catalyst since there is no band observed at ~550 cm^{-1}.[5,8]
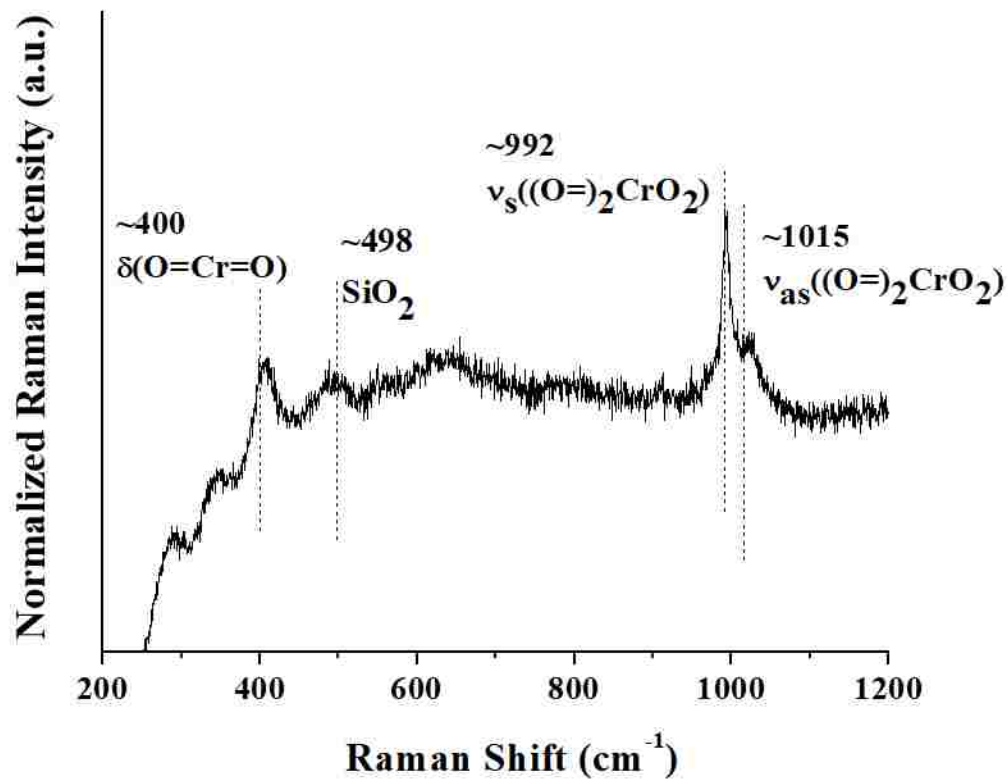
Figure 3.2. *In situ* Raman spectrum of the initial oxidized supported 3% CrO$_x$/SiO$_2$ catalyst taken in flowing 5% O$_2$/He at 100 °C. The spectrum was taken with a 442 nm wavelength laser (20% laser power) and a moving stage.

3.2.3 *In situ* Raman Spectroscopy During Ethylene Polymerization

The time-resolved *in situ* Raman spectra of the supported CrO_x/SiO_2 catalyst during ethylene polymerization are reported in Figure 3.3. The spectrum of the dehydrated silica support was subtracted from each Raman spectrum to emphasize observation of the chromia sites. During ethylene polymerization, the intensity of the Raman band for the dioxo sites (~986 cm^{-1}) diminishes over time. This demonstrates that the dioxo surface chromia sites are either reducing by or interacting with the gas-phase ethylene.[5]
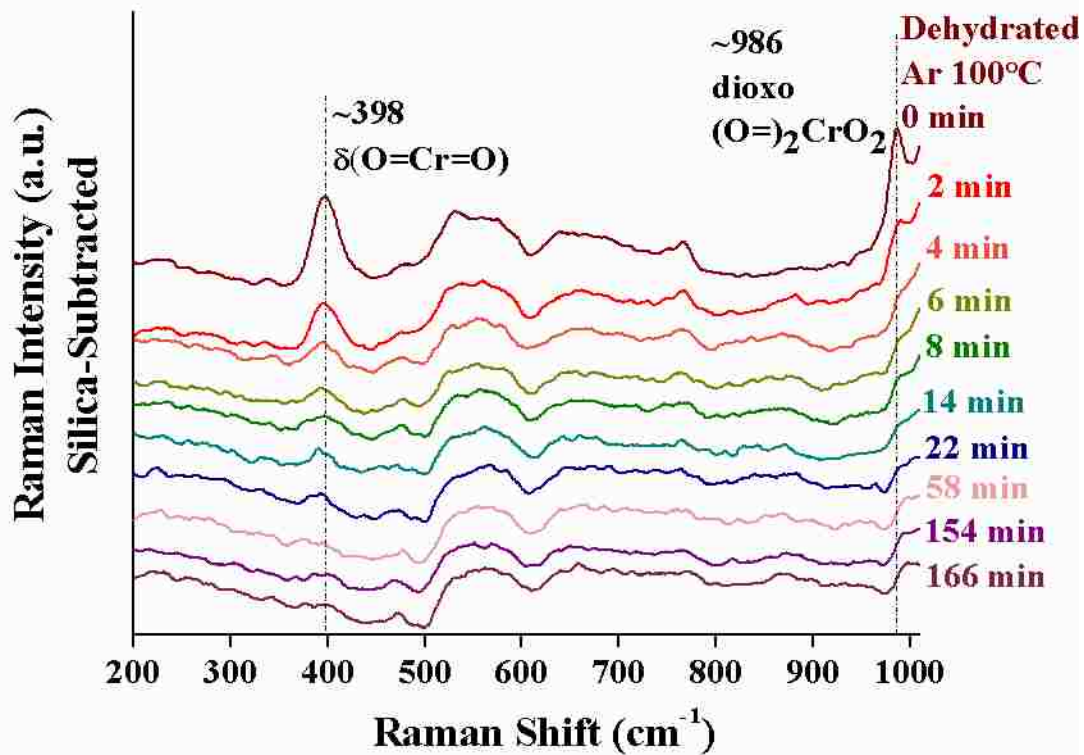
Figure 3.3. Time-resolved *in situ* Raman spectra of supported 3% CrO_x/SiO_2 catalyst taken in flowing 1% C_2H_4/Ar at T = 100 °C. Spectra were taken with a 442 nm wavelength laser.[5]

3.2.4 *In situ* UV-vis DRS During Ethylene Polymerization

The time-resolved *in situ* UV-vis spectra of the supported 3% CrO_x/SiO_2 catalyst are presented in Figure 3.4. Multiple ligand-to-metal charge transfer (LMCT) bands are present at ~250, ~340, and ~460 nm (see Figure 3.4 A) that are characteristic of surface $Cr^{+6}O_x$ sites on silica[12]. The surface CrO_x E_g value is ~2.4 eV, corresponding to isolated surface chromia sites[8]. The intensity of the $Cr^{+6}O_x$ LMCT bands is minimally decreased under these reaction conditions suggesting minimal reduction (see Figure S 3.3). The difference curves in Figure 3.4 B were obtained by subtracting the UV-vis spectrum of the initial dehydrated catalyst from each UV-vis spectrum taken during ethylene polymerization and allowed for improved observation of the weak d–d transition bands at 425 and 587 nm that have been assigned to pseudo-octahedral $Cr^{+3}O_6$ sites[12]. A UV-vis d-d band from surface Cr^{+5} sites is not apparent, but a small amount may be also present under the broad d–d band from the surface Cr^{+3} site at 587 nm.[5]
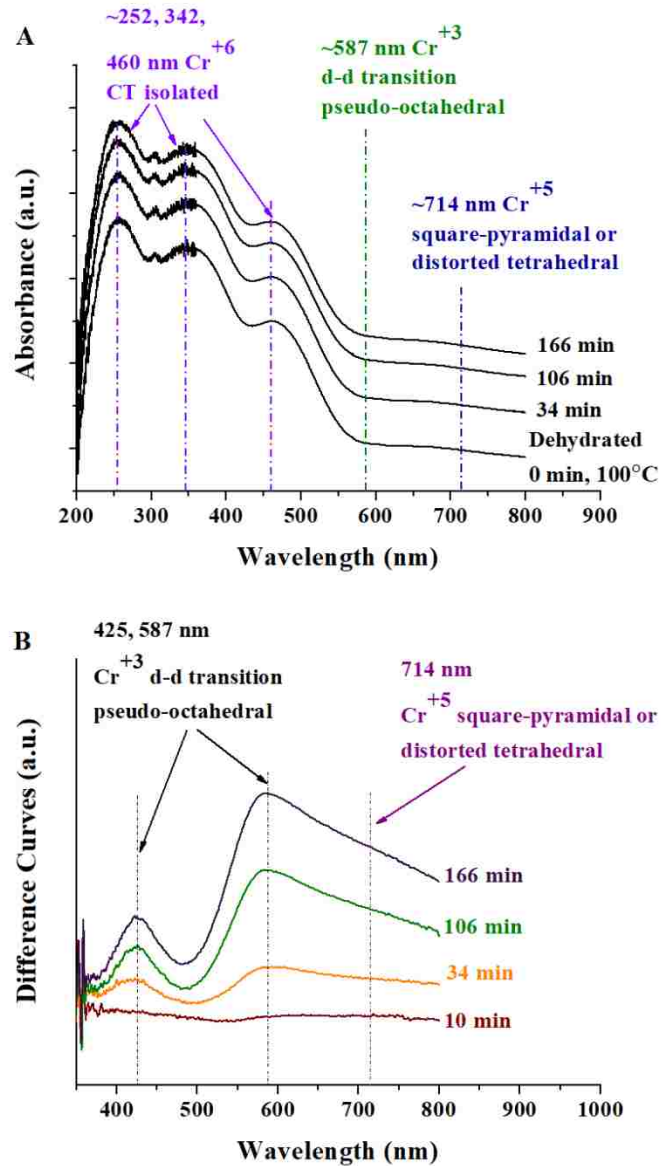
Figure 3.4. Time-resolved *in situ* UV-vis spectra of the supported 3% CrO$_x$/SiO$_2$ catalyst in flowing 1% C$_2$H$_4$/Ar at 100 °C highlighting the LMCT region (A) and magnified to show the d-d transition bands (B).[5]

3.2.5 C₂H₄-TPSR

C$_2$H$_4$-TPSR spectroscopy was performed to determine the reduced states formed from the initial surface dioxo CrO$_x$ sites as shown in Figure 3.5. The formation of CO$_2$ during C$_2$H$_4$-TPSR demonstrates that ethylene is reducing the initial surface Cr^{+6} sites to lower chromia oxidation states via the removal of oxygen. CO$_2$ was the only oxidation product detected, and H$_2$O was not detected since the line from the reactor to the MS was not heated and caused condensation. The two CO$_2$ peaks at ~280 °C and ~410 °C represent the two-step reduction of the chromia sites of Cr^{+6} → Cr^{+4} and Cr^{+4} → Cr^{+3}, respectively. The ratio of CO$_2$(280 °C)/CO$_2$(410 °C) is approximately 1.7 and indicates that ~63% of the sites are in a Cr^{+4} oxidation state while ~37 % of the reduced sites are in a Cr^{+3} oxidation state. This demonstrates that not all the surface chromia sites reduce to the same oxidation state. The CO$_2$/C$_2$H$_4$-TPSR spectrum also allows for calculation of the ethylene reduction kinetics of the two surface chromia sites. Application of the Redhead equation[13] yields the first-order kinetic constants of k$_{6/4}$ = 92 s^{-1} and k$_{4/3}$ = 0.48 s^{-1} for the activation of the dioxo and mono-oxo sites, respectively. The ratio of k$_{6/4}$/k$_{2/3}$ is ~400 indicating that the reduction by ethylene of the surface chromia sites from Cr^{+6} to Cr^{+4} is significantly easier than the reduction of the Cr^{+4} sites to Cr^{+3} sites.[5]
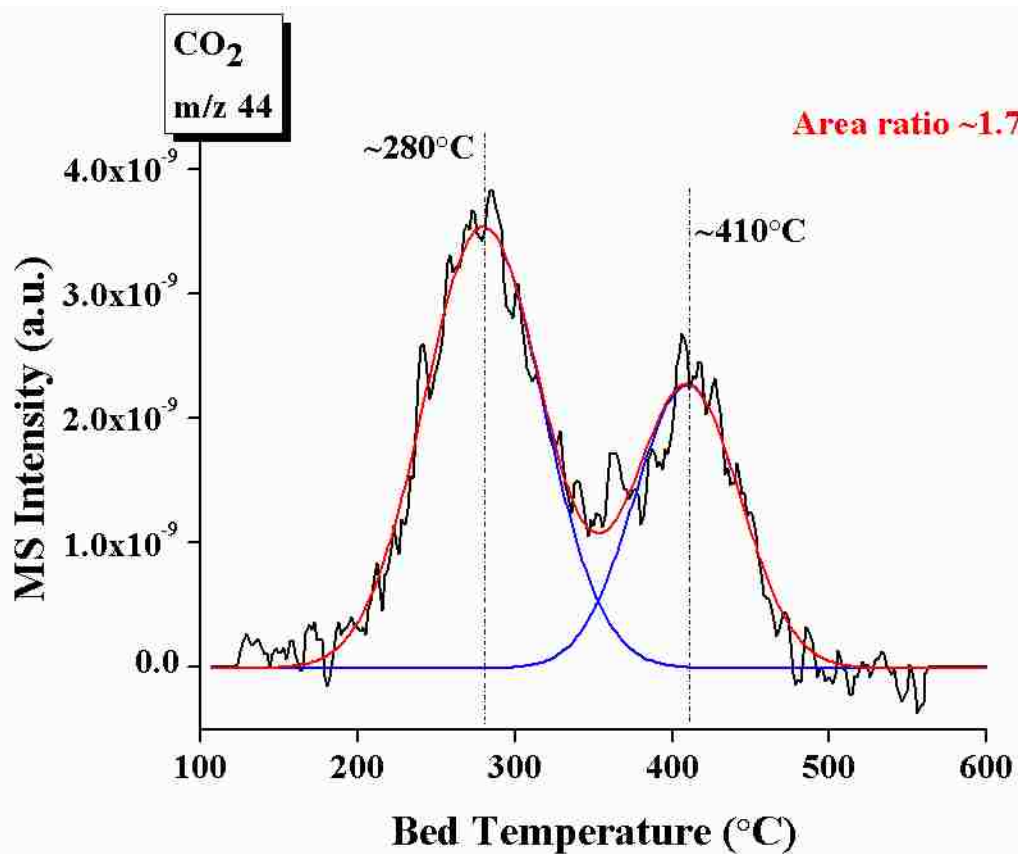
Figure 3.5. The CO_2/C_2H_4-TPSR spectrum of the supported 3% CrO_x/SiO_2. The temperature was ramped from 100 to 800 °C with a heating rate of 10 °C/min in flowing 1% C_2H_4/Ar.[5]

3.2.6 *In situ* and *Operando* DRIFTS During Ethylene Polymerization

The time-resolved *in situ* IR spectra during ethylene polymerization are presented in Figure 3.6. The IR difference spectra were obtained by subtracting the IR spectrum of the initial dehydrated catalyst from each IR spectrum taken during ethylene polymerization, after normalizing against the SiO_2 vibration at 1350 cm^{-1}. The entire range (650-4000 cm^{-1}) is presented in Figure 3.6 A, and the zoomed region (2700-3200 cm^{-1}) is given in Figure 3.6 B. Positive IR bands represent bands being formed while negative IR bands represent bands being consumed. Gas phase ethylene gives rise to bands at ~950, ~1450, ~1900, and 2950–3200 cm^{-1} in Figure 3.6[14]. The band at 3745 cm^{-1} for isolated silanols[15-19] decreases with reaction time, and the bands at 3700 and 3400 cm^{-1} increase with reaction time because the isolated silanols interact with the PE chain[18,20]. In the bending region, the increasing IR bands at ~805 and 985 cm^{-1} are assigned to $\delta(=CH_2)$ modes of PE[20,21]. The band at 1574 cm^{-1} also increases with reaction time and is assigned to $\nu_{as}(C=C)$ of the PE chain[20,21]. The 906 cm^{-1} band from bridging Cr-O-Si decreases in intensity with time reflecting the interaction of the surface intermediates and PE with this bond.[5]

The area in Figure 3.6 labeled as ''Zoomed Region'' is replotted in Figure 3.6 B to allow better observation of the relevant IR bands. This region contains significant IR bands that increase with reaction time and are assigned to the surface intermediates, PE product, and gas phase ethylene vibrations (2950-3200 cm^{-1})[14]. The band at 2898 cm^{-1} is assigned to the ν_s(-CH2-CH2) vibration of the bulk PE chain since it is expected to vibrate in the 2850-3000 cm^{-1} range, and the band at 2865 cm^{-1} is assigned to ν_s(Cr-CH2-) of the PE forming close to the Cr site; it would be expected to vibrate with lower energy than the bulk PE since it is closer to the Cr center [20,21]. The bulk PE bands in the literature are seen

at ~2850 cm-1 for ν_s(-CH$_2$-CH$_2$) and ~2920 cm^{-1} for ν_{as}(-CH$_2$-CH$_2$). The ~Δ50 cm^{-1} red

shift previously reported could be related to the higher temperature used for the current

measurements (room temperature vs. 100 °C) that are more aligned with industrial reaction

conditions (85-150 °C)[1,3,4]. An Ar flush was performed at the end of the experiment to

detect any additional bands that may have been obscured by the gas-phase ethylene

reactant. After the Ar flush, two new IR bands are also present at 2973 cm^{-1} from the mas

(-CH$_2$-CH$_2$) of the bulk PE chain, which is ~70 cm^{-1} higher than the ν_s(-CH$_2$-CH$_2$) of the

bulk PE, a typical difference in wavenumber between asymmetric and symmetric

vibrations, and a second band at 2960 cm^{-1} that is assigned to the ν(C-H) of the vinyl

reaction intermediate Cr^{+3}-CH=CH$_2$[20,21]. In general, the C-H stretch vibrations for a vinyl

group fall in the range of 2980-3110 cm^{-1}, and specifically for σ-bonded olefinic metal

compounds, the CH$_2$ and CH stretches fall in the 2900-3100 cm^{-1} range. In the case of a

vinyl active reaction intermediate bonded to the Cr metal center, this vibration would shift

to lower wavenumbers because of the bond to the metal center and the reduced symmetry

of the coordinated ethylene molecule.[5]
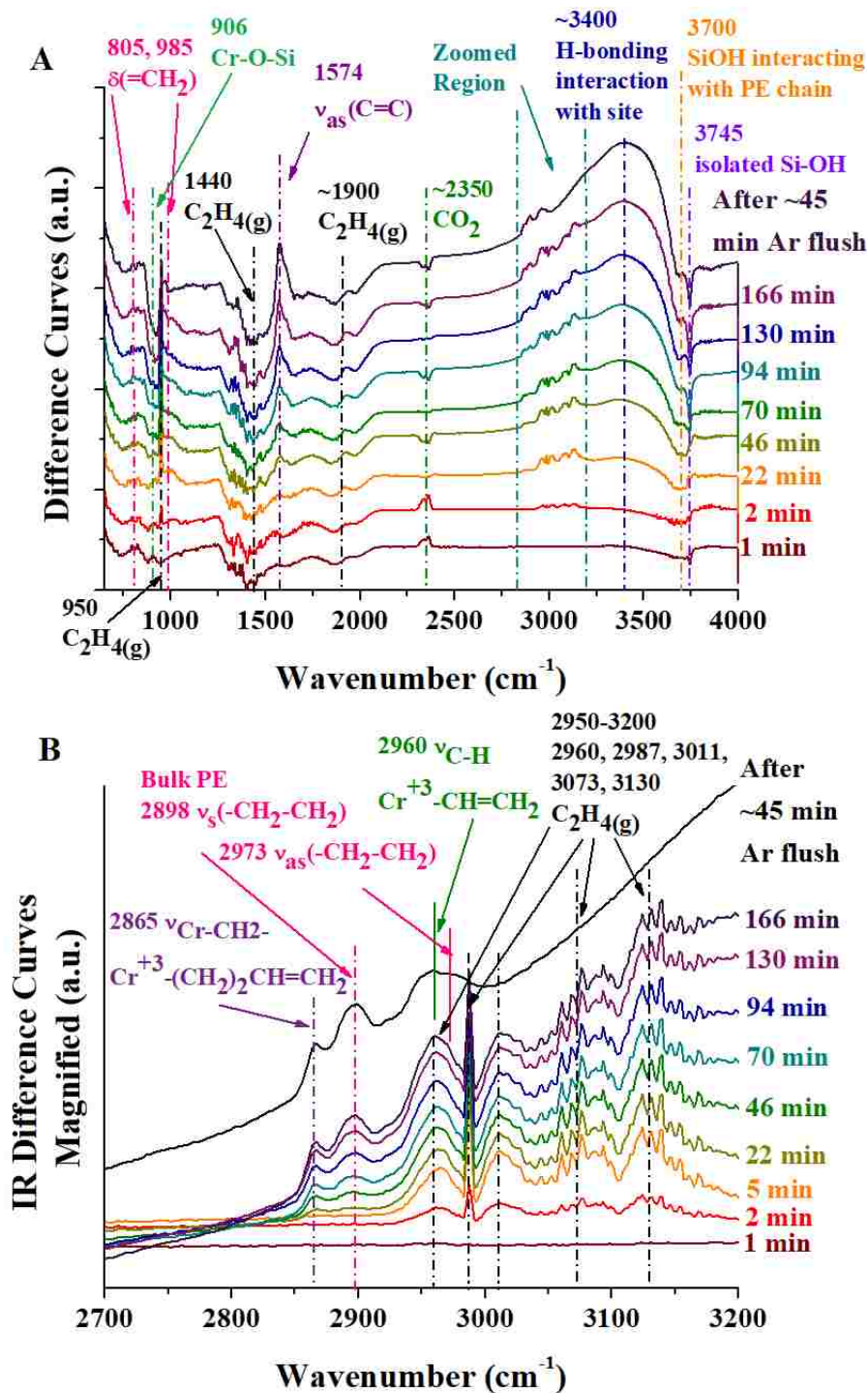
Figure 3.6. *In situ* DRIFT spectra of supported 3% CrO_x/SiO_2 in flowing 1% C_2H_4/Ar at 100 °C as a function of time with an Ar flush after 3 h. (A) Difference curves of the entire spectrum (650-4000 cm^{-1}) and (B) Difference curves magnified to show the growing surface species and polyethylene product (2700-3200 cm^{-1}).[5]

3.2.7 Kinetics of Formation of PE Product and Surface Cr^{+3} Sites

The evolution of the IR bands for formation of PE product, surface Cr^{+3}-$(CH_2)_2CH=CH_2$, and surface Cr^{+3}-$CH=CH_2$ sites during the ethylene polymerization reaction is plotted as a function of reaction time in Figure 3.7. The initial positive slope for IR band of the formation of the surface Cr^{+3}-$(CH_2)_2CH=CH_2$ reveals that this is one of the initial reaction intermediates during ethylene polymerization by surface CrO_x on silica. At slightly longer times, the IR band for the surface Cr^{+3}-$(CH_2)_2CH=CH_2$ reaction intermediates appears to saturate. The formation of the PE product, however, initially exhibits a slope of zero indicating that it is a secondary product during ethylene polymerization by supported CrO_x/SiO_2 and is formed by reaction of ethylene with surface reaction intermediates. At longer reaction times (>20 min), the slope for PE formation linearly increases and is greater than the decreasing slope for formation of the surface Cr^{+3}-$(CH_2)_2CH=CH_2$ reaction intermediates. The continued modest increase in the IR band area for the surface Cr^{+3}-$(CH_2)_2CH=CH_2$ intermediates even at ~180 min suggests that not all the surface chromia sites have been activated at this time under these experimental conditions. The IR band area for the surface Cr^{+3}-$CH=CH_2$ intermediate at 2960 cm^{-1} could not be directly monitored because of overlap with the IR bands of gas phase ethylene. The gas phase contribution of ethylene, however, could be determined by subtracting the IR spectrum collected after ~178 min in flowing Ar with the spectrum collected at ~178 min in flowing ethylene. This difference was then subtracted from the time-resolved spectra at ~2960 cm^{-1}. The resulting plot for the intensity of surface Cr^{+3}-$CH=CH_2$ intermediates seems to track the evolution of the PE reaction product.[5]

The evolution of the UV-vis bands of the two distinct surface Cr^{+3} sites as a function of reaction time of ethylene polymerization by the supported CrO_x/SiO_2 catalyst is presented in Figure 3.8. Both UV-vis Cr^{+3} bands initially increase linearly with reaction time and their lines go through the origin suggesting that they are initial reaction intermediates during ethylene polymerization. At longer reaction times (>20 min), the slope of the band at ~587 nm remains constant while the slope of the band at ~425 nm band decreases and appears to approach saturation. Comparison of evolution of the UV-vis and IR bands suggests that the UV-vis bands at ~425 and ~587 nm follow the time dependent trends observed for the IR bands for the surface Cr^{+3}-$(CH_2)_2CH=CH_2$ and Cr^{+3}-$CH=CH_2$ reaction intermediates, respectively (see Figure 3.9). The non-zero slopes of both UV-vis Cr^{+3} bands at ~170 min indicates that not all the surface chromia sites have been activated at this initial stage of the ethylene polymerization reaction under the current reaction conditions.[5]
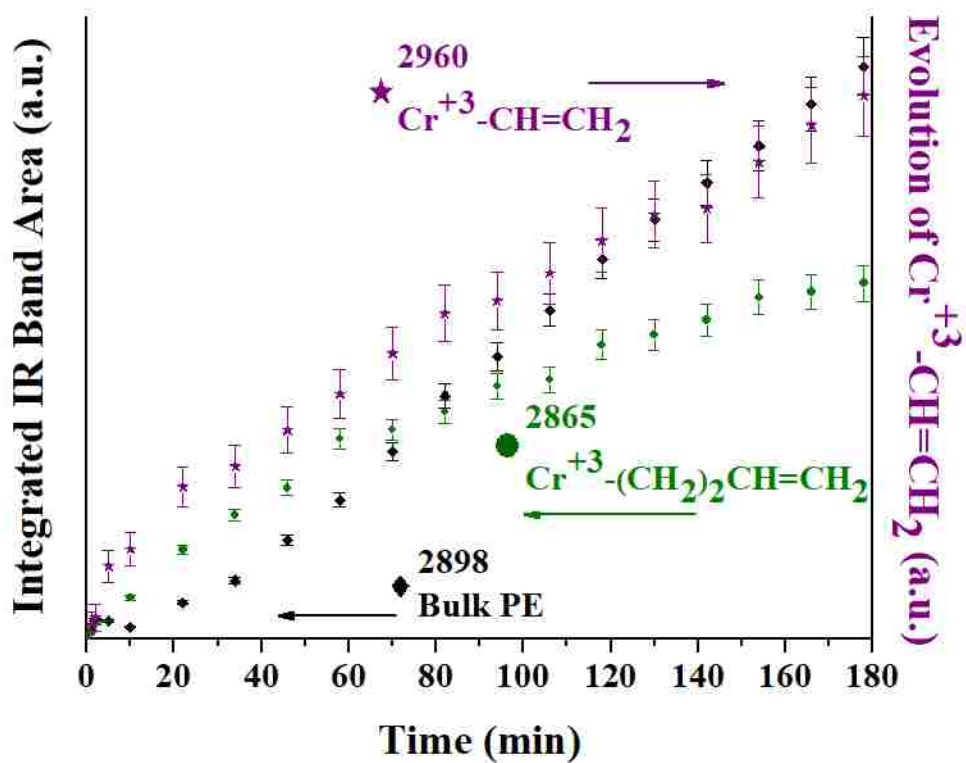
Figure 3.7. Evolution of DRIFTS bands from PE product, surface Cr^{+3}-CH=CH$_2$, and surface Cr^{+3}-(CH$_2$)$_2$CH=CH$_2$ as a function of reaction time.[5]
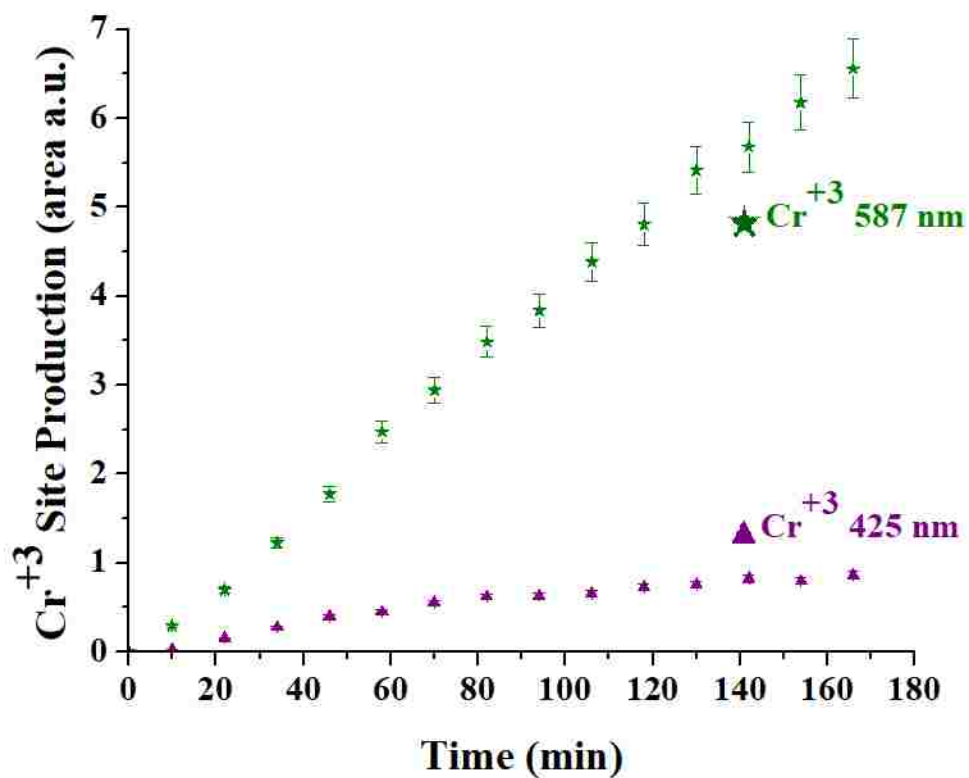
Figure 3.8. The production of UV-vis detectable surface Cr^{+3} sites as a function of ethylene polymerization reaction time by supported CrO_x/SiO_2 catalysts at 100 °C (1% C_2H_4/Ar).[5]
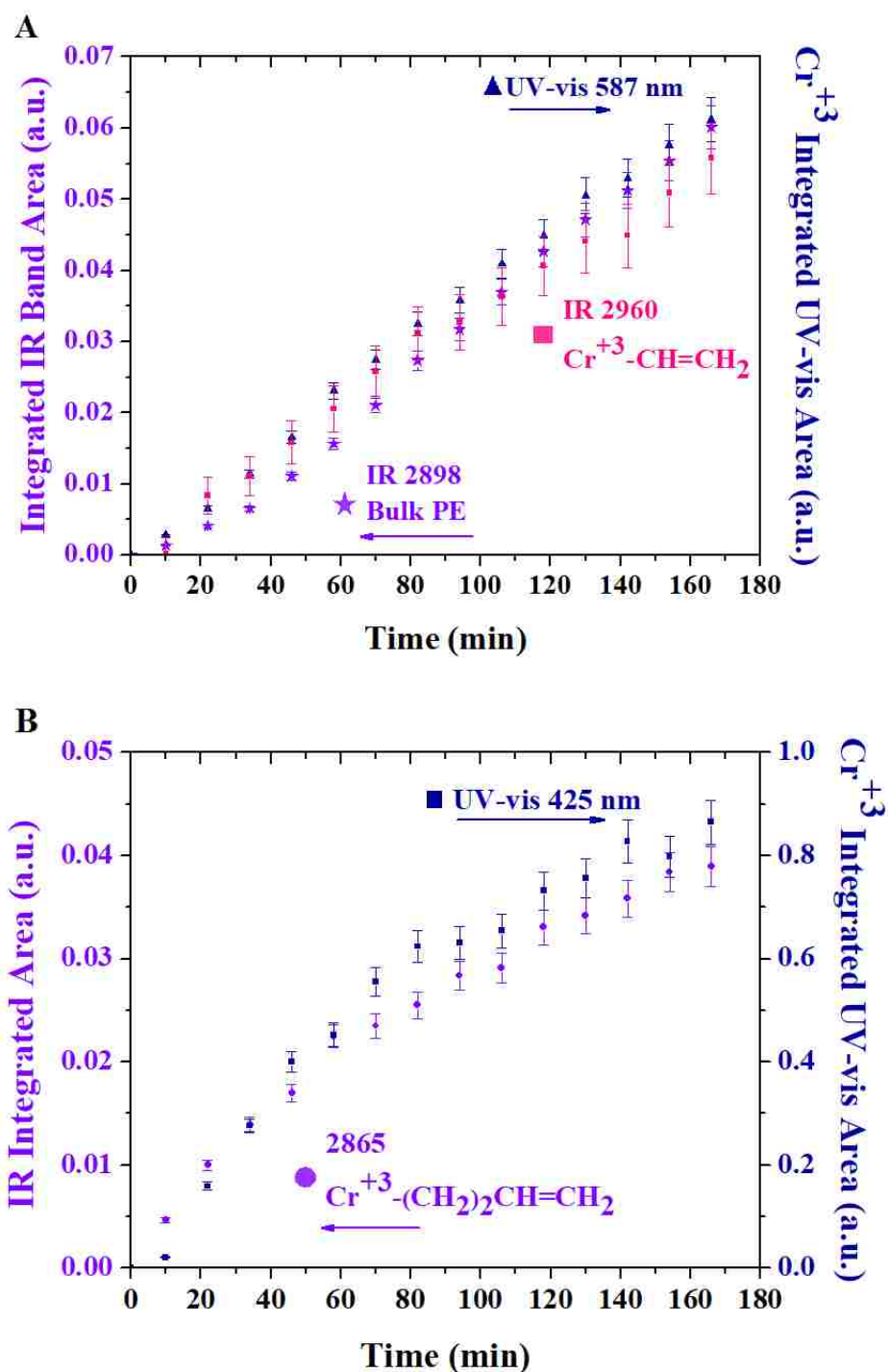
Figure 3.9. Comparison of the evolution of UV-vis and DRIFTS bands. (A) Cr^{+3} 587 nm band area with Cr^{+3}-$CH=CH_2$ 2960 cm^{-1} intensity and bulk PE 2898 cm^{-1} and (B) Cr^{+3} 425 nm area with 2865 cm^{-1} Cr^{+3}-$(CH_2)_2CH=CH_2$ area.[5]

3.2.8 Density Functional Theory (DFT)

Two proposed models of surface Cr^{+3} oxide sites are shown in Figure 3.10. Proposed models of isolated surface Cr^{+3} oxide sites: (A) ($\equiv SiO)_2Cr^{+3}$-OH and (B) ($\equiv SiO)_3Cr^{+3}$. The surface ($\equiv SiO)_3Cr^{+3}$ site (B) was recently postulated in the literature[22-24]; however, the existence of hydroxylated surface ($\equiv SiO)_2Cr^{+3}$-OH sites (A) cannot be excluded. We have calculated initiation mechanisms for ethylene polymerization, considering both potential surface Cr^{+3} sites on silica as the precursors of the active site complexes. The Gibbs energy profile at T = 73 K for the initiation mechanism for surface site A is presented in Figure 3.11. The coordination of an ethylene molecule to chromium, resulting in π-complex A1, is predicted to be an equilibrium process (ΔG and 0 kJ mol^{-1}), allowing both A and A1 structures to exist on the surface of the reduced catalyst in the presence of gaseous ethylene. After A1 formation, the subsequent hydrogen transfer from the p-coordinated ethylene to the hydroxyl group can take place. It directly leads to the vinyl Cr^{+3}-CH=CH$_2$ active site (A2), which is experimentally confirmed in this work. This elementary step is endergonic (61 kJ mol^{-1}) and proceeds with a rather high predicted activation barrier (ΔG = 135 kJ mol^{-1}), but recently calculated activation Gibbs energies for other initiation mechanisms of ethylene polymerization are comparable[22-24]. Desorption of the by-product water molecule is calculated to be a moderately endergonic process (46 kJ mol^{-1}) under water vapor pressure of 1 atm (Figure 3.11). Under more dehydrated conditions, expected during the catalytic process, the desorption step will be less endergonic, for instance 32 and 10 kJ mol^{-1} for water vapor pressures of 0.01 and 10^{-5} atm, respectively. Thus, the water molecule can easily desorb to leave a bare surface ($\equiv SiO)_2Cr^{+3}$-CH=CH2 site (A3) for ethylene adsorption during the propagation stage. The initiation mechanism for surface ($\equiv SiO)_3Cr^{+3}$

site (B) as the precursor of the active site (Figure 3.12) is different than that calculated for the surface site A. The coordination of ethylene leading to the π-complex B1 is predicted to be a slightly more exergonic process (-4 kJ mol^{-1}) than the A → A1 step (Figure 3.11), but it can still be regarded as an equilibrium step. The subsequent ethylene insertion into the Cr-O σ-bond, resulting in an oxachromacycle site B2, is endergonic (78 kJ mol^{-1}) and proceeds with an activation barrier of 111 kJ mol^{-1}. The Cr-O distance is only moderately increased during the formation of B2, from 1.77 to 2.06 Å, indicating that the threefold coordination of the chromium atom to the surface is still preserved. The coordination of another ethylene molecule to B2 is an endergonic step (47 kJ mol^{-1}), therefore the complex B3 is thermodynamically unstable. Instead of considering the insertion of ethylene into the oxachromacycle, like Peters *et al.*[24] did in the case of surface Cr^{+2} sites, we propose another activation mechanism, in which the active site having a vinyl substituent is formed (B4) by the subsequent hydrogen transfer from π-bounded ethylene to the oxachromacycle moiety. The formation of surface ethoxy group during this transformation effectively prevents proton transfer to the growing chain and the termination step is avoided. On the other hand, the overall predicted activation Gibbs energy for this initiation route is very high (198 kJ mol^{-1}) suggesting that such mechanism is rather unlikely.[5]
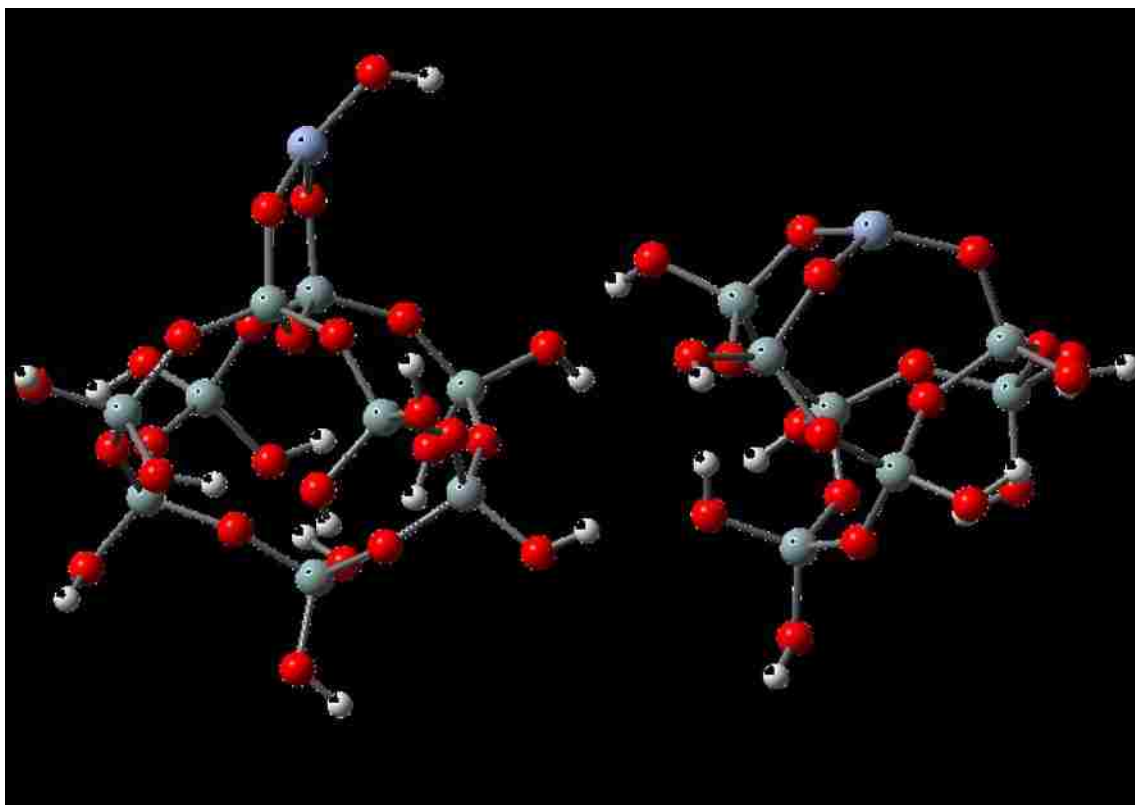
Figure 3.10. Proposed models of isolated surface Cr^{+3} oxide sites: A $(\equiv SiO)_2Cr^{+3}$-OH and B $(\equiv SiO)_3Cr$.[5]
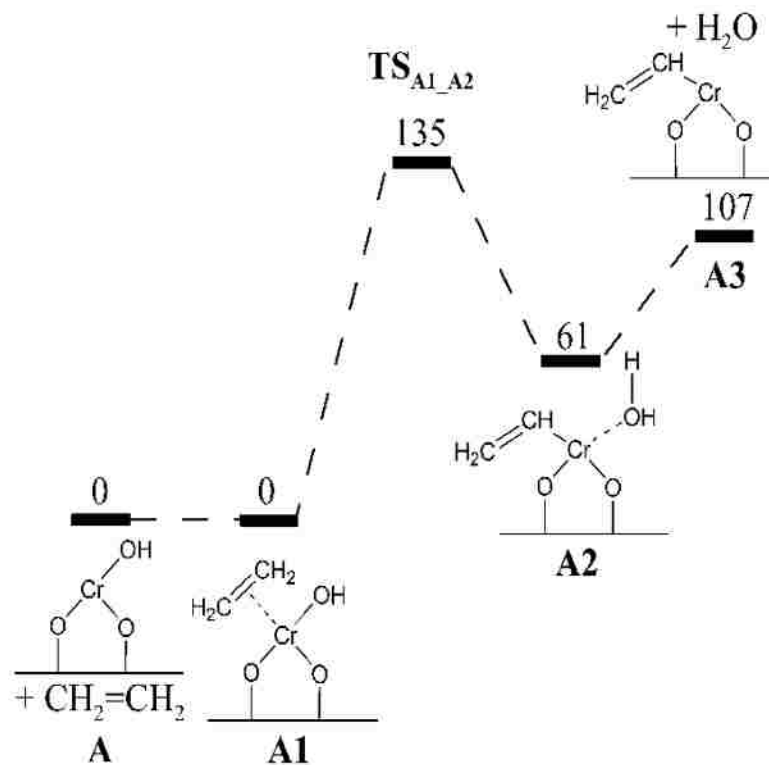
Figure 3.11. The Gibbs energy profile (kJ mol^{-1}) at T = 373 K for the initiation stage of ethylene polymerization over surface ($\equiv$SiO)$_2$Cr^{+3}-OH site (A).[5]
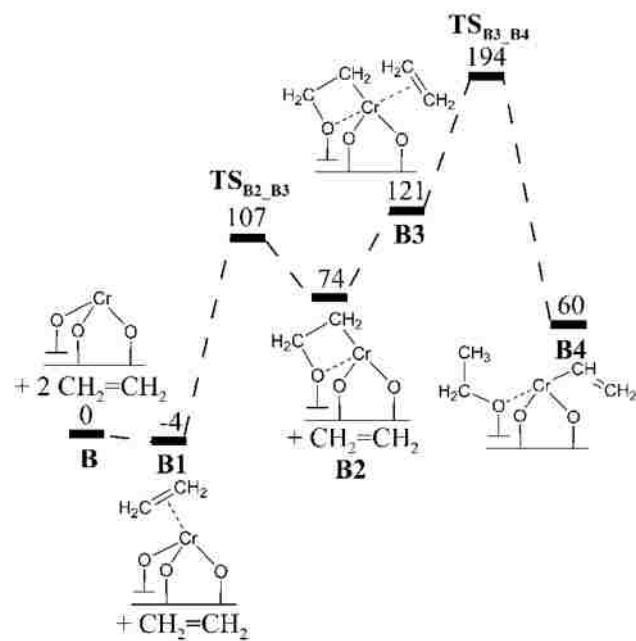
Figure 3.12. The Gibbs energy profile (kJ mol^{-1}) at T = 373 K for the initiation stage of ethylene polymerization over surface ($\equiv$SiO)$_3$Cr^{+3} site (B).[5]

3.3 Discussion

3.3.1 Initial Surface CrO_x Sites on SiO_2

The initial surface CrO_x sites on the SiO_2 support are fully oxidized as indicated by Cr^{+6} UV-vis bands at 252, 342, and 460 nm[12] and XANES leading edge energy (see Figure 3.1). The isolated nature of the initial surface $Cr^{+6}O_x$ sites is demonstrated by *in situ* Raman (absence of ~230 cm^{-1} band for bridging Cr-O-Cr bands)[8] and UV-vis (high E_g value of ~2.4 eV). There is no experimental evidence supporting the presence of dimeric surface Cr_2O_x sites. There is only one distinct isolated surface CrO_x site on silica in the initial oxidized catalyst: dioxo $\nu_s((O=)_2CrO_2)$ (Raman band at ~986 cm^{-1}). More recent results have shown that the "mono-oxo" site is most likely a combination of laser-induced reduction and the weak asymmetric stretching mode of the isolated dioxo site. The band at ~1015 cm^{-1} arises due to reduction by laser and is an experimental artifact. Most studies in the literature determined the presence of one distinct surface CrO_x sites for the initial oxidized supported CrO_x/SiO_2 catalyst.[2,18,24-32] The band at ~1015 cm^{-1} only appears when a 442 nm laser is used and has been previously assigned both to the $\nu_s(O=CrO_4)$ of an isolated mono-oxo site[8,9] and to the $\nu_{as}((O=)_2CrO_2)$ vibration for the isolated dioxo site[11]. DFT studies support both assignments[10]. The presence of dimeric Cr_2O_x sites on SiO_2 was first proposed by Hogan based on titration of silica surface hydroxyls[25]. The Cr/OH stoichiometry, however, was assumed to be 1:2 for isolated dioxo $(O=)_2Cr(-O-Si)_2$ sites and 1:1 for dimeric dioxo Si-O-Cr$(=O)_2$-O-$(O=)_2$Cr-O-Si sites. The titration calculations assume a molecular structure and anchoring stoichiometry without direct evidence of the actual molecular structures and anchoring sites. Thus, titration cannot provide proof of a dimeric surface Cr_2O_x site on silica.[5]

3.3.2 Catalyst Activation

The surface $Cr^{+6}O_x$ dioxo site is activated by reduction with ethylene in the present study. The *in situ* UV-vis spectroscopic measurements indicate that only a small number of surface $Cr^{+6}Ox$ sites become reduced (see Figure 3.4) while the *in situ* Raman spectra suggest extensive reduction of the surface $Cr^{+6}O_x$ sites (see Figure 3.3). The reason for this discrepancy is that the laser is heating the catalyst during the Raman analysis thereby inducing the reduction of the surface chromia sites by ethylene as well as the appearance of the ~1015 cm^{-1} artifact band. Consequently, the actual extent of reduction of the surface chromia sites is better reflected by the UV-vis spectra that do not stimulate the reduction of the surface chromia sites. Nevertheless, the Raman results, as well as the C_2H_4-TPSR spectra (see Figure 3.5), indicate that the dioxo surface CrO_4 sites reduce readily during ethylene polymerization. The extent of reduction under the present experimental conditions (1% C_2H_4/Ar and 100 °C) is minimal since the UV-vis Cr^{+6} band is barely reduced and indicates that the reaction conditions are representative of the initiation stage of the ethylene polymerization reaction. The reduction during ethylene polymerization at 100 °C yields two distinct pseudo-octahedral surface Cr^{+3} sites exhibiting UV-vis at bands at 425 and 587 nm (see Figure 3.4). The different time-resolved evolution trajectories of the two bands confirms that they arise from two independent Cr^{+3} sites (see Figure 3.8). These two reduced Cr^{+3} sites derive from the surface dioxo CrO_4 sites during ethylene polymerization. Supported CrO_x/SiO_2 catalysts activated with CO, and then exposed to ethylene exhibit UV-vis bands at 463 and 676 nm, which are different than those found in the present study with ethylene activation (425 and 587 nm). This suggests that the activated chromia sites may not be the same when initially activated with CO or C_2H_4[27]. Many studies in the

literature have used methods that are not molecular in nature (e.g., XANES, EXAFS, XPS, etc.); however, methods such as these only yield a signal that is an ensemble average of multiple sites if more than one site is present, and cannot provide molecular level information. Consequently, surface CrO_x molecular structures on silica derived from such ensemble averaging spectroscopic techniques are suspect since more than one surface chromia site is always present.[5]

Formaldehyde (HCHO) has been proposed to be the major oxygenated product during catalyst activation of supported CrO_x/SiO_2 catalysts with ethylene and thought to be responsible for the slow catalyst activation because it acts as a poison that bonds to the activated chromia sites and blocks ethylene coordination[1,3,33,34]. The current measurements, however, did not detect HCHO as an initial reaction product and only combustion of ethylene was initially observed. Hydrolysis of the bridging Cr-O-Si bonds has been proposed to be responsible for the agglomeration of surface chromia on silica to form crystalline Cr_2O_3 NPs during ethylene polymerization, but direct evidence was not provided[1,35,36]. The present *in situ* and *operando* spectroscopy measurements during ethylene polymerization demonstrate that the bridging Cr-O-Si bond is indeed perturbed by the reaction environment (see Figure 3.6), but this does not lead to formation of Cr_2O_3 NPs that would give a strong Raman band at ~550 cm^{-1} (see Figure 3.3).[5]

3.3.3   Surface Reaction Intermediates and Initiation Mechanism

Many initiation mechanisms have been proposed for ethylene polymerization by supported CrO_x/SiO_2 catalysts. Most of the studies did not even have IR bands for the proposed reaction intermediates, and this has led to much speculation and ambiguity in the literature. The current *operando* IR spectroscopy measurements reveal that both surface

Cr-(CH$_2$)$_2$CH=CH$_2$ and Cr-CH=CH$_2$ reaction intermediates are present during the initiation stage of the ethylene polymerization reaction (see Figure 3.7 and Figure 3.9) with the concentration of the former saturating, and the concentration of the latter linearly increasing with reaction time. The surface Cr-vinyl hydride (H-Cr-CH=CH$_2$) and Cr-carbene (Cr=CH$_2$) reaction intermediates[28] were proposed from *in vacuo* IR studies of a CO-reduced catalyst, but the IR bands for these intermediates were not observed, with only the bands for the PE product and adsorbed ethylene detected. The proposed initiation mechanism assumed that ethylene dissociation is the first step. It was proposed that surface Cr=CH$_2$ carbene is the most likely reaction intermediate since it was detected earlier with adsorption of propylene and 1-hexene. This study, however, does not provide any direct evidence for any reaction intermediates and was performed under vacuum. A surface Cr-alkylidene (Cr=CH-CH$_3$) reaction intermediate[30,31] has also been proposed from *in vacuo* IR studies of a CO-activated catalyst. In this case, a few bands were seen for the intermediate in addition to the bands for the PE product. An IR band at 3700 cm^{-1} was detected from the weak interaction of silica hydroxyl groups with polymer chains, and a second band was present at 2750 cm^{-1} that was assigned to methylene. Like the study proposing the Cr-vinyl hydride or Cr-carbene structures, this study was performed under vacuum. Furthermore, the IR band at 2750 cm^{-1} overlaps with many other possible structures and typically two bands are seen for a methyl group. The surface metallacycle reaction intermediate was previously proposed from in situ IR studies of a CO-reduced CrO$_x$/SiO$_2$[15-18,26]. When the temperature was increased from ~100 K to room temperature, bands for polyethylene were seen. Right before PE is detected, IR bands are observed at 2915 and 2893 cm^{-1}, and at short polymerization times, bands were present at 2931, 2861,

and 2965 cm^{-1}. These five ''anomalous'' IR bands are overshadowed by the growing polyethylene bands at increasing times, and disappear when the cell is evacuated. This reversible phenomenon led the authors to conclude it is more likely that the reaction intermediate is cyclic rather than containing a methyl group (the ethylene molecules would not need to transfer H making it more easily reversible)[15-18,26]. Two of the IR bands were also observed at 2865 and 2960 cm^{-1} in the present study during ethylene polymerization and after flushing with Ar, indicating that they are both from strongly bound surface reaction intermediates. In the present study, the band at 2865 cm^{-1} is assigned to the v_s(Cr-CH$_2$-) of the surface Cr^{+3}-(CH$_2$)$_2$CH=CH$_2$ or the PE forming close to the Cr metal center, while the band at 2960 cm^{-1} is assigned to the v(C–H) of the surface Cr^{+3}-CH=CH$_2$ vinyl reaction intermediate. An organo-Cr^{+3} reaction intermediate has also been proposed[27] based on previous EXAFS analysis and computational modeling[32]. *In vacuo* IR of CO adsorption on the CO-reduced catalyst showed the possibility of two Cr^{+2} structures. Using EXAFS analysis and computational modeling, it was also proposed that these two surface Cr^{+2} structures are likely three-coordinated with trigonal pyramidal coordination and four-coordinated with square pyramidal coordination, with the former more dominant and active than the latter. Given the EXAFS is an ensemble averaging spectroscopy, it is not possible to deconvolute and curve fit a system simultaneously containing two sites. In the study of the redox processes of ethylene polymerization, a general organo-Cr^{+3} site was proposed as the active site, but the primary focus was on the oxidation state. Based on the earlier study, it was concluded that the two structures are likely for the CO-reduced catalyst. Concerning the structure of the active site proposed, it was only said that it would be in a higher coordination since the UV-vis bands shifted to lower wavelengths. Although these

studies included discussion of the catalyst structure, only the structure of the CO-reduced Cr^{+2} catalyst was discussed at length, and it was remarked that this structure is affected by the bonding with CO. Of the different initiation mechanisms proposed in literature, the IR spectra presented in the current study provide direct evidence for a surface Cr^{+3}-CH=CH$_2$ vinyl reaction intermediate during ethylene polymerization by the supported CrO_x/SiO_2 catalyst. Additional insights about formation of the surface Cr-vinyl reaction intermediate come from the DFT calculations.[5]

3.3.4 DFT

In the recent proposals of mechanisms for ethylene polymerization, based on computational studies[22-24,37], there are two main obstacles. The first one is the high activation barrier for formation of the active sites. The second one is that the termination reaction can be more preferred then the propagation steps, so shorter oligomers of ethylene would be expected instead of the polyethylene product. Copéret *et al.*[22,23] and Peters *et al.*[24] recently studied initiation mechanisms, in which monoalkylchromium(+2) or (+3) sites are formed by the proton transfer from ethylene to the surface Si-O-Cr bridging oxygen, resulting in a surface Si(OH)Cr-vinyl site. They found that the initiation occurs with a high activation barrier, in contrast to the propagation reaction. The termination step, however, can compete with the propagation step or can even be more kinetically preferred because the proton transfer from Si(OH)Cr-alkyl site to the growing chain can occur more easily than the insertion of another ethylene molecule into the Cr-alkyl σ-bond[24,38]. Based on the presently proposed mechanism (Figure 3.11), the predicted overall Gibbs energy barrier for the initiation reaction (135 kJ mol^{-1}) is reasonable and it is in a similar range as the barriers calculated for the formation of surface Si(OH)Cr^{+2}-vinyl site[24] and

Si(OH)Cr^{+3}-vinyl site[22-24]. It should be noted, however, that different models and computational methodologies were used in those works. After slow initiation, according to the proposed mechanism (Figure 3.11), further chain growing reaction is expected to easily occur via the standard Cossee-type mechanism, i.e., insertion of ethylene into the Cr-Cr bond[24]. What is worth noting, the advantage of our new proposal of the initiation mechanism (Figure 3.11) is that the too fast termination reaction is no longer a drawback. After water desorption, there is no reactive hydrogen near the active Cr site, hence, the premature termination step will not take place and the formation of oligomers, instead of the polyethylene product, should not be facilitated.[5]

Gierada *et al.* later expanded on the preliminary results involving the initiation mechanism proposed in Figure 3.11 for a Cr^{+3}-OH/SiO$_2$, including propagation and termination mechanisms as well[39]. For this mechanism, a Cr^{+3}-CH=CH$_2$ vinyl site would be formed through hydrogen transfer from ethylene to the hydroxy ligand, forming a coordinated water molecule in the process. Once the water molecule is released, there is a vacancy, allowing coordination of other ethylene monomers. The water that desorbed can either hydrate another surface Cr^{+3} site to make Cr^{+3}-OH/SiO$_2$ site, which would increase the number of hydroxylated sites, so the initial water amount would be low. Otherwise, if the water vapor pressure is too high, the catalyst may deactivate due to the hydrolysis of Cr-O-Si bonds, which has been shown experimentally[40]. Assuming low water vapor pressure, the most likely propagation mechanism occurs via insertion of ethylene molecules into the Cr-C bond. The first insertion of an ethylene molecule into the Cr^{+3}-CH=CH$_2$ initiation site occurs with a low activation barrier of 34 kJ/mol, the product of which can coordinate another ethylene molecule with an activation barrier of 78 kJ/mol

and undergo further propagation to a Cr^{+3} hexenyl complex. Alternative to the propagation step, the termination reactions were proposed to occur through either β-H transfer from the ethylene monomer to the butenyl ligand (ΔG = 118 kJ/mol) or β-H elimination giving a Cr^{+3} hydride intermediate with a butadiene ligand (ΔG = 117 kJ/mol). Both termination pathways were less favorable compared to propagation.[39]

3.3.5 Structure-Activity Relationships

Prior to ethylene polymerization, the oxidized supported CrO_x/SiO_2 catalyst consists of one distinct isolated surface chromia site: dioxo CrO_4. The dioxo surface CrO_4 site is activated by ethylene by reducing to two surface Cr^{+3} sites: Cr-CH=CH$_2$ and Cr-$(CH_2)_2$CH=CH$_2$ reaction intermediates. The time-resolved evolution of the surface Cr^{+3}-CH=CH$_2$ reaction intermediate appears to track the formation of the PE product, which implicates it as the active reaction intermediate. The time-resolved evolution of the surface Cr^{+3}-$(CH_2)_2$CH=CH$_2$ reaction intermediate seems to saturate in the early stages of the ethylene polymerization reaction possibly implicating it as a spectator species.[5]

3.4 Conclusions

This is the first study to monitor the evolution of the supported CrO_x/SiO_2 catalyst during activation with ethylene and the ethylene polymerization reaction. The initial oxidized supported CrO_x/SiO_2 catalyst consists of one distinct and isolated surface chromia species in a Cr^{+6} oxidation state – the tetrahedrally-coordinated dioxo (O=)$_2$CrO$_2$ site. The reduction step of $Cr^{+6} \rightarrow Cr^{+4}$ is ~400 times easier than the reduction from $Cr^{+4} \rightarrow Cr^{+3}$. Two distinct surface Cr^{+3} reaction intermediates were detected upon activation: Cr^{+3}-$(CH_2)_2$CH=CH$_2$ (PE oligomers forming nearer to the metal center) and Cr^{+3}-CH=CH$_2$. The concentration of the surface Cr^{+3}-$(CH_2)_2$CH=CH$_2$ structure saturates in the early stages

of ethylene polymerization and may represent a spectator intermediate. The evolution of the surface Cr^{+3}-CH=CH$_2$ reaction intermediate tracks the formation of the PE product after the early induction period, which implicates it as the active reaction intermediate during ethylene polymerization by supported CrO_x/SiO_2 catalysts. The computational results indicate the possibility of formation of Cr^{+3} active sites on SiO_2 for ethylene polymerization and agree with the experimental findings presented in this work.[5]

Acknowledgements

Chapter 3 References

1. McDaniel, M. P. A Review of the Phillips Supported Chromium Catalyst and Its Commercial Use for Ethylene Polymerization. *Advances in Catalysis* 2010, *53*, 123-606.

2. Hogan, J. P. Catalysis of the Phillips Petroleum Company Polyethylene Process. In *Applied Industrial Catalysis*; Leach, B. E., Ed.; Academic Press, Inc.: New York, 1983; Vol. 1, pp 149-176.

3. Groppo, E.; Lamberti, C.; Bordiga, S.; Spoto, G.; Zecchina, Z. The Structure of Active Centers and the Ethylene Polymerization Mechanism on the Cr/SiO_2 Catalyst: A Frontier for the Characterization Methods. *Chem. Rev.* 2005, *105*, 115-183.

4. Hogan, J. P.; Banks, R. L. Polymers and Production Thereof. 2825721. March 4, 1958.

5. Chakrabarti, A.; Gierada, M.; Handzlik, J.; Wachs, I. E. Operando Molecular Spectroscopy During Ethylene Polymerization by Supported CrO_x/SiO_2 Catalysts: Active Sites, Reaction Intermediates, and Structure-Activity Relationship. *Top. Catal.* 2016, *59*, 725-739.

6. Weckhuysen, B. M.; Schoonheydt, R. A.; Jehng, J. M.; Wachs, I. E.; Cho, S. J.; Ryoo, R.; Kljlstra, S.; Poels, E. Combined DRS-RS-EXAFS-XANES-TPR Study of Supported Chromium Catalysts. *J. Chem. Soc. Far. Trans.* 1995, *91*, 3245-3253.

7. Groppo, E.; Prestipino, C.; Cesano, F.; Bonino, F.; Bordiga, S.; Lamberti, C.; Thune, P. C.; Niemantsverdriet, J. W.; Zecchina, A. In situ, Cr *K*-edge XAS study on the Phillips catalyst: activation and ethylene polymerization. *J. Catal.* 2005, *230*, 98-108.

8. Lee, E. L.; Wachs, I. E. In Situ Spectroscopic Investigation of the Molecular and Electronic Structures of SiO_2 Supported Surface Metal Oxides. *J. Phys. Chem. C* 2007, *111*, 14410-14425.

9. Lee, E. L.; Wachs, I. E. *J. Phys. Chem. C* 2008, *112*, 6487-6498.

10. Handzlik, J.; Grybos, R.; Tielens, F. Structure of Monomeric Chromium(VI) Oxide Species Supported on Silica: Periodic and Cluster DFT Studies. *J. Phys. Chem. C* 2013, *117*, 8138-8149.

11. Groppo, E.; Damin, A.; Bonino, F.; Zecchina, A.; Bordiga, S.; Lamberti, C. New Strategies in the Raman Study of the Cr/SiO_2 Phillips Catalyst: Observation of Molecular Adducts on Cr(II) Sites. *Chem. Mater.* 2005, *17*, 2019-2027.

12. Weckhuysen, B. M.; Wachs, I. E.; Schoonheydt, R. A. Surface Chemistry and Spectroscopy of Chromium in Inorganic Oxides. *Chem. Commun.* 1996, *96*, 3327-3349.

13. Redhead, P. A. Thermal Desorption of Gases. *Vacuum* 1962, *12*, 203-211.

14. National Institute of Standards and Technology NIST Chemistry WebBook. *http://webbook.nist.gov/chemistry/*.

15. Groppo, E.; Lamberti, C.; Bordiga, S.; Spoto, G.; Damin, A.; Zecchina, A. FTIR Investigation of the H_2, N_2, and C_2H_4 Molecular Complexes Formed on the Cr(II) Sites in the Phillips Catalyst: a Preliminary Step in the understanding of a Complex System. *J. Phys. Chem. B* 2005, *109*, 15024-15031.

16. Groppo, E.; Lamberti, C.; Bordiga, S.; Spoto, G.; Zecchina, A. In situ FTIR spectroscopy of key intermediates in the first stages of ethylene polymerizaton on the

Cr/SiO$_2$ Phillips catalyst: Solving the puzzle of the initiation mechanism? *J. Catal.* 2006*, 240*, 172-181.

17. Groppo, E.; Estephane, J.; Lamberti, C.; Spoto, G.; Zecchina, A. Ethylene, propylene and ethylene oxide in situ polymerization on the Cr(II)/SiO$_2$ system: A temperature- and pressure-dependent investigation. *Catal. Today* 2007*, 126*, 228-234.

18. Barzan, C.; Groppo, E.; Quadrelli, E. A.; Monteil, V.; Bordiga, S. Ethylene polymerization on a SiH$_4$-modified Phillips catalyst: detection of *in situ* produced a-olefins by operando FT-IR spectroscopy. *Phys. Chem. Chem. Phys.* 2012*, 14*, 2239-2245.

19. Vuurman, M.; Wachs, I. E.; Stufkens, D. J.; Oskam, A. Characterization of chromium oxide supported on Al$_2$O$_3$, ZrO$_2$, TiO$_2$, and SiO$_2$ under dehydrated conditions. *J. Mol. Catal.* 1993*, 80*, 209-227.

20. Davydov, A. *Molecular Spectroscopy of Oxide Catalyst Surfaces;* John Wiley & Sons Ltd.: West Sussex, England, 2003.

21. Socrates, G. *Infrared and Raman Characteristic Group Frequencies: Tables and Charts;* John Wiley & Sons Ltd: West Sussex, England, 2001.

22. Delley, M. F.; Nunez-Zarur, F.; Conley, M. P.; Comas-Vives, A.; Siddiqi, G.; Norsic, S.; Monteil, V.; Safonova, O. V.; Coperet, C. Proton transfers are key elementary steps in ethylene polymerization on isolated chromium(III) silicates. *PNAS* 2014*, 111*, 11624-11629.

23. Conley, M. P.; Delley, M. F.; Núñez-Zarur, F.; Comas-Vives, A.; Copéret, C. *Inorg. Chem.* 2015*, 54*, 5065-5078.

24. Fong, A.; Yuan, Y.; Ivry, S. L.; Scott, S. L.; Peters, B. Computational Kinetic Discrimination of Ethylene Polymerization Mechanisms for the Phillips (Cr/SiO$_2$) Catalyst. *ACS Catal.* 2015, *5*, 3360-3374.

25. Hogan, J. P. Ethylene Polymerization Catalysis over Chromium Oxide. *J. Polym. Sci. , Part A: Polym. Chem.* 1970, *8*, 2637-2652.

26. Bordiga, S.; Bertarione, S.; Damin, A.; Prestipino, C.; Spoto, G.; Lamberti, C.; Zecchina, A. On the first stages of the ethylene polymerization on Cr^{2+}/SiO$_2$ Phillips catalyst: time and temperature resolved IR studies. *J. Mol. Catal. A: Chem.* 2003, *204-205*, 527-534.

27. Brown, C.; Krzystek, J.; Achey, R.; Lita, A.; Fu, R.; Meulenberg, R. W.; Polinski, M.; Peek, N.; Wang, Y.; van de Burgt, L. J.; Profeta, J., S.; Stiegman, A. E.; Scott, S. L. Mechanism of Initiation in the Phillips Ethylene Polymerization Catalyst: Redox Processes Leading to the Active Site. *ACS Catal.* 2015, *5*, 5574-5583.

28. Zielinski, P.; Dalla Lana, I. G. An FTIR Spectroscopic View of the Initiation of Ethylene Polymerization on Cr/SiO$_2$ Catalyst. *J. Catal.* 1992, *137*, 368-376.

29. Kantcheva, M.; Dalla Lana, I. G.; Szymura, J. A. FTIR Spectroscopic Investigation of the Initiation of Ethylene Polymerization on Cr/Silica. *J. Catal.* 1995, *154*, 329-334.

30. Ghiotti, G.; Garrone, E.; Zecchina, A. IR Investigation of Polymerization Centres of the Phillips Catalyst. *J. Mol. Catal.* 1988, *46*, 61-77.

31. Ghiotti, G.; Garrone, E.; Coluccia, S.; Morterra, C.; Zecchina, A. Evidence for Alkylidenic Configuration of Polymethylene Chains on the Phillips Catalyst. *J. C. S. Chem. Comm.* 1979, 1032-1033.

32. Zhong, L.; Lee, M. Y.; Liu, Z.; Wanglee, Y. J.; Liu, B.; Scott, S. L. Spectroscopic and structural characterization of Cr(II)/SiO$_2$ active site precursors in model Phillips polymerization catalysts. *J. Catal.* 2012*, 293*, 1-12.

33. Baker, L. M.; Carrick, W. L. Oxidation of Olefins by Supported Chromium Oxide. *J. Org. Chem.* 1968*, 33*, 616-618.

34. Liu, B.; Nakatani, H.; Terano, M. New aspects of the induction period of ethene polymerization using Phillips CrOx/SiO$_2$ catalyst probed by XPS, TPD and EPMA. *J. Mol. Catal. A: Chem.* 2002*, 184*, 387-398.

35. McDaniel, M. P.; Collins, K. S.; Benham, E. A.; Cymbaluk, T. H. The activation of Phillips Cr/silica catalysts V. Stability of Cr(VI). *Appl. Catal. A: Gen.* 2008*, 335*, 252-261.

36. McDaniel, M. P.; Collins, K. S.; Benham, E. A.; Cymbaluk, T. H. The activation of Phillips Cr/silica catalysts VI. Influence of hold time. *Appl. Catal. A: Gen.* 2008*, 335*, 180-186.

37. Zhong, L.; Liu, Z.; Cheng, R.; Tang, S.; Qiu, P.; He, X.; Terano, M.; Liu, B. *ChemCatChem* 2012*, 4*, 872-881.

38. Peters, B.; Scott, S. L.; Fong, A.; Wang, Y.; Stiegman, A. E. *PNAS* 2015*, 112*, E4160-E4161.

39. Gierada, M.; Handzlik, J. Active sites formation and their transformations during ethylene polymerization by the Phillips CrO$_x$/SiO$_2$ catalyst. *J. Catal.* 2017*, 352*, 314-328.

40. Gierada, M.; Michorczyk, P.; Tielens, F.; Handzlik, J. Reduction of chromia-silica catalysts: A molecular picture. *J. Catal.* 2016*, 340*, 122-135.

Chapter 3 Supporting Information
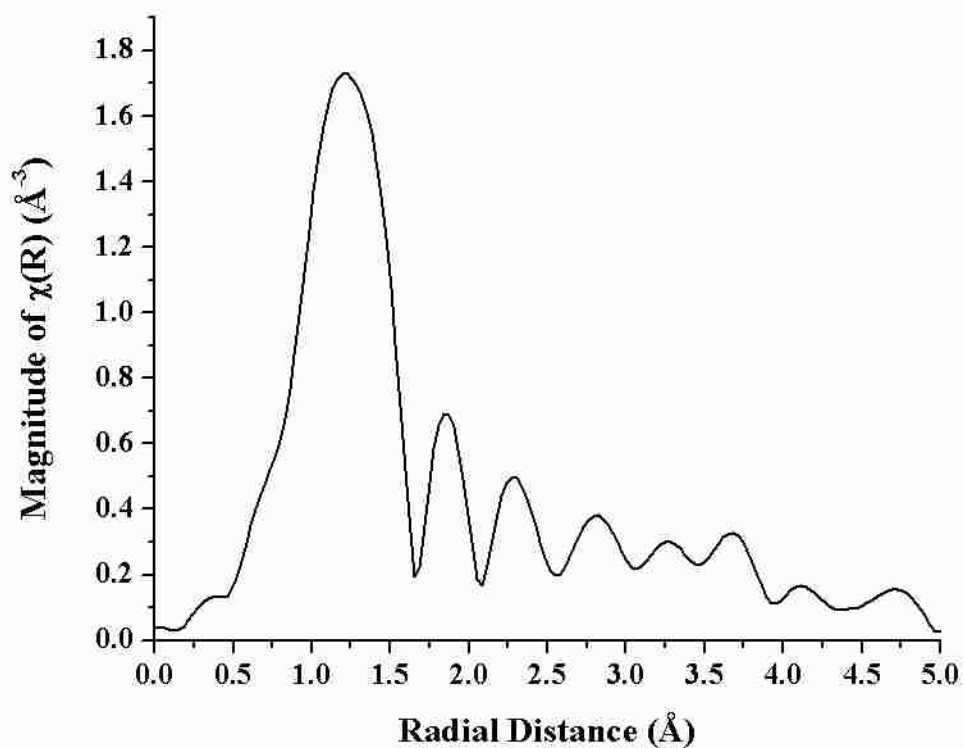
Figure S 3.1. *In situ* k^2-weighted, phase uncorrected Fourier Transform (FT) EXAFS spectrum of the dehydrated supported 3% CrO_x/SiO_2 catalyst taken at 100 °C in flowing He. The absence of a peak at ~3.1 Å for Cr-Cr distance is consistent with the presence of isolated chromia sites on the silica support.
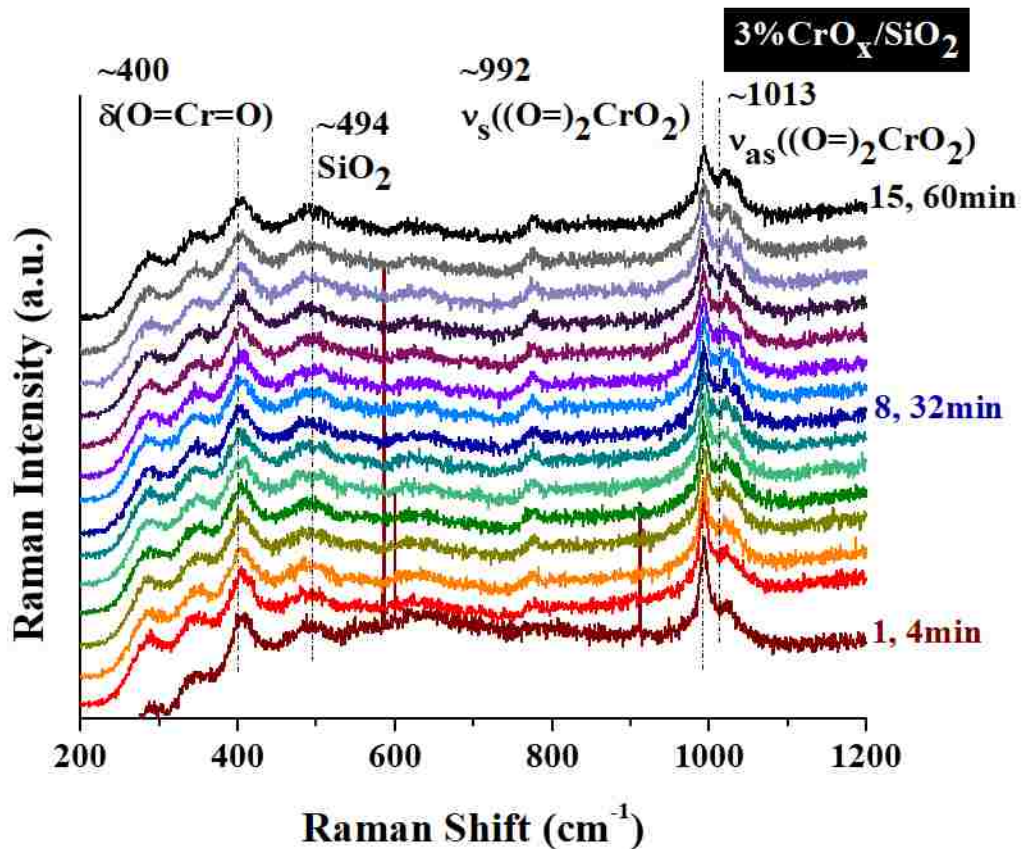
Figure S 3.2. *In situ* Raman spectra of the supported 3% CrO$_x$/SiO$_2$ catalyst taken in flowing 5% O$_2$/He at 100°C. Spectra were taken using a 442 nm wavelength laser (20% laser power) and a moving stage.
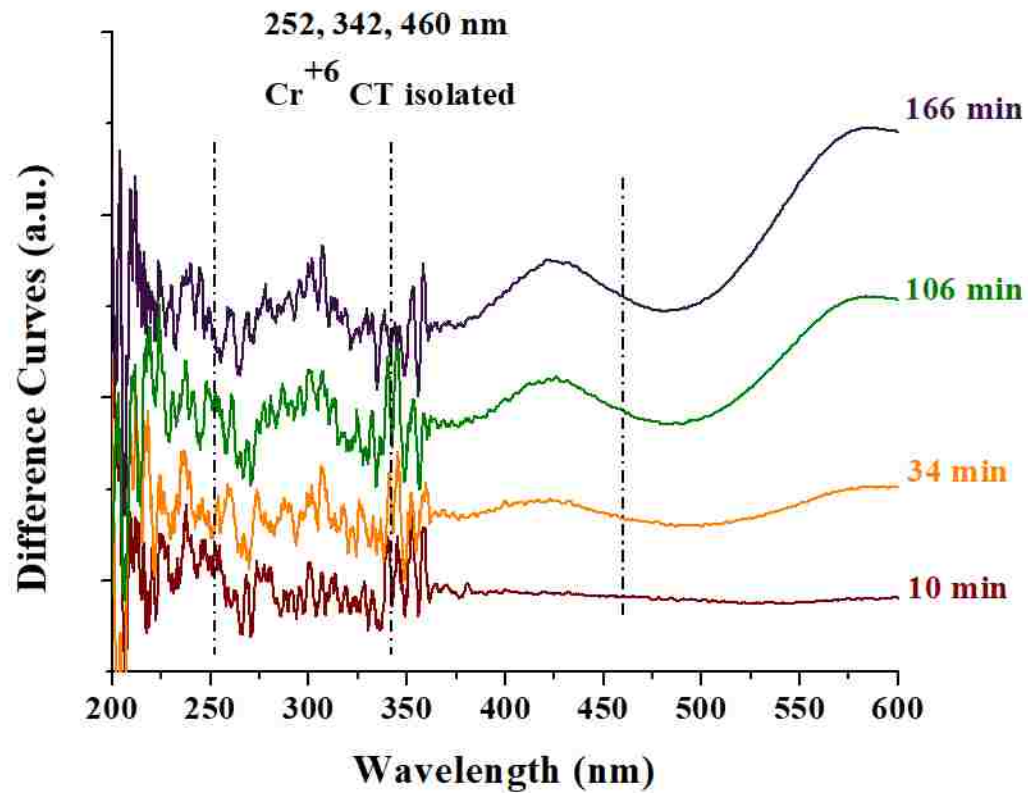
Figure S 3.3. Time-resolved *in situ* UV-vis difference spectra showing reduction of the Cr^{+6} LMCT bands (consumed bands) of the supported 3% CrO_x/SiO_2 in flowing 1% C_2H_4/Ar at 100 °C.

Chapter 4 | *Operando* **Ethylene Polymerization by Supported CrO$_x$/SiO$_2$**

    Catalysts: Role of Promoters

Abstract

Time-resolved *operando* molecular spectroscopy was applied during ethylene polymerization by supported and promoted CrO$_x$/MO$_x$/SiO$_2$ catalysts to investigate the role of promoter oxides (AlO$_x$, TiO$_x$, ZrO$_x$). A combination of spectroscopic techniques (Raman, UV-vis, XAS, DRIFTS, and TPSR) during ethylene polymerization allows for the first time to monitor the molecular events taking place during activation of supported CrO$_x$/MO$_x$/SiO$_2$ catalysts by ethylene and establishment of the role of promoters for this reaction. During reaction, the initial surface Cr^{+6}O$_x$ sites reduce to Cr^{+3} sites (AlO$_x$ and ZrO$_x$) or Cr^{+3} and Cr^{+2} (TiO$_x$) to form Cr-CH=CH$_2$ (AlO$_x$ and ZrO$_x$) or Cr-CH=CH$_2$ and Cr-(CH$_2$)$_2$CH=CH$_2$ (TiO$_x$) reaction intermediates. While AlO$_x$ was determined to not promote the ethylene polymerization reaction, the role of the ZrO$_x$ promoter oxide is to have a higher TOF and the role of the TiO$_x$ promoter oxide is to create a higher number of active sites.

4.1   Introduction

In an effort to improve the catalytic activity, multiple promoters have been examined over the years, most notably TiO$_x$ and AlO$_x$, and ZrO$_x$ has also been found to exhibit a similar effect.[1] As demonstrated in the literature review, the limitation of many of the studies is that they were not performed on dehydrated initially oxidized catalysts, activated catalysts or during the ethylene polymerization reaction. Furthermore, in most cases only indirect information was provided about the catalytic active chromia sites (e.g., NO chemisorption, ^{1}H NMR, or H$_2$-TPR).

Here, a modern approach has been applied using a combination of techniques that can directly monitor the catalytic active chromia sites (before, during ethylene activation, and during ethylene polymerization), surface reaction intermediates and polyethylene products to study silica-supported chromia catalysts promoted with TiO_x, ZrO_x, or AlO_x, and this has allowed for development of a molecular level model of ethylene polymerization by oxide promoted silica-supported chromia catalysts.

4.2   Results

4.2.1   *In Situ* Raman Spectroscopy of Oxidized Supported $CrO_x/MO_x/SiO_2$ Catalysts

The normalized silica-subtracted *in situ* dehydrated Raman spectra of the supported $CrO_x/MO_x/SiO_2$ catalysts are presented in Figure 4.1. The spectrum of the silica support was subtracted from each spectrum of the catalyst during reaction to highlight the changing chromia surface structures. The symmetric and asymmetric vibrations for the surface dioxo $\nu_s((O=)_2CrO_2)$ site are observed at ~992 cm^{-1} and ~1015 cm^{-1}, respectively.[2] Some of the ~1015 cm^{-1} band is due to an experimental artifact caused from laser-induced reduction of the surface dioxo site (see Figure S 4.1). This effect is greater for the promoted catalysts as compared to the standard CrO_x/SiO_2 catalyst since the addition of promoter oxides has been shown to decrease the stability of the surface chromia sites.[3] Surface modification causes the appearance of broad bands at ~860-900 cm^{-1} assigned to the ν_s(Cr-O-M) bridging bond vibrations[4], which demonstrates the preferential bonding of the chromia to the dispersed promoter metal rather than the inert SiO_2 surface. The presence of the Cr-O-M bridging bonds does not exclude the possibility of Cr-O-Si bonds also being present, suggesting the presence of at least two different sites present on these promoted catalysts.[3,5] The corresponding bending mode for CrO_x δ(O=Cr=O) appears at ~400 cm^{-1}.

The absence of Raman bands in the ~200-300 cm^{-1} region demonstrates that bridging Cr-O-Cr bonds are not present, indicating that the surface CrO$_x$ sites are isolated on the silica support.[4,6,7] Additionally, the absence of a band at ~550 cm^{-1} for Cr$_2$O$_3$ crystalline nanoparticles (NPs) indicates that the initial oxidized catalysts consist only of dispersed CrO$_x$ surface sites.
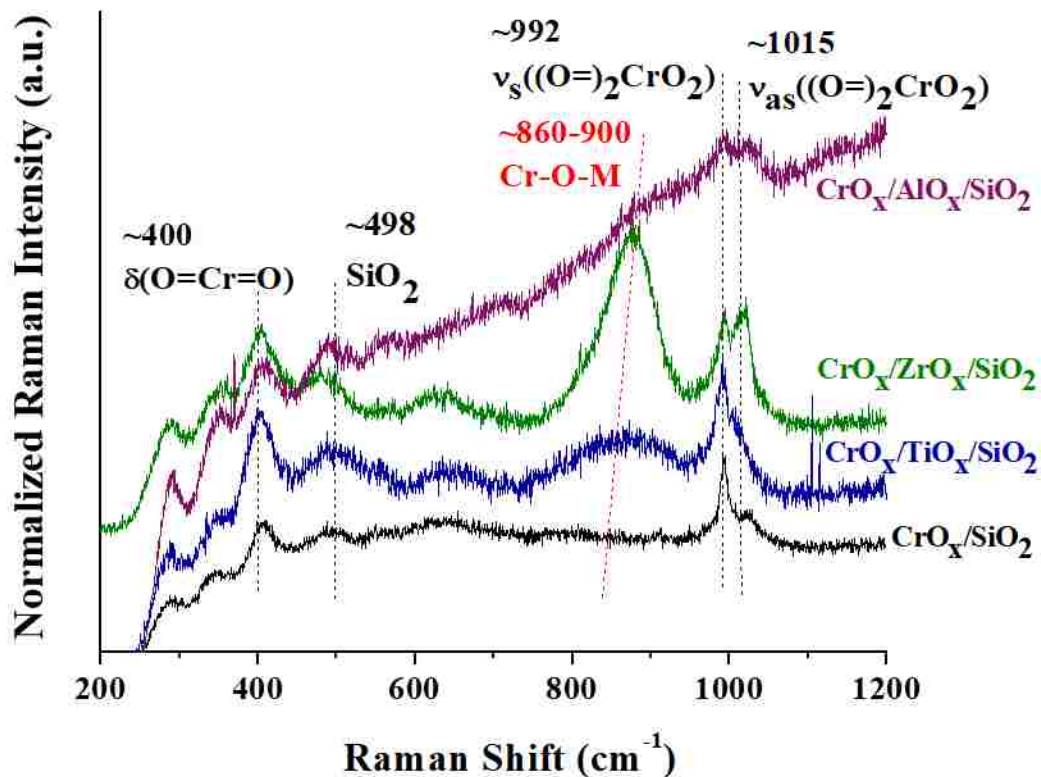
Figure 4.1. *In situ* Raman spectra of the initial oxidized supported $CrO_x/MO_x/SiO_2$ catalysts (3% CrO_x/SiO_2, 3% CrO_x/5% TiO_x/SiO_2, 3% CrO_x/5% ZrO_x/SiO_2, and 3% CrO_x/5% AlO_x/SiO_2) taken in flowing 5% O_2/He at 100 °C. The spectra were taken with a 442 nm wavelength laser (20% laser power) and a moving stage.

4.2.2 *In situ* Raman Spectroscopy During Ethylene Polymerization

Figure S 4.2 reports the *in situ* Raman spectra taken during ethylene polymerization of the supported $CrO_x/MO_x/SiO_2$ catalysts. Figure 4.2 presents the *in situ* Raman spectra taken in flowing He after ethylene polymerization of the Zr- and Al-promoted catalysts. To minimize laser heating, a D2 filter (1% laser power) was used during spectra collection in flowing 1% C_2H_4/Ar. The spectrum of the dehydrated silica support was subtracted from each Raman spectrum to emphasize observation of the chromia sites. During the ~3 h of ethylene polymerization, the intensities of the Raman bands from the surface dioxo CrO_4 site (~992 cm^{-1}) decreases. This indicates that the dioxo surface chromia sites are easily activated at 100°C with ethylene. After the reaction, the spectra in Figure 4.2 suggest that the dioxo CrO_4 sites (Raman bands at ~977-980 cm^{-1}) were perturbed both by ethylene at 100 °C and the strong laser, since the band at ~1015 cm^{-1} remains and is stronger than before reaction. The bands at ~860-900 cm^{-1} for the bridging Cr-O-M sites are unperturbed, indicating that they do not participate in the ethylene polymerization reaction. These *in situ* Raman spectroscopy results also demonstrate that adding the promoter oxides increases the ease of ethylene reduction and decreases the stability of the CrO_x sites since the bands for the dioxo site and bending mode vibration decrease more quickly compared to the standard 3% CrO_x/SiO_2 catalyst previously studied.[3,7]
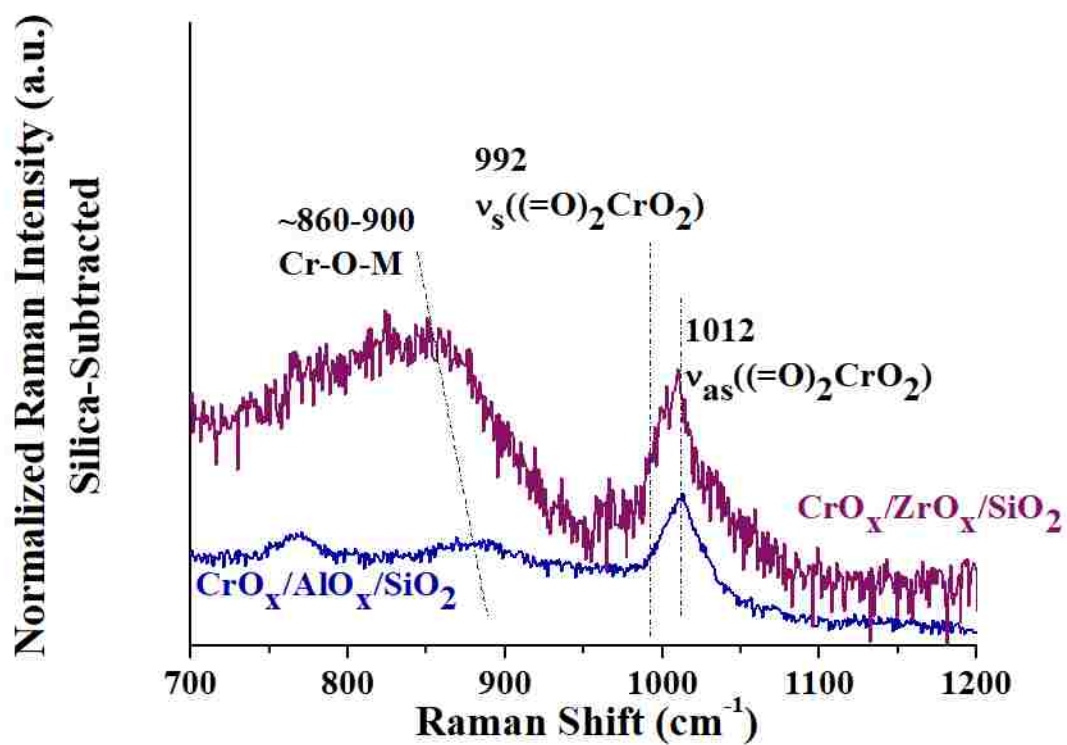
Figure 4.2. *In situ* Raman spectra taken after ~3h of ethylene polymerization conditions in flowing He at 100 °C. Spectra were taken with a 442 nm laser without a filter.

4.2.3 *In situ* UV-vis DRS During Ethylene Polymerization

The *in situ* dehydrated UV-vis DRS results of the initial oxidized $CrO_x/MO_x/SiO_2$ catalysts are presented in Figure 4.3. In the fully oxidized states, the *in situ* dehydrated UV-vis spectra of the Al- and Zr-promoted catalysts exhibit three bands at ~255, ~356-360, and ~460 nm characteristic of the $O \rightarrow Cr^{+6}$ ligand-to-metal charge transfer (LMCT).[7-10] The *in situ* dehydrated UV-vis spectrum (100 °C, UHP He) of the 5% TiO_x/SiO_2 support has a single absorbance at ~246 nm assigned to the $O \rightarrow Ti^{+4}$ LMCT[10], while the spectra of the 5% ZrO_x/SiO_2 and 5% AlO_x/SiO_2 supports do not contain any UV-vis absorbances. Thus, the spectrum of the 5% TiO_x/SiO_2 was subtracted from the spectra of the Ti-promoted catalyst to emphasize the UV-vis absorbance bands deriving from the CrO_x sites on silica. Before subtraction, the Ti-promoted catalyst exhibits three LMCT bands at ~255, ~350, and ~460 nm, while after subtraction of the *in situ* dehydrated UV-vis spectrum of the support, the bands are at ~270, ~350, and ~460 nm. Since the subtraction highlights the absorbance bands due to the CrO_x, the bands at ~270, ~350, and ~460 nm were assigned to the $O \rightarrow Cr^{+6}$ LMCT. The location of the first LMCT band shifts due to the overlap of the $O \rightarrow Ti^{+4}$ and $O \rightarrow Cr^{+6}$ LMCT.[7-10] The surface CrO_x edge energy (E_g) values of the $CrO_x/MO_x/SiO_2$ catalysts vary between ~2.4-2.5 eV (see Table 4.1), corresponding to isolated surface chromia sites.[4,6,7,9]

Compared to the standard CrO_x/SiO_2 catalyst, the position of the second LMCT band (~350-356 nm) is red-shifted, while the positions of the bands at ~255 and ~460 nm do not shift. The shift occurs because of the replacement of the Si atom by the less electronegative Zr, Ti, and Al atoms. The decreased electronegativity pulls the electron cloud closer to the O atom nearest to the Cr atom to occupy its energy levels, thereby narrowing the $O \rightarrow Cr^{+6}$

LMCT energy gap and decreasing the energy required for the CT to occur.[10] Only the second LMCT band shifts (~350-356 nm), suggesting that it may arise from the ligands. It would be expected that the band would shift to increasingly lower energies with decreasing electronegativity of the substituted atom. However, this relation is not seen in these studies, but this may just be due to the broad nature of UV-vis DRS bands.
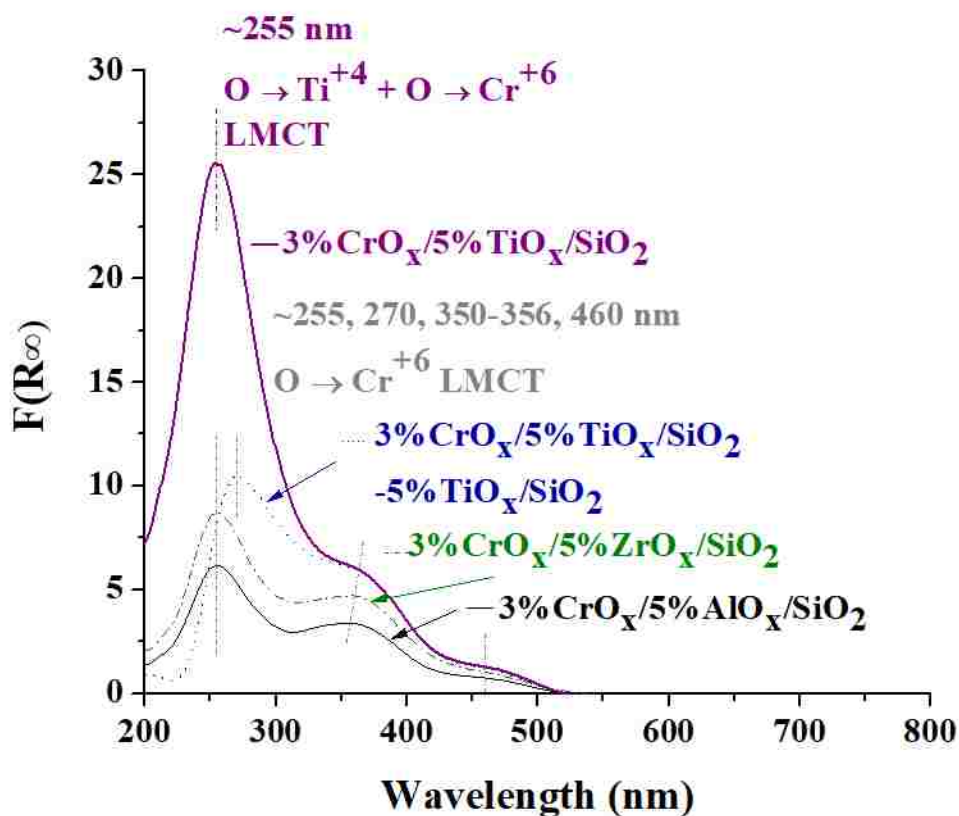
Figure 4.3. Time-resolved *in situ* dehydrated UV-vis spectra taken in flowing UHP He at T=100 °C of promoted and supported CrO_x/SiO_2 catalysts before the ethylene polymerization reaction (3% CrO_x/5% AlO_x/SiO_2, 3% CrO_x/5% TiO_x/SiO_2 with 5% TiO_x/SiO_2 subtracted, and 3% CrO_x/5% ZrO_x/SiO_2).

Figure 4.4 reports the time-resolved difference spectra of the *in situ* UV-vis DRS spectra taken during ethylene polymerization of the supported $CrO_x/MO_x/SiO_2$ catalysts. The difference curves were obtained by subtracting the UV-vis spectrum of the corresponding initial dehydrated catalyst from each UV-vis spectrum taken during ethylene polymerization, allowing for better observation of the d-d transition bands. The spectra are displayed with units of absorbance because the Kubelka-Munk transformation emphasizes the LMCT bands, and the d-d transitions are most visible using absorbance. During the ~3 h of ethylene polymerization, the intensities of the LMCT bands decrease while multiple d-d transition bands appear ranging from ~428-441 nm and ~576-720 nm depending on the promoter metal oxide (see Table 4.1) and increase monotonically in intensity with time. The Zr-promoted catalyst exhibits a single increasing absorbance band at ~576 nm, while the Al-promoted catalyst exhibits two increasing absorbance bands at ~428 and ~618 nm. These three bands are assigned to Cr^{+3}_{Oh} d-d transitions.[7-9] The band maximum for Cr^{+2}_{Oh} would be expected at ~800 nm, and the absorbance for Cr^{+2}_{Th} would be expected at ~1000 nm.[8,11,12]

Both the Zr- and Al-promoted catalysts also exhibit isosbestic points at ~500 nm. Isosbestic points most usually appear in reactions with two absorbing species, such as Cr^{+6} and Cr^{+3},[13] and this suggests that there are no Cr^{+2} sites present on the catalyst. However, the Ti-promoted catalyst exhibits one increasing absorbance band at ~441 nm assigned to a Cr^{+3}_{Oh} d-d transition, and another absorbance band at ~720 nm. The band at ~720 nm has been assigned to a combination of Cr^{+2}_{Oh} and Cr^{+3}_{Oh}.[8,11,12] The UV-vis spectra during ethylene polymerization of the Ti-promoted catalyst lacks the clean isosbestic point seen

with the Zr- and Al-promoted catalysts, which would be more expected to occur with a higher number of different species present on the surface of the catalyst.[13]

The band at ~720 nm observed in these studies has also been assigned to a combination of Cr^{+2} and Cr^{+3} in other recent studies.[12] To determine the relative amount of Cr^{+3}_{Oh} and Cr^{+2}_{Oh}, the UV-vis band at ~720 nm was deconvoluted. Only the spectra taken during the first two hours could be deconvoluted (see Figure 4.5) since the results for the last hour failed.
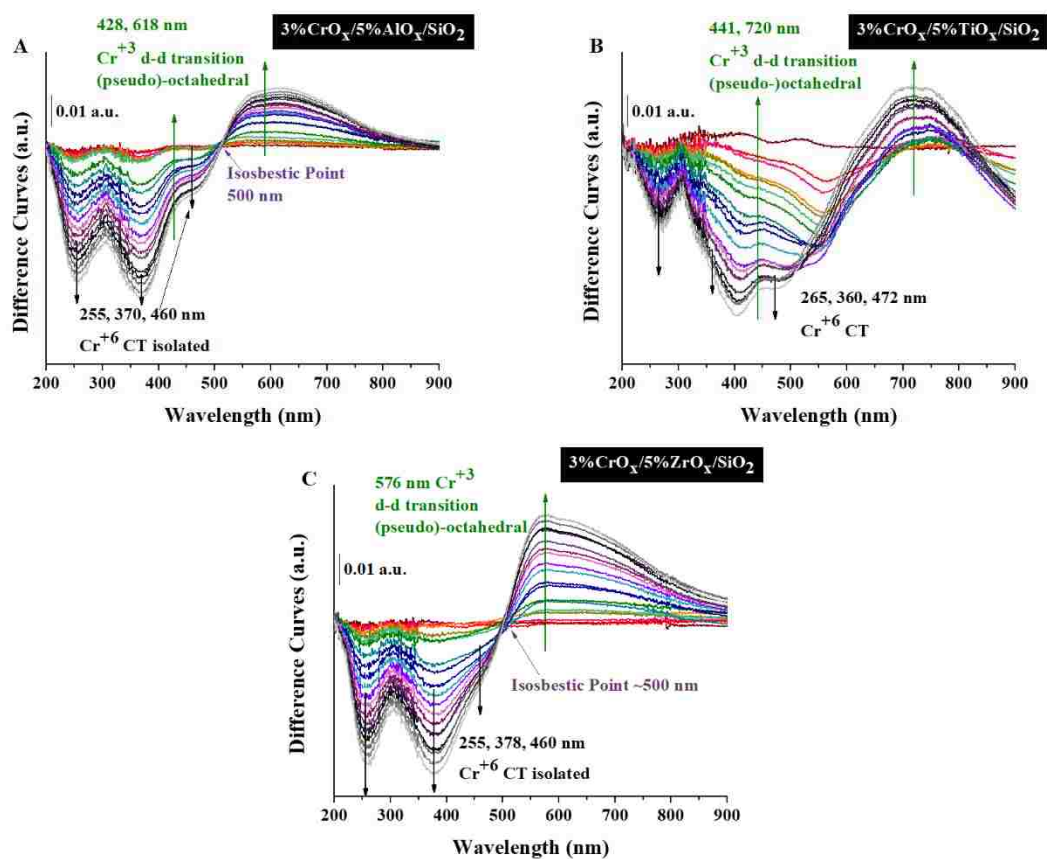
Figure 4.4. Time-resolved *in situ* UV-vis absorbance difference spectra of catalysts: (A) 3% CrO$_x$/5% AlO$_x$/SiO$_2$, (B) 3% CrO$_x$/5% TiO$_x$/SiO$_2$, and (C) 3% CrO$_x$/5% ZrO$_x$/SiO$_2$ during ethylene polymerization at 100 °C.
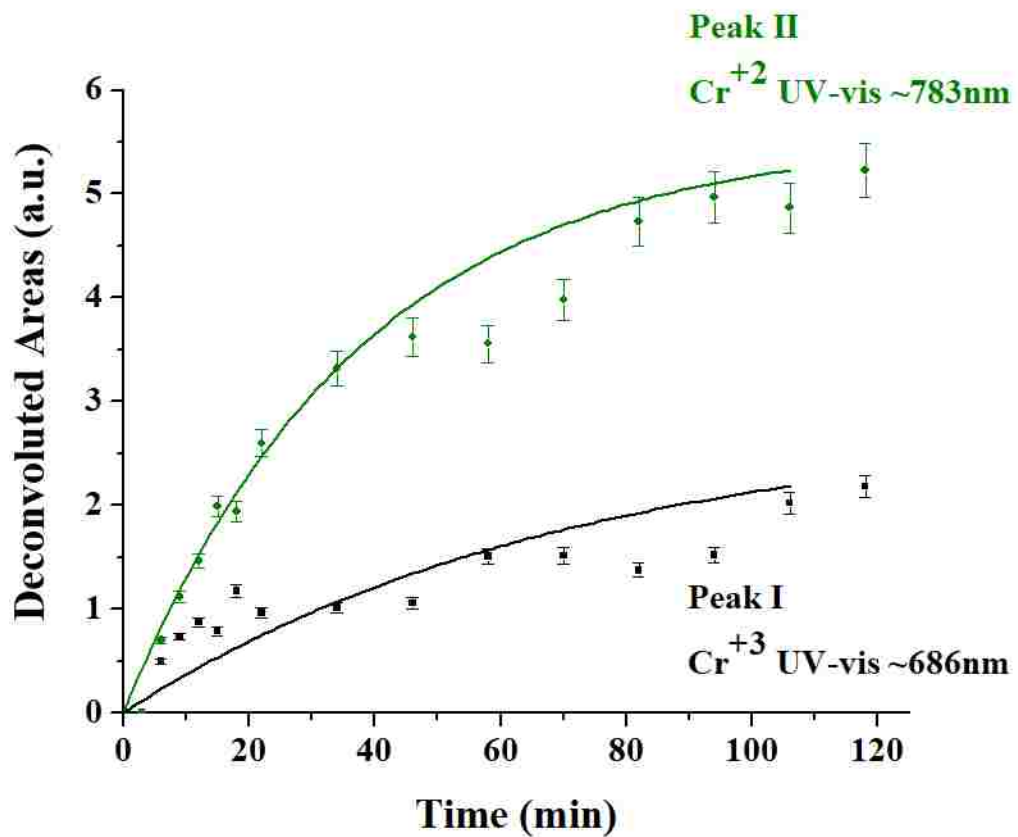
Figure 4.5. Evolution of areas of bands at ~686 nm and ~783 nm resulting from deconvolution of ~720 nm UV-vis band observed during ethylene polymerization of 3% CrO_x/5% TiO_x/SiO_2.

During the first ~2 h of ethylene polymerization, the band at ~720 nm could be deconvoluted into two bands, which were observed to blue-shift as time progressed. In the first ~20 min, the lower wavelength deconvoluted peak (Peak I) shifted from ~686-667 nm, while the higher wavelength deconvoluted peak (Peak II) shifted from ~783-765 nm. By the end of ~2 h, Peak I maximum is at ~645 nm, while the Peak II maximum is at ~757 nm. The location of Peak I is characteristic of Cr^{+3}_{Oh}, while the location of Peak II is closer to the characteristic absorbance of Cr^{+2}_{Oh}. There is thus a combination of Cr^{+2}_{Oh} and Cr^{+3}_{Oh} present on the surface of the Ti-promoted catalyst, and the presence of more than two surface species (Cr^{+6}, Cr^{+3}_{Oh}, and Cr^{+2}_{Th}) explains the lack of an isosbestic point in the difference curves of the Ti-promoted catalyst. Additionally, the blue-shifting to lower wavelength of the bands, particularly of Peak II, indicates that the Cr^{+2}_{Oh} sites are re-oxidizing to $Cr^{+3}_{Oh.}$

The UV-vis spectra during ethylene polymerization of the Zr- and Al-promoted catalysts were also deconvoluted into two bands. For the Zr-promoted catalyst, the location of Peak I_{Zr} in the first ~20 min shifted from ~671-565 nm, while the position of Peak II_{Zr} shifted from ~765-694 nm, and at the end of ~2 h, the positions were ~555 and ~666 nm, respectively. In the case of the Al-promoted catalyst, Peak I_{Al} shifted from ~594-566 nm, while Peak II_{Al} shifted from ~723-675 nm, and at the end of ~2 h, the positions were ~568 and ~674 nm, respectively. However, these band positions are characteristic of the Cr^{+3} Cr_2O_3 reference standard[9], indicating that these catalysts do not have any Cr^{+2} surface sites.

Table 4.1. Summary of *in situ* UV-vis Studies During Ethylene Polymerization			
MO_x	E_g (eV)	CT band location (nm)	d-d transition band location (nm)
None[b]	2.4	252, 342, 460	425, 587
ZrO_x	2.5	255, 356, 460	576
TiO_x	2.4	255, 348, 460	441, 720 (686, 783)
AlO_x	2.4	255, 354, 460	428, 618

[b] The standard un-promoted 3% CrO_x/SiO_2 catalyst has been previously studied.[7]

4.2.4   C₂H₄-TPSR of Supported CrOₓ/MOₓ/SiO₂ Catalysts

The CO_2/C_2H_4-TPSR results of the supported CrO_x/MO_x/SiO_2 catalysts are presented in Figure 4.6. The only gaseous product detected was CO_2, the formation of which demonstrates that ethylene is reducing the initial Cr^{+6} surface sites to lower chromia oxidation states. The two CO_2 peaks at ~286-308 °C and ~428-494 °C represent a two-step reduction process for the chromia sites. For all the catalysts, the first reduction step is $Cr^{+6} \rightarrow Cr^{+4}$. The *in situ* UV-vis results (see Figure 4.4 and Figure 4.5) suggest that the second step differs depending on the promoter oxide. For the Zr- and Al-promoted catalysts, the reduction step is $Cr^{+4} \rightarrow Cr^{+3}$, but for the Ti-promoted catalyst, the co-existence of surface Cr^{+2} with Cr^{+2} suggests that T_{p2} is due to $Cr^{+4} \rightarrow Cr^{+2/+3}$.

Table 4.2 compares the C_2H_4-TPSR results and presents the results of calculation of the ethylene reduction kinetics. From deconvolution of the TPSR results, it appears that the $Cr^{+6/+4}$:$Cr^{+4/+3/+2}$ ratio is only very slightly perturbed. From the ratio of $CO_2(T_{p1})$/$CO_2(T_{p2})$, ~60-65% of the reduced sites are present as Cr^{+4} and ~35-40% are in a Cr^{+3} or Cr^{+2} state. Calculation of the reduction kinetics by applying the Redhead equation with first-order kinetics[14] shows that the ratios of $k_{6/4}$/$k_{4/3/2}$ are high (see Table 4.2) and suggests that reduction of $Cr^{+6} \rightarrow Cr^{+4}$ with ethylene is substantially more facile than the reduction of $Cr^{+4} \rightarrow Cr^{+3/+2}$.
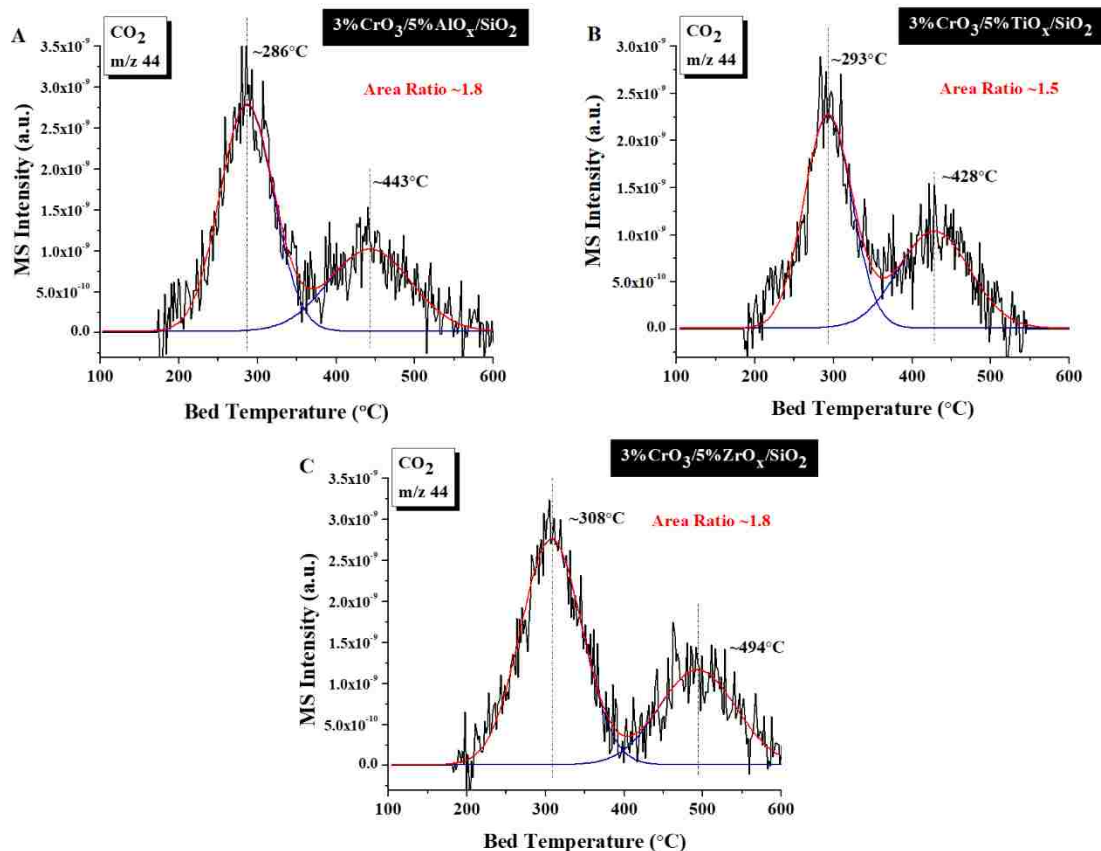
Figure 4.6. The CO_2/C_2H_4-TPSR spectrum of the supported $CrO_x/MO_x/SiO_2$ catalysts (A) 3% CrO_x/5% AlO_x/SiO_2, (B) 3% CrO_x/5% TiO_x/SiO_2, (C) 3% CrO_x/5% ZrO_x/SiO_2. The temperature was ramped from 100 to 800 °C with a heating rate of 10 °C/min in flowing 1% C_2H_4/Ar. The reactor outlet was connected to an online MS to monitor the gaseous products.

Table 4.2. Summary of TPSR Spectroscopy Studies

MO$_x$	T$_{p1}$ (°C)	T$_{p2}$ (°C)	Ratio[a]	k$_{6/4}$ (s^{-1})[c]	k$_{4/3 \text{ or } 2}$ (s^{-1})[c, d]	k$_{6/4}$/k$_{4/3 \text{ or } 2}$[c, d]
None[b]	280	410	1.7	6.1×10^{-10}	2.5×10^{-15}	2×10^5
ZrO$_x$	300	494	1.8	9×10^{-11}	1×10^{-17}	7×10^6
TiO$_x$	280	410	1.5	6.1×10^{-10}	2.5×10^{-15}	2×10^5
AlO$_x$	290	475	1.8	6.1×10^{-10}	5×10^{-18}	1×10^8

[a] The ratios of the reduction peaks were calculated by baseline correction and deconvolution with Gaussian peak fitting of the CO_2 spectrum.

[b] The standard 3% CrO$_x$/SiO$_2$ catalyst has been previously studied in Reference [7].

[c] The k$_{rds}$ constants were calculated using the Redhead equation for first-order kinetics at a reference temperature of 100 °C.[14]

[d] The 3% CrO$_x$/5% TiO$_x$/SiO$_2$ catalyst reduces to Cr^{+3} and Cr^{+2}

4.2.5 *In situ* and *Operando* DRIFTS During Ethylene Polymerization

The time-resolved *in situ* DRIFTS spectra taken of the supported $CrO_x/MO_x/SiO_2$ catalysts during ethylene polymerization are shown in Figure S 4.3. DRIFTS difference spectra were used to emphasize the surface intermediates and products that appear (positive DRIFTS bands) or are consumed (negative DRIFTS bands) during the reaction. The difference spectra were obtained by subtracting the IR spectrum of the initial dehydrated catalyst from each IR spectrum taken during ethylene polymerization, after normalization using the SiO_2 support vibration at ~1350 cm^{-1}. The DRIFTS spectra of the supported $CrO_x/MO_x/SiO_2$ catalysts are similar to those of the standard CrO_x/SiO_2 catalyst. Gas phase ethylene gives rise to bands at ~950, ~1440, ~1900, and ~2950-3200 cm^{-1}, and the gas phase CO_2 vibration is at ~2350 cm^{-1} in Figure S 4.3.[7,15] The band at ~3745 cm^{-1}, well-known and characteristic of isolated silanol groups,[7,16-20] decreases with reaction time since the isolated silanols interact with the polyethylene chains forming.[10] The bands at ~3400-3548 cm^{-1} and ~3700 cm^{-1} increase and broaden with reaction time due to the silanols interacting with the active site via hydrogen bonding and the PE chain, respectively.[7,19,21]

In the bending region, the DRIFTS bands at ~805 and ~985 cm^{-1} arise due to the $\delta(=CH_2)$ modes of the PE chain, while the band at ~1574-1600 cm^{-1} for the $\nu_{as}(C=C)$ of the PE chain increases with reaction time.[7,21,22] The band at ~906 cm^{-1} is assigned to the Cr-O-Si bridging bond and decreases with reaction time, indicating its interaction with the surface intermediates and PE chain.[7] The appearance of the Cr-O-Si bond also demonstrates that both Cr-O-M-O-Si bands (see Figure 4.1) and Cr-O-Si bonds are present in the supported $CrO_x/MO_x/SiO_2$ catalysts.

The areas in Figure S 4.3 labeled as "Zoomed Region" are replotted in Figure 4.7 to allow for closer observation of the significant DRIFTS bands that increase with reaction time and are assigned to surface intermediates, PE product, and gas phase ethylene vibrations (~2950-3200 cm^{-1}).[7,15] The bands at ~2895, 2889, and 2906 cm^{-1} are assigned to the ν_s(-CH$_2$-CH$_2$) vibration of the bulk PE chain since they would be expected between 2850 and 3000 cm^{-1}. The band at ~2840 cm^{-1} seen for the Ti-promoted catalyst in Figure 4.7 B is similar to the band observed in the case of the standard CrO$_x$/SiO$_2$ catalyst at ~2865 cm^{-1} and assigned to Cr^{+3}-(CH$_2$)$_2$CH=CH$_2$. However, in the case of the Ti-promoted catalyst, its formation does not begin until ~45 min into the reaction. In one study of ethylene polymerization at 95 °C with a Cr/silica-titania catalyst, the reaction was stopped various times to collect samples of PE produced over different lengths of time.[1] It was determined that early samples yielded PE with lower molecular weight than that of the standard CrO$_x$/SiO$_2$ catalyst that is known to produce only high-density PE. At later times, the PE samples had a higher molecular weight, and the average molecular weight increased over time. This suggested that, compared to the standard CrO$_x$/SiO$_2$ catalyst that is known to produce only high molecular weight PE, the addition of titania caused the development of new sites responsible for the lower molecular weight polymer. It also suggested that these Ti-associated sites are more active since the lower molecular weight polymer was seen earlier in the polymerization reaction. Thus, this band is assigned to the ν_s(Cr-CH$_2$) of the Cr^{+3}-(CH$_2$)$_2$CH=CH$_2$ site of the PE forming with higher molecular weight at the Cr-O-Si sites not associated with Ti. The slight red shift of ~25 cm^{-1} from 2865 cm^{-1} of the standard CrO$_x$/SiO$_2$ catalyst[7] may be due interaction with the nearby Ti-associated sites.[10,21,22]

To detect any additional bands that may have been obscured by the gas phase ethylene reactant, UHP Ar was flushed for ~45 min. Like the standard catalyst, after the Ar flush, new IR bands are observed for the Zr- and Ti-promoted catalysts at ~2978 and 2968 cm^{-1}, respectively, for ν_{as}(-CH$_2$-CH$_2$) of the bulk PE chain. This is ~80 cm^{-1} higher than the corresponding ν_s(-CH$_2$-CH$_2$) of the bulk PE and is a typical difference between the symmetric and asymmetric band vibrations.[7,21] A second band is also observed after the Ar flush for all three promoted catalysts at ~2939-2960 cm^{-1} assigned to the ν(C-H) of the Cr^{+3}-CH=CH$_2$ vinyl reaction intermediate.[7,21,22] For the Zr- and Ti-promoted catalysts, the bands for the Cr^{+3}-CH=CH$_2$ vinyl reaction intermediate shift to lower wavenumbers, presumably due to the increased reduced mass of the functional groups,[10,21] and indicate that these sites are forming on the Cr-O-Zr and Cr-O-Ti bridging bonds, respectively. However, the band does not shift for the Al-promoted catalyst, suggesting that the key vinyl Cr^{+3}-CH=CH$_2$ intermediate could be forming on the Cr-O-Si bonds, as for the standard CrO$_x$/SiO$_2$ catalyst.
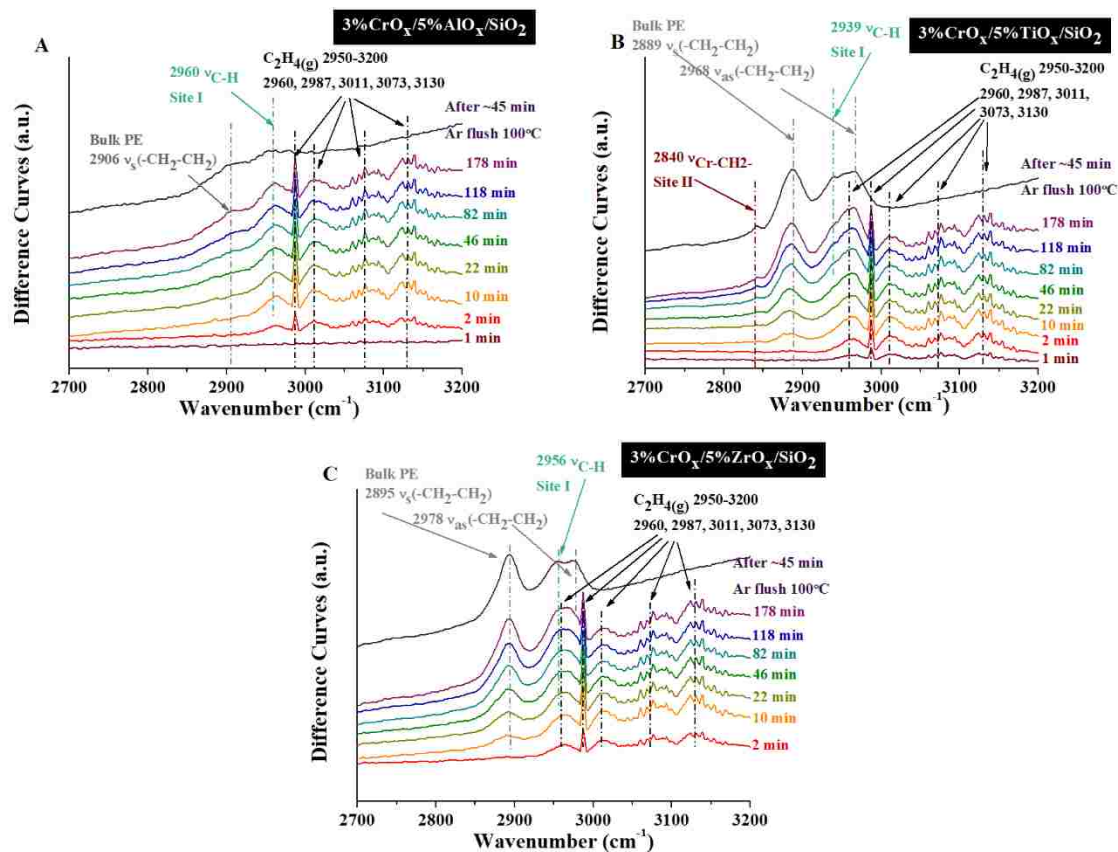
Figure 4.7. Time-resolved *in situ* DRIFT spectra of the C-H region for the supported promoted CrO_x/SiO_2 catalysts (A) 3% CrO_x/5% AlO_x/SiO_2, (B) 3% CrO_x/5% TiO_x/SiO_2, (C) 3% CrO_x/5% ZrO_x/SiO_2 during ethylene polymerization at 100 °C with an Ar flush after ~3 h.

4.2.6 Kinetics

Plots of the evolution of the IR bands for the formation of PE product, surface Cr^{+3}-$(CH_2)_2CH=CH_2$, and Cr^{+3}-$CH=CH_2$ sites during ethylene polymerization are in Figure 4.8. Formation of the Cr^{+3}-$(CH_2)_2CH=CH_2$ reaction intermediate was only observed with the Ti-promoted catalyst. Previously, in ethylene polymerization by the standard CrO_x/SiO_2 catalyst, an initial positive slope was observed in the progression of the Cr^{+3}-$(CH_2)_2CH=CH_2$ reaction intermediate that indicated it is an initial reaction intermediate.[7] However, the Cr^{+3}-$(CH_2)_2CH=CH_2$ reaction intermediate in the experiment with the Ti-promoted catalyst does not form until after ~45 min (Figure 4.8 A). This indicates that the Cr^{+3}-$(CH_2)_2CH=CH_2$ intermediate is a secondary reaction intermediate for ethylene polymerization by $CrO_x/TiO_x/SiO_2$, which is expected since this reaction intermediate is associated with the Cr-O-Si sites, and not the Cr-O-Ti bridging bonds.[1] The formation of the Cr^{+3}-$(CH_2)_2CH=CH_2$ reaction intermediate appears to saturate after ~2.5 h. For both the Zr- and Ti-promoted catalysts, the evolution of the bulk PE band exhibits an initial positive slope, in contrast to the initial zero slope observed with the standard catalyst,[7] demonstrating it is the primary product formed during ethylene polymerization by $CrO_x/ZrO_x/SiO_2$ and $CrO_x/TiO_x/SiO_2$, and not related to the formation of the Cr^{+3}-$(CH_2)_2CH=CH_2$ reaction intermediates. The variance between these catalysts and the standard catalyst also indicates that ZrO_x and TiO_x are promoting the ethylene polymerization reaction, since formation of the PE product starts more quickly. However, formation of the bulk PE in the case of the Al-promoted catalyst does not appear to begin until after ~30 min into the ethylene polymerization reaction, suggesting that it does not promote the ethylene polymerization reaction.

At times greater than ~20 min, the slopes of the bulk PE evolution for the Zr- and Ti-promoted catalysts become more linear, while that of the Al-promoted appears to begin to increase exponentially after ~2 h. The IR band area for the surface Cr^{+3}-CH=CH$_2$ reaction intermediate at ~2939-2960 cm^{-1} could not be monitored directly due to the overlap of them with the IR bands of gas phase ethylene. However, following a method used previously for the standard CrO_x/SiO_2 catalyst,[7] the gas phase ethylene contribution could be determined and subtracted to find the amount of the Cr^{+3}-CH=CH$_2$ intermediate. The resulting plot of the intensity of the surface Cr^{+3}-CH=CH$_2$ seems to track the evolution of the PE product for both the Zr- and Ti-promoted catalysts. On the other hand, for the Al-promoted catalyst, the evolutions of the bulk PE band and Cr^{+3}-CH=CH$_2$ reaction intermediate do not appear to track each other for more than ~2 h, which suggests there may be another reaction intermediate contributing to the formation of the PE that is not detectable in these experiments. The evolutions of the Cr^{+3}-(CH$_2$)$_2$CH=CH$_2$ reaction intermediate and bulk PE for the Ti-promoted catalyst also track each other. The continued increase in amount of bulk PE and Cr^{+3}-CH=CH$_2$ reaction intermediate even at ~180 min indicates that not all the surface chromia site have been activated.

The UV-vis band evolution plots as a function of reaction time of ethylene polymerization are in Figure 4.9. The progressions of both reduced surface chromia sites on the surface of the Ti-promoted catalyst initially exhibit positive slopes, and it appears that at times earlier than ~20 min, the area of the combination Cr^{+3}+Cr^{+2} band at ~720 nm is greater than that of the Cr^{+3} band at ~441 nm, suggesting that these sites are first reduced to Cr^{+2}, then re-oxidize to Cr^{+3}. The slopes of the evolution of both these bands go through the plot origin, indicating that they are both initial reaction intermediates during ethylene

polymerization by the Ti-promoted catalyst, and that they likely originate from two different sites. The evolutions of the UV-vis band of the Cr^{+3} surface chromia sites in the Zr-promoted (576 nm) and Al-promoted (428 and 618 nm) exhibit an initial lag since the slopes are close to zero. The production of Cr^{+3} sites appears to increase after ~10 min for the Zr-promoted catalyst, but does not grow for the Al-promoted catalyst until after ~20-30 min. At reaction times longer than ~20 min, the areas of these bands are more closely aligned, and the slopes decrease but remain linear, indicating the continued catalyst reduction since not all the surface chromia sites have been activated since this is an early stage of ethylene polymerization under the current reaction conditions.
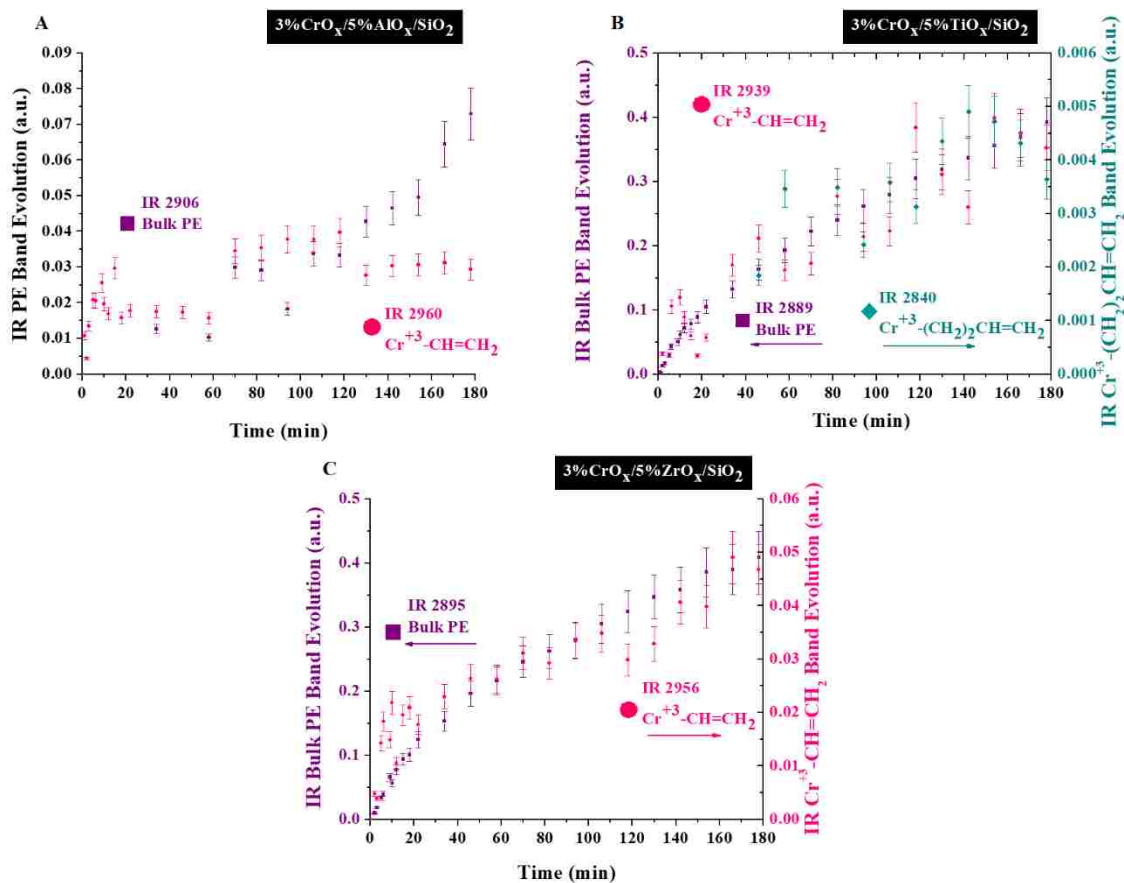
Figure 4.8. Evolution of IR bands from PE product and surface intermediates during ethylene polymerization at 100 °C. (A) evolution of IR bands from bulk PE and surface Cr^{+3}-CH=CH$_2$ growing on 3% CrO$_x$/5% AlO$_x$/SiO$_2$; (B) evolution of IR bands from PE product, surface Cr^{+3}-(CH$_2$)$_2$CH=CH$_2$, and surface Cr^{+3}-CH=CH$_2$ growing on 3% CrO$_x$/5% TiO$_x$/SiO$_2$; and (C) evolution of IR bands from bulk PE and surface Cr^{+3}-CH=CH$_2$ growing on 3% CrO$_x$/5% ZrO$_x$/SiO$_2$.
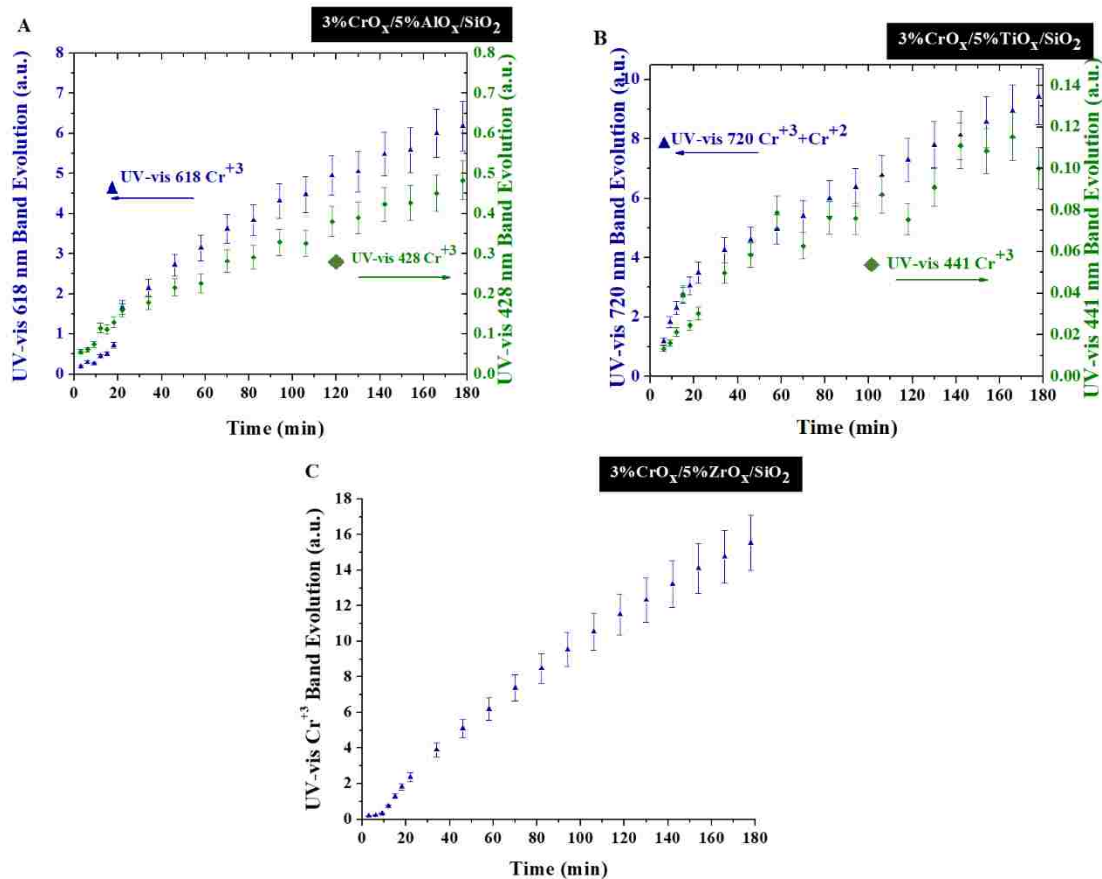
Figure 4.9. Evolution of UV-vis bands from reduced CrO_x sites at 100 °C. (A) evolution of UV-vis bands at 618 nm and 428 nm for Cr^{+3} for 3% CrO_x/5% AlO_x/SiO_2; (B) evolution of UV-vis bands at 720 nm ($Cr^{+3} + Cr^{+2}$) and 441 nm (Cr^{+3}) for 3% CrO_x/5% TiO_x/SiO_2; (C) evolution of UV-vis band at 576 nm for Cr^{+3} for 3% CrO_x/5% ZrO_x/SiO_2.
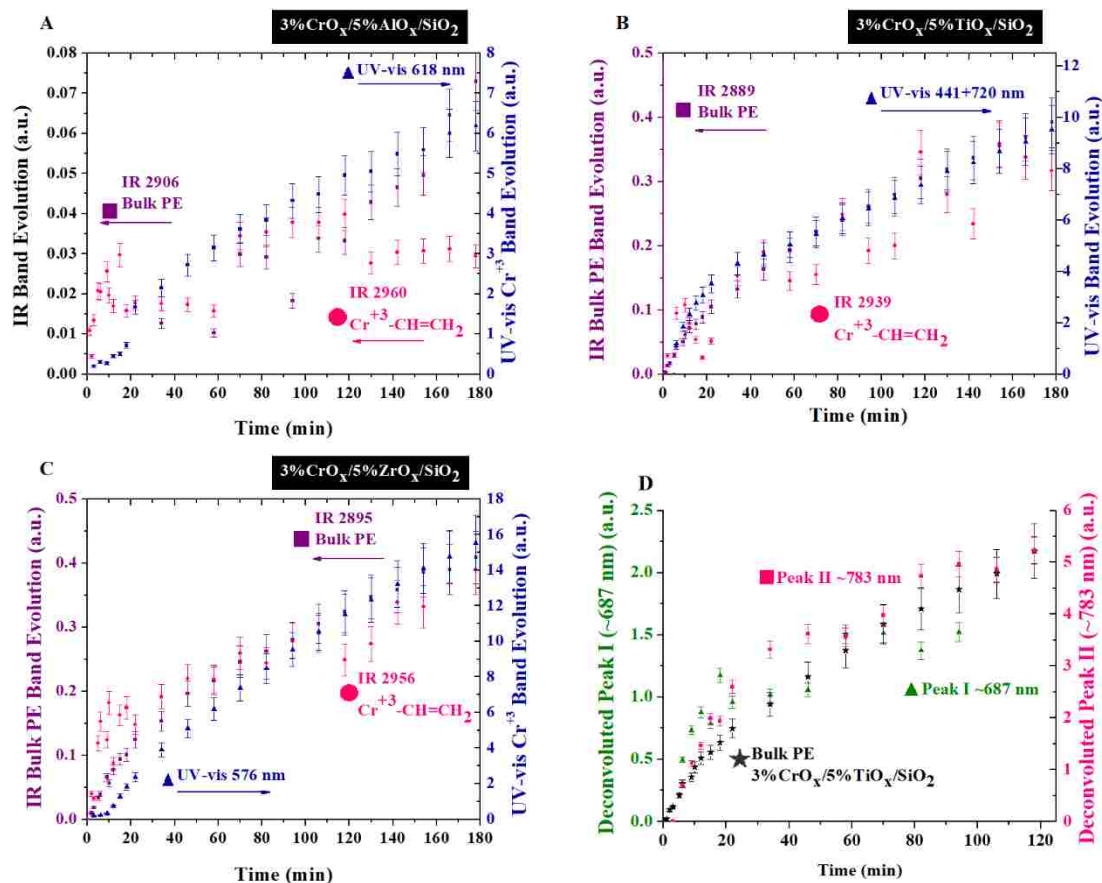
Figure 4.10. Evolution of IR and UV-vis bands from surface intermediates and reduced CrO_x sites, respectively, at 100 °C. (A) 3% CrO_x/5% AlO_x/SiO_2; (B) 3% CrO_x/5% TiO_x/SiO_2; (C) 3% CrO_x/5% ZrO_x/SiO_2; (D) deconvolution of ~720 nm $Cr^{+3}+Cr^{+2}$ combination band during reduction of 3% CrO_x/5% TiO_x/SiO_2.

Comparisons of the evolution of the UV-vis and DRIFTS bands are plotted in Figure 4.10 to follow the time-dependent trends. For the Zr-promoted catalyst, the UV-vis band at 576 nm tracks the progression of the DRIFTS band at 2956 cm^{-1} for the Cr^{+3}-CH=CH$_2$ reaction intermediate (see Figure 4.10). The plots for the Ti-promoted catalyst demonstrate that the UV-vis bands at 720 nm and 441 nm track the trends of the Cr^{+3}-CH=CH$_2$ and the Cr^{+3}-(CH$_2$)$_2$CH=CH$_2$ reaction intermediates, respectively (see Figure 4.10). It is difficult to determine whether the polymerization is occurring on the Cr^{+2} sites as well since there is always a co-existence of Cr^{+3} and Cr^{+2} sites, and evolutions of both the deconvoluted Cr^{+3} band at ~686 nm and mixed Cr^{+2}+Cr^{+3} band at ~783 nm track the progression of the bulk PE produced by the Ti-promoted catalyst (see Figure 4.10). However, the deconvoluted peak location progressions tending towards typical Cr^{+3} locations as discussed earlier and the increasing amount of PE suggest that the surface sites most likely re-oxidize to Cr^{+3} before creating polyethylene. Thus, the lower molecular weight polymer is produced on the vinyl Cr^{+3}-CH=CH$_2$ sites located on the Ti-associated sites (Cr-O-Ti bridging bonds). These are formed by reduction of $Cr^{+6}_{Th} \rightarrow Cr^{+2}_{Th}$ before re-oxidization to Cr^{+3}_{Oh}. The Ti-promoted catalyst also produces the higher molecular weight polymer made by the standard catalyst. The higher molecular weight polymer is produced with the Cr^{+3}-(CH$_2$)$_2$CH=CH$_2$ reaction intermediate located on the sites without Ti (Cr-O-Si bond). The comparison plots of the Al-promoted catalyst suggest that both the UV-vis bands at 618 and 428 nm track the evolution of the bulk PE, although neither of them appears to follow the time-dependent progression of the Cr^{+3}-CH=CH$_2$ past the first two hours (see Figure 4.10).

By directly comparing the amount of PE produced by each catalyst (Figure 4.11), it becomes obvious that the Zr- and Ti-promoted catalysts are the most active, while the Al-promoted catalyst is only as active as, if not less active than, the standard catalyst. By also comparing the number of active UV-vis sites produced by each catalyst (Al – 618 nm; Ti – 441, 720 nm; Zr – 576 nm), it becomes apparent that both the Zr- and Ti-promoted catalysts are creating more active sites.

Although the PE production shows the Zr- and Ti-promoted catalysts to be about equal, the comparison of the number of sites in Figure 4.11 demonstrates that the Zr-promoted catalyst produces fewer sites than the Ti-promoted catalyst, suggesting that the activity is affected by more than just the number of sites. The turnover frequency (TOF) of these catalysts was calculated using   Equation 4.1.

$$TOF\ (s^{-1}) = \frac{dPE/dt}{N_S}$$

Equation 4.1

Values for dPE/dt were found using the slope of the best fit line through PE formation and N_S is the number of sites, as determined by the integrations of the active UV-vis bands. Comparison of the initial TOF values across all the catalysts (see Table 4.3) allows for observing that the sites in the Zr-promoted sites are the most catalytically active for ethylene polymerization, as evidenced by the relatively high TOF values, and the TOF decreases in the order $ZrO_x > TiO_x > SiO_2 \sim AlO_x$. Over time, the TOF values decrease due to mass transfer limitations occurring because of the increasing amounts of PE. Thus, using ZrO_x as a promoter allows creation of higher activity sites.
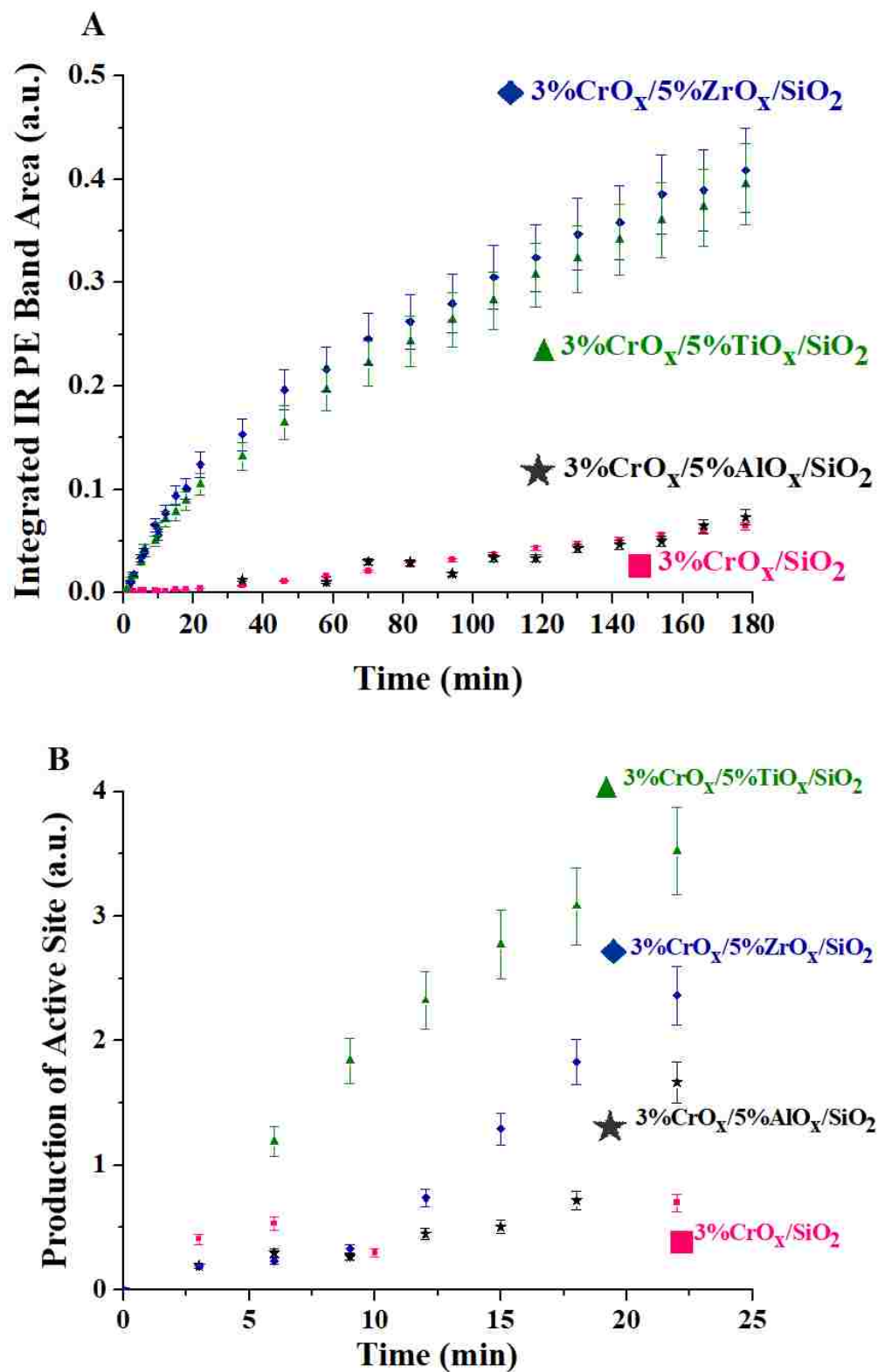
Figure 4.11. Comparison of PE and active Cr^{+3} sites produced from all $CrO_x/MO_x/SiO_2$ catalysts. (A) total PE produced; (B) initial UV-vis active sites produced.

143

Table 4.3. TOF Values Calculated from IR and UV-vis Areas at 6 min			
Catalyst	**dPE/dt**	**TOF (s^{-1})**	**Relative TOF**
CrO_x/SiO_2	3.5×10^{-6}	6.6×10^{-6}	1
$CrO_x/AlO_x/SiO_2$	$<< 1 \times 10^{-6}$	$<< 1 \times 10^{-6}$	$<< 1 \times 10^{-6}$x
$CrO_x/TiO_x/SiO_2$	1.5×10^{-4}	1.2×10^{-4}	18x
$CrO_x/ZrO_x/SiO_2$	1.2×10^{-4}	5.1×10^{-5}	77x

4.3 Discussion

4.3.1 Initial Surface CrO_x Sites on MO_x/SiO_2

The initial surface CrO_x sites on the promoted MO_x/SiO_2 supports are fully oxidized since there are Cr^{+6} UV-vis bands at 255, 348-356, and 460 nm (see Figure 4.3).[7-10] *In situ* Raman (absence of ~230 cm^{-1} band for bridging Cr-O-Cr bonds) and UV-vis (high E_g values of ~2.4-2.5 eV). No experimental evidence is present to support the presence of dimeric surface Cr_2O_x sites as proposed in literature.[1]

One distinct isolated surface CrO_x sites on silica exist in the initial oxidized catalyst: dioxo $\nu_s((O=)_2CrO_2)$ (Raman bands at ~992 and 1015 cm^{-1}).[2,6] The surface CrO_x sites preferentially bond to the Cr-O-M bridging bonds (Raman bands at ~860-900 cm^{-1}).[4]

4.3.2 Catalyst Activation

In the present study, the surface $Cr^{+6}O_x$ sites are activated by reduction with ethylene. Reduction during ethylene polymerization at 100 °C yields different reduced active sites depending upon the metal oxide promoter in the catalyst. While reduction of the standard CrO_x/SiO_2 catalyst yielded two surface Cr^{+3}_{Oh} sites,[7] reduction of the Zr-promoted catalyst yields just one type of surface Cr^{+3}_{Oh} site, since only one increasing d-d transition band is observed at ~576 nm (see Figure 4.4). On the other hand, reduction of the Al-promoted catalyst is more similar to the standard catalyst, yielding two distinct pseudo-octahedral surface Cr^{+3} surface sites assigned from two UV-vis bands at ~428 and ~618 nm. The extent of reduction is highest for the Ti-promoted catalyst since there are two bands at ~441 and ~720 nm, for one Cr^{+3}_{Oh} surface site and a mixture of Cr^{+3}_{Oh} and Cr^{+2}_{Oh} surface sites, respectively, suggesting a possible presence of three distinct surface sites. Contact of an industrially-made Cr/SiO_2 catalyst with a TEAl co-catalyst resulted in the appearance of d-

d transition bands of Cr^{+3}_{Oh} at ~625 nm and Cr^{+2}_{Oh} at ~1000 nm, which were still present after contacting with ethylene. These band maxima are different than those observed in the present study with direct ethylene contact, demonstrating that the types of activated chromia sites are not necessarily the same when the activation procedures are altered.[10]

The Raman and C_2H_4-TPSR results indicate that the surface CrO_4 sites are easily reduced in the first step ($Cr^{+6} \rightarrow Cr^{+4}$) during ethylene polymerization. The TPSR results indicate that the reduction kinetics do not change significantly with promoter oxide since the ratios of $k_{6/4}/k_{4/3/2}$ only vary ~1.5-1.8 compared to ~1.7 for the initial oxidized standard catalyst.[7] The easier reduction of Cr^{+6} to Cr^{+4} is corroborated by DFT results[12] that showed this step was thermodynamically favorable.

The UV-vis results, however, indicate a greater extent of reduction for the promoted catalysts as compared to the standard catalyst, as demonstrated by the decreasing negative Cr^{+6} LMCT bands. The presence of Cr^{+2} sites (see Figure 4.4 and Figure 4.5) in the Ti-promoted catalyst indicate that TiO_x promotion causes a greater extent of reduction.

It has been argued that the addition of titania creates new sites that are more easily reducible and thereby increase the catalytic activity.[1] DFT studies[5] have suggested that an increase in electron deficiency facilitates reduction of the surface chromia sites and results in a shorter induction period. Shifts in the peak temperatures for TPSR relate to the relative reactivity of the sites, so the peak temperatures of more reducible catalysts would be expected to shift to lower temperatures; however for the first reduction step, the peak temperatures are relatively constant (see Figure 4.6 and Table 4.2). The second reduction step is relatively easier for the Ti-promoted catalyst compared to the Zr- and Al-promoted catalysts, since T_{p2}'s for the latter occurred at relatively higher temperatures (see Figure

4.6 and Table 4.2). The peak temperatures only change slightly from those observed for the standard CrO_x/SiO_2 catalyst, shifting only slightly higher for the most active Zr-promoted catalyst, and not at all for the Ti-promoted catalyst, although it is much more active than the standard CrO_x/SiO_2 catalyst, suggesting that there is another reason for the increased activity observed with the TiO_x and ZrO_x promoter oxides. These studies indicate that for the Ti-promoted catalyst, only the extent of reduction is greater, since Cr^{+3} and Cr^{+2} reduced sites co-exist on the catalyst surface during ethylene polymerization (see Figure 4.4 and Figure 4.5).

Similar to the standard CrO_x/SiO_2 catalyst, it has been proposed that formaldehyde (HCHO) is the major oxygenated product in the activation of the CrO_x/SiO_2 catalysts.[1] However, HCHO was not detected in these measurements as an initial reaction product, in agreement with recent studies[23,24], and only combustion of ethylene was observed. More recently, however, oxygenated products were proposed to remain in the coordination sphere.[24,25] In agreement with these studies, Potter *et al.*[24] did not detect oxygenates during activation of a supported 1% Cr/SiO_2 catalyst. However, their calculated heats of reaction were high, indicating a redox process, suggesting that the oxygenates remained in the coordination sphere. To determine the nature of the surface oxygenates, the products were thermally decomposed (TPD-MS) and monitored. In addition to combustion products (water and carbon dioxide), ethylene/carbon monoxide (m/z = 28), hydrogen (m/z = 2), alkyl fragments (m/z = 15), and fragments of unsaturated hydrocarbons (m/z = 26, 27, and 41) were observed. Ethylene oxide (m/z = 29) and HCHO (m/z 29, 30, and 28) were not observed.[24] In these studies, m/z = 26 and 15 were not monitored, and the other MS traces (m/z = 41 and 2) were not observed, most likely due to the different experimental

conditions. Potter *et al.* first activated the CrO_x sites with ethylene, and then heated in Ar,[24] but in these studies, the catalyst was heated in ethylene since focus was on activation of the CrO_x sites.

4.3.3 Surface Reaction Intermediates and Initiation Mechanism

From the literature review of the studies concerning the promoted CrO_x/SiO_2 catalysts, it was apparent that most of the studies did not use *in situ* methods to study the catalyst surface, and many of the techniques used were not molecular spectroscopy (i.e. XPS or XAS).[1,26-35] As indicated in previous work,[7,9] characterization methods such as XAS or XPS which are not molecular in nature yield signals that are the average of multiple sites.[7,9] The studies in the literature also mostly focused on demonstrating how the modifications by promoters can alter activation time, activity, or polyethylene product, rather than determining how the surface of the catalyst changes from the addition of promoters and promotion mechanisms.

The current *operando* DRIFTS measurements show that the key surface intermediates present during the initiation stage of ethylene polymerization with the promoted $CrO_x/MO_x/SiO_2$ catalysts are similar to those of the standard CrO_x/SiO_2 catalyst. The Zr-promoted catalyst only contains one active surface intermediate – Cr^{+3}-$CH=CH_2$ site formed on Cr-O-Zr bridging bonds that continues to increase after ~3h, while the Ti-promoted catalyst contains two active surface sites – surface Cr^{+3}-$CH=CH_2$ site formed on Cr-O-Ti bridging bonds, which continues to grow at the end of ~3h, and the surface Cr^{+3}-$(CH_2)_2CH=CH_2$ site formed on the Cr-O-Si bonds, which appears to saturate. Although recent studies of a CrO_x/TiO_2 catalyst demonstrated that the active sites are Ti^{4-n} defect sites located in the band gap evidenced by a broad, featureless UV-vis absorbance

throughout the visible, NIR, and MIR regions,[36] in this case, the UV-vis spectra of the 5% TiO_x/SiO_2 support during ethylene polymerization does not undergo any changes, indicating that the silica support stabilizes the surface promoter titania and defect sites are not a factor.

The DRIFT spectra also exhibited bands at ~3400-3548 cm^{-1} from the interaction of the Si-OH groups and the active site through hydrogen bonding.[7,19,21] The size of the shift of the band relative to the standard catalyst may be dependent on the nature of the OH group.[21] Lee *et al.*[37] studied the surface chemistry and reactivity of several multilayered catalysts and determined that the selectivity pattern of bulk zirconia, titania, and alumina materials during CH_3OH-TPSR minimally changed when anchored on silica, and thus the intrinsic redox (HCHO), basic (CO_2), and acidic (DME) properties of each metal oxide is retained, except for TiO_x, which becomes mostly redox rather than acidic. When CrO_x was added, the selectivity during methanol TPSR reflected a much higher redox property, although a certain amount of basic and acidic property was still retained, which may explain the shift. The amount of DME, reflecting the acidic character of the catalyst, produced in the multilayer catalysts decreased in the order $SiO_2 \sim ZrO_x/SiO_2 > TiO_x/SiO_2 > AlO_x/SiO_2$.[37] The upward shift of the ~3400-3548 cm^{-1} also follows the trend $SiO_2 \sim ZrO_x/SiO_2 > TiO_x/SiO_2 > AlO_x/SiO_2$, indicating that the shift of this interaction band is derived from the acidic nature of the supports. This is also related to the amount of ethylene adsorption on the catalyst surface, so the Al-promoted catalyst would be expected to adsorb the least amount of ethylene, possibly explaining the low activity of the Al-promoted catalyst.

The similarity of the surface reaction intermediates and reduced chromia sites for the Zr- and Al-promoted CrO_x catalysts as compared to the standard CrO_x/SiO_2 catalyst suggests that the initiation reaction mechanism is also similar for these catalysts, in which the precursor site Cr^{+3}-OH transforms to Cr^{+3}-CH=CH$_2$ active site after ethylene interaction. This reaction mechanism has been proven to be a plausible pathway in recent DFT studies, with reasonable activation barriers, and the propagation steps being more kinetically favored than the termination pathways.[7,38] However, the addition of TiO_x allows for deeper reduction to Cr^{+2} sites that then re-oxidize to Cr^{+3} sites (see Figure 4.4 and Figure 4.5), indicating that the CrO_x sites are activated slightly differently in this case, although the similarity of the surface reaction intermediates still indicates that the active vinyl site forms after the Cr^{+2} sites are re-oxidized to Cr^{+3} sites.

4.3.4   Structure-Activity Relationships and Role of Promoters

The initial oxidized supported $CrO_x/MO_x/SiO_2$ catalysts consist of one distinct isolated surface chromia site: dioxo (O=)$_2$CrO$_2$. The surface dioxo CrO_4 sites are activated during ethylene polymerization to three different reduced surface sites, depending on the promoter oxide. Modifying the silica surface with ZrO_x and AlO_x causes formation of one Cr^{+3}-CH=CH$_2$, while promotion with TiO_x causes formation of two surface Cr^{+3} sites, Cr^{+3}-CH=CH$_2$ and Cr^{+3}-(CH$_2$)$_2$CH=CH$_2$. While the time-resolved evolution of the surface Cr^{+3}-CH=CH$_2$ reaction intermediate track the formation of the PE product for the Zr-promoted catalyst, the vinyl reaction intermediate only tracks the PE product formation for ~2h in the Al-promoted catalyst. Both reduced sites on the surface of the Ti-promoted catalyst track the bulk PE formation, although the Cr^{+3}-(CH$_2$)$_2$CH=CH$_2$ reaction intermediate does not form until ~45 min and saturates at the end of the ~3h, similarly to

the standard CrO_x/SiO_2 catalyst[7], suggesting it is anchored to the Cr-O-Si bridging bond and forms the higher molecular weight polymer, while the Cr^{+3}-$CH=CH_2$ site is anchored to the Ti-associated Cr-O-Ti-O-Si sites and responsible for the lower molecular weight polymer.

The Cr-O-Al bonds in the Al-promoted catalyst does not allow ethylene polymerization to take place on them, since the polymerization activity is even lower than that of CrO_x/SiO_2, and only the surface Cr^{+3}-$CH=CH_2$ site (un-shifted in position compared to standard CrO_x/SiO_2) is observed, which seems to form on the Cr-O-Si bonds, exhibiting very modest growth and appearing to saturate after just ~2h. As remarked in the introduction, according to recent DFT studies[3], formation of the mono-oxo site is thermodynamically preferred when there are two Cr-O-Al bridges and two Brönsted acid sites near each Cr center, which allows for deeper dehydration and modification from the usual square pyramidal geometry to pseudo-tetrahedral coordination that is more stable. These structural changes may explain the lack of activity for ethylene polymerization that is observed with the Al-promoted catalyst, and show that AlO_x is an inhibitor rather than a promoter. It may be that the continuing PE production observed after saturation of the Cr^{+3}-$CH=CH_2$ site is due to a surface reaction intermediate perhaps deriving from the pseudo-tetrahedral mono-oxo site which would be more symmetric, and therefore unlikely to be detected using *operando* DRIFTS, due to the selection rules.

The higher TOF exhibited by the Zr-promoted sites does not explain the higher activity observed in the Ti-promoted catalyst. Calculating the surface coverage of the metal promoter atoms demonstrates that the Ti-promoted catalyst exhibits the highest surface coverage by the Ti metal promoter atoms at ~1.1 atoms/nm^2, followed by the Al-promoted

catalyst (~0.9 Al atoms/nm^2), and finally the Zr-promoted catalyst (~0.7 Zr atoms/nm^2). With higher surface coverage by the metal promoter atom, the number of active sites would increase. Although the Ti-promoted catalyst has fewer overall active surface sites than the Zr-promoted catalyst, in the first ~20 min of ethylene time-on-stream, the Ti-promoted catalyst has a higher number of active sites (see Table 4.3). The higher activity of the vinyl sites in the cases of the Zr- and Ti-promoted catalysts compared to the standard catalyst (see Figure 4.11 and Table 4.3) also implies that they are a new kind of active site, in agreement with previous studies,[1] anchored to the Cr-O-M bonds. The increased activity of the Ti-promoted catalyst is due to both the ability of deeper reduction of the new sites, as evidenced by the combination band for Cr^{+3} and Cr^{+2}, and the slight increase in the number of active sites (both surface intermediates detected in DRIFTS are active).

4.4 Conclusions

The initial oxidized catalysts contain one distinct and isolated surface chromia species in Cr^{+6} oxidation state: the dioxo $(O=)_2CrO_2$ in tetrahedral coordination. However, the Al-promoted catalyst may also contain tetrahedral mono-oxo, which may explain its lower relative TOF. The dioxo CrO_4 site is easily activated with ethylene, and reduction kinetics indicate the first reduction step of $Cr^{+6} \rightarrow Cr^{+4}$ (~60-65%) is more facile than the second $Cr^{+4} \rightarrow Cr^{+3/+2}$ (~35-40%), in agreement with recent DFT studies.[12] Various distinct surface reaction intermediates were found after activation: promotion with TiO_x yielded both the Cr^{+3}-$(CH_2)_2CH=CH_2$ anchored to the Cr-O-Si bonds (responsible for higher molecular weight polymer) and the Cr^{+3}-$CH=CH_2$ site anchored to the Cr-O-Ti-O-Si bonds (responsible for the lower molecular weight polymer), while with ZrO_x only the Cr^{+3}-$CH=CH_2$ site anchored to Cr-O-Zr bonds results, and promotion with AlO_x yields one

Cr^{+3}-CH=CH$_2$ site that is not very active since it saturates after ~2h. The progressions of the reaction intermediates on the surfaces of the Zr- and Ti-promoted catalysts track the evolution of the bulk PE produced, implying they are active reaction intermediates. The promotion mechanisms differ depending on the promoter metal. While TiO_x promotes the creation of a higher number of active sites, ZrO_x exhibits a higher initial TOF. Addition of AlO_x inhibits ethylene polymerization.

Acknowledgements

Chapter 4 References

1. McDaniel, M. P. A Review of the Phillips Supported Chromium Catalyst and Its Commercial Use for Ethylene Polymerization. *Advances in Catalysis* **2010**, *53*, 123-606.

2. Handzlik, J.; Grybos, R.; Tielens, F. Structure of Monomeric Chromium(VI) Oxide Species Supported on Silica: Periodic and Cluster DFT Studies. *J. Phys. Chem. C* **2013**, *117*, 8138-8149.

3. Handzlik, J.; Grybos, R.; Tielens, F. Isolated Chromium(VI) Oxide Species Supported on Al-Modified Silica: A Molecular Description. *J. Phys. Chem. C* **2016**, *120*, 17594-17603.

4. Lee, E. L.; Wachs, I. E. Molecular Design and In Situ Spectroscopic Investigation of Multilayered Supported $M_1O_x/M_2Ox/SiO_2$ Catalysts. *J. Phys. Chem. C* **2008**, *112*, 20418-20428.

5. Guesmi, H.; Tielens, F. Chromium Oxide Species Supported on Silica: A Representative Periodic DFT Model. *J. Phys. Chem. C* **2012**, *116*, 994-1001.

6. Lee, E. L.; Wachs, I. E. In Situ Spectroscopic Investigation of the Molecular and Electronic Structures of SiO_2 Supported Surface Metal Oxides. *J. Phys. Chem. C* **2007**, *111*, 14410-14425.

7. Chakrabarti, A.; Gierada, M.; Handzlik, J.; Wachs, I. E. Operando Molecular Spectroscopy During Ethylene Polymerization by Supported CrO_x/SiO_2 Catalysts: Active Sites, Reaction Intermediates, and Structure-Activity Relationship. *Top. Catal.* **2016**, *59*, 725-739.

8. Weckhuysen, B. M.; Wachs, I. E.; Schoonheydt, R. A. Surface Chemistry and Spectroscopy of Chromium in Inorganic Oxides. *Chem. Rev.* **1996***, 96*, 3327-3349.

9. Chakrabarti, A.; Wachs, I. E. The Nature of CrOₓ Sites in Different Environments. *Catal. Lett.* **2015***, 145*, 985-994.

10. Cicmil, D.; van Ravenhorst, I. K.; Meeuwissen, J.; Vantomme, A.; Weckhuysen, B. M. Structure-performance relationships of Cr/Ti/SiO$_2$ catalysts modified with TEAl for oligomerisation of ethylene: tuning the selectivity towards 1-hexene. *Catal. Sci. Tech.* **2016***, 6*, 731-743.

11. Weckhuysen, B. M.; Verberckmoes, A. A.; De Baets, A. R.; Schoonheydt, R. A. Diffuse Reflectance Spectroscopy of Supported Chromium Oxide Catalysts: A Self-Modeling Mixture Analysis. *J. Catal.* **1997***, 166*, 160-171.

12. Gierada, M.; Michorczyk, P.; Tielens, F.; Handzlik, J. Reduction of chromia-silica catalysts: A molecular picture. *J. Catal.* **2016***, 340*, 122-135.

13. Pouet, M. -.; Baures, E.; Vaillant, S.; Thomas, O. Hidden Isosbestic Point(s) in Ultraviolet Spectra. *Appl. Spectrosc.* **2004***, 58*, 486-490.

14. Redhead, P. A. Thermal Desorption of Gases. *Vacuum* **1962***, 12*, 203-211.

15. National Institute of Standards and Technology NIST Chemistry WebBook. *http://webbook.nist.gov/chemistry/*.

16. Groppo, E.; Lamberti, C.; Bordiga, S.; Spoto, G.; Damin, A.; Zecchina, A. FTIR Investigation of the H$_2$, N$_2$, and C$_2$H$_4$ Molecular Complexes Formed on the Cr(II) Sites in the Phillips Catalyst: a Preliminary Step in the understanding of a Complex System. *J. Phys. Chem. B* **2005***, 109*, 15024-15031.

17. Groppo, E.; Lamberti, C.; Bordiga, S.; Spoto, G.; Zecchina, A. In situ FTIR spectroscopy of key intermediates in the first stages of ethylene polymerization on the Cr/SiO$_2$ Phillips catalyst: Solving the puzzle of the initiation mechanism? *J. Catal.* **2006***, 240*, 172-181.

18. Groppo, E.; Estephane, J.; Lamberti, C.; Spoto, G.; Zecchina, A. Ethylene, propylene and ethylene oxide in situ polymerization on the Cr(II)/SiO$_2$ system: A temperature- and pressure-dependent investigation. *Catal. Today* **2007***, 126*, 228-234.

19. Barzan, C.; Groppo, E.; Quadrelli, E. A.; Monteil, V.; Bordiga, S. Ethylene polymerization on a SiH$_4$-modified Phillips catalyst: detection of *in situ* produced a-olefins by operando FT-IR spectroscopy. *Phys. Chem. Chem. Phys.* **2012***, 14*, 2239-2245.

20. Vuurman, M.; Wachs, I. E.; Stufkens, D. J.; Oskam, A. Characterization of chromium oxide supported on Al$_2$O$_3$, ZrO$_2$, TiO$_2$, and SiO$_2$ under dehydrated conditions. *J. Mol. Catal.* **1993***, 80*, 209-227.

21. Davydov, A. *Molecular Spectroscopy of Oxide Catalyst Surfaces;* John Wiley & Sons Ltd.: West Sussex, England, 2003.

22. Socrates, G. *Infrared and Raman Characteristic Group Frequencies: Tables and Charts;* John Wiley & Sons Ltd: West Sussex, England, 2001.

23. Barzan, C.; Damin, A. A.; Budnyk, A.; Zecchina, A.; Bordiga, S.; Groppo, E. Pre-reduction of the Phillips Cr^{VI}/SiO$_2$ catalyst by cyclohexene: A model for the induction period of ethylene polymerization. *J. Catal.* **2016***, 337*, 45-51.

24. Potter, K. C.; Beckerle, C. W.; Jentoft, F. C.; Schwerdtfeger, E.; McDaniel, M. P. Reduction of the Phillips catalyst by various olefins: Stoichiometry, thermochemistry, reaction products and polymerization activity. *J. Catal.* **2017**, *344*, 657-668.

25. Barzan, C.; Piovano, A.; Braglia, L.; Martino, G. A.; Lamberti, C.; Bordiga, S.; Groppo, E. Ligands Make the Difference! Molecular Insights into Cr^{VI}/SiO_2 Phillips Catalyst during Ethylene Polymerization. *J. Am. Chem. Soc.* **2017**, Ahead of Print.

26. McDaniel, M. P. Supported Chromium Catalysts for Ethylene Polymerization. *Advances in Catalysis* **1985**, *33*, 47-98.

27. Conway, S. J.; Falconer, J. W.; Rochester, C. H. Chromia/Silica-Titania Cogel Catalysts for Ethene Polymerisation Kinetics. *Journal of Chemical Society, Faraday Transactions 1* **1989**, *85*, 71-78.

28. Conway, S. J.; Falconer, J. W.; Rochester, C. H. Chromia/Silica-Titania Cogel Catalysts for Ethene Polymerisation IR Study. *Journal of Chemical Society, Faraday Transactions 1* **1989**, *85*, 79-90.

29. Conway, S. J.; Falconer, J. W.; Rochester, C. H. Chromia/Silica-Titania Cogel Catalysts for Ethene Polymerisation Polymer Characteristics. *Journal of Chemical Society, Faraday Transactions 1* **1989**, *85*, 1841-1851.

30. Finch, J. N. Reduction Studies on Supported Chromic Anhydride Catalysts. *Journal of Catalysis* **1976**, *43*, 111-121.

31. Holm, V. C. F.; Clark, A. Reduction Studies on Supported Metal Oxide Catalysts. *Journal of Catalysis* **1968**, *11*, 305-316.

32. Ellison, A.; Overton, T. L. Characterisation of Cr/Silica Catalysts. *Journal of Chemical Society Faraday Transactions* **1993**, *89*, 4393-4395.

33. Ellison, A.; Overton, T. L. Characterisation of modified Cr-silica catalysts. *Journal of Molecular Catalysis* **1994**, *90*, 81-86.

34. Ma, Y.; Wang, L.; Liu, Z.; Cheng, R.; Zhong, L.; Yang, Y.; He, X.; Fang, Y.; Terano, M.; Liu, B. High-resolution XPS and DFT investigations into Al-modified Phillips CrO_x/SiO_2. *J. Mol. Catal. A: Chem.* **2015**, *401*, 1-12.

35. Cheng, R.; Xu, C.; Liu, Z.; Dong, Q.; He, X.; Fang, Y.; Terano, M.; Hu, Y.; Pullukat, T. J.; Liu, B. High-resolution spectroscopy (XPS, ^{1}H MAS solid-state NMR) and DFT investigations into Ti-modified Phillips CrO_x/SiO_2 catalysts. *Journal of Catalysis* **2010**, *273*, 103-115.

36. Barzan, C.; Groppo, E.; Bordiga, S.; Zecchina, A. Defect Sites in H_2-Reduced TiO_2 Convert Ethylene to High Density Polyethylene without Activator. *ACS Catal.* **2014**, *4*, 986-989.

37. Lee, E. L.; Wachs, I. E. Surface chemistry and reactivity of well-defined multilayered supported $M_1O_x/M_2O_x/SiO_2$ catalysts. *J. Catal.* **2008**, *258*, 103-110.

38. Gierada, M.; Handzlik, J. Active sites formation and their transformations during ethylene polymerization by the Phillips CrO_x/SiO_2 catalyst. *J. Catal.* **2017**, *352*, 314-328.

Chapter 4 Supporting Information
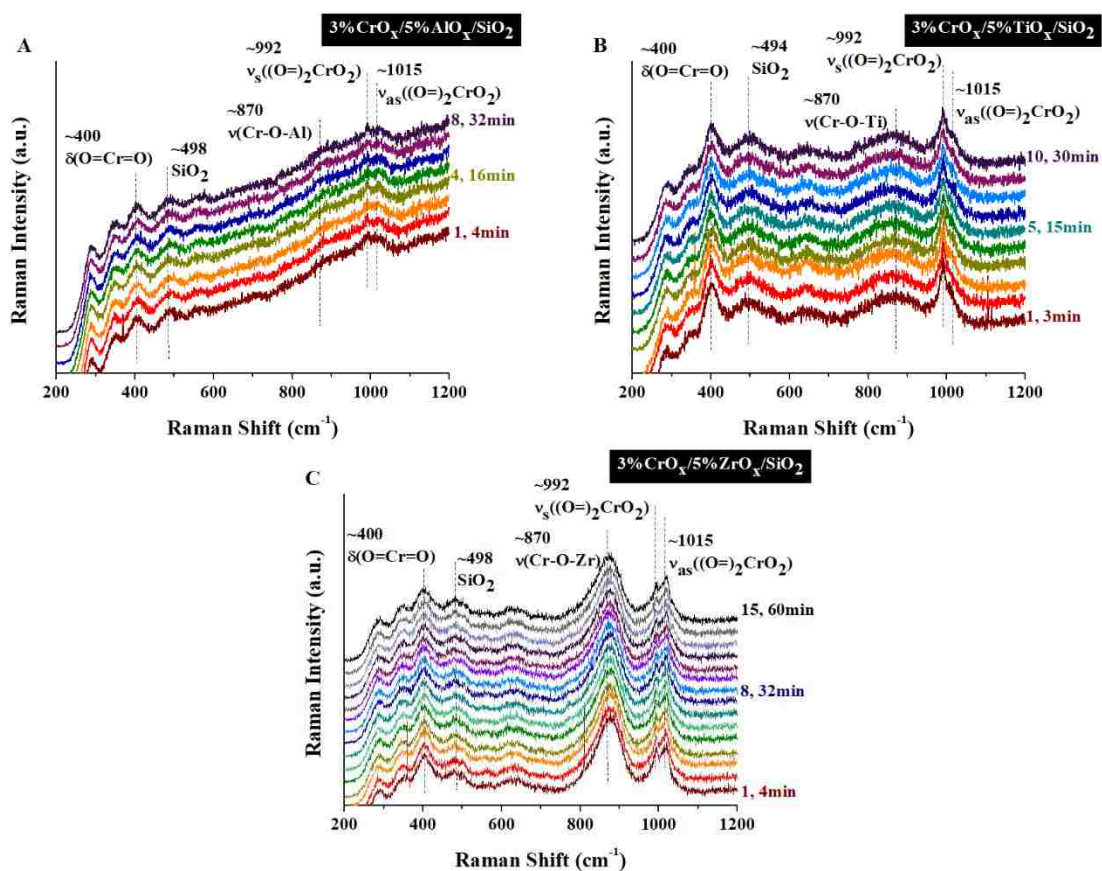
Figure S 4.1. *In situ* Raman spectra of the initial oxidized supported $CrO_x/MO_x/SiO_2$ catalysts in flowing 5% O_2/He at 100 °C. The spectra were taken with a 442 nm wavelength laser (20% laser power) and a moving stage. (A) 3% CrO_x/5% AlO_x/SiO_2 (8 scans x 4min); (B) 3% CrO_x/5% TiO_x/SiO_2 (10 scans x 3 min); (C) 3% CrO_x/5% ZrO_x/SiO_2 (15 scans x 4 min).
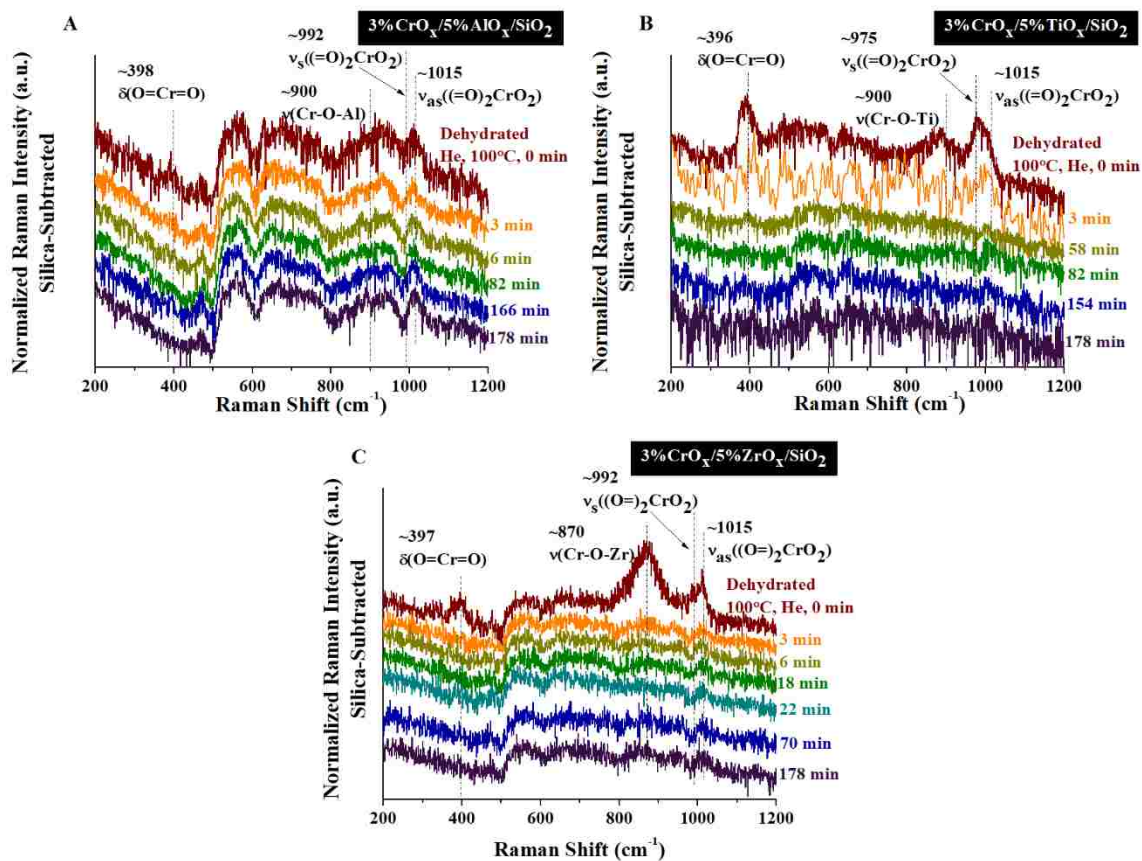
Figure S 4.2. Time-resolved *in situ* Raman spectra of the supported promoted $CrO_x/MO_x/SiO_2$ catalysts taken in flowing 1% C_2H_4/Ar at 100 °C. The spectra were taken with a 442 nm wavelength laser (D2 filter, 1% power). (A) 3% CrO_x/5% AlO_x/SiO_2; (B) 3% CrO_x/5% TiO_x/SiO_2; (C) 3% CrO_x/5% ZrO_x/SiO_2.
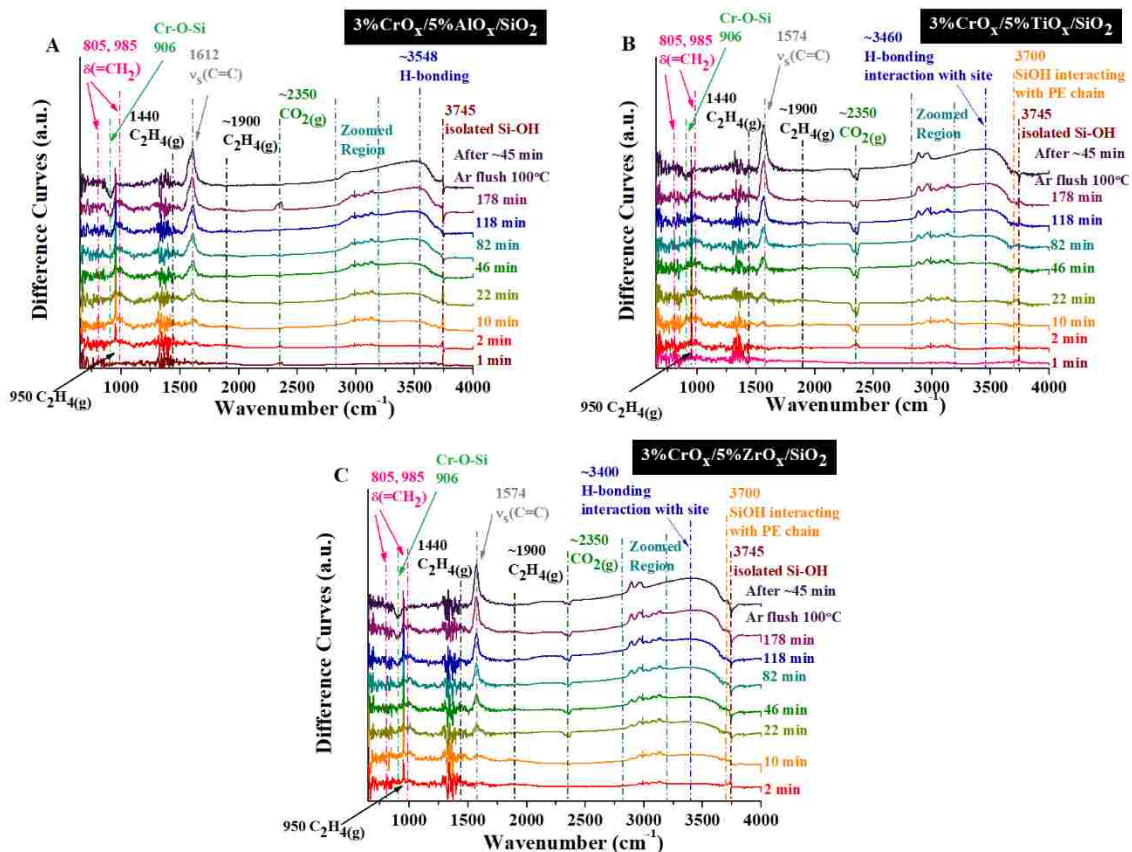
Figure S 4.3. Time-resolved *in situ* DRIFT spectra of the C-H region for the supported promoted CrO_x/SiO_2 catalysts (A) 3% CrO_x/5% AlO_x/SiO_2, (B) 3% CrO_x/5% TiO_x/SiO_2, (C) 3% CrO_x/5% ZrO_x/SiO_2 during ethylene polymerization at 100 °C with an Ar flush after ~3 h.
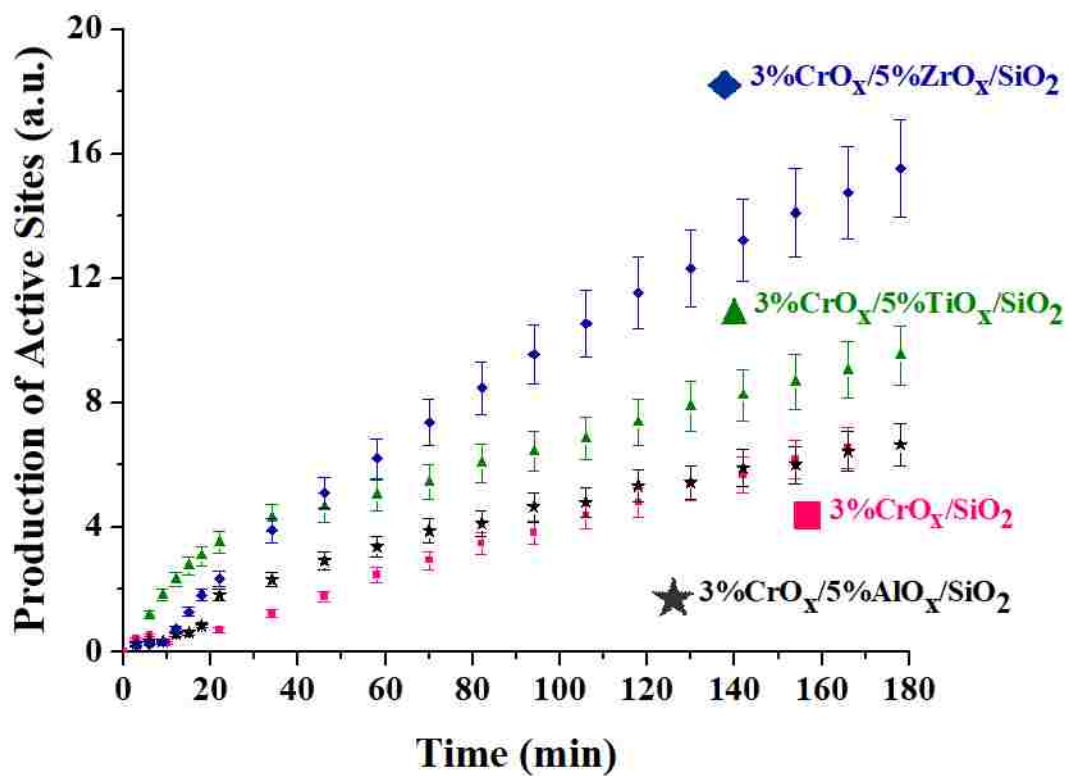
Figure S 4.4. Relative number of active sites produced by supported CrO_x/SiO_2 catalysts for ethylene polymerization. The active sites were taken from the areas of the UV-vis bands.

Chapter 5 | **Literature Review of Olefin Metathesis by Supported MoO$_x$/Al$_2$O$_3$**

    Catalysts

Abstract

The literature of olefin metathesis by heterogeneous supported MoO$_x$/Al$_2$O$_3$ catalysts is reviewed. The current global shortage of propylene has increased the interest in on-purpose propylene production by olefin metathesis. This literature review demonstrates that although there have been numerous studies conducted on olefin metathesis by MoO$_x$/Al$_2$O$_3$ catalysts, little progress has been made in the elucidation of the fundamental details of the catalyst, including the molecular structures and oxidation states of the catalytic active sites, surface reaction intermediates, reaction mechanism, and role of promoters. Thus far, there have only been a few applications of *in situ* and *operando* spectroscopy techniques, and using a combination of these modern techniques in systematic studies will greatly improve fundamental understanding of olefin metathesis by supported MoO$_x$/Al$_2$O$_3$ catalysts.

5.1 Introduction

Olefin metathesis is the cleavage and reformation of olefinic double bonds.[1] Olefin metathesis by molybdena catalysts was originally discovered by Banks and Bailey at Phillips Petroleum using heterogeneous alumina-supported molybdenum catalysts to transform two molecules of propylene into one ethylene and one butene molecule, and first commercialized in 1966 and dubbed the Phillips Triolefin Process.[2] The reversibility of the olefin metathesis reaction also allows for propylene to be produced from ethylene and butene, now known as olefins conversion technology (OCT).[1,3] Heterogeneous supported MoO$_x$/Al$_2$O$_3$ catalysts are used in the Shell Higher Olefin Process (SHOP), which was

established in 1968.[3-5] The SHOP process is used to produce linear higher olefins from ethylene and consists of three main stages – oligomerization (homogeneous nickel-phosphine catalyst in a polar solvent), isomerization (solid potassium metal catalyst), and olefin metathesis (alumina-supported molybdate catalyst) – to convert ethylene into linear higher olefins.[3] The current high global demand for propylene and higher olefins is projected to significantly increase in the future, indicating the continued importance of olefin metathesis.[6-8]

5.2   Structure of the MoO_x/Al_2O_3 Catalysts in the Initial Oxidized Catalyst

The molecular structure of molybdenum oxide in initial oxidized supported MoO_x/Al_2O_3 catalysts has been established in recent years using *in situ* Raman[9-12], UV-vis[9,12], XAS spectroscopy[10-12], and DFT calculations[13-15]. At low surface coverage ($< \sim 1$ Mo atoms/nm^2), only isolated surface dioxo $(O=)_2MoO_2$ species are present on oxidized, dehydrated supported MoO_x/Al_2O_3 catalysts. At intermediate surface coverage (~ 1-4.5 Mo atoms/nm^2), both isolated dioxo $(O=)_2MoO_2$ and oligomeric mono-oxo $O=MoO_4$ surface species co-exist on the alumina support. Above monolayer surface coverage (>4.6 Mo atoms/nm^2), crystalline MoO_3 nanoparticles (NPs) form since there are no remaining exposed Al-OH sites to which the MoO_x species can anchor on the support.[9]

Periodic DFT calculations of MoO_x sites on alumina have provided some insights into the more stable oxidized MoO_x and activated species.[13] It was concluded that under strictly dehydrating conditions, a square pyramidal mono-oxo site is dominant on the most exposed alumina (110) surface, but that 4- and 5-coordinated dioxo sites are most likely present on the minor alumina (100) surface. The presence of 3-fold bonded mono-oxo sites (especially on the (100) surface), however, cannot be excluded. Periodic DFT calculations of dimeric

Mo(VI) sites on the (100) and (110) surfaces of alumina[14] predicted that the most stable

dimeric species on the (100) plane are mixed dioxo-mono-oxo (dimer possessing one dioxo

fragment and one mono-oxo fragment) or double mono-oxo structures that are 3-, 4-, or at

most 5-fold bonded to the surface, and the Mo in these exhibits mostly MoO_4 coordination.

When the energetic stabilities of the monomeric species were compared to those of the

dimeric structures on the alumina (100) surface, it was determined that the dimeric

structures were always more stable than their monomeric analogues and, therefore, Mo

oligomer chains are expected to exist on the alumina (100) surface. On the alumina (110)

surface, however, the most stable dimeric structures are double-mono-oxo that are 6- or 5-

fold bonded to the surface, and these are most frequently in distorted square pyramidal

geometry, although distorted MoO_6 or distorted MoO_4 may also be present. The

monomeric structures are more stable than the dimeric structures on the alumina (110)

plane. Thus, even at high Mo oxide surface coverage, the monomeric Mo species are still

present on the alumina (110) surface and will co-exist with the oligomeric molybdate

species.

The absence of reported *in situ* characterization studies that directly probe activated

supported MoO_x/Al_2O_3 catalysts during olefin metathesis has hampered the establishment

of the fundamental details of this important heterogeneous catalyst system and comparison

of experimental data with findings from DFT calculations.

5.3   Anchoring Al-OH Sites of the MoO$_x$ Sites

In situ IR studies of supported MoO_x/Al_2O_3 catalysts synthesized from decomposition

of $Mo(CO)_6$ on Al_2O_3[16] and of reaction of $MoO_2(acac)_2$ with alumina[17] found a preferential

consumption of the surface hydroxyl IR band at 3740 cm^{-1} (tentatively assigned to more

basic hydroxyls and subsequently assigned to the basic HO-μ_1-Al$_{IV}$ surface hydroxyls by Digne and Sautet via DFT studies)[18,19].

5.4 Nature of the Activated Supported MoO$_x$/Al$_2$O$_3$ Catalysts

In contrast to the detailed molecular information about oxidized, dehydrated supported MoO$_x$/Al$_2$O$_3$ catalysts from *in situ* characterization studies, little is known concerning the structures of the activated MoO$_x$ surface sites during olefin metathesis.

5.4.1 Activation with Olefins

In the earliest characterization studies, activated MoO$_x$ surface sites on Al$_2$O$_3$ were exposed to propylene metathesis reaction conditions and subsequently exposed to ambient conditions and examined with *ex situ* XPS and EPR spectroscopy[20,21]. These studies detected both Mo^{+6} and Mo^{+4} oxidation states, and it was suggested that other Mo oxidation states are not active for olefin metathesis. From *ex situ* solid-state ^{27}Al NMR of mesoporous Al$_2$O$_3$-supported MoO$_x$ catalysts[22], it was proposed that surface MoO$_x$ sites anchored to AlO$_6$ sites are the most active sites. However, these *ex situ* spectroscopic studies are irrelevant since the catalysts were exposed to O$_2$ and moisture that compromised the molybdena oxidation states and structures present during olefin metathesis.

5.4.2 Activation with CO or H$_2$

Reduction with CO suggested that the surface MoO$_x$ sites anchored at basic surface hydroxyls are not active and do not reduce at 500 °C, although surface MoO$_x$ sites anchored at non-basic surface hydroxyls are active and do reduce to Mo^{+4} sites.[23-28]

Gruenert *et al.*[20,21] examined alumina-supported molybdena catalysts for propylene metathesis activity by initial activation with H$_2$ or thermal treatment in Ar and employed XPS to determine the resulting Mo oxidation states.[21] The resulting H$_2$-activated catalysts

were subsequently examined for propylene metathesis at 200 °C using a conventional flow reactor, and it was concluded that the surface molybdena sites derived from Mo^{+4} or Mo^{+6} sites are active for metathesis. Other studies by Klimov *et al.*[29] investigated the oxidation states of conventional supported MoO_x/Al_2O_3 catalysts by first activating the catalysts with CO or H_2 at 500 °C, testing the propylene metathesis activity at room temperature, and subsequently pulsing oxygen to determine the oxidation state by oxygen consumption. The estimated Mo oxidation state was found to decrease with increasing Mo loading (1.4% Mo/Al_2O_3 (Mo^{+5}), 3.3% Mo/Al_2O_3 (Mo^{+4}), and 6.2% Mo/Al_2O_3 (Mo^{+2})). These findings, however, are clouded by the presence of surface $Mo=CH_2$ and $Mo=CHCH_3$ reaction intermediates after the metathesis reaction that may contribute to O_2 consumption and yield results suggesting deep reduction of the surface MoO_x sites (e.g., Mo^{+2}).

5.4.3 Density Functional Theory (DFT) Studies

DFT calculations of the active sites (Mo-methylidene structures variously located on the (100) and (110) surfaces of alumina)[23,30] determined that the relative stabilities of the surface MoO_x sites on Al_2O_3 depend on temperature and water vapor pressure, and that the location of the MoO_x active site on the alumina surface influences the reactivity towards ethylene addition. The studies also predicted that Mo sites on the alumina (110) surface are more stable than the analogous structures on the alumina (100) surface.

On the alumina (100) surface[23], it was determined that if the Mo-methylidene replaces two basic OH groups anchored to AlO_6 sites, ethylene addition is endothermic with a relatively high activation energy. However, if there is replacement of only one basic OH, and the Mo is also directly bonded to a bridging oxygen of the alumina surface, the site is less stable, the electron density of the active site moiety decreases, and the geometry is

more suitable for alkene addition. Similar findings were determined from cluster studies comparing the reactivity of monomeric and dimeric Mo-methylidene structures on the (100) and (110) surfaces.[31] These cluster studies also showed that both the MoO_x monomers and dimers can be active sites. Although the activation energies for ethylene addition were close for both types of sites, the activation energy was found to be more facile for the dimeric sites (more exothermic). The DFT studies also concluded that the monomeric sites are less likely to be the active sites, since they are more likely to undesirably transform the active trigonal bipyramidal molybdacyclobutane complex into a more stable square pyramidal molybdacyclobutane structure. The exact activation pathways of the surface MoO_x active sites on Al_2O_3 were not discussed in these DFT studies.

5.5   Surface Reaction Intermediates During Olefin Metathesis

Not much is known concerning the surface reaction intermediates during olefin metathesis. Early *in situ* studies[16] concluded that propylene becomes π-bonded to oxidized and CO-reduced catalyst surface of the MoO_x/Al_2O_3 catalysts. An IR band at 1600 cm^{-1} was seen and assigned to the C=C bond of the π-bond, which was red-shifted from the band seen at 1645 cm^{-1} when propylene is adsorbed on pure Al_2O_3. It was, thus, concluded that the adsorption of propylene is reversible, and that this π-bonded complex could be a reaction intermediate during propylene metathesis. These early studies did not consider that propylene directly adsorbs on the Al_2O_3 support and no attempt was made to distinguish between propylene bonded to Mo sites and Al sites.

From DFT studies[30], it has been suggested also that Mo-cyclobutane intermediates anchored to AlO_6 cause the high reactivity. However, cyclic intermediates are usually less

stable surface species.[12] To conclusively determine the surface intermediates and discriminate between active and spectator surface reaction intermediates, transient experiments are needed.[12]

5.6 Number of Catalytic Active Sites

Studies in the literature concerning the number of catalytic active sites for olefin metathesis have reported that as little as 1%, but also as high as 15%, of the surface MoO_x sites are involved in the metathesis reaction.[32,33] Early studies using $Mo(CO)_6/Al_2O_3$ at 53 °C[34] concluded that only 1% of the surface MoO_x sites are active in the metathesis reaction. However, using NO poisoning experiments, other studies[32] concluded for a Co--promoted MoO_x/Al_2O_3 catalyst that at room temperature, 15% of the surface MoO_x sites were active. Yet another group[33] concluded that only 1% of the MoO_x sites are active at 50 °C, but that promoting with Sn allowed 4.5% of the MoO_x sites to be active at 50 °C.

These discrepancies are due to inconsistencies in catalyst preparation and a range of surface MoO_x coverages. Additionally, as seen in recent work with supported ReO_x/Al_2O_3 catalysts for olefin metathesis[35-37], the activation temperature and olefin partial pressure can have a significant effect on the number of activated surface MoO_x sites.

5.7 Surface Kinetics and Reaction Mechanism

The studies in literature found that the supported MoO_x/Al_2O_3 showed the highest activity at about monolayer coverage.[38,39] Thus, it was assumed that the active surface MoO_x sites that are most likely either isolated or oligomeric, and not MoO_3 or $Al_2(MoO_4)_3$ nanoparticles, since at above monolayer coverage both of the latter tend to form. However, the structures of the active sites and the structure-activity/selectivity relationship of these isolated and oligomeric sites are still unknown.

Isotope exchange studies proposed that the initiation mechanism for the olefin metathesis of long chain olefins by supported MoO_x/Al_2O_3 catalysts proceeds via surface π-allyl species.[40] This suggests that a C-H bond could be involved. However, transient isotope studies are needed to provide additional details about the active reaction intermediates and spectator species.

5.8 Promoters

The standard MoO_x/Al_2O_3 catalysts have often been modified with a promoter. The specific roles of these promoters have not yet been elucidated, although surface modification by SiO_2 [39,41-43], MCl_4 (M = Si or Ge)[44], CoO[32], and $(CH_3)_4Sn$[33] are claimed to increase the number of active sites. The promotion mechanisms, however, are still not understood.

It has been claimed that olefin metathesis activity is improved by using mixed SiO_2-Al_2O_3[12,39,41-43,45-49] or zeolite[12,50-52] supports. Debecker et al.[39,41-43,45,46] proposed that using alternative catalyst synthesis methods improved catalytic activity of propylene metathesis as compared to that of standard SiO_2-Al_2O_3 supported MoO_x catalysts prepared via the traditional incipient wetness impregnation. Methods included nonhydrolytic sol-gel route in a non-aqueous medium[42], thermal spreading[39], flame pyrolysis[43], and one-pot aerosol synthesis. It was claimed that the superior activity of the alternatively prepared catalysts was due to higher MoO_x dispersion that lowered the amount of inactive MoO_3 crystalline nanoparticles formed, as well as the presence of more monomeric MoO_x sites. In studies of the catalysts synthesized via flame pyrolysis, an inverse relationship between the metathesis activity and number of Mo-O-Mo bonds was claimed to exist, and thus, the monomeric species were proposed to be the active sites.[12,43] In studies of a one-pot aerosol

synthesis of MoO_x-SiO_2-Al_2O_3 from an aqueous solution of tetraethyl orthosilicate and ethanol with block copolymer (Brij58), $AlCl_3$, $12MoO_3H_3PO_4 \bullet xH_2O$, or $MoCl_5$[12,45,46], the catalysts displayed higher activity compared to traditionally synthesized catalysts, and NMR detected no $Al_2(MoO_4)_3$ or MoO_3 crystals.

Ex situ EPR was used to detect surface Mo^{+5} possessing MoO_5 or MoO_6 coordination after exposure to propylene metathesis conditions and subsequent evacuation at room temperature and 200 °C.[47] However, EPR does not detect other Mo oxidation states, such as Mo^{+4}, and no other methods were used to detect active oxidation states. Complementary *ex situ* L_3-XANES of fresh and spent catalysts suggested that the active surface MoO_x consist of poorly formed oligomeric species containing some partially reduced Mo cations. The use of *ex situ* techniques means that the measurements are performed after reaction on samples that are evacuated and exposed to moisture in the ambient atmosphere, making them irrelevant. Furthermore, these spectroscopic findings are dominated by just one Mo oxidation state. For instance, Mo^{+5} is dominant in EPR, while XANES is dominated by Mo^{+6} sites since only a minority of MoO_x sites are expected to be reduced. Thus, there is a need for spectroscopic techniques that can directly characterize the catalyst during olefin metathesis.

In other studies of the metathesis of ethylene and butene to propylene, it was proposed that SiO_2-Al_2O_3 supported molybdena catalysts exhibited higher activity in olefin metathesis due to Brönsted acidity, with the most efficient catalysts containing moderate MoO_x loadings.[12,48-52] Side reactions such as cracking and isomerization were attributed to excessive Brönsted acidity.[50-52] Li *et al.*[50-52] proposed the existence of an interfacial interaction between MoO_x sites and the Hβ zeolite, and the addition of Al_2O_3 to the support

may stabilize the zeolite support. ^{27}Al MAS NMR in initial studies[50] showed that the Hβ zeolite dealuminated, forming crystalline $Al_2(MoO_4)_3$ (corroborated by XRD measurements). The amount of silanols and Brönsted acid sites decreased with increasing Mo coverage, according to corresponding ^{29}Si and ^{1}H MAS NMR, and the catalytic activity of ethylene and butene metathesis decreased. In later studies[51,52], the catalytic activity improved with the addition of Al_2O_3 to the Hβ zeolite (optimal catalyst 4-6 wt% MoO_x/70 wt% Hβ-30 wt% Al_2O_3). Hyperpolarized [129]Xe NMR, HR TEM, and SEM results demonstrated that the Mo species disperse in the Al_2O_3 rather than in the zeolites. It was thus proposed that the addition of Al_2O_3 to Hβ zeolite supports helps maintain the zeolitic structure, and therefore the presence of Brönsted acid sites, since dealumination of the framework and appearance of $Al_2(MoO_4)_3$ crystals did not occur.[50-52]

Hahn *et al.*[48,49] also proposed that Brönsted acidity increases the catalytic activity of supported MoO_x catalysts for the metathesis of ethylene and butene to propylene. They suggested that tetrahedral MoO_x species possessing Brönsted acid character are only created on supports with Brönsted acidity, while polymeric Brönsted acidic octahedral MoO_x sites can be created on supports without any Brönsted acid character. *In situ* UV-vis and ambient Raman spectroscopy results were correlated and detected isolated MoO_4 and polymeric MoO_6 sites. It was proposed that increasing the Brönsted acidity of these sites is the cause of the higher metathesis activity.[48] However, it has been proven unequivocally that there are issues with comparing ambient and *in situ*, since the surface structures vary significantly depending on the moisture content.[9,12] In another study, it was reported that the side reactions (self-metathesis of butene and 2 to 1 butene isomerization) are more favorable for isolated species, while metathesis is preferred over polymeric species.[12,49]

These conclusions were in contradiction with earlier studies by Li *et al.* showing that higher Brönsted acidity increased the amount of side reactions.[12,50-52] Thus, it is clear that more systematic *in situ* studies are necessary to determine the promotion mechanisms for the SiO_2-Al_2O_3 and zeolite surfaces.

5.9 Patents

The prolific patent literature demonstrates the recent increased importance of the olefin metathesis reaction to industry.[4,5,12,53-87]

Mostly γ-Al_2O_3 support is used, although mesoporous alumina[53,76] and silica-alumina[79,88] supports have also been claimed to be effective. The catalysts have also been treated with various promoters, such as halides[71], B_2O_3[76], CoO[80]; alkyl-Sn[81]; and alkyl-Pb[72,81]. The patent literature indicates interest in metathesis of smaller olefins[53,60-65,67,71,80,82-85] as well as higher olefins such as used in the SHOP process[3-5,55,68-70,74,75,77-79,87].[12]

5.10 Summary and Conclusions

The literature review of olefin metathesis by supported MoO_x/Al_2O_3 catalysts demonstrates that despite the significant industrial applications, there is still a lack of fundamental understanding in the literature of this catalyst technology. The absence of molecular level information of heterogeneous supported molybdena catalysts during catalyst activation and the olefin metathesis reaction has hindered the fundamental progress. Systematic *in situ* and *operando* molecular spectroscopy studies would greatly improve the fundamental understanding of the heterogeneous alumina supported molybdena catalysts for olefin metathesis, providing a foundation for the rational design of improved catalysts for this catalytic reaction system.

The objective of this research is to determine the molecular/electronic structure-catalytic activity/selectivity relationships for heterogeneous supported molybdena-based olefin metathesis catalysts by combining modern methods of time-resolved *in situ* and *operando* molecular/electronic spectroscopic techniques both during catalyst activation and under reaction conditions. The resulting experimental findings will be combined with theory to develop a fundamental structure-activity model with predictive capabilities, and the resulting model will guide the rational design of improved olefin metathesis catalysts.

5.11 Thesis Outline – Olefin Metathesis

The above literature review indicates the need for elucidation of fundamental details for olefin metathesis by heterogeneous supported MoO_x/Al_2O_3 catalysts to achieve understanding of structure-reactivity/selectivity relationships. This will be achieved by combining multiple *in situ* spectroscopic techniques capable of directly characterizing the catalyst under relevant olefin metathesis conditions. The chapters pertaining to olefin metathesis are outlined below.

Chapter 6: Molecular Structure-Reactivity Relationships for Olefin Metathesis by Supported MoO_x/Al_2O_3 Catalysts

A series of synthesized MoO_x/Al_2O_3 will be characterized before and during olefin metathesis reaction conditions. The molecular structure, electronic transitions, and catalytic reactivity will be determined using *in situ* Raman spectroscopy, *in situ* UV-vis

DRS, *in situ* DRIFTS, and TPSR-MS. This will allow for development of the molecular structure-reactivity relationships of MoO_x/Al_2O_3 catalysts for olefin metathesis.

Chapter 7: Activation Mechanism and Surface Intermediates for Olefin Metathesis by Supported MoO$_x$/Al$_2$O$_3$ Catalysts

The activation mechanism and surface intermediates for the supported MoO_x/Al_2O_3 catalysts during olefin metathesis will be examined. A variety of experiments will be presented, primarily using *in situ* DRIFTS to detect the surface intermediates during reaction. Results from C_4H_8-C_2H_4 titration, C_3H_6 adsorption-TP, C_3H_8O adsorption-C_3H_6 TP, C_3H_6O adsorption-C_3H_6 TP, and C_3D_6-C_3H_6 isotope exchange studies will be correlated.

Chapter 8: Conclusions

The important conclusions of the research presented in this dissertation will be summarized. Future work for both ethylene polymerization and olefin metathesis will be discussed. A general perspective on the similarities between these two industrial reactions will be given.

Chapter 5 References

1. Rouhi, A. M. Olefin Metathesis: Big-Deal Reaction. *C&EN* **2002**, *80*, 29-33.

2. Banks, R. L. Olefin Metathesis: Technology and Applications. In *Applied Industrial Catalysis*; Leach, B. E., Ed.; Academic Press: Orlando, FL, 1984; pp 215-239.

3. Mol, J. C. Industrial applications of olefin metathesis. *J. Mol. Catal. A: Chem.* **2004**, *213*, 39-45.

4. Brown, D. S.; Ginestra, J. M. Metathesis catalyst and process. U.S. Patent 20060116542 A1. June 1, 2006.

5. Lutz, E. F. Metathesis process and catalysts for the preparation of α-olefins from internal olefins and ethylene. U.S. Patent 5672802. September 30, 1997.

6. Pieper, L.; Stryk, A. Market Watch. *http://www.cbi.com/getattachment/47eebcf7-2176-44ab-8f8d-4a1e64505018/Market-Watch.aspx*2017).

7. Shell *www.shell.com. (*2017).

8. Plotkin, J. S. The Propylene Quandary.
   https://www.acs.org/content/acs/en/pressroom/cutting-edge-chemistry/the-propylene-quandary.html (accessed 08, 2017).

9. Tian, H.; Roberts, C. A.; Wachs, I. E. Molecular Structural Determination of Molybdena in Different Environments: Aqueous Solutions, Bulk Mixed Oxides, and Supported MoO_3 Catalysts. *J. Phys. Chem. C* **2010**, *114*, 14110-14120.

10. Hu, H.; Wachs, I. E.; Bare, S. R. Surface Structures of Supported Molybdenum Oxide Catalysts: Characterization by Raman and Mo L_3-Edge XANES. *J. Phys. Chem.* **1995**, *99*, 10897-10910.

11. Chen, K.; Xie, S.; Bell, A. T.; Iglesia, E. Structure and Properties of Oxidative Dehydrogenation Catalysts Based on MoO_3/Al_2O_3. *J. Catal.* **2001***, 198*, 232-242.

12. Lwin, S.; Wachs, I. E. Olefin Metathesis by Supported Metal Oxide Catalysts. *ACS Catal.* **2014***, 4*, 2505-2520.

13. Handzlik, J.; Sautet, P. Structure of Isolated Molybdenum(VI) Oxide Species on y-Alumina: A Periodic Density Functional Theory Study. *J. Phys. Chem. C* **2008***, 112*, 14456-14463.

14. Handzlik, J.; Sautet, P. Structure of Dimeric Molybdenum(VI) Oxide Species on y-Alumina: A Periodic Density Functional Theory Study. *J. Phys. Chem. C* **2010***, 114*, 19406-19414.

15. Chempath, S.; Zhang, Y.; Bell, A. T. DFT Studies of the Structure and Vibrational Spectra of Isolated Molybdena Species Supported on Silica. *J. Phys. Chem. C* **2007***, 111*, 1291-1298.

16. Olsthoorn, A. A.; Moulijn, J. A. An In Situ Infrared Spectroscopic Study of the Activity of y-Alumina Supported $Mo(CO)_6$ for Metathesis and Ethene Polymerization. *J. Mol. Catal.* **1980***, 8*, 147-160.

17. Van Veen, J. A. R. A Method for the Quantitative Determination of the Basic Hydroxyl Groups on an Alumina Surface. *J. Colloid Interface Sci* **1988***, 121*, 214-219.

18. Digne, M.; Sautet, P.; Raybaud, P.; Euzen, P.; Toulhoat, H. Hydroxyl Groups on y-Alumina Surfaces: A DFT Study. *J. Catal.* **2002***, 211*, 1-5.

19. Digne, M.; Sautet, P.; Raybaud, P.; Euzen, P.; Toulhoat, H. Use of DFT to achieve a rational understsanding of acid-basic properties of y-alumina surfaces. *J. Catal.* **2004***, 226*, 54-68.

20. Grunert, W.; Stakheev, A. Y.; Morke, W.; Feldhaus, R.; Anders, K.; Shpiro, E. S.; Minachev, K. M. Reduction and Metathesis Activity of MoO_3/Al_2O_3 Catalysts I. An XPS Investigation of MoO_3/Al_2O_3 Catalysts. *J. Catal.* **1992***, 135*, 269-278.

21. Grunert, W.; Stakheev, A. Y.; Feldhaus, R.; Anders, K.; Shpiro, E. S.; Minachev, K. M. Reduction and Metathesis Activity of MoO_3/Al_2O_3 Catalysts II. The Activation of MoO_3/Al_2O_3 Catalysts. *J. Catal.* **1992***, 135*, 287-299.

22. Aguado, J.; Escola, J. M.; Castro, M. C. Metathesis of 1-hexene over MoO_3 and Re_2O_7 supported on mesostructured y-Al_2O_3 prepared with cationic surfactants. *Stud. Surf. Sci. Catal.* **2005***, 156*, 835-842.

23. Handzlik, J.; Ogonowski, J.; Tokarz-Sobieraj, R. Dependence of metathesis activity of Mo-methylidene sites on their location on (100) y-Al_2O_3 - a theoretical study. *Catal. Today* **2005***, 101*, 163-173.

24. Imamoglu, Y.; Zumeroglu-Karan, B.; Amass, A. J. *Olefin Metathesis and Polymerization Catalysts: Synthesis, Mechanism and Utilization;* Kluwer Academic Publishers: 1989; Vol. 326.

25. Kazansky, V. B.; Shelimov, B. N.; Vikulov, K. A. *Stud. Surf. Sci. Catal.* **1993***, 75*, 515-527.

26. Vikulov, K. A.; Shelimov, B. N.; Kazansky, V. B.; Martra, G.; Marchese, L.; Coluccia, S. *Spec. Publ. R. Soc. Chem.* **1992***, 114*, 87-96.

27. Vikulov, K. A.; Elev, I. V.; Shelimov, B. N.; Kazansky, V. B. IR and UV-vis Spectroscopic Studies of the Stable $Mo=CH_2$ Carbene Complexes Over Photoreduced Silica-Molybdena Catalysts with Chemisorbed Cyclopropane, and Their Role in Olefin Metathesis Reactions. *J. Mol. Catal.* **1989***, 55*, 126-145.

28. Vikulov, K. A.; Elev, I. V.; Shelimov, B. N.; Kazansky, V. B. *Catal. Lett.* **1994**, *2*, 121-123.

29. Klimov, O. V.; Alekseev, O. S.; Startsev, A. N. Study of reduced Mo/Al_2O_3 metathesis catalysts prepared via metal complexes. *React. Kinet. Catal. Lett.* **1995**, *56*, 143-150.

30. Handzlik, J.; Sautet, P. Active sites of olefin metathesis on molybdena-alumina system: A periodic DFT study. *J. Catal.* **2008**, *256*, 1-14.

31. Handzlik, J. Properties and metathesis activity of monomeric and dimeric Mo centres variously located on y-alumina - A DFT study. *Surf. Sci.* **2007**, *601*, 2054-2065.

32. Hardee, J. R.; Hightower, J. W. *J. Catal.* **1983**, *83*, 182-191.

33. Handzlik, J.; Ogonowski, J. *Catal. Lett.* **2003**, *88*, 119-122.

34. Brenner, A.; Burwell, R. L. *J. Catal.* **1978**, *52*, 364-374.

35. Lwin, S.; Keturakis, C.; Handzlik, J.; Sautet, P.; Li, Y.; Frenkel, A. I.; Wachs, I. E. Surface ReO_x Sites on Al_2O_3 and Their Molecular Structure-Reactivity Relationships for Olefin Metathesis. *ACS Catal.* **2015**, *5*, 1432-1444.

36. Lwin, S.; Li, Y.; Frenkel, A. I.; Wachs, I. E. Activation of Surface ReO_x Sites on Al_2O_3 Catalysts for Olefin Metathesis. *ACS Catal.* **2015**, *5*, 6807-6814.

37. Lwin, S.; Wachs, I. E. Determination of Number of Activated Sites Present during Olefin Metathesis by Supported ReO_x/Al_2O_3 Catalysts. *ACS Catal.* **2015**, *5*, 6823-6827.

38. Ivin, K. J.; Mol, J. C. *Olefin Metathesis and Metathesis Polymerization;* Academic Press: San Diego, CA, 1997.

39. Debecker, D. P.; Stoyanova, M.; Rodemerck, U.; Eloy, P.; Leonard, A.; Su, B. L.; Gaigneaux, E. M. Thermal Spreading as an Alternative for the Wet Impregnation

Method: Advantages and Downsides in the Preparation of $MoO_3/SiO_2-Al_2O_3$ Metathesis Catalysts. *J. Phys. Chem. C* **2010***, 114*, 18664-18673.

40. Grubbs, R.; Swetnick, S. Mechanism of olefin metathesis over a supported molybdenum catalyst. *J. Mol. Catal.* **1980***, 8*, 25-36.

41. Debecker, D. P.; Stoyanova, M.; Rodemerck, U.; Gaigneaux, E. M. Preparation of $MoO_3/SiO_2-Al_2O_3$ metathesis catalysts via wet impregnation with different Mo precursors. *J. Mol. Catal. A: Chem.* **2011***, 340*, 65-76.

42. Debecker, D. P.; Bouchmella, K.; Poleunis, C.; Eloy, P.; Bertrand, P.; Gaigneaux, E. M.; Mutin, P. H. Design of $SiO_2-Al_2O_3-MoO_3$ Metathesis Catalysts by Nonhydrolytic Sol-Gel. *Chem. Mater.* **2009***, 21*, 2817-2824.

43. Debecker, D. P.; Schimmoeller, B.; Stoyanova, M.; Poleunis, C.; Bertrand, P.; Rodemerck, U.; Gaigneaux, E. M. Flame-made $MoO_3/SiO_2-Al_2O_3$ metathesis catalysts with highly dispersed and highly active molybdate species. *J. Catal.* **2011***, 277*, 154-163.

44. Bykov, V. I.; Belyaev, B. A.; Butenko, T. A.; Finkelshtein, E. S. Kinetics of a-Olefin Metathesis over the Heterogeneous Catalytic System $(MoOCl_4/SiO_2)$-$SnMe_4$. *Kinet. Catal.* **2012***, 53*, 353-356.

45. Debecker, D. P.; Stoyanova, M.; Colbeau-Justin, F.; Rodemerck, U.; Boissiere, C.; Gaigneaux, E. M.; Sanchez, C. One-Pot Aerosol Route to $MoO_3-SiO_2-Al_2O_3$ Catalysts with Ordered Super Microporosity and High Olefin Metathesis Activity. *Angew. Chem. Int. Ed.* **2012***, 51*, 2129-2131.

46. Debecker, D. P.; Colbeau-Justin, F.; Sanchez, C.; Chaumonnot, A.; Berthod, M. PCT Int. WO 2013011209 A1. January 24, 2013.

47. Aritani, H.; Fukuda, O.; Miyaji, A.; Hasegawa, S. Structural change of molybdenum on silica-alumina in contact with propene studied by ESR and Mo L$_{III}$-edge XANES. *Appl. Surf. Sci.* **2001***, 180*, 261-269.

48. Hahn, T.; Bentrup, U.; Armbruster, M.; Kondratenko, E. V.; Linke, D. The Enhancing Effect of Bronsted Acidity of Supported MoO$_x$ Species on their Activity and Selectivity in Ethylene/*trans*-2-Butene Metathesis. *ChemCatChem* **2014***, 6*, 1664-1672.

49. Hahn, T.; Kondratenko, E. V.; Linke, D. The effect of supported MoO$_x$ structures on the reaction pathways of propene formation in the metathesis of ethylene and 2-butene. *Chem. Commun.* **2014***, 50*, 9060-9063.

50. Li, X.; Zhang, W.; Liu, S.; Han, X.; Xu, L.; Bao, X. A high-resolution MAS NMR study on the potential catalysts Mo/HBeta for olefin metathesis: The interaction of Mo species with HBeta zeolite. *J. Mol. Catal. A: Chem.* **2006***, 250*, 94-99.

51. Li, X.; Zhang, W.; Liu, S.; Xu, L.; Han, X.; Bao, X. The role of alumina in the supported Mo/HBeta-Al$_2$O$_3$ catalyst for olefin metathesis: A high-resolution solid-state NMR and electron microscopy study. *J. Catal.* **2007***, 250*, 55-66.

52. Li, X.; Zhang, W.; Liu, S.; Xu, L.; Han, X.; Bao, X. Olefin Metathesis over Heterogeneous Catalysts: Interfacial Interaction between Mo Species and a HB-Al$_2$O$_3$ Composite Support. *J. Phys. Chem. C* **2008***, 112*, 5955-5960.

53. Takai, T.; Ikenaga, H.; Kotani, M.; Miyazoe, S. Olefin manufacturing method. PCT Int. WO 2010024319 A1. March 4, 2010.

54. Takai, T.; Kubota, T. Method for producing olefins by metathesis reaction of olefins under hydrogen using catalysts. PCT Int. WO 2006093058 A1. September 8, 2006.

55. Euzen, P.; Guibert, S.; Kruger-Tissot, V.; Vidouta, G. Catalyst compound for the metathesis of olefins. U.S. Patent 20030023125 A1. January 30, 2003.

56. Gartside, R. J.; Greene, M. I.; Jones, Q. J. Metathesis process for producing propylene and hexene from C4 olefin streams. U.S. Patent 20030176754 A1. September 18, 2003.

57. Twu, F.; Christensen, S. A.; Hensey, S.; Rost, W. R. Process for Well Fluids Base Oil via Metathesis of Alpha-Olefins. U.S. Patent 20030224945 A1. December 4, 2003.

58. Matkovskii, P. E.; Startseva, G. P.; Aldoshin, S. M.; Mihailovic, D.; Stankovic, V. Process for production of olefinic oligomers by cationic oligomerization of isomeric decenes with nickel-aluminum catalyst systems. RU 2199516 C2. February 27, 2003.

59. Fuerstner, A.; Heppekausen, J. Molybdenum and tungsten metal complexes and use thereof as precatalysts for olefin metathesis. PCT Int. WO 2012116695 A1. September 7, 2012.

60. Van Hal, J. W.; Stevenson, S. A.; Allman, J.; Sullivan, D. L.; Conant, T. A process for producing propylene and aromatics from butenes by metathesis and aromatization. PCT Int. WO 2011136983 A1. November 3, 2011.

61. Miyazoe, S.; Ikenaga, H.; Kotani, M. Process for producing olefin. PCT Int. WO 2010113993 A1. October 7, 2010.

62. Shum, P. S. Catalyst regeneration with coke removal from pores. U.S. Patent 20100167911 A1. July 1, 2010.

63. Halsey, R. B.; Coleman, S. T. Olefin metathesis process using a fluidized bed reactor. U.S. Patent 20090203950 A1. August 13, 2009.

64. Halsey, R. B. Metathesis process using a moving phase reactor. U.S. Patent 20090281364 A1. November 12, 2009.

65. Bridges, R. S. Multi-step process for propylene and gasoline manufacture from tert-butanol and ethylene. U.S. Patent 20050250969 A1. November 10, 2005.

66. Botha, J. M.; Spamer, A.; Mbatha, M.; Mthokozi, J.; Nkosi, B. S.; Reynhardt, J. P. K.; Jacobus, K. S.; Scwikkard, G. W. High-temperature metathesis process for the conversion of C5-C15 alkenes into C9 - C18 alkenes. PCT Int. WO 2001002324 A1. January 11, 2001.

67. Conant, T.; Stevenson, S. A. Mixed-phase operation of butenes metathesis process for maximizing propylene production using metathesis catalysts. U.S. Patent 20130150643. June 13, 2013.

68. Xuan, D.; Wang, Y.; Liu, S. Method for preparing 2,3-dimethyl-2-butene by metathesis of isobutylene. CN 102464552. May 23, 2012.

69. Kinkead, S. A. Olefin metathesis for kerogen upgrading. U.S. Patent 20090133935 A1. May 28, 2009.

70. Basset, J.; Merle, N.; Stoffelbach, F.; Taoufik, M.; Thivolle-Cazat, J. Solid metal compound, preparations and uses thereof. PCT Int. WO 2009044107. April 15, 2010.

71. Bridges, R. S.; Coleman, S. T. Integrated cracking and metathesis process for the manufacture of propylene from ethane. U.S. Patent 20070112236. May 17, 2007.

72. Kruger, T. V.; Guibert, S.; Commereuc, D. Method for improving the regeneration of a metathesis catalyst. U.S. Patent 20030008766. January 9, 2003.

73. Maas, H.; Wiebelhaus, D.; Stephan, J.; Paciello, R. Method for producing C6 - C20 linear α-olefins using transalkylation with isomerization and metathesis. DE 10103309. August 1, 2002.

74. Mukerjee, S. L.; Kyllingstad, V. L. Ring-opening metathesis polymerization (ROMP) of cycloolefins with molybdenum atalysts with outstanding reactivity. U.S. Patent 20020111446. August 15, 2002.

75. Endo, Z.; Yamada, T. Metathesis polymerization catalyst solution and system for preparing cross-linked polymers. EP 0815155 B1. August 7, 2002.

76. Inagaki, S.; Fukushima, Y.; Ichikawa, M.; Oonishi, R. Olefin metathesis catalysts. JP 8215565. August 27, 1996.

77. Kelly, J. Preparation of C4-alkene streams by olefin metathesis. EP 691318 A1. January 10, 1996.

78. Nicolaides, C. P. Production of C4 - C6 olefins for manufacture of gasoline octane boosters using a metathesis catalyst. ZA 9207693. April 15, 1993.

79. Quann, R. J. Alpha-olefins from light olefins. U.S. Patent 4665245. May 12, 1987.

80. Motz, K. L.; Poe, R. L.; Washecheck, P. H.; Yates, J. E. Olefins. EP 139774. May 8, 1985.

81. Tanaka, K. Catalyst for metathesis reaction. JP 61125438. June 13, 1986.

82. Vermeiren, W.; Adam, C.; Minoux, D. Production of propylene via simultaneous dehydration and skeletal isomerization of isobutanol on acid catalysts followed by metathesis. PCT Int. WO 2011113836 A1. September 22, 2011.

83. Ikenaga, H. Process for reactivation of metathesis catalysts and process for production of olefins comprising the reactivation. PCT Int. WO 2009013964 A1. January 29, 2009.

84. Liu, S.; Wang, Y.; Xu, Z.; Yang, W. Olefin metathesis catalyst for preparing propylene. CN 1915510 A. February 21, 2007.

85. Kukes, S. G.; Banks, R. L. Metathesis process and catalyst. U.S. Patent 4465890. August 14, 1984.

86. Kukes, S. G.; Banks, R. L. Olefin metathesis and catalyst. U.S. Patent 4517401. May 14, 1985.

87. Tupy, M. J.; Amore, F.; Kaido, H.; Meng, X. Method of making hydrogenated metathesis products. PCT Int. WO 2007081987 A2. July 19, 2007.

88. Noweck, K.; Hoffmann, A. Aluminosilicate Carrier for Metathesis Catalysts. U.S. Patent 5883272. March 16, 1999.

Chapter 6 | Molecular Structure-Reactivity Relationships for Olefin Metathesis by Supported MoO_x/Al_2O_3 Catalysts
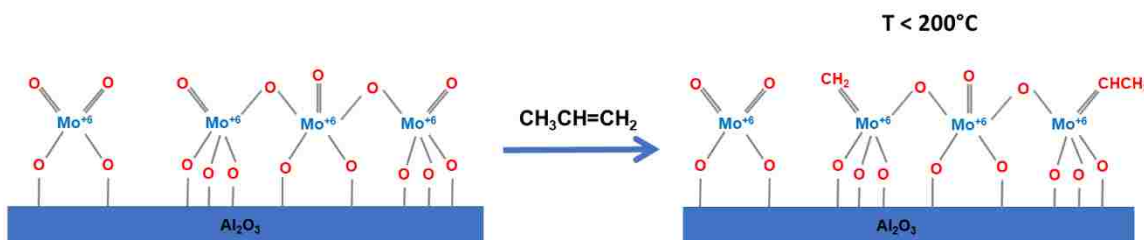
Abstract

Supported MoO_x/Al_2O_3 catalysts were synthesized by incipient-wetness impregnation of aqueous ammonium heptamolybdate, dried at room temperature and 110 °C, and finally calcined at 500 °C in air. The catalysts were spectroscopically characterized with *in situ* Raman, UV-vis, DRIFTS, and TPSR, both after calcination and during propylene metathesis reaction conditions. Three distinct MoO_x species on the Al_2O_3 support were identified: isolated surface dioxo $(O=)_2MoO_2$, anchored to the basic $HO-\mu_1-Al_{IV}$ sites (<1 Mo atom/nm^2), oligomeric surface mono-oxo $O=MoO_{4/5}$ anchored to more acidic $HO-\mu_1-Al_{V/VI}$ sites (1-4.6 Mo atoms/nm^2), and crystalline MoO_3 nanoparticles also present above monolayer coverage (>4.6 Mo atoms/nm^2). During propylene metathesis, activation proceeds by removal of oxo Mo=O bonds and insertion of $=CH_2$ and $=CHCH_3$ alkyls, which maintain the surface MoO_x species in the Mo^{+6} oxidation state. The surface oligomeric mono-oxo $O=MoO_{4/5}$ species easily activate at mild temperatures 25-200 °C while the isolated surface dioxo $(O=)_2MoO_2$ species require very high temperatures for activation (>400 °C). The crystalline MoO_3 nanoparticles decrease the number of accessible activated surface MoO_x sites by their physical blocking. This study establishes the structure-reactivity relationship for olefin metathesis by supported MoO_x/Al_2O_3

catalysts and demonstrates the significant role that the anchoring surface hydroxyl sites on alumina have on the reactivity of surface MoO_x species.

6.1 Introduction

Olefin metathesis is a cleavage and reformation of double bonds in olefins [1]. The reaction was originally discovered by Banks and Bailey at Phillips Petroleum using heterogeneous alumina-supported molybdenum catalysts to transform two molecules of propylene into one ethylene and one butene molecule, and first commercialized in 1966 and dubbed the Phillips Triolefin Process.[2] The reversibility of the olefin metathesis reaction also allows for propylene to be produced from ethylene and butene, now known as olefins conversion technology (OCT).[1,3] Heterogeneous supported MoO_x/Al_2O_3 catalysts are find use in the Shell Higher Olefin Process (SHOP), which was established in 1968. The SHOP process is used to produce linear higher olefins from ethylene and consists of three main stages – oligomerization (homogeneous nickel-phosphine catalyst in a polar solvent), isomerization (solid potassium metal catalyst), and olefin metathesis (alumina-supported molybdate catalyst) – to convert ethylene into linear higher olefins.[3] The current high global demand for propylene and higher olefins is projected to significantly increase in the future, indicating the continued importance of olefin metathesis.[4-6]

The molecular structure of molybdenum oxide in initial oxidized supported MoO_x/Al_2O_3 catalysts has been established in recent years using *in situ* Raman[7-10], UV-vis[7,10], XAS spectroscopy[8-10], and DFT calculations[11-13]. At low surface coverage ($< \sim 1$ Mo atoms/nm^2), only isolated surface dioxo $(O=)_2MoO_2$ species are present on oxidized, dehydrated supported MoO_x/Al_2O_3 catalysts. At intermediate surface coverage (~ 1-4.5 Mo atoms/nm^2), both isolated dioxo $(O=)_2MoO_2$ and oligomeric mono-oxo $O=MoO_4$ surface

species coexist on the alumina support. Above monolayer surface coverage (>4.6 Mo atoms/nm^2), crystalline MoO_3 nanoparticles (NPs) form since there are no remaining exposed Al-OH sites to which the MoO_x species can anchor to the support.[7]

In contrast to the detailed molecular information about oxidized, dehydrated supported MoO_x/Al_2O_3 catalysts from in situ characterization studies, little is known concerning the structures of the activated MoO_x surface sites during olefin metathesis. The earliest characterization studies of activated MoO_x surface sites on Al_2O_3 had been exposed to propylene metathesis reaction conditions and subsequently exposed to ambient conditions and examined with *ex situ* XPS and EPR spectroscopy[14,15]. These studies detected both Mo^{+6} and Mo^{+4} oxidation states, and it was suggested that other Mo oxidation states are not active for olefin metathesis. From *ex situ* solid-state ^{27}Al NMR of mesoporous Al_2O_3-supported MoO_x catalysts[16], it was proposed that surface MoO_x sites anchored to AlO_6 sites are the most active sites. However, these *ex situ* spectroscopic studies are not relevant since the catalysts were exposed to O_2 and moisture that compromised the molybdena oxidation states and structures present during olefin metathesis.

Periodic DFT calculations of MoO_x sites on alumina have provided some insights into the more stable oxidized MoO_x and activated species[11]. It was concluded that under strictly dehydrating conditions, a square pyramidal mono-oxo site is dominant on the most exposed alumina (110) surface, but that 4- and 5-coordinated dioxo sites are most likely present on the minor alumina (100) surface. The presence of 3-fold bonded mono-oxo sites (especially on the (100) surface), however, cannot be excluded. Periodic DFT calculations of dimeric Mo(VI) sites on the (100) and (110) surfaces of alumina[12] predicted that the most stable dimeric species on the (100) plane are mixed dioxo-mono-oxo (dimer possessing one dioxo

190

fragment and one mono-oxo fragment) or double mono-oxo structures that are 3-, 4-, or at most 5-fold bonded to the surface, and the Mo in these exhibits mostly MoO_4 coordination. When the energetic stabilities of the monomeric species were compared to the dimeric structures on the alumina (100) surface were compared, it was determined that the dimeric structures were always more stable than their monomeric analogues and, therefore, Mo oligomer chains are expected to exist on the alumina (100) surface. On the alumina (110) surface, however, the most stable dimeric structures are double-mono-oxo that are 6- or 5-fold bonded to the surface, and these are most frequently in distorted square pyramidal geometry, although distorted MoO_6 or distorted MoO_4 may also be present. The monomeric structures are more stable than the dimeric structures on the alumina (110) plane. Thus, even at high Mo oxide surface coverage, the monomeric Mo species are still present on the alumina (110) surface and will co-exist with the oligomeric molybdate species.

DFT calculations of the active sites (Mo-methylidene structures variously located on the (100) and (110) surfaces of alumina)[17,18] determined that the relative stabilities of the surface MoO_x sites on Al_2O_3 depend on temperature and water vapor pressure, and that the location of the MoO_x active site on the alumina surface influences the reactivity towards ethylene addition. The studies also predicted that Mo sites on the alumina (110) surface are more stable than the analogous structures on the alumina (100) surface. On the alumina (100) surface[18], it was determined that if the Mo-methylidene replaces two basic OH groups anchored to AlO_6 sites, ethylene addition is endothermic with a relatively high activation energy. However, if there is replacement of only one basic OH, and the Mo is also directly bonded to a bridging oxygen of the alumina surface, the site is less stable, the

electron density of the active site moiety decreases, and the geometry is more suitable for alkene addition. Similar findings were determined from cluster studies comparing the reactivity of monomeric and dimeric Mo-methylidene structures on the (100) and (110) surfaces[19]. These cluster studies also showed that both the MoO_x monomers and dimers can be active sites. Although the activation energies for ethylene addition were close for both types of sites, the activation energy was found to be more facile for the dimeric sites (more exothermic). The DFT studies also concluded that the monomeric sites are less likely to be the active sites, since they are more likely to undesirably transform the active trigonal bipyramidal molybdacyclobutane complex into a more stable square pyramidal molybdacyclobutane structure. The formation process of the surface MoO_x active sites on Al_2O_3 was not discussed in these DFT studies.

The absence of reported *in situ* characterization studies that directly probe activated supported MoO_x/Al_2O_3 catalysts during olefin metathesis has hampered the establishment of the fundamental details of this important heterogeneous catalyst system and comparison of experimental data with findings from DFT calculations. The objective of the current studies is to apply *in situ* characterization studies (Raman, IR, UV-vis, and TPSR) during olefin metathesis to establish the molecular/electronic structure-reactivity relationships for olefin metathesis by heterogeneous supported MoO_x/Al_2O_3 catalysts. Such new

fundamental insights should be able to guide the rational design of improved supported

MoO_x/Al_2O_3 catalysts for olefin metathesis.

6.2   Results

6.2.1   Structure of the Initial Oxidized Supported MoO_x/Al_2O_3 Catalysts

6.2.1.1   In situ UV-vis DRS

The UV-vis spectra of several bulk molybdate reference compounds are presented in

Figure S 6.1. The $MgMoO_4$ compound consists of only isolated MoO_4 units and its UV-vis

spectrum exhibits only one strong ligand-to-metal charge transfer (LMCT) absorption band

at ~250 nm with a corresponding high UV-vis energy (E_g) value of 4.5 eV as previously

found for other bulk molybdates with isolated MoO_4/MoO_6 units[7]. The $(NH_4)_2Mo_2O_7$

compound is made up of a chain of alternating MoO_4/MoO_6 units and its UV-vis spectrum

possesses two LMCT absorption bands at ~250 nm (m) and ~320 nm (s) with an E_g value

of 3.5 eV. The lower UV-vis E_g value and the stronger LMCT absorption band at ~320 nm

are characteristic of oligomeric molybdates[7]. The UV-vis spectrum of crystalline MoO_3,

which consists of infinite sheets of highly distorted MoO_6 units, also contains two LMCT

absorption bands at ~250 nm (m) and ~320 nm (s) and an E_g value of 3.5 eV that reflect

the presence of oligomeric molybdates.

The *in situ* UV-vis spectra of the series of oxidized supported $MoO_x/S-Al_2O_3$ catalysts

under dehydrated conditions are presented in Figure 6.1. The UV-vis spectrum of the Sasol

Catalox Al_2O_3 support exhibits a very small absorbance in the charge transfer region and

this background feature was subtracted from the dehydrated spectra. The *in situ* UV-vis

spectra of the dehydrated alumina-supported molybdena catalysts exhibit two LMCT bands

at ~245 nm (s) and ~280-320 nm (m). The stronger LMCT band at ~245 nm indicates the

presence of a significant fraction of isolated surface molybdates and the weaker LMCT band at ~280-320 nm reflects the presence of a significant fraction of oligomeric surface molybdates.
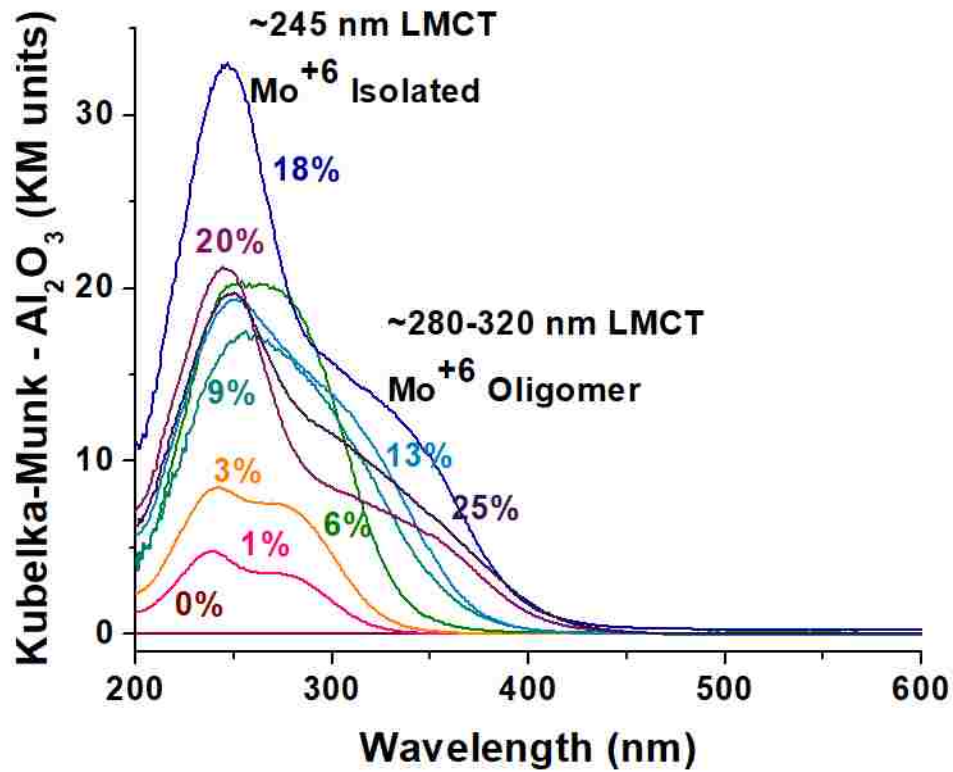
Figure 6.1. *In situ* UV-vis DRS spectra of the dehydrated supported $MoO_x/S\text{-}Al_2O_3$ catalysts. The spectrum of the dehydrated $S\text{-}Al_2O_3$ support taken at 30 °C under flowing UHP Ar (200-800 nm) was subtracted from the spectra of the dehydrated catalysts.

The UV-vis E_g reflects the degree of oligomerization of molybdates and decreases as the number of bridging Mo-O-Mo bonds increases[7]. The UV-vis E_g values of the reference bulk molybdate compounds *vs*. number of bridging Mo-O-Mo bonds are plotted in Figure 6.2 with the E_g values generally decreasing with increasing number of bridging Mo-O-Mo bonds[7]. The measured *in situ* UV-vis E_g values for the oxidized, dehydrated supported MoO_x/Al_2O_3 catalysts are plotted *vs*. the corresponding estimated number of bridging Mo-O-Mo bonds[7] in Figure 6.2. The UV-vis E_g values of the supported MoO_x phase monotonically decrease from 4.0 to 3.2 eV with increasing molybdate loading reflecting an increasing fraction of bridging Mo-O-Mo bonds associated with surface MoO_x oligomers. The number of bridging Mo-O-Mo bonds for the supported MoO_x phase was determined from the E_g *vs*. Mo-O-Mo relationship previously developed[7]. The supported 1% MoO_x/Al_2O_3 (0.2 Mo atoms/nm^2) catalysts exhibits an E_g value of ~4.0 eV that reflects a high concentration of isolated MoO_x structures and the absorption band at ~280-320 nm also reflects the presence of oligomeric MoO_x sites. The E_g value slightly decreases to ~3.9 eV for the supported 3-6% MoO_x/Al_2O_3 (0.7-1.4 Mo atoms/nm^2) catalysts and to ~3.8 eV for the supported 9% MoO_x/Al_2O_3 (2.1 Mo atoms/nm^2) catalyst, indicating slight increases in the concentration of oligomeric MoO_x structures. For supported 13% MoO_x/Al_2O_3 (3.0 Mo atoms/nm^2), the E_g value decreases to ~3.5 eV, indicating increasing concentration of oligomeric molybdate structures. For the supported 18-25% MoO_x/Al_2O_3 (4.1-5.8 Mo atoms/nm^2) catalysts, the E_g values further decrease to ~3.2-3.3 eV, reflecting increasing concentrations of oligomeric MoO_x structures. In summary, the fraction of oligomeric molybdates increases with molybdena loading on the alumina support.
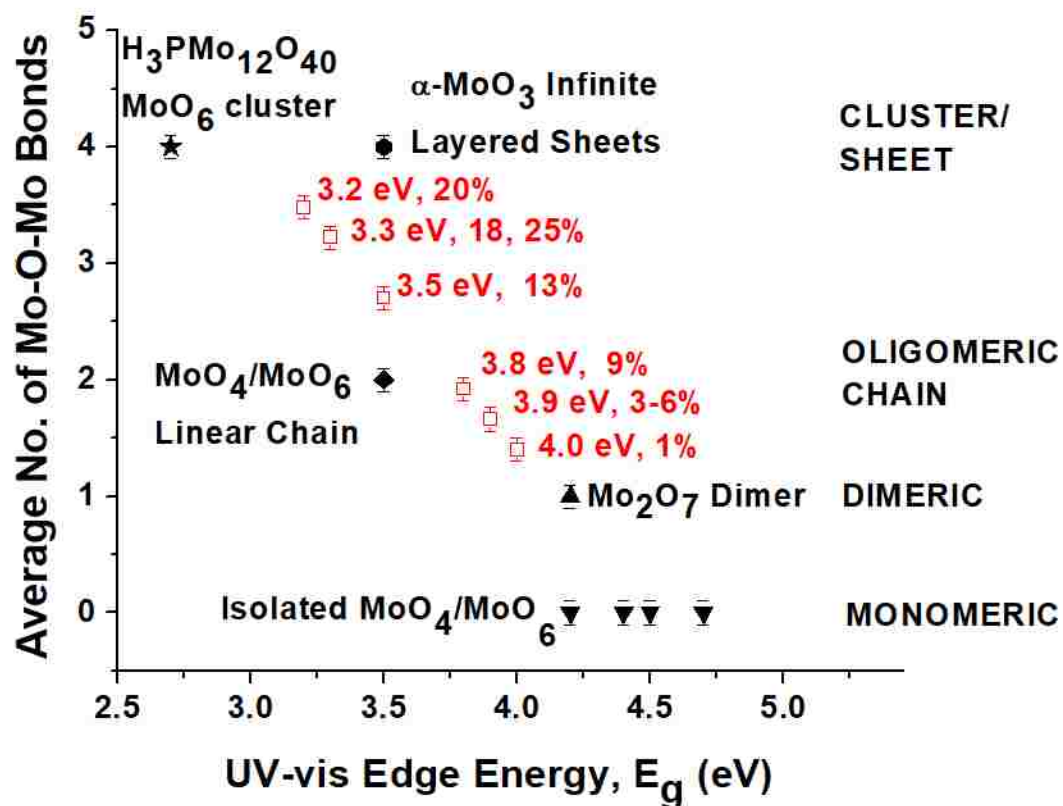
Figure 6.2. *In situ* UV-vis DRS E_g values of reference bulk molybdate compounds (black filled-in shapes) and dehydrated supported $MoO_x/S-Al_2O_3$ catalysts (open red squares). The percent represents the weight percent of the molybdena loading on the alumina support. The E_g values were calculated from the UV-vis spectra with the spectrum of the dehydrated Sasol alumina subtracted.

6.2.1.2 *In situ Raman Spectroscopy*

The *in situ* Raman spectra of the supported MoO_x/H-Al_2O_3 catalysts under dehydrated conditions are presented in Figure 6.3. The H-Al_2O_3 support does not give rise to any Raman bands. The Raman spectrum of the dehydrated supported 3% MoO_x/H-Al_2O_3 (0.7 Mo atoms/nm^2) catalyst exhibits weak bands at ~993, $\nu_s((O=)_2MoO_2$, ~970, $\nu_{as}((O=)_2MoO_2$, and ~840 cm^{-1}, ν_s(Mo-O-Al), of isolated surface dioxo sites[7,11,13]. The corresponding band at ~344 cm^{-1} from the associated $\delta(MoO_4)$ bending vibration, however, is not readily apparent because of its weak signal. A vibrational band from oligomeric molybdena surface species detected with UV-vis is not apparent in the Raman spectrum, most likely because of its weaker Raman scattering. For the supported 6% MoO_x/H-Al_2O_3 (1.4 Mo atoms/nm^2) catalyst, the Mo=O vibration shifts slightly to ~1006 cm^{-1}, reflecting oligomerization of some surface MoO_x species, as detected by UV-vis. Weak vibrations also appear at ~580 cm^{-1} for the bridging ν_s(Mo-O-Mo). In the bending region, a weak vibration appears at ~344 cm^{-1} assigned to $\delta(MoO_4)$ of surface MoO_x sites. For the supported 9-13% MoO_x/H-Al_2O_3 (2.1-3.0 Mo atoms/nm^2) catalysts, the Mo=O vibration at ~1006 cm^{-1} increases in intensity compared to the supported 6% MoO_x/H-Al_2O_3 catalyst due to formation of more oligomeric surface mono-oxo $(O=MoO_{4/5})_n$ sites[7]. The bands from bridging ν_{as}(Mo-O-Mo) and ν_s(Mo-O-Mo) bonds increase and a new band appears at ~205 cm^{-1} assigned to δ(Mo-O-Mo) vibrations, reflecting the increasing number of oligomeric surface MoO_x sites. In the bending region, the band at ~344 cm^{-1} that has been assigned to $\delta(MoO_4)$ of surface MoO_x sites increases[7]. Further increasing the MoO_x loading to supported 18% MoO_x/H-Al_2O_3 (4.1 Mo atoms/nm^2), which approaches monolayer coverage of 4.6 Mo atoms/nm^2, increases the intensities of the oligomeric mono-oxo bands.

For the supported 20-25% MoO_x/H-Al_2O_3 (4.6-5.8 Mo atoms/nm^2) catalysts, which correspond to about monolayer coverage and above monolayer coverage, crystalline MoO_3 NPs are also present and reflected by its characteristic strong bands at ~996, ~820, ~665, and ~200-400 cm^{-1}.[7] In summary, isolated dioxo surface sites predominate at low coverage (<1 Mo atoms/nm^2), both isolated dioxo and oligomeric mono-oxo O=$MoO_{4/5}$ sites co-exist at higher coverage (>1-4.5 Mo atoms/nm^2), and both surface MoO_x sites and crystalline MoO_3 are present above monolayer coverage. The current observations agree with previous experimental findings[7,8] and theoretical calculations[11,13].
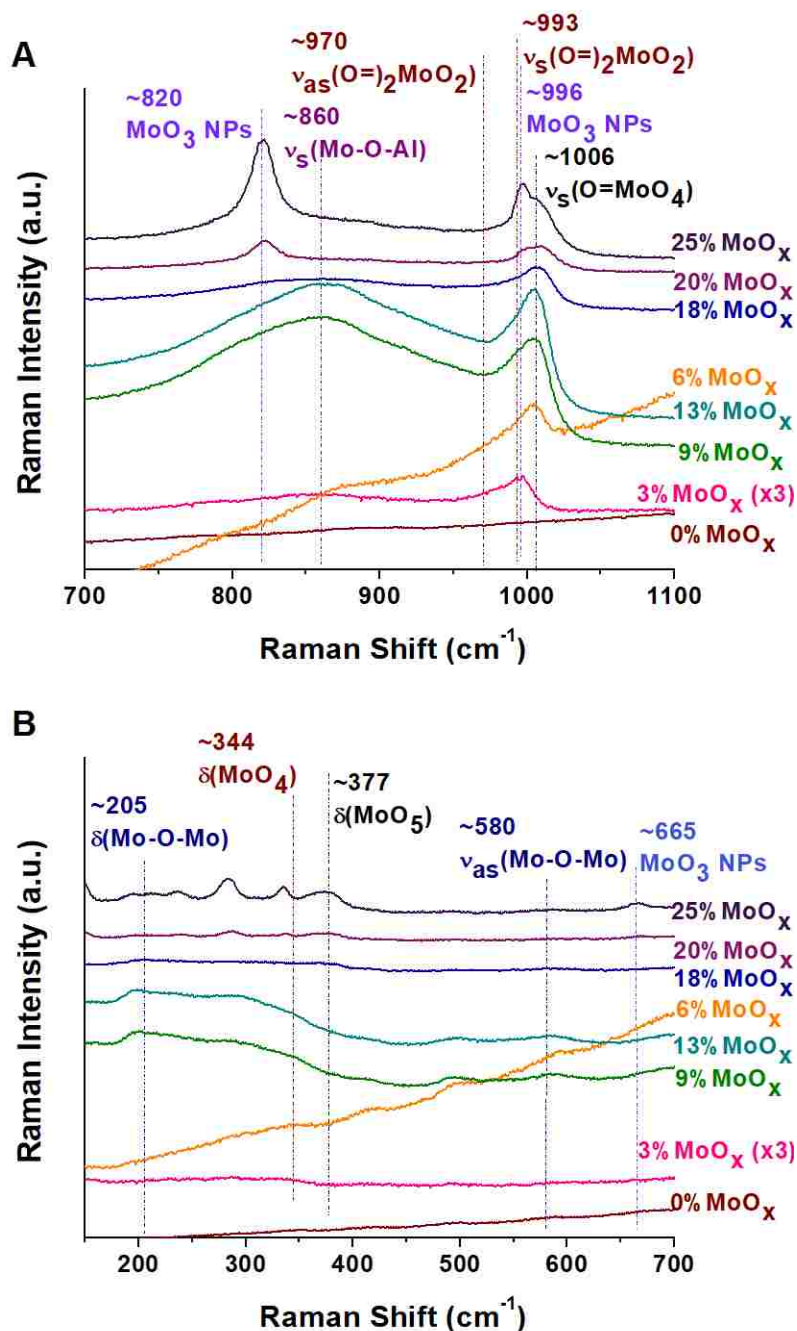
Figure 6.3. *In situ* Raman spectra of dehydrated supported $MoO_x/H-Al_2O_3$ catalysts as a function of molybdena loading in the (A) 700-1100 cm^{-1} and (B) 150-700 cm^{-1} regions. Spectra were collected at 30 °C under flowing UHP Ar using a 442 nm laser without a filter. For the spectrum of the supported 3% $MoO_x/H-Al_2O_3$ catalyst, the intensity was multiplied by 3x to enhance the spectrum since the bands are weak compared to the other spectra with higher molybdena loadings.

6.2.1.3 In situ DRIFTS

6.2.1.3.1 Overtone Region

The overtone region from the *in situ* DRIFTS of the dehydrated supported MoO_x/S-Al_2O_3 catalysts is depicted in Figure 6.4. Strong absorption of the IR radiation by the Al_2O_3 support obscures the primary Mo=O vibrations in the fundamental frequency region ($\sim$1000 cm^{-1} and below). The spectra were normalized using the S-Al_2O_3 support DRIFTS band at $\sim$1041 cm^{-1}, and the spectrum of the dehydrated S-Al_2O_3 support was subtracted to highlight the MoO_x vibrations. The supported 3% MoO_x/S-Al_2O_3 catalyst possesses a very weak overtone band that appears to be centered at $\sim$1975 cm^{-1}. The overtone band shifts slightly to higher wavenumbers as the MoO_x loading is increased to 6% MoO_x/S-Al_2O_3. For higher MoO_x loading, a well-resolved overtone band is present at $\sim$1988 cm^{-1} and assigned to the overtone vibration from the surface mono-oxo $O=MoO_{4/5}$ oligomeric structures.[20,21] The blue shift of the overtone band from the MoO_x species is indicative of the increasing number of oligomeric mono-oxo sites with molybdena loading.
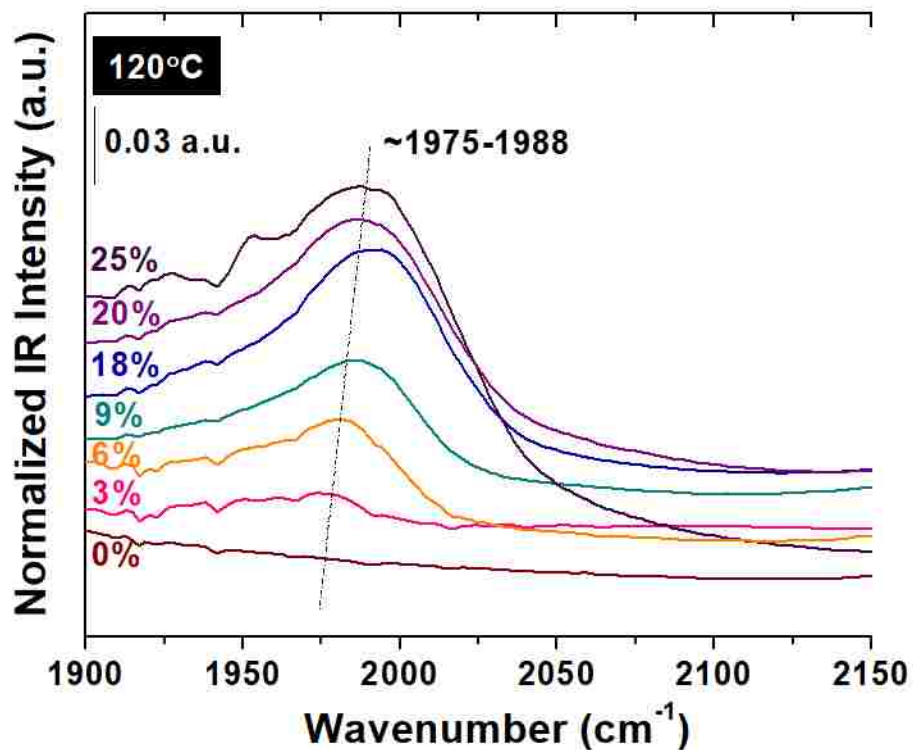
Figure 6.4. *In situ* DRIFT spectra of the overtone region from the supported MoO_x/S-Al_2O_3 catalysts under dehydrated conditions at 120 °C. The spectrum of the dehydrated Sasol alumina support was subtracted from the DRIFT spectra of the dehydrated MoO_x/S-Al_2O_3 catalysts.

6.2.1.3.2 Surface Hydroxyl Groups

The *in situ* DRIFTS of the alumina surface hydroxyl region for the dehydrated supported $MoO_x/S-Al_2O_3$ catalysts are shown in Figure 6.5. Previous experimental and theoretical studies have demonstrated that the surface hydroxyls can be used to determine which alumina surface hydroxyl sites anchor the surface MoO_x structures[22-25], and the various alumina surface hydroxyl types and vibrational positions reported in the literature can be found in Ref.[22]. At low surface coverage of MoO_x (3% $MoO_x/S-Al_2O_3$, 0.7 Mo atoms/nm^2), the HO-μ_1 bands (μ_1-Al_{IV} at 3787 cm^{-1} on the (110) facet, μ_1-Al_{VI} at 3764 cm^{-1} on the (100) facet, and μ_1-Al_V at 3743 cm^{-1} and 3720 cm^{-1} on the (110) facet) are mostly consumed reflecting anchoring of MoO_x at these sites. There is also some consumption of the HO-μ_3 sites (μ_3-Al_{VI} at 3670 cm^{-1} on the (100) facet) of the alumina support. As the molybdena loading is increased to intermediate coverage (9-18% $MoO_x/S-Al_2O_3$, 2.1-4.1 Mo atoms/nm^2), the Al_2O_3 μ_1 and μ_3 surface hydroxyls are completely consumed by anchoring of the surface molybdena. For the 18% $MoO_x/S-Al_2O_3$, there is also consumption of the IR band at 3694 cm^{-1} from Al_2O_3 μ_2-Al_V surface hydroxyls located on the (110) facet. At the highest loadings of 20-25% MoO_x/Al_2O_3 (4.6-5.8 Mo atoms/nm^2), the Al_2O_3 μ_2-Al_V surface hydroxyls are completely consumed. The *in situ* DRIFTS of the Al_2O_3 surface hydroxyl region, thus, reveals that the surface MoO_x species anchor at distinct surface Al-OH sites. At low surface MoO_x coverage (<1 Mo atom/nm^2), the predominant isolated surface $(O=)_2MoO_2$ sites anchor to more basic Al_2O_3 HO-μ_1-Al_{IV} hydroxyls, and at higher surface molybdena loading (>1-4.5 W atoms/nm^2), the oligomeric surface $O=MoO_{4/5}$ species anchor to more acidic Al_2O_3 HO-$\mu_{1/3}$-$Al_{V/VI}$ hydroxyls.
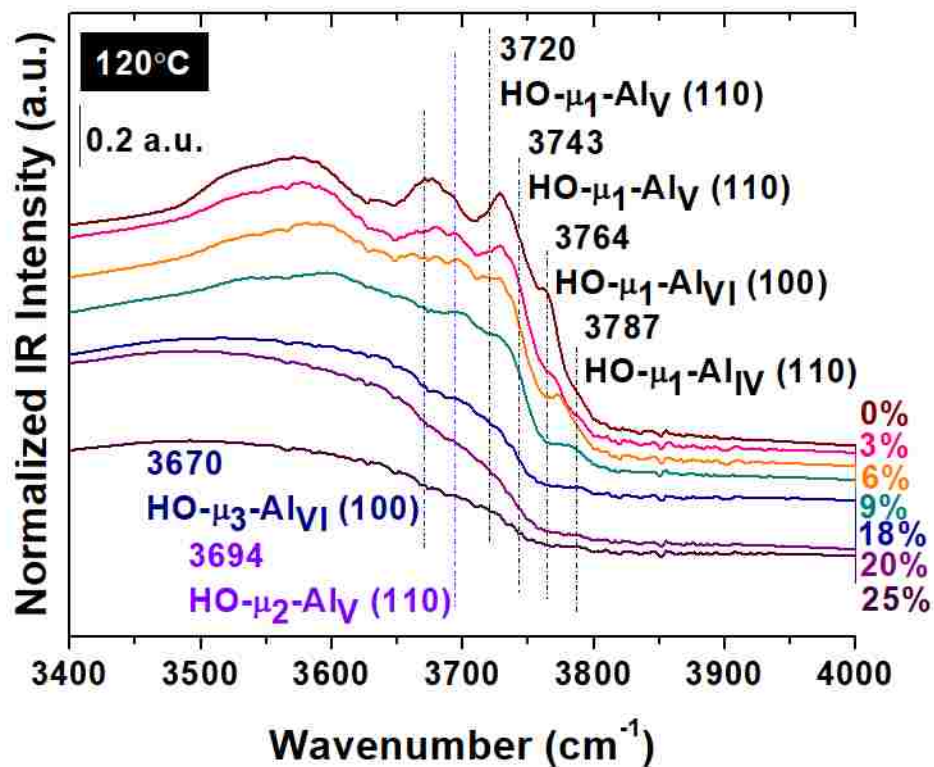
Figure 6.5. *In situ* DRIFT spectra of the surface hydroxyl region from the supported $MoO_x/S-Al_2O_3$ catalysts under dehydrated conditions at 120 °C.

6.2.2 Structure of Supported MoO$_x$/Al$_2$O$_3$ Catalysts During Olefin Metathesis

6.2.2.1 *In situ UV-vis Spectroscopy*

The *in situ* UV-vis spectra taken during propylene metathesis are presented in Figure 6.6. Difference curves were taken to highlight the changes in the catalyst during the reaction with the reference spectrum being that of the corresponding dehydrated catalyst.

At low molybdena loadings (3% MoO$_x$/S-Al$_2$O$_3$, 0.7 Mo atoms/nm^2), there are negative Mo^{+6} LMCT bands (~240 and ~280 nm) that modestly decrease over the one hour at 30°C during propylene metathesis. There are no d-d transition bands from reduced MoO$_x$ sites present, and the decrease in the LMCT bands is not visible unless difference curves are taken, suggesting that there is only a minor perturbation caused by propylene chemisorption. When the temperature is increased to 200 °C under Ar, the LMCT bands further decrease without the detection of d-d transitions from reduced surface MoO$_x$ sites. During propylene metathesis at 200 °C, the absorbance of the LMCT bands increases, and there are still no d-d transition bands present, suggesting that the sites are not being appreciably reduced, but are only slightly perturbed by the adsorbed propylene. The positive bands at ~250 ~ 350 nm are artifacts of the subtraction since there is negligible change in intensity as compared to the negative bands. Furthermore, the catalyst surface did not darken in color during exposure to propylene suggesting that at low surface molybdena coverages (<1 Mo atom/nm^2), in which the isolated (O=)$_2$MoO$_2$ sites dominate, there is just minor perturbation of the surface molybdena species in the presence of propylene.

At higher molybdena loadings (20% MoO$_x$/S-Al$_2$O$_3$, 4.6 Mo atoms/nm^2) where oligomeric surface MoO$_x$ sites are more plentiful, the catalyst quickly darkened in color at

30 °C upon exposure to propylene reflecting either reduction of the surface MoO_x sites and/or the presence of significant surface organic intermediates. The corresponding *in situ* UV-vis spectrum in Figure 6.6 B exhibits only a small d-d transition band maximum at ~460 nm, similar to Mo^{+4} in bulk MoO_2 (see Figure S 6.1)[26], that grows with time-on-stream and absence of changes in the LMCT region. The UV-vis Mo^{+4} absorbance band at 460 nm further increases upon increasing the temperature to 200°C in flowing Ar indicating that some surface intermediates become activated at the higher temperature. The UV-vis absorbance band of Mo^{+4} at 460 nm, however, only mildly increases during propylene metathesis at 200 °C suggesting that the number of reduced Mo^{+4} sites has reached a maximum. The presence of the UV-vis Mo^{+4} d-d transition band demonstrates that the catalysts containing higher amounts of oligomeric surface MoO_x sites during propylene metathesis at 200 °C can possess some reduced sites. The lack of the extensive decrease in the UV-vis Mo^{+6} LMCT band during propylene metathesis at 200 °C, however, demonstrates that the concentration of surface Mo^{+4} sites is very low and surface Mo^{+6} sites are the dominant molybdena oxidation state during propylene metathesis.
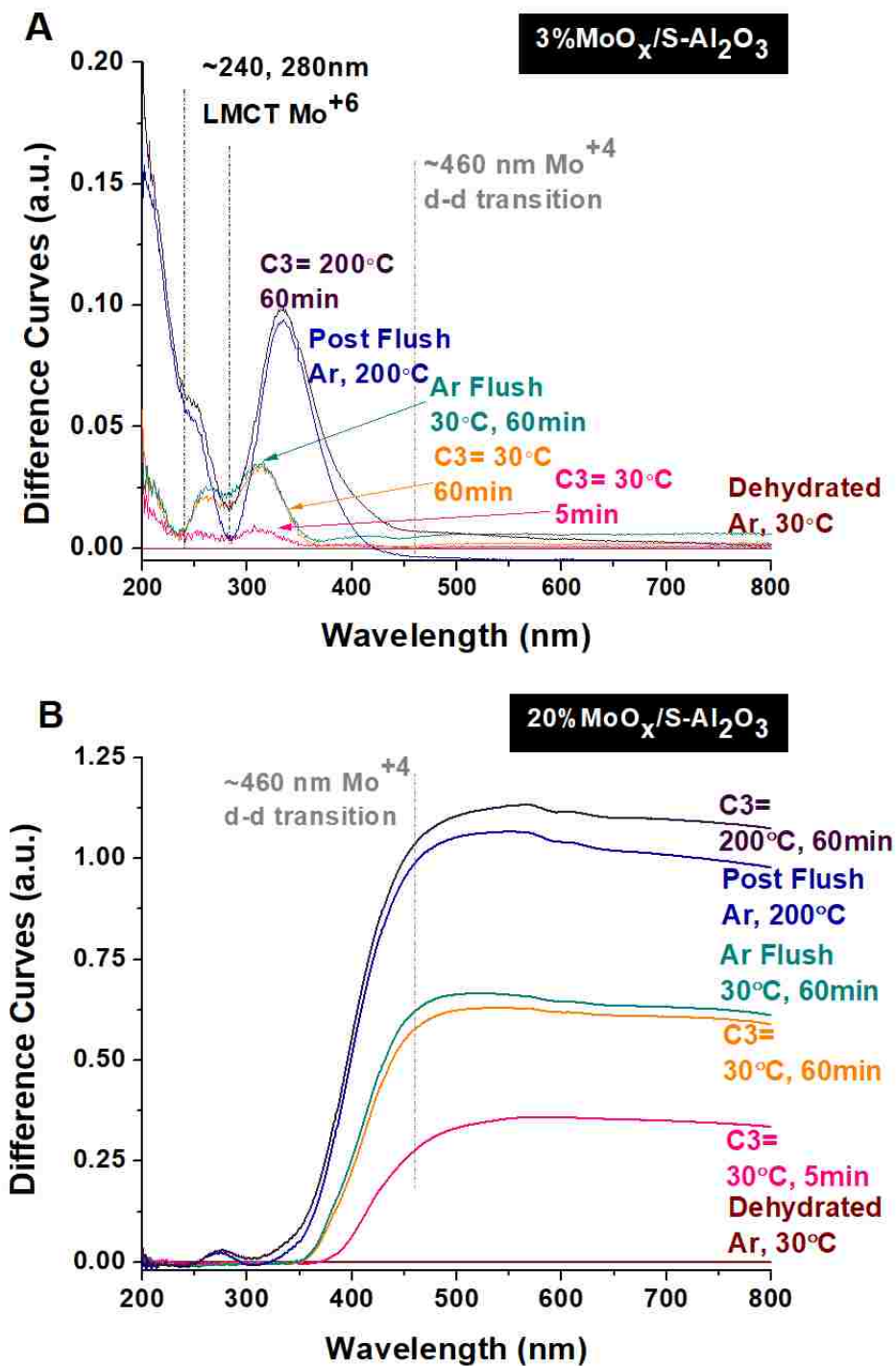
Figure 6.6. *In situ* UV-vis absorbance difference spectra of catalysts: (A) 3% MoO_x/S-Al_2O_3 (0.7 Mo atoms/nm^2) and (B) 20% MoO_x/S-Al_2O_3 (4.6 Mo atoms/nm^2) monolayer coverage during propylene metathesis.

6.2.2.2 *In situ* Raman Spectroscopy

The *in situ* Raman spectra during propylene metathesis reaction conditions at low and about monolayer surface coverage are presented in Figure 6.7. At low molybdena coverage (3% MoO_x/H-Al_2O_3, 0.7 Mo atoms/nm^2), the Raman bands for the isolated dioxo site at ~970 and ~993 cm^{-1} are minimally perturbed by exposure to the propylene metathesis reaction (30 °C and 200 °C) indicating that the isolated dioxo sites are not being activated for olefin metathesis. For the supported 18% MoO_x/H-Al_2O_3 catalyst (4.1 Mo atoms/nm^2), the Raman band at ~1006 cm^{-1} of the surface oligomeric mono-oxo O=$MoO_{4/5}$ sites decreases during the propylene metathesis reaction. The weak bands at ~205 cm^{-1} and ~377 cm^{-1} from the bending modes of Mo-O-Mo and MoO_5, respectively, and the band at ~580 cm^{-1} for the symmetric stretch of the Mo-O-Mo bonds decrease during the propylene metathesis reaction as well (see Figure S 6.2). After flushing the catalyst with UHP Ar for 60 min, there is still a band maximum at ~1006 cm^{-1}, indicating that not all the oligomeric surface MoO_x sites have reacted during propylene metathesis at 30 °C. At the end of the propylene metathesis reaction at 200 °C, the ~1006 cm^{-1} band observed after reaction at 30°C is now a broader band at ~993 ~ 996 cm^{-1}, indicating that the oligomeric sites are now fully activated at the higher temperature of 200 °C. Additionally, the presence of band maxima at ~240, ~285, ~336, ~665, ~820, and ~990-996 cm^{-1} demonstrates that crystalline NPs are not activated during propylene metathesis, and that the isolated dioxo sites may still also be present on the catalyst surface (see Figure S 6.3).
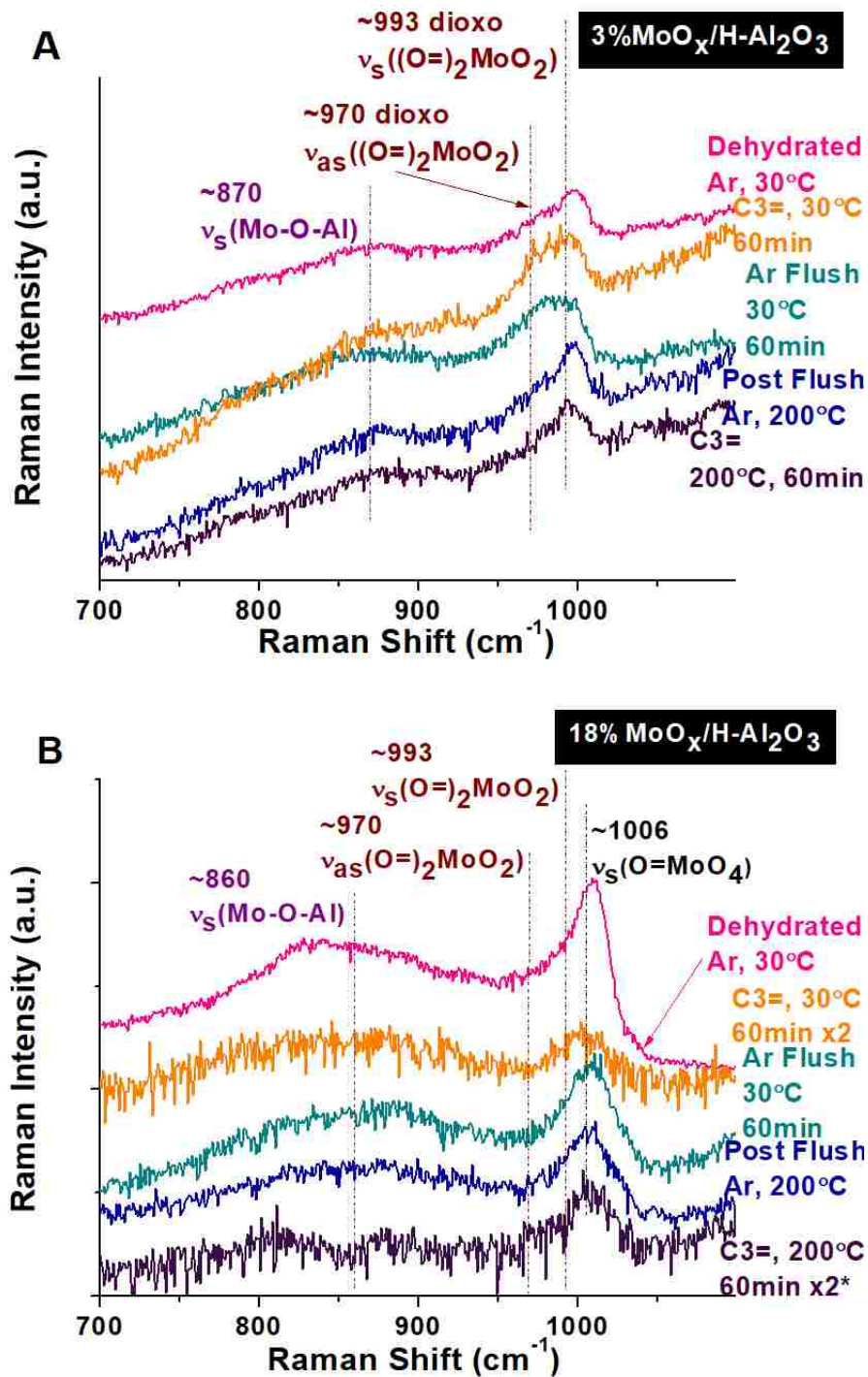
Figure 6.7. *In situ* Raman spectra of catalysts: (A) 3% MoO_x/H-Al_2O_3 (0.7 Mo atoms/nm^2) and (B) 18% MoO_x/H-Al_2O_3 (4.1 Mo atoms/nm^2) during propylene metathesis in the 700-1100 cm^{-1} vibrational region. A D0.6 (*D1) filter was employed to minimize surface heating and induced reduction by the laser. In some cases, the spectral bands were weaker because of the darkened sample, so the signal intensity was multiplied so that the bands could be seen more clearly.

The *in situ* Raman spectra in the hydrocarbon region (1200-1800 cm^{-1}) of the supported 3% MoO$_x$/H-Al$_2$O$_3$ and 18% MoO$_x$/H-Al$_2$O$_3$ catalysts during propylene metathesis are presented in Figure 8. For the supported 3% MoO$_x$/Al$_2$O$_3$ catalyst, Raman bands from surface hydrocarbon species are absent at both 30 °C and 200 °C. This indicates that surface hydrocarbons do not adsorb on the alumina support sites, and that the surface dioxo MoO$_4$ sites are not able to adsorb and activate propylene for the metathesis reaction. For the supported 18% MoO$_x$/Al$_2$O$_3$ catalyst, however, Raman bands from surface hydrocarbon species (~1365 and ~1560 ~ 1600 cm^{-1}, assigned to the characteristic D (disordered) and G (graphite) peaks of sp^2-bonded carbon, respectively)[27,28] immediately appeared and increased in intensity with propylene metathesis time on-stream. The D peak represents the disorder in the graphitic structure, and the broad nature of the G peak is related to the degree of disorder and/or inhomogeneity. The G peak also red shifts to lower wavenumbers with propylene time-on-stream suggesting that as the reaction progresses, a more ordered sp^2-bonded carbon species forms.[27,28]
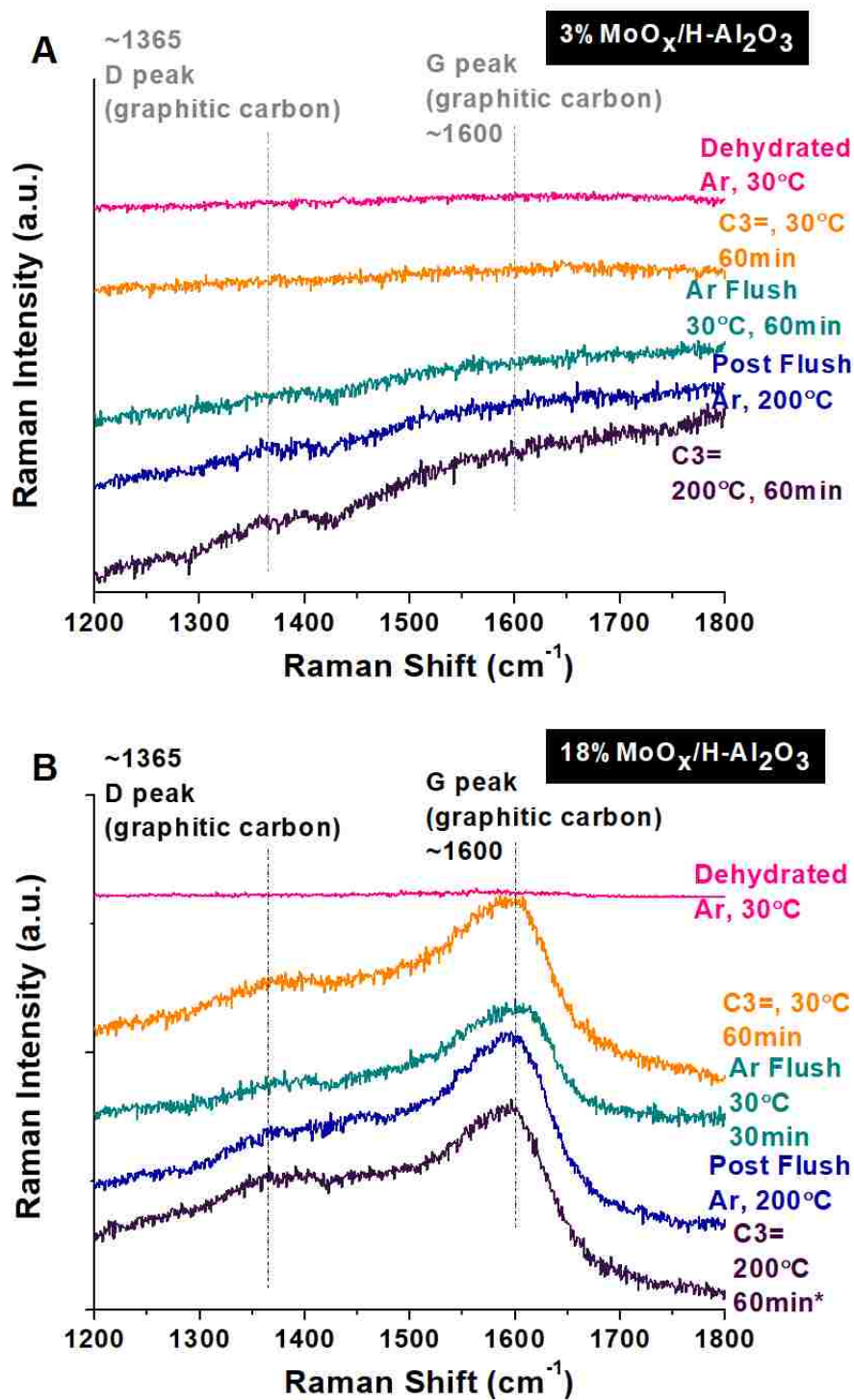
Figure 6.8. *In situ* Raman spectra of supported catalysts during propylene metathesis in the carbon/hydrocarbon vibrational region (1200-1800 cm^{-1}): (A) 3% MoO$_x$/H-Al$_2$O$_3$ (0.7 Mo atoms/nm^2) and (B) 18% MoO$_x$/H-Al$_2$O$_3$ (4.1 Mo atoms/nm^2) during propylene metathesis. A D0.6 (*D1) filter was employed to minimize surface heating and induced reduction by the laser.

6.2.2.3 C_3H_6-TPSR

The C_4H_8/C_3H_6-TPSR spectra are presented in Figure 6.9. The formation of oxygenated reaction products (Figure S 6.6) (acetaldehyde (CH_3CHO), acetone (CH_3COCH_3), formaldehyde ($HCHO$), CO, CO_2, and H_2O) occurs during activation of the MoO_x sites on alumina. For supported 3% MoO_x/Al_2O_3 (0.7 Mo atoms/nm^2), there is only one peak temperature (T_p) for butene formation at ~544 °C and only a small amount of oxygenated products is formed below 400 °C (Figure S 6.6). As molybdena loading is increased from 6-18% MoO_x/Al_2O_3 (1.4-3.0 Mo atoms/nm^2), the T_p values for butene formation progressively shift to lower temperatures from 544 to 74 °C indicating the presence of MoO_x sites that are much more reactive for metathesis. This is also consistent with the much lower temperatures of ~200 °C for the appearance of oxygenated products (Figure S 6.4) for high loaded molybdena catalysts. The presence of crystalline MoO_3 NPs for the supported 20-25% MoO_x/Al_2O_3 catalysts (4.6-5.8 Mo atoms/nm^2) results in less production of butene revealing the detrimental influence of crystalline MoO_3 NPs on the accessibility of olefins to the surface MoO_x sites for propylene metathesis. All the supported MoO_x/Al_2O_3 catalysts exhibit a butene production peak at ~500 °C, representative of reaction from the isolated surface dioxo MoO_4 species that are always present on the supported MoO_x/Al_2O_3 catalysts.

The corresponding C_2H_4/C_3H_6-TPSR spectra are shown in Figure 6.10 and qualitatively follow the same trend as for butene production, but usually with different T_p values suggesting that both ethylene and butene are not produced by the same rate-determining-step. For the supported 3-13% MoO_x/S-Al_2O_3 catalysts, C_2H_4 was formed at two temperature ranges (T_p~50 °C and ~300-450 °C), with the lower T_p constant and the

higher T_p decreasing with molybdena loading. Although for the supported 3% MoO_x/S-Al_2O_3 catalyst the high temperature T_p value was the same for ethylene and butene formation, at higher molybdena loadings the T_p values for butene formation were lower than the corresponding high temperature T_p values for ethylene formation. Further increasing the molybdena loading on alumina decreases the amount of ethylene formed by blocking propylene access to the active sites. In addition, the low temperature reaction pathway is not observed at these high molybdena loadings.
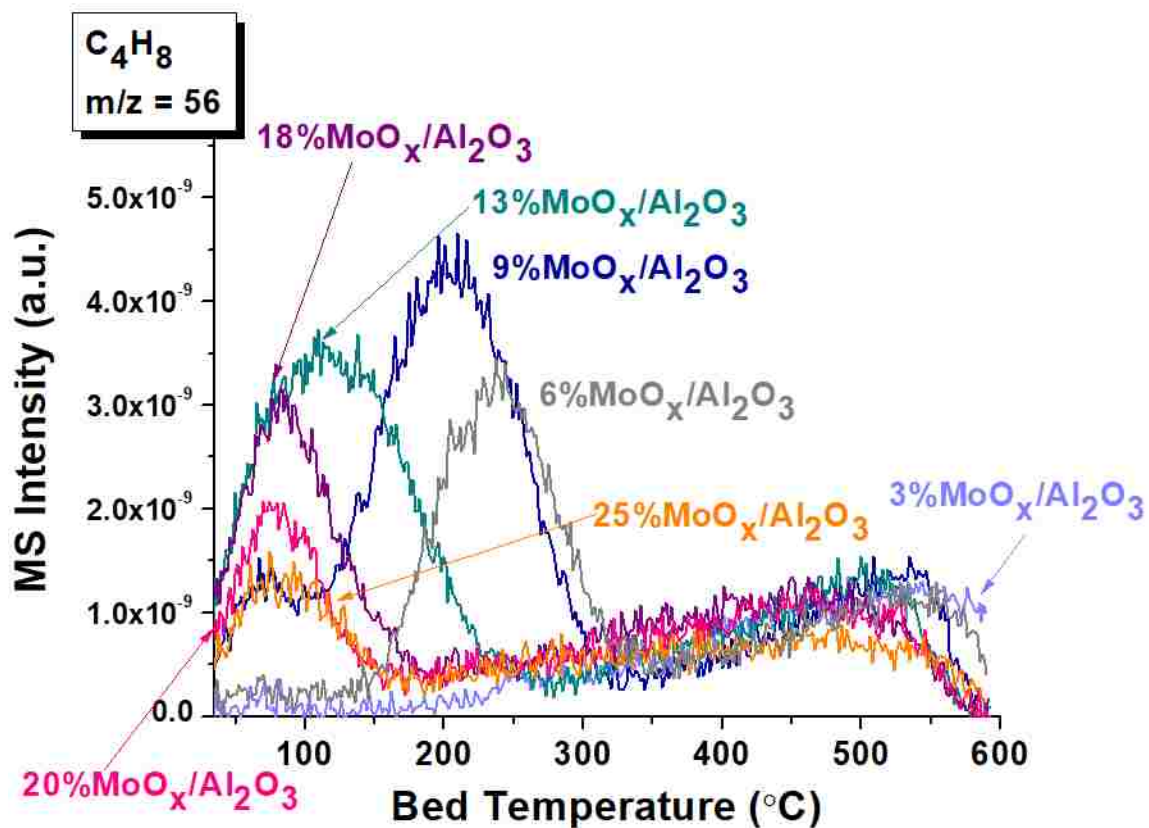
Figure 6.9. The C_4H_8/C_3H_6-TPSR spectra from the supported MoO_x/S-Al_2O_3 catalysts as a function of MoO_x loading. The butene product was monitored with the mass spectrometer $m/z=56$ ratio.
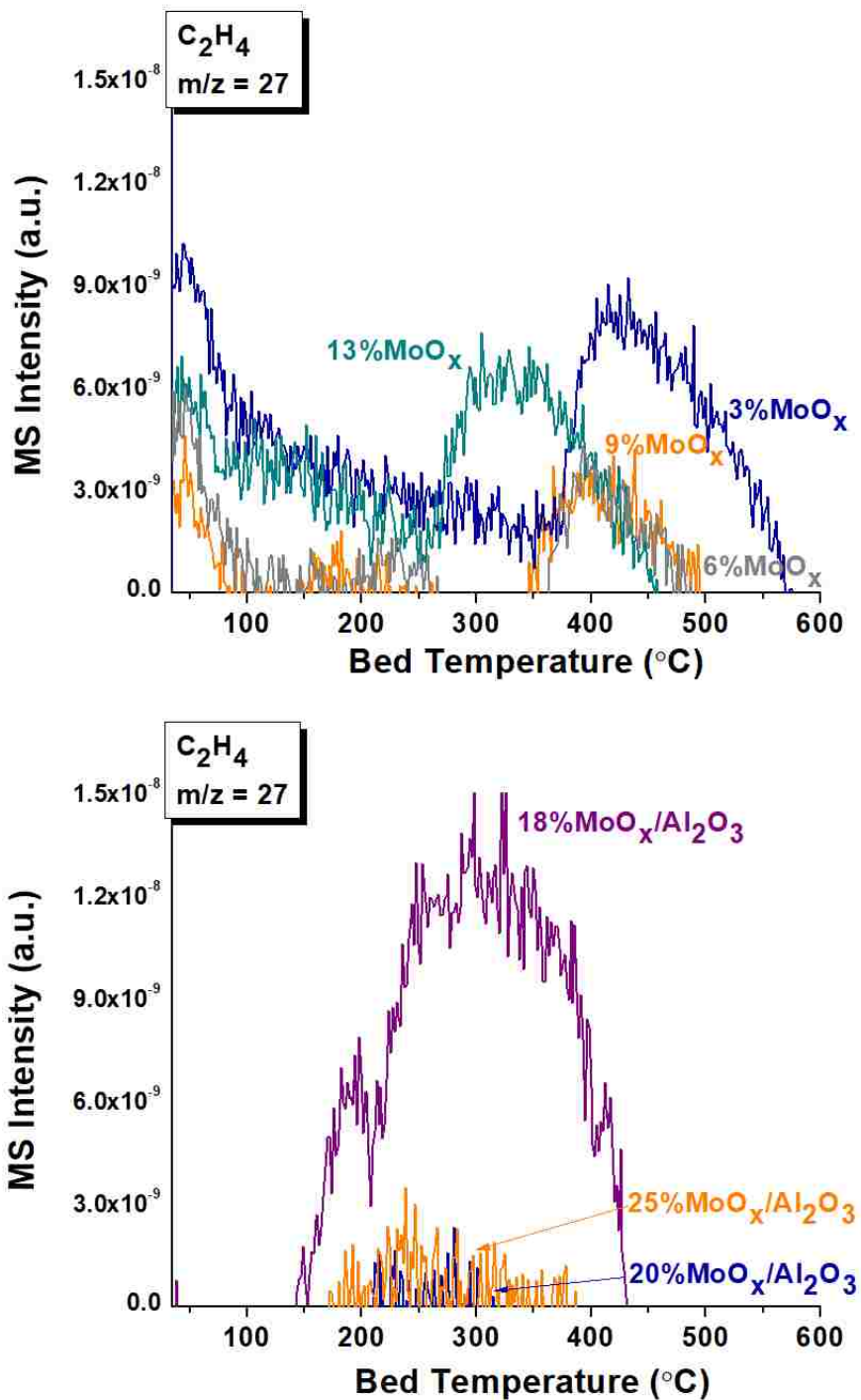
Figure 6.10. The C_2H_4/C_3H_6-TPSR spectra from the supported $MoO_x/S-Al_2O_3$ catalysts: (A) 3-13% $MoO_x/S-Al_2O_3$ and (B) 18-25% $MoO_x/S-Al_2O_3$. The ethylene product was monitored with the mass spectrometer m/z=27 ratio. The MS m/z=27 signal was corrected for contributions from cracking of the C_3H_6 and C_4H_8 molecules in the MS.

6.3   Discussion

6.3.1   Initial Molecular Structures and Anchoring Sites of the Dehydrated

The initial oxidized, dehydrated surface MoO_x sites on Al_2O_3 are present as $Mo^{+6}O_x$ and consist of both isolated dioxo $(O=)_2MoO_2$ sites and oligomeric mono-oxo $O=MoO_{4/5}$ sites as shown by *in situ* UV-vis (Figure 6.1) and Raman (Figure 6.3) spectroscopy, and summarized in Table 6.1.

Table 6.1: Summary of Al$_2$O$_3$-Supported Surface MoO$_x$ Sites and Butene/Propylene–TPSR T$_p$ Values

wt% Mo (Mo/nm^2)	Type of Surface MoO$_x$ Sites	T$_p$ (°C)		
3 (0.7)	Isolated			544
6 (1.4)	Isolated		237	544
9 (2.1)	Isolated + oligomeric	70	204	535
13 (3.0)	Isolated + oligomeric	112		500
18 (4.1)	Isolated + oligomeric	83		450
20 (4.6)	Isolated + oligomeric + NPs	74		450
25 (5.8)	Isolated + oligomeric + NPs	74		450

At low surface MoO_x coverage (<1 Mo atoms/nm^2), the isolated dioxo (O=)$_2$MoO$_2$ sites predominate. At higher surface MoO_x coverage (1-4.6 Mo atoms/nm^2), both the isolated dioxo MoO_4 and oligomeric O=MoO$_{4/5}$ species co-exist, with the latter primarily increasing with surface molybdena coverage. Above monolayer coverage (>4.6 Mo atoms/nm^2), crystalline MoO_3 nanoparticles are also present on top of the surface MoO_x monolayer on Al_2O_3 as shown by *in situ* Raman spectroscopy (Figure 6.3). The various dehydrated supported MoO_x structures on Al_2O_3 are shown in Scheme 6.1.
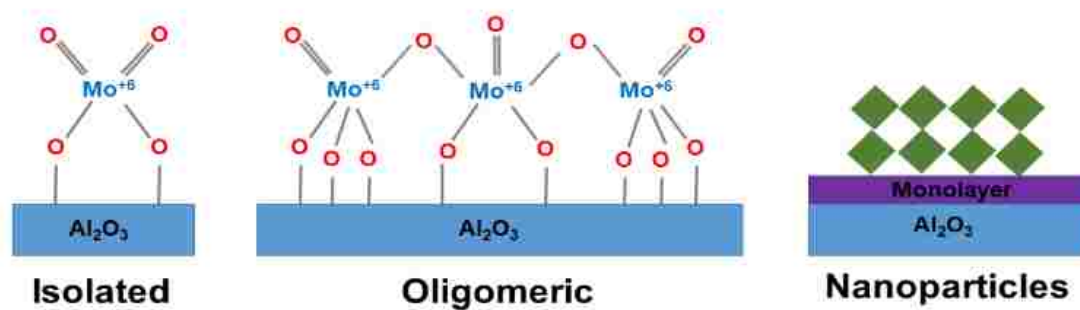
Scheme 6.1. Molecular structures of dehydrated isolated surface $(O=)_2MoO_2$ sites, oligomeric surface $O=MoO_4$ sites, and crystalline MoO_3 nanoparticles on the Al_2O_3 support.

The molecular structures of the alumina-supported MoO_x sites depicted in Scheme 6.1 are in agreement with the structures proposed from previous characterization studies of dehydrated supported MoO_x/Al_2O_3 catalysts: *in situ* XANES[8,9], *in situ* Raman[8,9], *in situ* UV-vis[7], and XPS[14].

The surface MoO_x sites preferentially anchor to the alumina support at more basic HO-μ_1-Al$_{IV}$ surface hydroxyls at low surface molybdena coverage and to some of the more acidic HO-$\mu_{1/3}$-Al$_{V/VI}$ surface hydroxyls. At high surface molybdena coverage, all the alumina HO-μ_1-Al$_{IV}$ surface hydroxyls are titrated by the isolated surface MoO_4 species and most of the alumina HO-$\mu_{1/3}$-Al$_{V/VI}$ surface hydroxyls are titrated by the oligomeric surface $MoO_{5/6}$ species. The crystalline MoO_3 NPs are not anchored to the Al_2O_3 support and reside on top of the surface MoO_x monolayer and interact via weak van der Waals forces with the monolayer.

Previous *in situ* IR studies of supported MoO_x/Al_2O_3 catalysts synthesized from decomposition of $Mo(CO)_6$ on Al_2O_3 [23] and of reaction of $MoO_2(acac)_2$ with alumina[29] also found a preferential consumption of the surface hydroxyl IR band at 3740 cm^{-1} (tentatively assigned to more basic hydroxyls and subsequently assigned to the basic HO-μ_1-Al$_{IV}$ surface hydroxyls by Digne and Sautet via DFT studies[24,25]).

6.3.2 Catalyst Structure During Olefin Metathesis

The surface $Mo^{+6}O_x$ sites on Al_2O_3 need to be activated by propylene during the propylene metathesis reaction conditions (~25-200 °C). Activation involves removal of an oxygen atom from the Mo=O oxo bond[30] as shown by initial formation of oxygenates (Figure S 6.6). While the oligomeric surface MoO_x sites readily form oxygenates at lower temperatures (~25-200 °C), the isolated surface MoO_x sites only form oxygenates at higher

temperatures (>400 °C). The oxidation state of the surface MoO_x sites during propylene metathesis is dominated by Mo^{+6} (Figure 6.6) because the initial Mo=O oxo bond is replaced by Mo=CH$_2$ and Mo=CHCH$_3$ alkyls that oxidize the surface Mo species back to the +6 oxidation state (as shown in Scheme 6.2). The trace of reduced surface Mo^{+4} sites may just be from the minor unselective reduction reactions that produce H_2O, CO, and CO_2 (Figure 6.6).
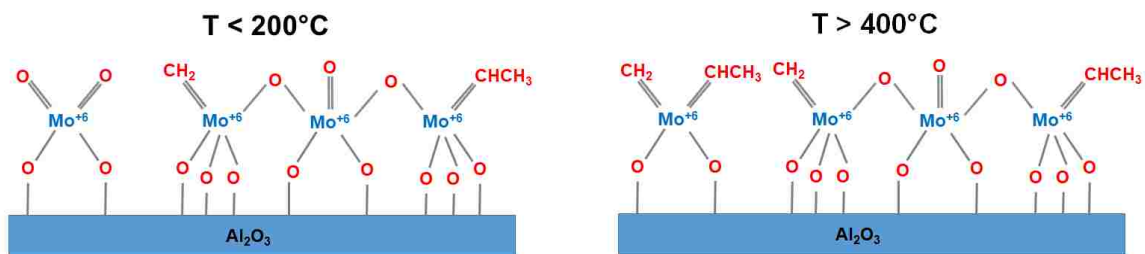
Scheme 6.2. Representation of the activated supported MoO_x/Al_2O_3 catalyst.

The structure and oxidation state(s) of activated surface MoO_x sites on Al_2O_3 during olefin metathesis have previously been addressed by a few studies, but the catalysts were activated with H_2 or CO rather than olefins.[14,15,31] In two separate studies, Gruenert *et al.*[14,15] examined the alumina-supported molybdena catalysts (0.5-13% MoO_x/Al_2O_3 prepared via impregnation of a solution of MoO_3 in NH_4OH (pH ≈ 8)) for propylene metathesis activity by initial activation of Al_2O_3-supported MoO_x with H_2 or thermal treatment in Ar and employed XPS to determine the resulting Mo oxidation states[15]. The resulting H_2-activated catalysts were subsequently examined for propylene metathesis at 200 °C using a conventional flow reactor. It was concluded that the surface molybdena sites derived from Mo^{+4} or Mo^{+6} sites are active for metathesis, while the surface molybdena sites derived from Mo^{+5}, Mo^{+2}, and Mo^0 sites are inactive for metathesis. This indicates that the initial Mo^{+6} and Mo^{+4} sites can transform to catalytic active sites during propylene metathesis and that the initial Mo^{+5}, Mo^{+2}, and Mo^0 sites are unable to transform to activated sites during propylene metathesis. The lack of metathesis activity for the initial Mo^{+5}, Mo^{+2}, and Mo^0 sites suggests that propylene cannot reduce or oxidize these oxidation states to an active Mo state. The nature of the activated site(s) during propylene metathesis, however, cannot be determined from such indirect measurements since the surface MoO_x oxidation states are dynamic and depend on the metathesis reaction conditions. Despite the limitations of this earlier study, these results qualitatively agree with the current *in situ* spectroscopic findings during propylene metathesis that the surface Mo sites on alumina

are primarily present as Mo^{+6} sites with a minor amount of Mo^{+4} sites during propylene metathesis.[14,15]

Klimov *et al.*[31] investigated the oxidation states of conventional supported MoO_x/Al_2O_3 catalysts (prepared via incipient-wetness impregnation of aqueous ammonium heptamolybdate) by first activating the catalysts with CO or H_2 at 500 °C, testing the propylene metathesis activity at room temperature, and subsequently pulsing oxygen to determine the oxidation state by oxygen consumption. The estimated Mo oxidation state was found to decrease with increasing Mo loading (1.4% Mo/Al_2O_3 (Mo^{+5}), 3.3% Mo/Al_2O_3 (Mo^{+4}), and 6.2% Mo/Al_2O_3 (Mo^{+2})). These findings, however, are clouded by the presence of surface $Mo=CH_2$ and $Mo=CHCH_3$ reaction intermediates after the metathesis reaction that may contribute to O_2 consumption and yield results suggesting deep reduction of the surface MoO_x sites (e.g., Mo^{+2}). In the present investigation, Mo^{+2} sites were not detected during propylene metathesis reaction conditions with *in situ* UV-vis.[32]

6.3.3   Structure-Reactivity Relationships

Prior to propylene metathesis, the dehydrated, oxidized supported MoO_x/Al_2O_3 catalysts consist of both isolated surface dioxo MoO_4 sites anchored to the alumina support at more basic μ_1-Al_{IV} surface hydroxyls, and surface oligomeric mono-oxo $MoO_{5/6}$ sites anchored to the alumina support at more acidic $\mu_{1/3}$-$Al_{V/VI}$ surface hydroxyls, with the oligomers predominant at medium and high coverage. The isolated surface MoO_4 sites anchored to the more basic OH sites on alumina are not activated during normal propylene metathesis reaction temperatures (~100 °C) and require very high temperature for activation by propylene, >400 °C (Figure 6.7, Figure 6.10, and Figure S 6.6). The surface

oligomeric $MoO_{5/6}$ sites anchored to the more acidic OH sites on alumina are activated at mild temperatures (~50-150 °C) reflecting the more facile conditions required for their activation by propylene (Figure 6.7-Figure 6.10 and Figure S 6.6). Additionally, crystalline MoO_3 NPs residing on the surface MoO_x monolayer block access of propylene to the surface MoO_x sites, which decreases the number of participating surface MoO_x active sites (Figure 6.9). The blocking of sites is demonstrated by the decrease in butene formation with the same T_p value, which reflects fewer activated sites with the same surface kinetics. The nature of the surface MoO_x species (isolated or oligomeric) is dependent on the specific anchoring alumina surface hydroxyls (more basic or more acidic, respectively).

Previous DFT calculations have examined the reactivity of surface Mo-alkylidene surface reaction intermediates on alumina[17-19,33], but did not examine the activation of the initial surface molybdenum oxide sites on alumina during olefin metathesis. The DFT studies concluded that the activity and stability of the surface Mo-alkylidenes depend on their anchoring location on the alumina support. In the three most reactive Mo-methylidene sites, the Mo was anchored to the more acidic hydroxyl sites: either two $HO-\mu_1-Al_V$ sites, one $HO-\mu_1-Al_{VI}$ and one $HO-\mu_3-Al_{VI}$ sites, or two $HO-\mu_3-Al_{VI}$ sites. The Mo anchored to the basic $HO-\mu_1-Al_{IV}$ sites was predicted to be less active. These studies have also proposed that isolated surface Mo-alkylidene sites are less likely to be the active sites since such sites tended to transform the active trigonal bipyramidal molybdacyclobutane complex into a more stable and less reactive square pyramidal molybdacyclobutane structure. This theoretical prediction agrees with the current finding that isolated surface MoO_x anchored at basic $HO-\mu_1-Al_{IV}$ sites are difficult to activate for propylene metathesis and that oligomeric surface MoO_x anchored at more acidic $HO-\mu_1-Al_V$ and $HO-\mu_1-Al_{VI}$ surface

hydroxyls are easily activated for propylene metathesis. Although the initial oligomeric surface $MoO_{5/6}$ species become the active sites, it is their anchoring to the more acidic alumina hydroxyls rather than their oligomeric structure that controls their activation. The DFT calculations proposed that the active surface Mo-alkylidene sites are pseudo-MoO_4 coordinated, but the current findings reveal that the activated surface Mo sites are derived from oligomeric pseudo-$MoO_{5/6}$ sites and not from isolated pseudo-MoO_4 sites.

Similar observations were made for activation of surface ReO_4 sites on Al_2O_3 during propylene metathesis[22] with surface ReO_4 sites on more basic alumina hydroxyls unable to become activated while surface ReO_4 sites on more acidic hydroxyls readily activated. Furthermore, both surface ReO_4 sites on alumina are isolated, again emphasizing the important role of the anchoring alumina surface hydroxyls in controlling the activation process.

6.4 Conclusions

The initial dehydrated, oxidized supported MoO_x/Al_2O_3 catalysts primarily consist of isolated dioxo MoO_4 surface sites at low coverage (<1 Mo atoms/nm^2), oligomeric mono-oxo $MoO_{5/6}$ surface species at intermediate coverage (1-4.6 Mo atoms/nm^2), and also crystalline MoO_3 nanoparticles above monolayer coverage (>4.6 Mo atoms.nm^2). The isolated MoO_4 surface species are quite stable and do not activate at mild propylene metathesis reaction conditions (~25-200 °C). The oligomeric $MoO_{5/6}$ surface species, however, readily activate during propylene metathesis at ~25-200 °C. Activation of the surface MoO_x species for propylene metathesis is strongly dependent on their anchoring surface hydroxyl sites on the Al_2O_3 support. The difficult to activate isolated surface dioxo MoO_4 species anchor at the more basic HO-μ_1-Al$_{IV}$ surface hydroxyls while the readily

activated oligomeric surface mono-oxo $MoO_{5/6}$ species anchor at the more acidic HO-$\mu_{1/3}$-$Al_{V/VI}$ surface hydroxyls. The crystalline MoO_3 nanoparticles are not active for propylene metathesis and their presence decreases the accessibility of propylene to the activated surface MoO_x species for metathesis. The catalytic active sites for propylene metathesis are the initial oligomeric mono-oxo $MoO_{5/6}$ surface species on the alumina support. The initial oligomeric mono-oxo $MoO_{5/6}$ surface species activate by removal of an oxo Mo=O and formation of Mo=CH$_2$ and Mo=CHCH$_3$ surface alkyls, thus, retaining the Mo^{+6} oxidation state. The present investigation experimentally establishes, for the first time, the structure-reactivity relationship for propylene metathesis by supported MoO_x/Al_2O_3 catalysts.

Chapter 6 References

1. Rouhi, A. M. Olefin Metathesis: Big-Deal Reaction. *C&EN* **2002**, *80*, 29-33.

2. Banks, R. L. Olefin Metathesis: Technology and Applications. In *Applied Industrial Catalysis*; Leach, B. E., Ed.; Academic Press: Orlando, FL, 1984; pp 215-239.

3. Mol, J. C. Industrial applications of olefin metathesis. *J. Mol. Catal. A: Chem.* **2004**, *213*, 39-45.

4. Pieper, L.; Stryk, A. Market Watch. *http://www.cbi.com/getattachment/47eebcf7-2176-44ab-8f8d-4a1e64505018/Market-Watch.aspx* (accessed 2017).

5. Plotkin, J. S. The Propylene Quandary. *https://www.acs.org/content/acs/en/pressroom/cutting-edge-chemistry/the-propylene-quandary.html* (accessed 08, 2017).

6. Shell *www.shell.com* (accessed 2017).

7. Tian, H.; Roberts, C. A.; Wachs, I. E. Molecular Structural Determination of Molybdena in Different Environments: Aqueous Solutions, Bulk Mixed Oxides, and Supported MoO_3 Catalysts. *J. Phys. Chem. C* **2010**, *114*, 14110-14120.

8. Hu, H.; Wachs, I. E.; Bare, S. R. Surface Structures of Supported Molybdenum Oxide Catalysts: Characterization by Raman and Mo L_3-Edge XANES. *J. Phys. Chem.* **1995**, *99*, 10897-10910.

9. Chen, K.; Xie, S.; Bell, A. T.; Iglesia, E. Structure and Properties of Oxidative Dehydrogenation Catalysts Based on MoO_3/Al_2O_3. *J. Catal.* **2001**, *198*, 232-242.

10. Lwin, S.; Wachs, I. E. Olefin Metathesis by Supported Metal Oxide Catalysts. *ACS Catal.* **2014**, *4*, 2505-2520.

11. Handzlik, J.; Sautet, P. Structure of Isolated Molybdenum(VI) Oxide Species on y-Alumina: A Periodic Density Functional Theory Study. *J. Phys. Chem. C* **2008**, *112*, 14456-14463.

12. Handzlik, J.; Sautet, P. Structure of Dimeric Molybdenum(VI) Oxide Species on y-Alumina: A Periodic Density Functional Theory Study. *J. Phys. Chem. C* **2010**, *114*, 19406-19414.

13. Chempath, S.; Zhang, Y.; Bell, A. T. DFT Studies of the Structure and Vibrational Spectra of Isolated Molybdena Species Supported on Silica. *J. Phys. Chem. C* **2007**, *111*, 1291-1298.

14. Grunert, W.; Stakheev, A. Y.; Morke, W.; Feldhaus, R.; Anders, K.; Shpiro, E. S.; Minachev, K. M. Reduction and Metathesis Activity of MoO_3/Al_2O_3 Catalysts I. An XPS Investigation of MoO_3/Al_2O_3 Catalysts. *J. Catal.* **1992**, *135*, 269-278.

15. Grunert, W.; Stakheev, A. Y.; Feldhaus, R.; Anders, K.; Shpiro, E. S.; Minachev, K. M. Reduction and Metathesis Activity of MoO_3/Al_2O_3 Catalysts II. The Activation of MoO_3/Al_2O_3 Catalysts. *J. Catal.* **1992**, *135*, 287-299.

16. Aguado, J.; Escola, J. M.; Castro, M. C. Metathesis of 1-hexene over MoO_3 and Re_2O_7 supported on mesostructured y-Al_2O_3 prepared with cationic surfactants. *Stud. Surf. Sci. Catal.* **2005**, *156*, 835-842.

17. Handzlik, J.; Sautet, P. Active sites of olefin metathesis on molybdena-alumina system: A periodic DFT study. *J. Catal.* **2008**, *256*, 1-14.

18. Handzlik, J.; Ogonowski, J.; Tokarz-Sobieraj, R. Dependence of metathesis activity of Mo-methylidene sites on their location on (100) y-Al_2O_3 - a theoretical study. *Catal. Today* **2005**, *101*, 163-173.

19. Handzlik, J. Properties and metathesis activity of monomeric and dimeric Mo centres variously located on y-alumina - A DFT study. *Surf. Sci.* **2007**, *601*, 2054-2065.

20. Wachs, I. E. Raman and IR studies of surface metal oxide species on oxide supports: Supported metal oxide catalysts. *Catal. Today* **1996**, *27*, 437-455.

21. Vuurman, M. A.; Stufkens, D. J.; Oskam, A.; Deo, G.; Wachs, I. E. Combined Raman and IR study of MO_x-V_2O_5/Al_2O_3 (MO_x = MoO_3, WO_3, NiO, CoO) catalysts under dehydrated conditions. *J. Chem. Soc. Faraday Trans.* **1996**, *92*, 3259-3265.

22. Lwin, S.; Keturakis, C.; Handzlik, J.; Sautet, P.; Li, Y.; Frenkel, A. I.; Wachs, I. E. Surface ReO_x Sites on Al_2O_3 and Their Molecular Structure-Reactivity Relationships for Olefin Metathesis. *ACS Catal.* **2015**, *5*, 1432-1444.

23. Olsthoorn, A. A.; Moulijn, J. A. An In Situ Infrared Spectroscopic Study of the Activity of y-Alumina Supported $Mo(CO)_6$ for Metathesis and Ethene Polymerization. *J. Mol. Catal.* **1980**, *8*, 147-160.

24. Digne, M.; Sautet, P.; Raybaud, P.; Euzen, P.; Toulhoat, H. Hydroxyl Groups on y-Alumina Surfaces: A DFT Study. *J. Catal.* **2002**, *211*, 1-5.

25. Digne, M.; Sautet, P.; Raybaud, P.; Euzen, P.; Toulhoat, H. Use of DFT to achieve a rational understsanding of acid-basic properties of y-alumina surfaces. *J. Catal.* **2004**, *226*, 54-68.

26. Aritani, H.; Tanaka, T.; Funabiki, T.; Yoshida, S.; Eda, K.; Sotani, N.; Kudo, M.; Hasegawa, S. Study of the Local Structure of Molybdenum-Magnesium Binary Oxides by Means of Mo L_3-Edge XANES and UV-Vis Spectroscopy. *J. Phys. Chem.* **1996**, *100*, 19495-19501.

27. Lin, L.; Lin, W.; Zhu, Y. X.; Zhao, B. Y.; Xie, Y. C. Uniformly Carbon-Covered Alumina and Its Surface Characteristics. *Langmuir* **2005***, 21*, 5040-5046.

28. Bare, S. R.; Vila, F. D.; Charochak, M. E.; Prabhakar, S.; Bradley, W. J.; Jaye, C.; Fischer, D. A.; Hayashi, S. T.; Bradley, S. A.; Rehr, J. J. Characterization of Coke on a Pt-Re/y-Al$_2$O$_3$ Re-Forming Catalyst: Experimental and Theoretical Study. *ACS Catal.* **2017***, 7*, 1452-1461.

29. Van Veen, J. A. R. A Method for the Quantitative Determination of the Basic Hydroxyl Groups on an Alumina Surface. *J. Colloid Interface Sci* **1988***, 121*, 214-219.

30. Imamoglu, Y.; Zumeroglu-Karan, B.; Amass, A. J. *Olefin Metathesis and Polymerization Catalysts: Synthesis, Mechanism and Utilization;* Kluwer Academic Publishers: 1989; Vol. 326.

31. Klimov, O. V.; Alekseev, O. S.; Startsev, A. N. Study of reduced Mo/Al$_2$O$_3$ metathesis catalysts prepared via metal complexes. *React. Kinet. Catal. Lett.* **1995***, 56*, 143-150.

32. Clark, R. J. H. Diffuse-reflectance Spectra of Some Anhydrous Transition-Metal Halides. *J. Chem. Soc.* **1964**, 417-425.

33. Handzlik, J. Metathesis Activity and Properties of Mo-Alkylidene Sites Differently Located on Silica. A Density Functional Theory Study. *J. Phys. Chem. B* **2005***, 109*, 20794-20804.

Chapter 6 Supporting Information
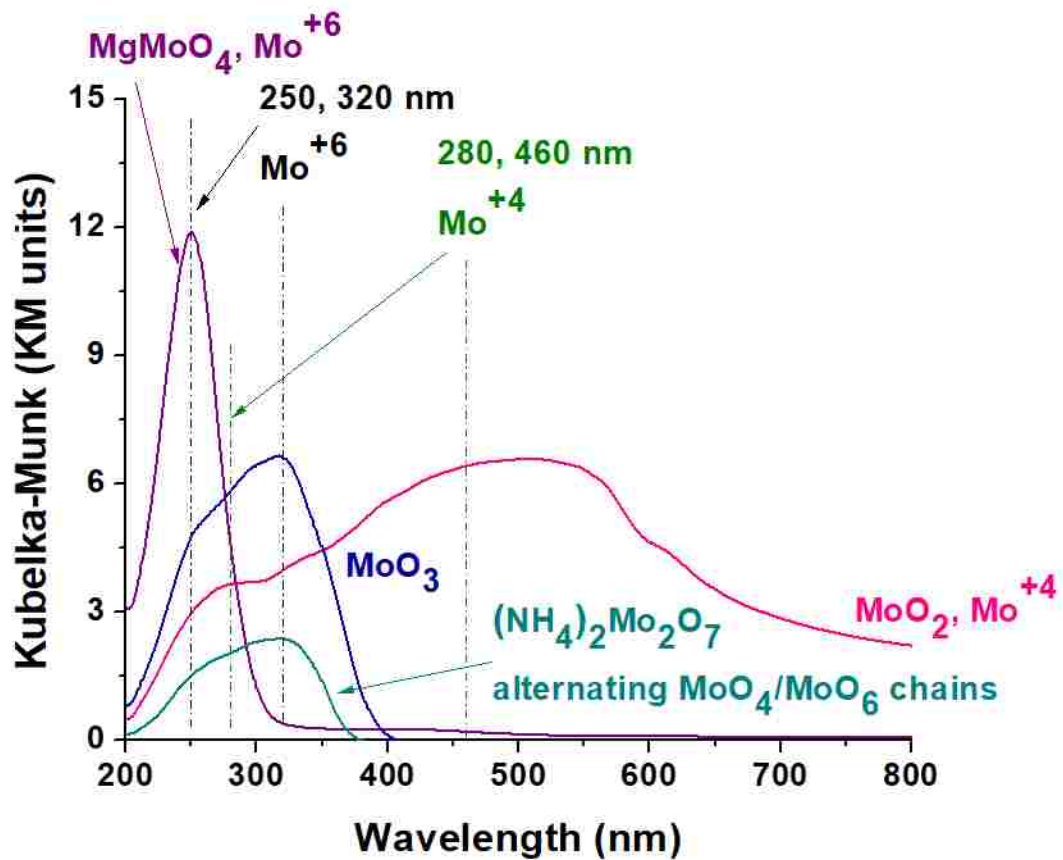
Figure S 6.1. UV-vis spectra of bulk molybdate reference compounds collected under ambient conditions (200-800 nm).
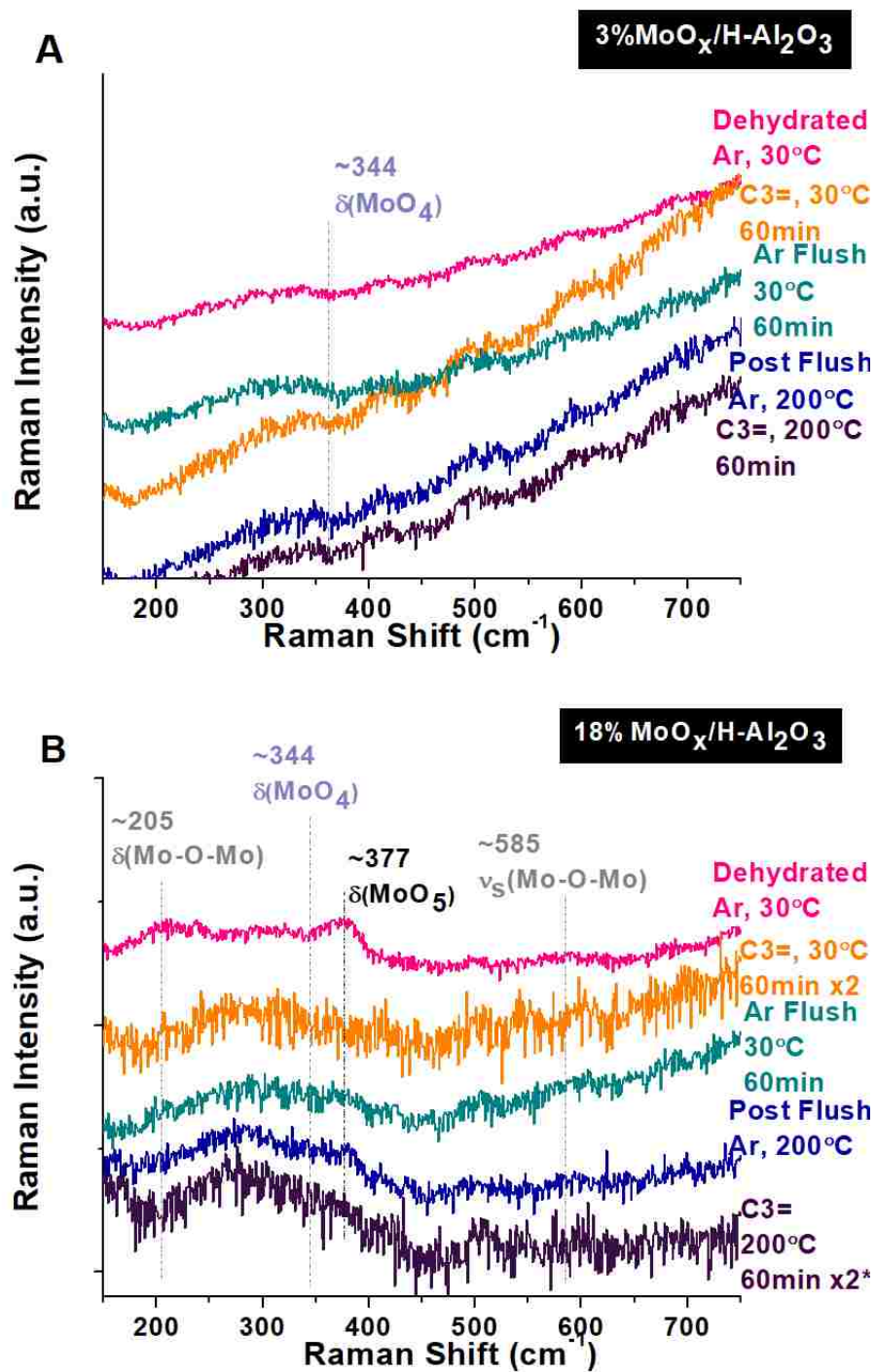
Figure S 6.2. *In situ* Raman spectra of catalysts during propylene: (A) 3% $MoO_x/H-Al_2O_3$ (0.7 Mo atoms/nm^2) and (B) 18% $MoO_x/H-Al_2O_3$ (4.6 Mo atoms/nm^2) (150-700 cm^{-1}). A D0.6 filter was employed to minimize surface heating and induced reduction by the laser. In some cases, the Raman spectral bands are either too weak because of the darkened sample or too strong because of the presence of MoO_3 NPs, so the signal intensity was adjusted to allow better observation of the bands.
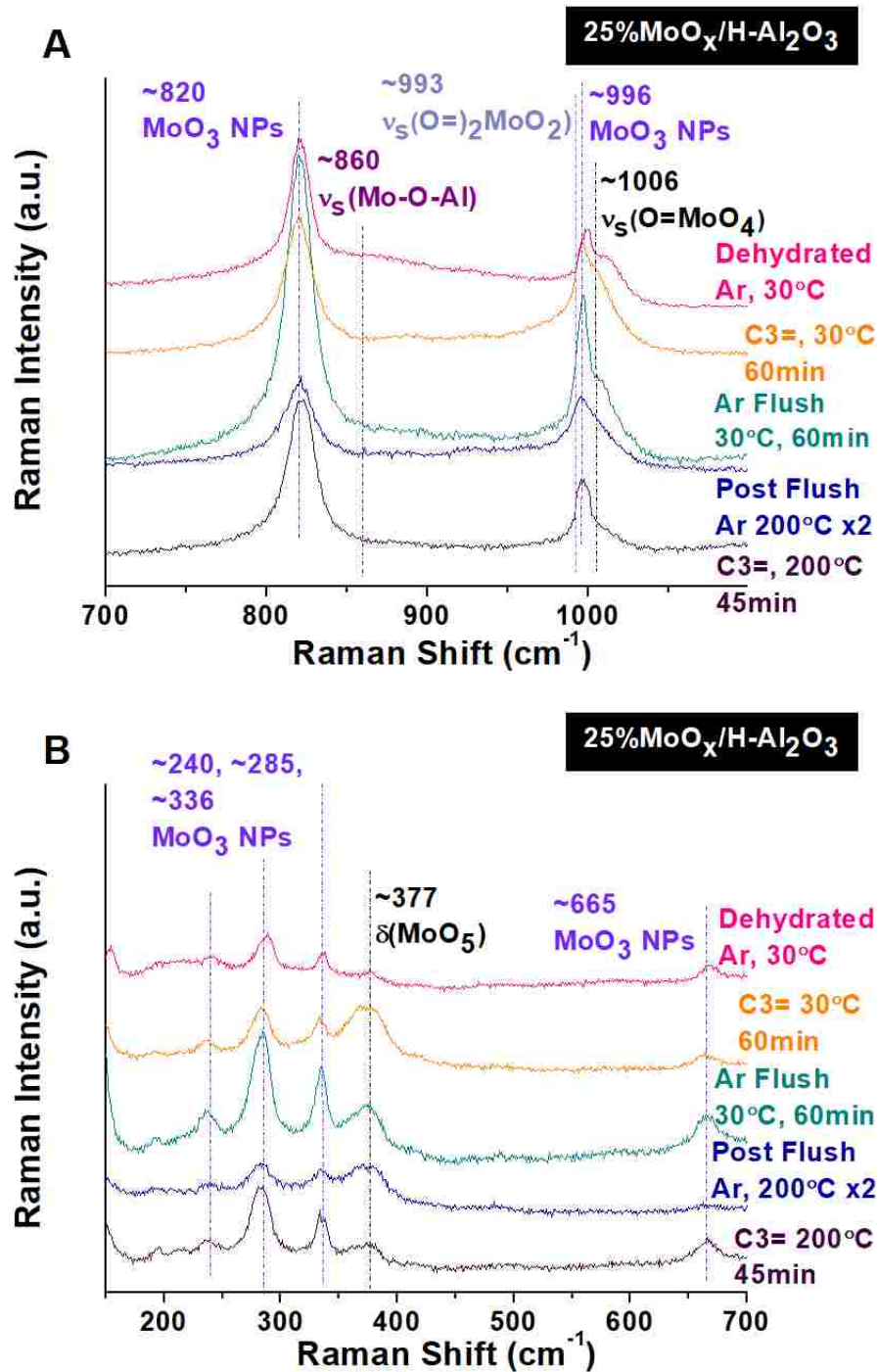
Figure S 6.3. *In situ* Raman spectra of the supported $25\%MoO_x/H-Al_2O_3$ catalyst (5.8 Mo atoms/nm^2) in the (A) 700-1100 cm^{-1} and (B) 150-700 cm^{-1} regions. A D0.6 filter was employed to minimize surface heating and induced reduction by the laser. In some cases, the Raman spectral bands were either too weak because of the darkened sample or too strong because of the presence of MoO_3 NPs, so the signal intensity was adjusted to allow better observation of the bands.

The Raman spectrum of the Harshaw alumina support does not yield any Raman vibrations. An internal standard was used to allow for normalization of the signal intensities of the spectra by physically mixing pure TiO_2 (anatase phase) with the catalysts following a previous procedure (S1). Approximately 0.5wt% of titanium (IV) oxide (TiO_2 anatase, ~45-55 m^2/g, Aldrich Chemical Company, Inc., 99.9%) was physically mixed with the already-prepared supported MoO_x/H-Al_2O_3 catalysts by grinding together for ~10 min to create the MoO_x/H-Al_2O_3+TiO_2. The TiO_2 band at ~636 cm^{-1} exhibited in the H-Al_2O_3+TiO_2 support was used to normalize all the Raman spectra. The normalized *in situ* Raman spectra are presented in Figure S 4. The strong TiO_2 bands in the 150-700 cm^{-1} region prevented observation of the bridging Mo-O-Mo stretching vibration at ~580 cm^{-1} and corresponding bending mode at ~205 cm^{-1}.
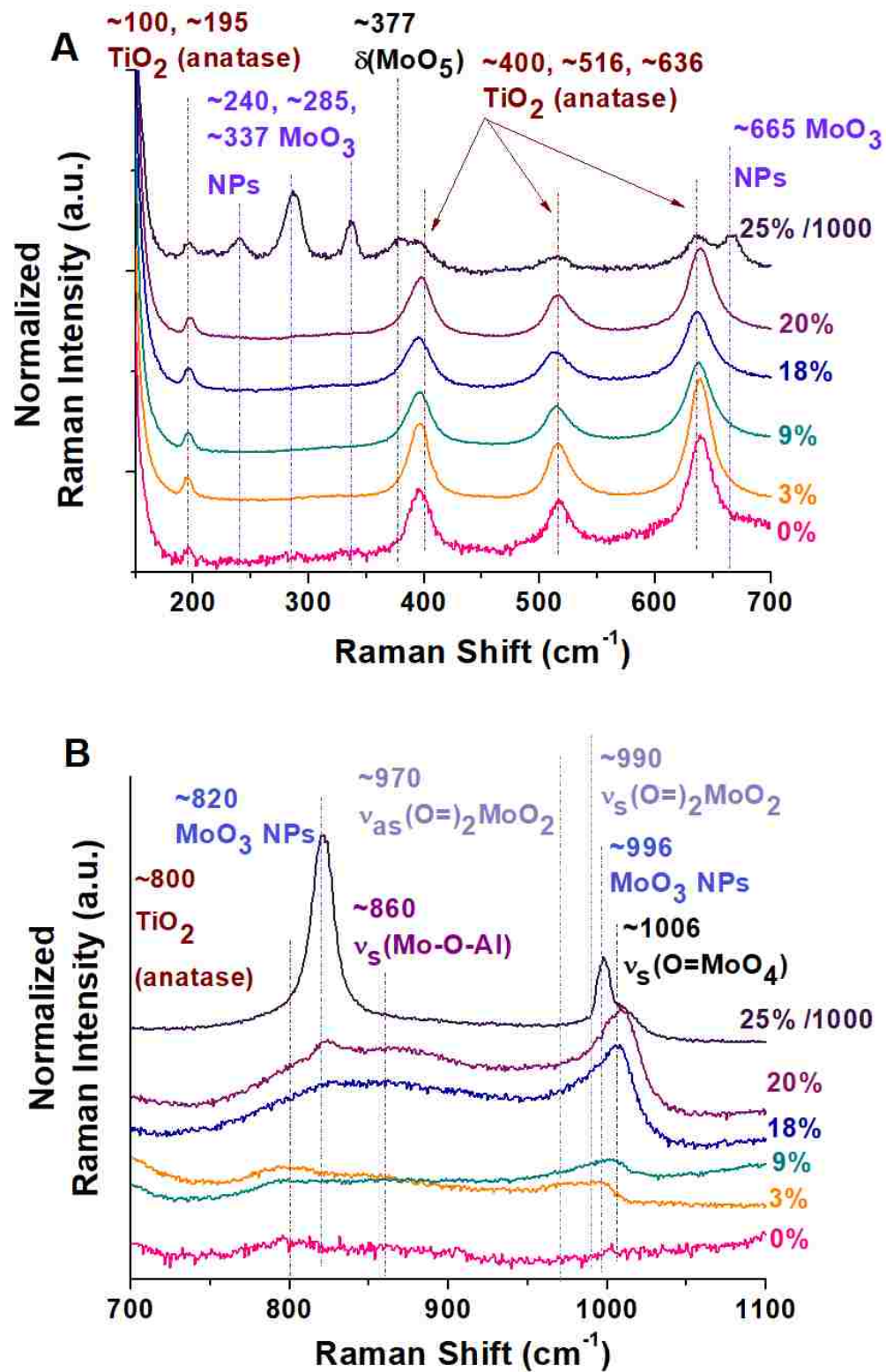
Figure S 6.4. Normalized *in situ* Raman spectra of dehydrated supported MoO_x/H-Al_2O_3+TiO_2 catalysts: (A) 150-700 cm^{-1} and (B) 700-1100 cm^{-1}.
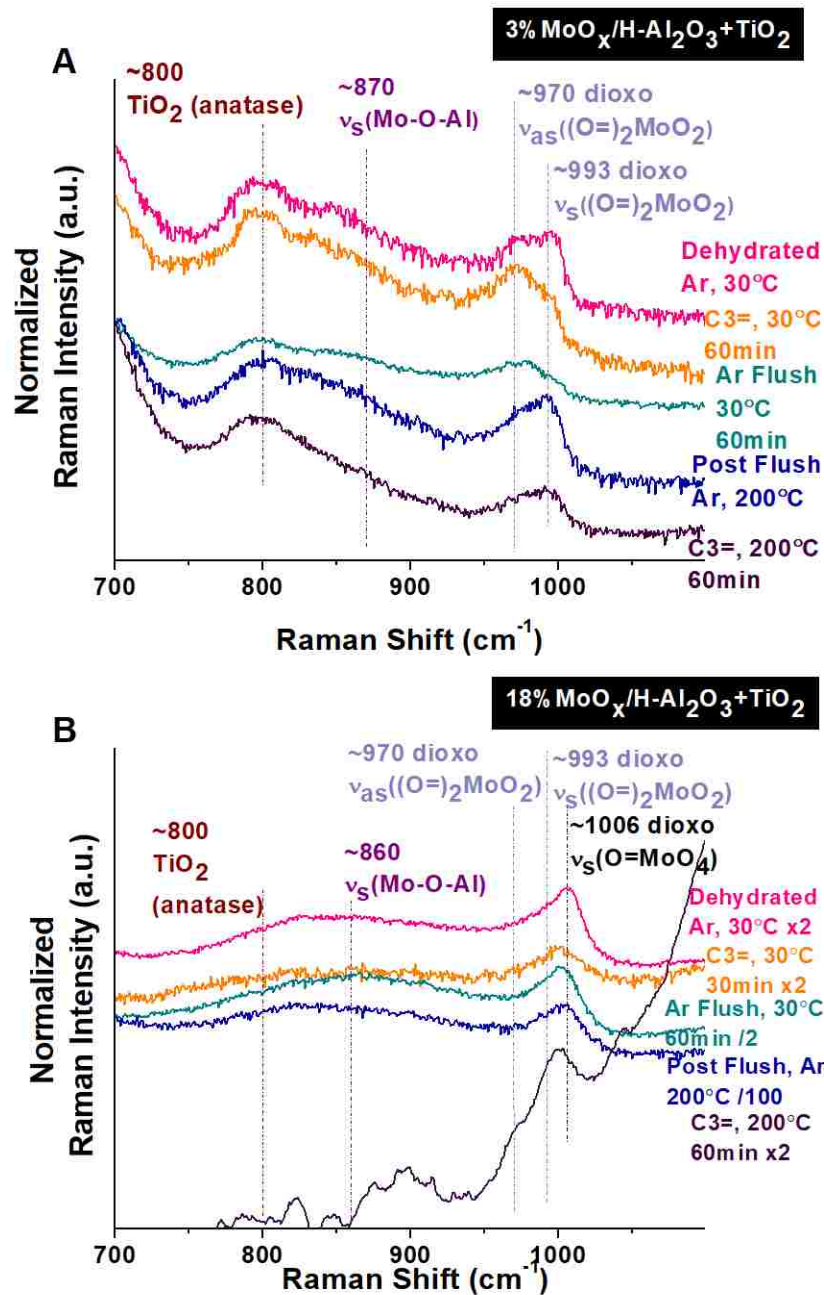
Figure S 6.5. Normalized *in situ* Raman spectra of supported MoO_x/H-Al_2O_3+TiO_2 catalysts during propylene metathesis (700-1100 cm^{-1} region): (A) low surface MoO_x coverage (3%MoO_x/H-Al_2O_3+TiO_2; 0.7 Mo atoms/nm^2) and (B) high surface MoO_x coverage (18%MoO_x/H-Al_2O_3+TiO_2; 4.1 Mo atoms/nm^2). A D0.6 filter was employed to minimize surface heating and induced reduction by the laser. In some cases, the Raman spectral bands were either too weak because of the darkened sample so the signal intensity was adjusted to allow better observation of the bands.
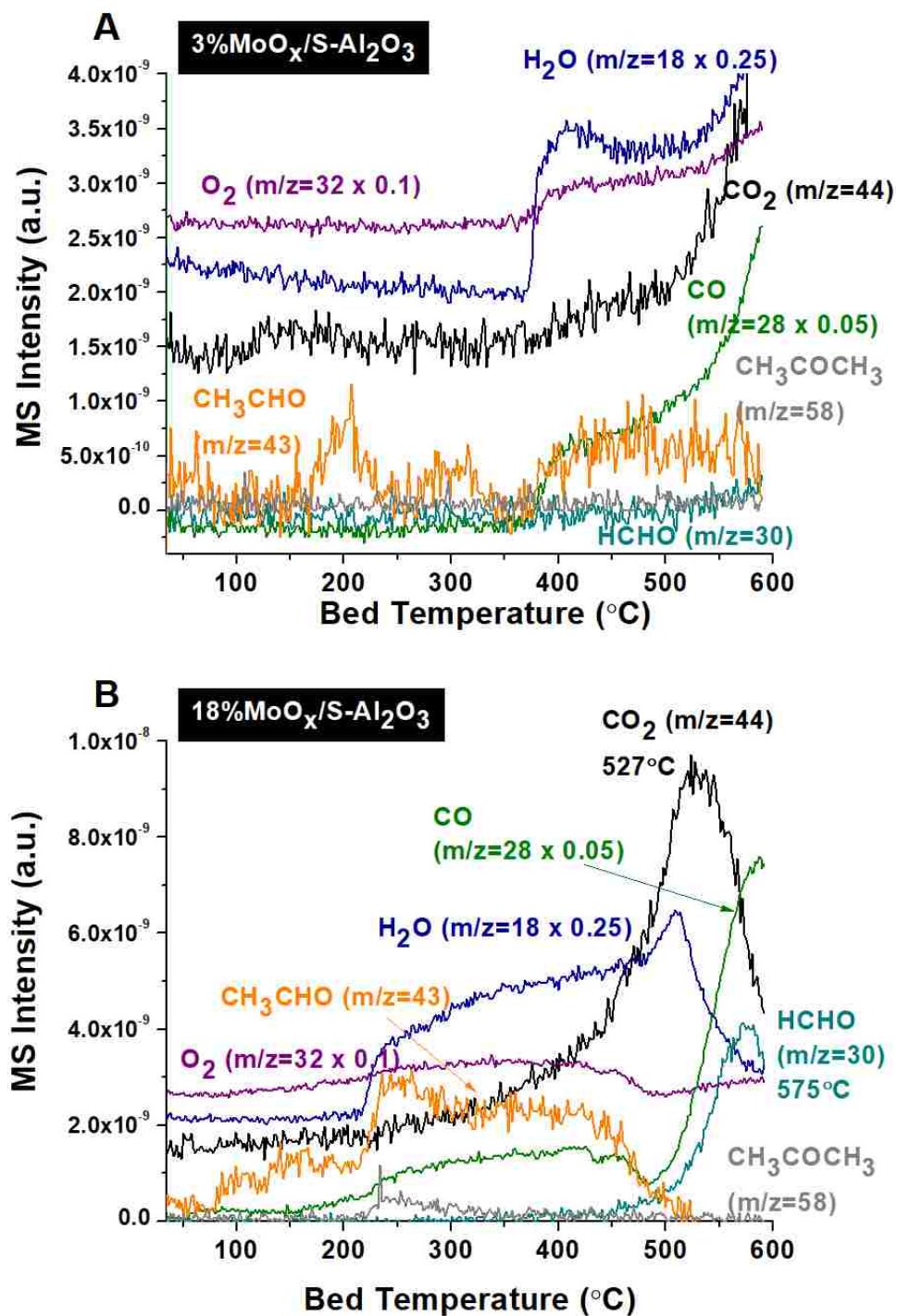
Figure S 6.6. Oxygenated products formed during C_3H_6-TPSR from supported molybdena catalysts: (A) 3% MoO_x/S-Al_2O_3 (0.7 Mo atoms/nm^2) and (B) 18% MoO_x/Al_2O_3 (4.1 Mo atoms/nm^2). The oxygenated products were monitored with an online MS connected to the reactor outlet.

239

Supporting Information References

(S1) Hu, H.; Wachs, I. E. Catalytic Properties of Supported Molybdenum Oxide Catalysts:

In situ Raman and Methanol Oxidation Studies. *J. Phys. Chem.* 1995, *99*, 10911-10922.

Chapter 7 | Activation Mechanism and Surface Intermediates for Olefin

   Metathesis by Supported MoO$_x$/Al$_2$O$_3$ Catalysts

Abstract

The activation mechanism of supported MoO$_x$/Al$_2$O$_3$ catalysts and surface intermediates are established using *in situ* DRIFTS during olefin metathesis reaction conditions with previously synthesized high molybdena content supported catalysts (20-25% MoO$_x$/Al$_2$O$_3$). Activation of the surface MoO$_x$ sites includes protonation of the propylene reactant isopropoxide surface species which then oxidize to coordinated acetone via reduction of the surface MoO$_x$ sites. The acetone desorbs from the catalyst surface, leaving a vacancy for the next propylene molecule to coordinate via oxidative addition and re-oxidize the surface sites back to Mo^{+6}. Thus, activation proceeds via removal of oxo Mo=O bonds and insertion of =CH$_2$ and =CHCH$_3$ alkyls and maintain the surface MoO$_x$ species in the Mo^{+6} oxidation state. This study establishes the active surface intermediates and activation mechanism of the surface MoO$_x$ sites.

7.1   Introduction

Little is known concerning the surface reaction intermediates during olefin metathesis and activation mechanism of the surface MoO$_x$ sites. Some early *in situ* studies[1] concluded that propylene becomes π-bonded to oxidized and CO-reduced catalyst surface of the MoO$_x$/Al$_2$O$_3$ catalysts. An IR band at 1600 cm^{-1} was detected and assigned to the C=C bond of the π-bond, which was red-shifted from the band seen at 1645 cm^{-1} when propylene is adsorbed on pure Al$_2$O$_3$. The adsorption of propylene was therefore concluded to be reversible, and this π-bonded complex was proposed to be a reaction intermediate during propylene metathesis. However, direct adsorption of propylene on the Al$_2$O$_3$ support was

not considered and attempts were not made to distinguish between propylene bonded to Mo sites and Al sites.[1]

From DFT studies[2], it has been suggested also that Mo-cyclobutane intermediates anchored to AlO_6 cause the high reactivity. However, cyclic intermediates are usually less stable surface species[3], and theoretical studies have not investigated the activation of the surface MoO_x sites during olefin metathesis.

This chapter presents *in situ* DRIFTS studies to determine the surface intermediates and activation mechanism of the surface MoO_x sites in olefin metathesis reaction conditions.

7.2 Results

7.2.1 C_4H_8-C_2H_4 Titration

Figure 7.1 presents the *in situ* DRIFT spectra taken during the C_4H_8-C_2H_4 titration of the 20% MoO_x/Al_2O_3 catalyst, which corresponds to approximately monolayer coverage of MoO_x, ensuring none of the detected IR bands correspond to species adsorbed directly on the alumina surface.

After normalizing the IR spectra against the Al_2O_3 vibration at ~1041 cm^{-1}, the difference spectra were obtained by subtracting the IR spectrum of the initial dehydrated catalyst from each IR spectrum taken during the titration experiment. Figure 7.1 A presents the 1200-1900 cm^{-1} range, while Figure 7.1 B presents the hydrocarbon region of 2800-3200 cm^{-1}. During butene adsorption at 120 °C, bands arise at 2864, 2923, and 3035 cm^{-1} characteristic of gas phase butene[4], which are removed during the subsequent Ar flush for 45 min. Several other bands that appeared during butene adsorption persisted through the Ar flush, indicating that they are related to strongly bound intermediates and may

242

participate in the olefin metathesis reaction. In Figure 7.1, bands are observed at 1390 and 1460 for the $\delta_s(CH_3)$ and $\delta_s(CH_2)$ deformation modes and 2880, 2939, and 2980 assigned to the corresponding stretching modes $\nu_s(CH_3)$, $\nu_{as}(CH_2)$, and $\nu_{as}(CH_3)$, respectively.[5-7] These bands characterize the surface intermediates Mo=CH$_2$ and Mo=CHCH$_3$.[8,9] A strong band is also observed at ~1680 cm^{-1} with a shoulder at ~1650 cm^{-1}, assigned to the $\nu(C=C)$ of an adsorbed butene π-complex.[6] The ~1680 cm^{-1} band is slightly red-shifted to lower wavenumbers from the characteristic $\nu(C=O)$ stretching region, suggesting that there may be formation of a surface intermediate containing a carbonyl group. During ethylene titration at a constant temperature of 120 °C after the argon flush, little to no change is observed in the bands. However, as the temperature is ramped from 120 °C under flowing ethylene, the bands at ~1650 and ~1680 cm^{-1} decrease, while a broad band at ~1555 cm^{-1} appears beginning at ~210 °C. In the bending region, the bands at 1390 and 1460 cm^{-1} for $\delta_s(CH_3)$ and $\delta_s(CH_2)$, respectively, decrease, while a band at ~1465 cm^{-1} increases starting at ~210 °C. The appearance of the bands at 1465 and 1555 cm^{-1} coincide with the disappearances of the bands at 1680 cm^{-1} for $\nu(C=O)$ and 1390 and 1460 cm^{-1} for $\delta(CH_3)$ and shift of the 2939 cm^{-1} band to 2935 cm^{-1}, suggesting these phenomena are due to the decomposition of a carboxylate, allowing assignment of the former bands to the $\nu_s(COO^-)$ and $\nu_{as}(COO^-)$, respectively.[10,11]

    In situ DRIFTS of propylene adsorption and temperature programming revealed similar IR bands to those of the C$_4$H$_8$-C$_2$H$_4$ titration (see Figure S 7.1). Gas-phase propylene gives rise to bands at 1339, 1384, and 1466 cm^{-1} in the bending region and 2920, 2943, 2953, 3082, and 3103 cm^{-1} in the CH stretching region[4], which are removed during the subsequent 45 min Ar flush. After the Ar flush, bands at 1375 cm^{-1} and 2877, 2929, and 2985 cm^{-1} are

still present for the deformation mode $\delta_s(CH_3)$ and stretching modes $\nu_s(CH_3)$, $\nu_{as}(CH_2)$, and $\nu_{as}(CH_2)$, respectively.[5-7] These bands are for strongly bound intermediates are related to the $Mo=CH_2$ and $Mo=CHCH_3$ surface intermediates[8,9] and agree with the bands observed after butene adsorption with subsequent Ar flushing. During subsequent propylene TP, the bands at 1653 and 1687 cm^{-1} for the $\nu(C=C)$ and $\nu(C=O)$ vibrations, respectively, and 1375 cm^{-1} for $\delta_s(CH_3)$ decrease, while broader bands appear at ~1470 and 1570 cm^{-1} resulting from decomposition of a carboxylate[10,11], as for butene-ethylene titration. The similarity in the bands observed in the forward (propylene adsorption and TP) and reverse (butene-ethylene titration) directions of the olefin metathesis reaction demonstrate that the activation mechanism of the surface MoO_x sites on Al_2O_3 does not depend on the specific reactant olefins.

In recent studies, a band for $\nu(C=O)$ was detected during propylene metathesis over supported MoO_x/SBA-15 catalysts.[9] It was proposed that adsorption of propylene causes formation of isopropoxide species that then oxidize and form acetone.[9]

To determine the origin of the $\nu(C=O)$ bond for supported MoO_x/Al_2O_3 catalysts, the *in situ* IR bands resulting from acetone and iso-propanol adsorption and subsequent temperature programming with propylene were determined (see Figure S 7.2 and Figure S 7.3, respectively).

Figure S 7.2 presents the *in situ* DRIFTS of acetone adsorption and subsequent temperature programming in flowing propylene. After 30 min of acetone adsorption at 30 °C, the characteristic bands for acetone are detected. Gas-phase acetone exhibits bands at ~1210-1230, 1720, 1736, 2923, 2970, 3008, and 3030 cm^{-1}.[4] Bands are also present at ~1365 and 1425 cm^{-1} for the deformation modes $\delta(CH_3)$.[5,9] With the introduction of

propylene at 30 °C, the gas-phase acetone bands in the ~1210-1750 cm^{-1} decrease since there is no more flow of acetone (see Figure S 7.2 A), although there is little change in the hydrocarbon stretching region (2800-3200 cm^{-1}) since in this region, the gas-phase propylene bands overlap with those of gas-phase acetone (see Figure S 7.2 B).[4] As the temperature is increased to 60 °C (above the boiling point of acetone) under flowing propylene, the bands for the acetone decrease because the acetone is evaporating from the catalyst.[12] The presence of a carbonyl-containing surface species is evidenced by the band at 1700 cm^{-1} that red-shifts to ~1680 cm^{-1} as the temperature continues increases, showing that the carbonyl group is anchoring to the catalyst surface. When the temperature is further increased to 210 °C in flowing propylene, the band at ~1683 decreases and broad bands are detected at ~1465 and 1570 cm^{-1} assigned to $\nu_s(COO^-)$ and $\nu_{as}(COO^-)$, respectively, arising from decomposition of a carboxylate group.[10,11] The latter three bands (~1683, 1465, and 1570 cm^{-1}) agree with those detected during C_4H_8-C_2H_4 titration (see Figure 7.1), propylene adsorption-TP (see Figure S 7.1), and iso-propanol adsorption with subsequent propylene TP (see Figure S 7.3). The shifting of the $\nu(C=O)$ band and formation of the $\nu_s(COO^-)$ and $\nu_{as}(COO^-)$ bands mirror the events taking place in olefin metathesis conditions (see Figure 7.1 and Figure S 7.1) as well as those during iso-propanol adsorption and propylene temperature programming (see Figure S 7.3), demonstrating that acetone is formed during activation of the surface MoO$_x$ sites.

Figure S 7.3 presents the *in situ* DRIFT spectra from adsorption of iso-propanol at 30 °C and subsequent temperature ramping under flowing propylene. After 30 min of iso-propanol adsorption at 30 °C, characteristic bands in the bending region are visible at ~1275 cm^{-1} for $\nu(C-O)$, 1338 cm^{-1} for in-plane $\delta(OH)$, and 1376, 1390, and 1465 cm^{-1} for

$\delta(CH_3)$ assigned to isopropoxide species[9], while in the hydrocarbon stretching region, bands arise from the corresponding stretching mode $\nu(CH_3)$ at ~2885, 2935, and 2980 cm^{-1}.[5,9]. When the reactant gas flow is switched to propylene and the temperature is increased, the bands for the isopropoxide species decrease, and when the temperature reaches 120 °C, a band appears at ~1700 cm^{-1} for the $\nu(C=O)$ of a carbonyl-containing species. As the temperature is increased to 180 °C under the propylene flow, the carbonyl band increases and red-shifts to ~1683 cm^{-1}, indicating that this surface species is binding to the surface of the MoO_x/Al_2O_3 catalyst. As the temperature is further increased to 210 °C in flowing propylene, the band at ~1683 decreases and broad bands are detected at ~1465 and 1555 cm^{-1} assigned to $\nu_s(COO^-)$ and $\nu_{as}(COO^-)$, respectively, arising from decomposition of the carboxylate.[10,11] The latter three bands (~1683, 1465, and 1555 cm^{-1}) match with those detected during C_4H_8-C_2H_4 titration (see Figure 7.1), propylene adsorption-TP (see Figure S 7.1), and acetone adsorption with subsequent C_3H_6-TP (see Figure S 7.2), demonstrating that isopropoxide species oxidize to acetone during activation of the surface MoO_x sites.
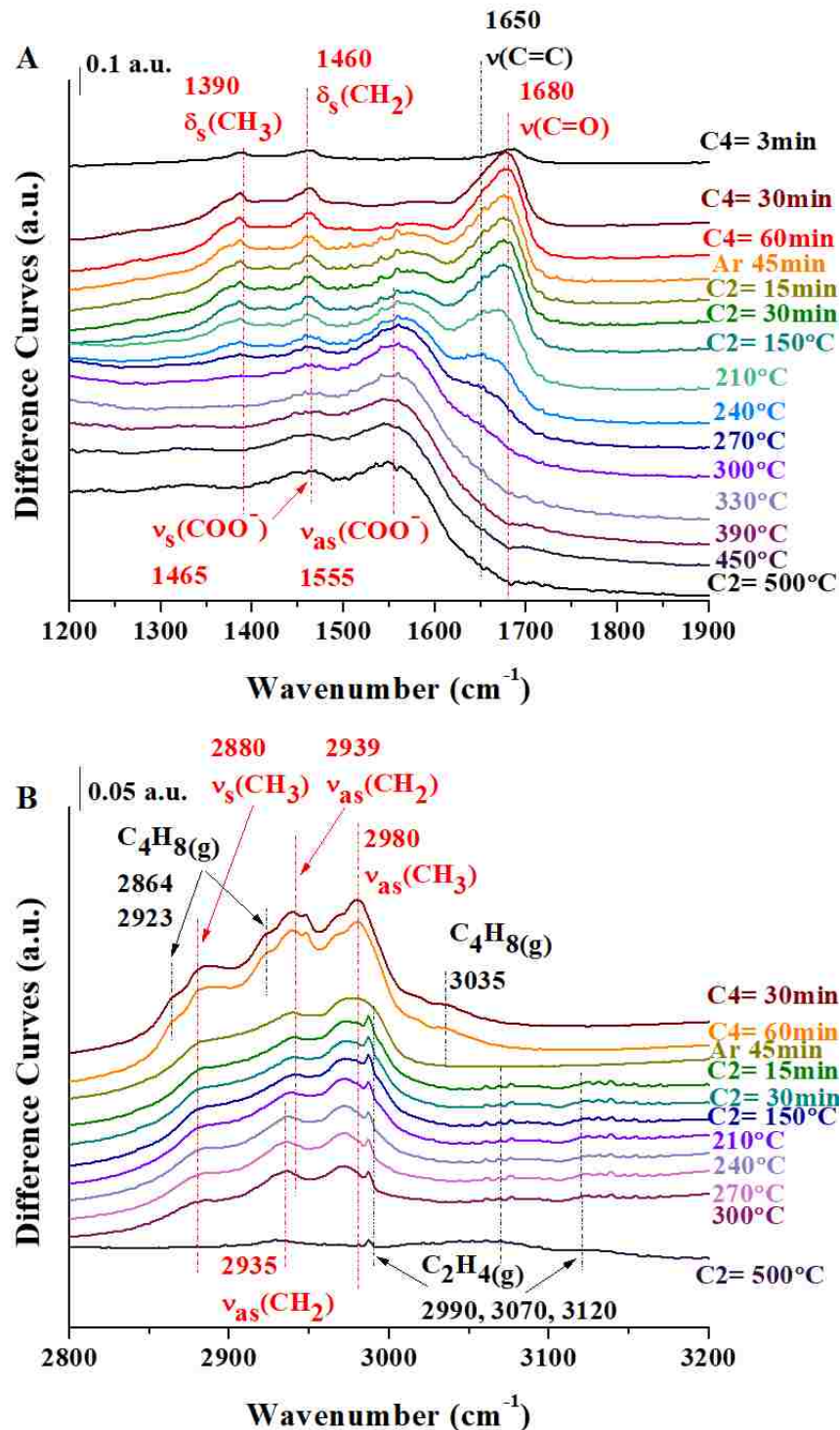
Figure 7.1. *In situ* DRIFT spectra during C_4H_8-C_2H_4 titration at 120 °C and subsequent temperature programming at 10 °C/min under flowing ethylene of the supported 20% MoO_x/Al_2O_3 catalyst. (A) 1200-1900 cm^{-1} and (B) 2800-3200 cm^{-1}.

7.2.2 C₃D₆-C₃H₆ Isotope Exchange

Figure 7.2 presents the *in situ* DRIFT spectra taken during C_3D_6-C_3H_6 isotope exchange of the supported 20% MoO_x/Al_2O_3 catalyst, which corresponds to approximately monolayer coverage of MoO_x, ensuring none of the detected IR bands correspond to species adsorbed directly on the alumina surface. After C_3D_6 adsorption at 120 °C, the hydrocarbon region exhibits three bands attributed to stretching modes $\nu_s(CD_3)$ and $\nu_{as}(CD_3)$ stretching modes at ~2070 and 2229 cm^{-1}, respectively, for the Mo=CDCD$_3$ surface intermediates, and ~2137 cm^{-1} for $\nu_{as}(CD_2)$ of the Mo=CD$_2$ surface intermediates.[8,9] The ν(C=C) and ν(C=O) vibrations that arose during C_4H_8-C_2H_4 titration and propylene adsorption-TP are also detected in these results at ~1580 cm^{-1} and ~1683 cm^{-1}, respectively (see Figure S 7.4), and broad band arises at ~2600 cm^{-1} assigned to ν(OD) of a D-labeled hydroxyl group. The former bands are associated with the D-labeled Mo=CD$_2$ and Mo=CDCD$_3$ surface intermediates[8,9] and would be expected to be red-shifted to lower wavenumbers compared to the bands for the H-labeled surface intermediate due to the mass effect of deuterium *vs.* hydrogen.[6,13,14] When the C_3D_6 flow is switched to C_3H_6, the CD$_3$ bands immediately begin to decrease, while bands arise at ~2877 and 2985 cm^{-1} for $\nu_s(CH_3)$ and $\nu_{as}(CH_3)$ of the Mo=CHCH$_3$ surface intermediates, respectively, and 2929 cm^{-1} for $\nu_{as}(CH_2)$ of the Mo=CH$_2$ intermediates.[5,7-9,13,14] The band for ν(OD) also decreases and shifts to ~3500 cm^{-1} for ν(OH) arising from hydrogen bonding[6] and indicates the involvement of hydroxyl groups in the activation of surface MoO_x sites. During C_3H_6-TP, the bands associated with D-labeled surface intermediates continue to decrease, while the H-labeled species bands continue to increase. The formation of the H-labeled surface species and increase in the CH$_2$ and CH$_3$ bands evidence the isotope exchange and

occurrence of the metathesis reaction via $Mo=CD_2$ and $Mo=CDCD_3$ surface intermediates. The $Mo=CD_2$ intermediate has been previously detected in C_2D_4 studies of $MoO_x/SBA-15$[9] and MoO_x/SiO_2[8]. At ~200 °C, broad bands appear at ~1450 and 1550 cm^{-1}, similar to those seen during all of the above results (see Figure 7.1, Figure S 7.1, and Figure S 7.2), assigned to $\nu_s(COO^-)$ and $\nu_{as}(COO^-)$, respectively. The isotopic shifts and ratios of the vibrational bands are presented in Table 7.1. The calculated $\nu(H)/\nu(D)$ ratios agree well with those calculated in adsorption studies of NH_3 and ND_3 on anatase phase TiO_2 for $\nu(NH3)/\nu(ND3)$.[13,14] All the ratios are about equal (~1.3) and confirm the above band assignments.
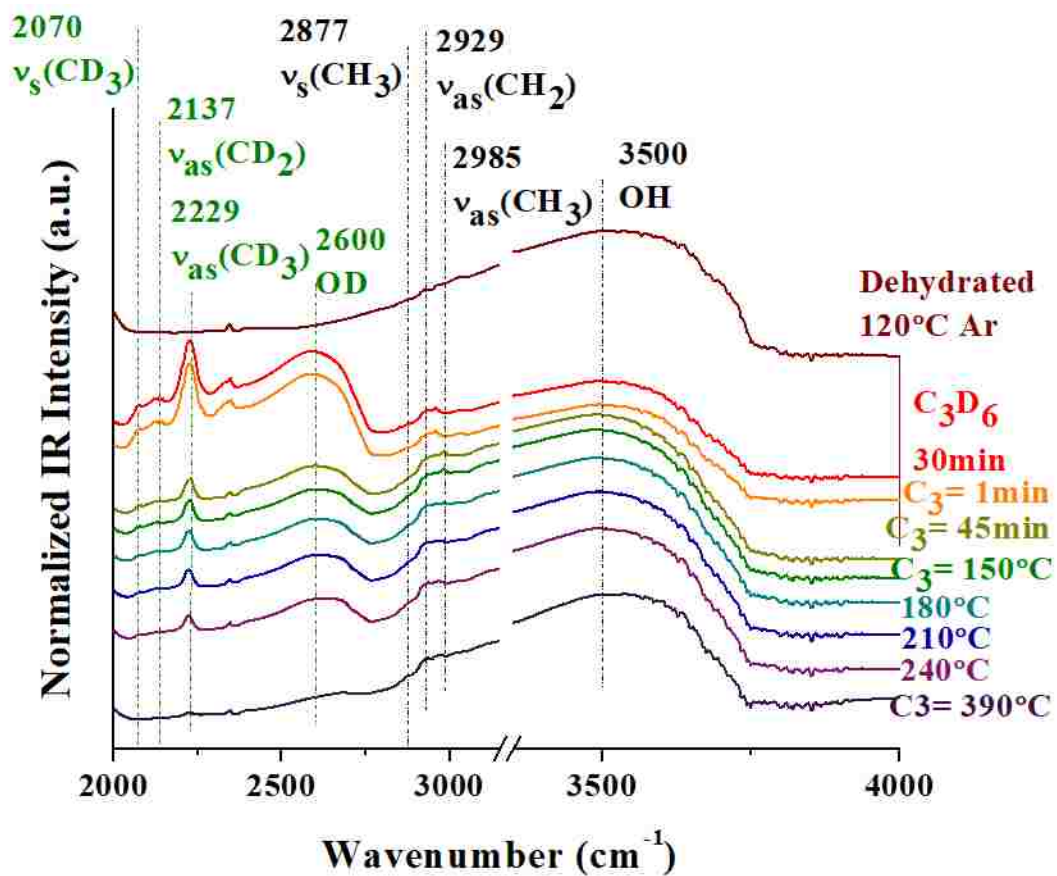
Figure 7.2. *In situ* DRIFT spectra during C_3D_6-C_3H_6 isotope exchange at 120 °C and subsequent temperature programming at 10 °C/min under flowing propylene of the supported 20% MoO_x/Al_2O_3 catalyst.

Table 7.1. Observed Isotopic Shifts			
Band Assignment	$\nu(H)$ (cm^{-1})	$\nu(D)$ (cm^{-1})	$\nu(H)/\nu(D)$
OH/OD	3500	2600	1.346
CH$_3$/CD$_3$ (symmetric)	2877	2070	1.339
CH$_2$/CD$_2$ (asymmetric)	2929	2137	1.371
CH$_3$/CD$_3$ (asymmetric)	2985	2229	1.390

7.3   Discussion

7.3.1   Activation Mechanism

The above results allow for proposing an activation mechanism for the MoO_x surface sites. The propylene reactant is protonated by the acidic hydroxyl site to form surface isopropoxide. *In situ* DRIFTS of the dehydrated supported MoO_x/Al_2O_3 catalysts revealed that at high MoO_x loadings (e.g., 20% MoO_x/Al_2O_3), the molybdena species anchor to the more acidic $HO-\mu_{1/3}-Al_{V/VI}$ sites. It was demonstrated that these sites are responsible for olefin metathesis. The isopropoxide oxidizes to acetone using oxygen from the surface MoO_x sites, which explains the $Mo^{+6} \rightarrow Mo^{+4}$ reduction step. The results of Chapter 6 demonstrated with *in situ* Raman spectroscopy and UV-vis DRS during propylene metathesis that the surface $Mo^{+6}O_x$ species lose oxygen and reduce to $Mo^{+4}O_x$ sites. Formation of acetone is evidenced by the appearance of the $\nu(C=O)$ stretching vibration at 1680 cm^{-1}, which matches the $\nu(C=O)$ vibration detected during acetone adsorption and subsequent C_3H_6-TP (see Figure S 7.2), as well as during iso-propanol adsorption and C_3H_6-TP (see Figure S 7.3). Acetone adsorption demonstrated that the $\nu(C=O)$ for gas-phase acetone is at ~1700 cm^{-1} which then red-shifts when it coordinates to the MoO_x surface sites. The acetone later desorbs from the surface, allowing for more propylene molecules to coordinate. C_3H_6-TPSR-MS in Chapter 6 revealed the formation of several surface oxygenates during activation of the MoO_x/Al_2O_3 catalysts, including CH_3CHO and acetone, the former being the most abundant oxygenate at low temperatures and forming first. The coordination of another propylene molecule is via oxidative addition and causes the Mo metal center to go through a re-oxidation step $Mo^{+4} \rightarrow Mo^{+6}$. This forms the Mo-carbene active site.

Oxidation of propylene to acetone via isopropoxy intermediates has been shown to take place in other instances as well, such as with mixed Co_3O_4-MoO_3[15], SnO_2-MoO_3[15], MoO_x/Al_2O_3[10,11], and MoO_x/SBA-15[9].

This activation mechanism for surface MoO_x sites has previously been proposed for supported MoO_x/SBA-15 catalysts[9] and MoO_x/Al_2O_3 catalysts[10,11]. Amakawa *et al.*[9] conducted *in situ* IR studies and detected the formation of methyl groups during propylene adsorption at 100 °C and subsequent evacuation. Bands for ν(C=C) were not detected, leading the authors to conclude that there are no strongly bound species with C=C bonds. The peaks were attributed to isopropoxy species adsorbed on a metal oxide surface, which was confirmed by adsorption of iso-propanol and acetone. The Mo^{+6}-alkylidene species were proposed to be generated by protonation of propylene driven by surface Brönsted acid sites, oxidation of isopropoxide to acetone, and oxidative addition of propylene to create the Mo^{+6}-alkylidene species. Ammonia adsorption detected both Lewis and Brönsted acid sites, although the structure of the hydroxyl sites and molybdena anchoring sites were not discussed. Acetone was proposed to be formed, and its desorption was assumed in the proposed mechanism; however, there was no direct evidence of the acetone leaving the catalyst surface.[9]

The current IR studies are in slight disagreement with the above conclusions. *In situ* DRIFTS during propylene adsorption and C_4H_8-C_2H_4 titration did detect ν(C=C) bands at ~1600 cm^{-1} that persist the Ar flush (see Figure 7.1 and Figure S 7.1), which suggests they are related to strongly bound surface intermediates. This is likely due to the higher adsorption temperature of 120 °C instead of 100 °C, which reduces the amount of water on the catalyst surface, a known poison for olefin metathesis.[3] Additionally, activation of

surface MoO_x supported on silica-type surfaces is more difficult than activation of surface MoO_x supported on alumina, and higher activation temperatures are necessary.[3] Acetone was a detected oxygenate during previous C_3H_6-TPSR-MS results, demonstrating that the acetone de-coordinates during activation of the surface MoO_x sites.

Davydov *et al.*[10,11] used *in situ* IR spectroscopy to elucidate the mechanism of acetone formation and role of Brönsted acid sites in propylene oxidation over supported MoO_x/Al_2O_3 catalysts since acetone is the main product of partial oxidation. Propylene adsorption of a 25% MoO_x/Al_2O_3 catalyst indicated the formation of an isopropylate complex with the appearance of IR bands at 1090 cm^{-1} ν(C-O), 1380 cm^{-1} δ(CH), 1465 cm^{-1} δ(CH), 2885 cm^{-1} ν(CH), 2940 cm^{-1} ν(CH), and 2980 cm^{-1} ν(CH). The complex was assumed to have formed due to the transfer of a mobile proton from the catalyst to the propylene molecule, which then stabilizes on the catalyst surface. Iso-propyl alcohol was adsorbed on the catalyst and corroborated the assignment, since the IR bands were similar. When the temperature was increased under propylene, the bands for the isopropylate complex decreased in intensity, while acetone appeared (ν(C=O) at 1680 cm^{-1} and ν(C-C) at 1250 cm^{-1}). As the temperature is further increased to 400 °C, destructive oxidation of a carboxylate group is attributed to the appearance of bands at 1480 and 1570 cm^{-1} assigned to ν_s(COO$^-$) and ν_{as}(COO$^-$), respectively. Thus, it was concluded that acetone formation on MoO_x/Al_2O_3 catalysts require strong Brönsted acid sites to protonate the propylene to form isopropylate complexes that are further oxidized to acetone.[10,11]

The results here agree well with the conclusions from Davydov *et al.* Propylene adsorption on 25% MoO_x/Al_2O_3 (see Figure S 7.1) and adsorption of iso-propanol on 20% MoO_x/Al_2O_3 (see Figure S 7.3) resulted in similar spectral bands to those detected by

Davydov *et al.* and confirms that propylene is protonated by a proton from the acid hydroxyl site to form surface isopropoxide.[10,11]
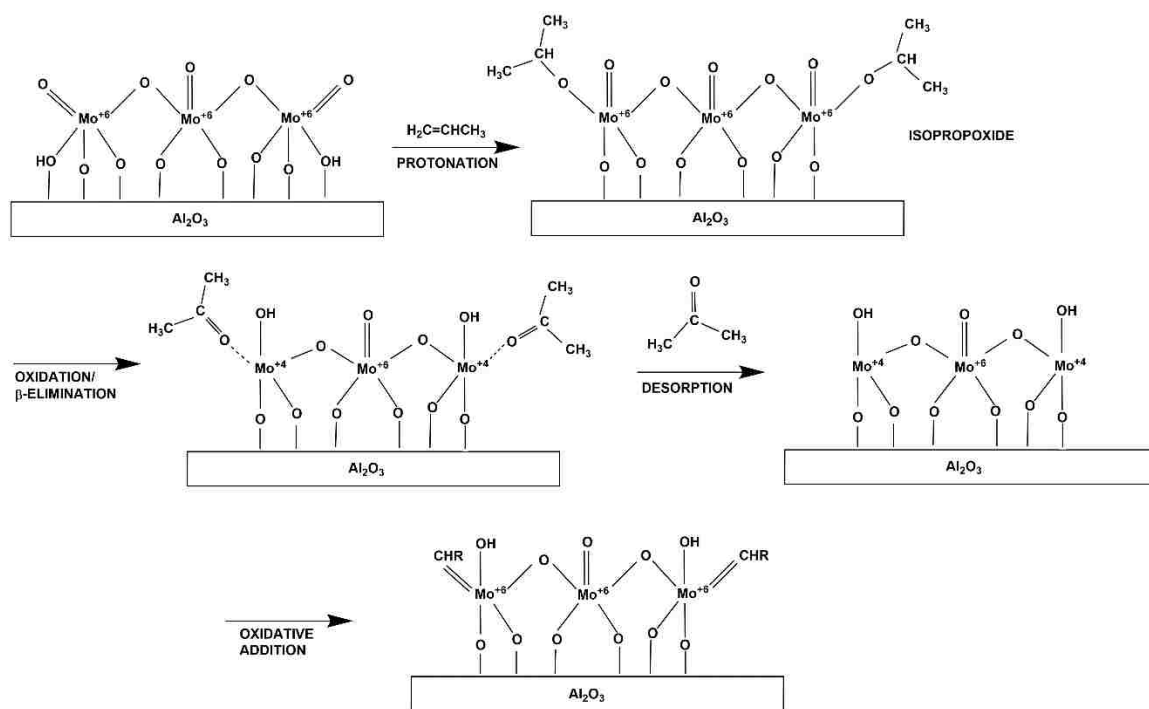
Scheme 7.1. Proposed activation mechanism for oligomeric MoO_x surface species anchored to acidic $OH-\mu_{1/3}-Al_{V/VI}$ sites.

7.3.2 Surface Reaction Intermediates

C_4H_8-C_2H_4 titration results indicate the appearance of CH_2 and CH_3 surface species, suggesting that the metathesis reaction proceeds via $Mo=CH_2$ and $Mo=CHCH_3$ surface intermediates (see Figure 7.1). The participation of these surface intermediates is corroborated by C_3D_6-C_3H_6 isotope exchange (see Figure 7.2 and Figure S 7.4).

Carbene intermediates have been previously proposed in the literature, primarily for experimental studies of silica-based supported MoO_x catalysts[8,9], but have also been proposed for MoO_x/Al_2O_3[10,11], although the reaction conditions were not always industrially-relevant to olefin metathesis conditions (e.g., photo- or CO-reduced).

An adsorbed propylene complex has been proposed based on *in situ* IR studies.[1] It was concluded that propylene becomes π-bonded to oxidized and CO-reduced catalyst surface of the MoO_x/Al_2O_3 catalysts as evidenced by the appearance of an IR band at 1600 cm^{-1} which is red-shifted from the propylene adsorbed on pure Al_2O_3 at 1645 cm^{-1},[1] and thus concluded to be irreversibly adsorbed, and the active surface intermediate was concluded to be a π-bonded propylene complex, although direct adsorption of propylene on the Al_2O_3 support was not considered and attempts were not made to distinguish between propylene bonded to Mo sites and Al sites. Furthermore, studies were not undertaken to determine if the π-bonded propylene complex transforms to other complexes during olefin metathesis conditions. The current studies also detect IR bands for $\nu(C=C)$, although they are at ~1650 cm^{-1}. The use of catalysts that are either approximately at or above monolayer coverage (monolayer $\approx$ 20% MoO_x/Al_2O_3[3,16,17]) demonstrates that any IR bands detected in these studies are related to adsorption on the surface MoO_x sites. The shift in the $\nu(C=C)$

band may be due to different reaction conditions (photo-reduction in CO at room temperature *vs.* olefin at 120 °C).[1]

In DFT studies, Handzlik *et al.*[2] concluded that the most likely active sites are Mo-cyclobutane anchored to AlO_6 sites. The IR bands observed in the current studies agree well with those in other studies concluding Mo-carbene species to be the active site. It is possible that Mo-cyclobutane species are formed after coordination of more reactant molecules to the Mo-carbene intermediate; however, Mo-cyclobutane species are known to be rather unstable[3] and have not been experimentally confirmed for heterogeneous catalysts. Furthermore, only monomeric active sites were discussed in the DFT studies, although the structure-activity study of Chapter 6 determined that the oligomeric sites are quite important for olefin metathesis by supported MoO_x/Al_2O_3 catalysts. More detailed DFT studies of the activation mechanism of the surface MoO_x sites are needed to corroborate the experimental evidence.

7.4 Conclusions

Overall, the initial oligomeric mono-oxo $MoO_{5/6}$ surface species activate by removal of the oxo Mo=O bond and formation of $Mo=CH_2$ and $Mo=CHCH_3$ surface alkyls which retains the Mo^{+6} oxidation state. The activation mechanism for the surface MoO_x sites consists first of protonation of the reactant to form surface isopropoxide species. Isopropoxide oxidizes to acetone that is coordinated to the catalyst surface. This oxidation step causes reduction of the surface MoO_x sites ($Mo^{+6} \rightarrow Mo^{+4}$). Acetone is removed from the surface, allowing coordination of another propylene molecule by oxidative addition. This step re-oxidizes the molybdena sites back to Mo^{+6}. The active surface intermediates were determined to be $=CH_2$ and $=CHCH_3$ alkyl surface species. This study establishes the

activation mechanism of the supported MoO_x/Al_2O_3 catalysts and surface intermediates during industrially relevant olefin metathesis conditions.

Chapter 7 References

1. Olsthoorn, A. A.; Moulijn, J. A. An In Situ Infrared Spectroscopic Study of the Activity of y-Alumina Supported $Mo(CO)_6$ for Metathesis and Ethene Polymerization. *J. Mol. Catal.* **1980**, *8*, 147-160.

2. Handzlik, J.; Sautet, P. Active sites of olefin metathesis on molybdena-alumina system: A periodic DFT study. *J. Catal.* **2008**, *256*, 1-14.

3. Lwin, S.; Wachs, I. E. Olefin Metathesis by Supported Metal Oxide Catalysts. *ACS Catal.* **2014**, *4*, 2505-2520.

4. National Institute of Standards and Technology NIST Chemistry WebBook. *http://webbook.nist.gov/chemistry/*.

5. Reusch, W. Infrared Spectroscopy. *https://www2.chemistry.msu.edu/faculty/reusch/virttxtjml/Spectrpy/InfraRed/infrared .htm*.

6. Davydov, A. *Molecular Spectroscopy of Oxide Catalyst Surfaces;* John Wiley & Sons Ltd.: West Sussex, England, 2003.

7. Lwin, S.; Li, Y.; Frenkel, A. I.; Wachs, I. E. Activation of Surface ReO_x Sites on Al_2O_3 Catalysts for Olefin Metathesis. *ACS Catal.* **2015**, *5*, 6807-6814.

8. Vikulov, K. A.; Shelimov, B. N.; Kazansky, V. B. IR and UV-Vis spectroscopic studies of the surface $Mo=CH_2$ and $Mo=CH-CH_3$ carbene complexes produced by methylcyclopropane chemisorption over photoreduced silica-molybdena catalysts. *J. Mol. Catal.* **1991**, *65*, 393-402.

9. Amakawa, K.; Wrabetz, S.; Krohnert, J.; Tzolova-Muller, G.; Schlogl, R.; Trunschke, A. In Situ Generation of Active Sites in Olefin Metathesis. *J. Am. Chem. Soc.* **2012***, 134*, 11462-11473.

10. Efremov, A. A.; Davydov, A. A. IR Spectroscopic Studies of Adsorption and Conversion of Isopropyl Alcohol on a Sn/Mo Oxide Catalyst. *React. Kinet. Catal. Lett.* **1981***, 18*, 363-366.

11. Goncharova, O. I.; Davydov, A. A. IR Spectroscopic Studies of the Interaction of Propylene with the Surface of Alumina-Supported MoO_3 Catalysts. *React. Kinet. Catal. Lett.* **1983***, 23*, 285-289.

12. National Center for Biotechnology Information PubChem Compound Database; CID=180. *https://pubchem.ncbi.nlm.nih.gov/compound/180*.

13. Went, G. T.; Bell, A. T. Laser Raman spectroscopy of NH_3 and ND_3 adsorbed on TiO_2(anatase). *Catal. Lett.* **1991***, 11*, 111-118.

14. Went, G. T.; Leu, L. J.; Lombardo, S. J.; Bell, A. T. Raman Spectroscopy and Thermal Desorption of NH_3 Adsorbed on TiO_2 (Anatase)-Supported V_2O_5. *J. Phys. Chem.* **1992***, 96*, 2235-2241.

15. Moro-oka, Y. The role of acidic properties of metal oxide catalysts in the catalytic oxidation. *Appl. Catal. A: Gen.* **1999***, 181*, 323-329.

16. Hu, H.; Wachs, I. E.; Bare, S. R. Surface Structures of Supported Molybdenum Oxide Catalysts: Characterization by Raman and Mo L_3-Edge XANES. *J. Phys. Chem.* **1995***, 99*, 10897-10910.

17. Tian, H.; Roberts, C. A.; Wachs, I. E. Molecular Structural Determination of Molybdena in Different Environments: Aqueous Solutions, Bulk Mixed Oxides, and Supported MoO$_3$ Catalysts. *J. Phys. Chem. C* **2010***, 114*, 14110-14120.

Chapter 7 Supporting Information
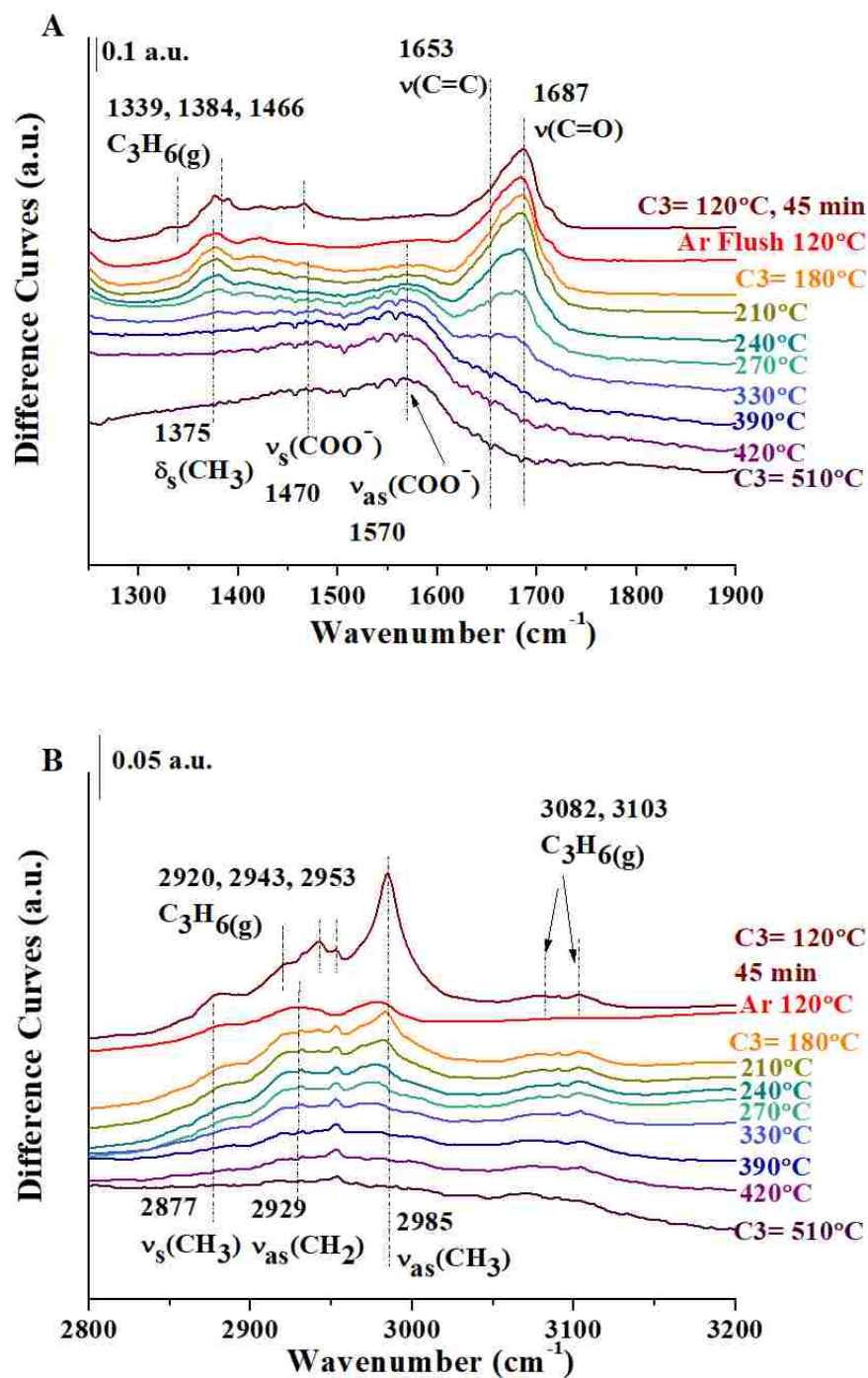
Figure S 7.1. *In situ* DRIFT spectra during propylene adsorption at 120 °C, Ar flush at 120 °C, and subsequent temperature programming at 10 °C under flowing propylene of the supported 25% MoO_x/Al_2O_3 catalyst. (A) 1250-1900 cm^{-1} and (B) 2800-3200 cm^{-1}.

Figure S 7.2. *In situ* DRIFT spectra of acetone adsorption at 30 °C and subsequent temperature programming at 10 °C/min under flowing of the supported 20% MoO_x/Al_2O_3 catalyst. (A) 1050-1900 cm^{-1} and (B) 2800-3200 cm^{-1}.
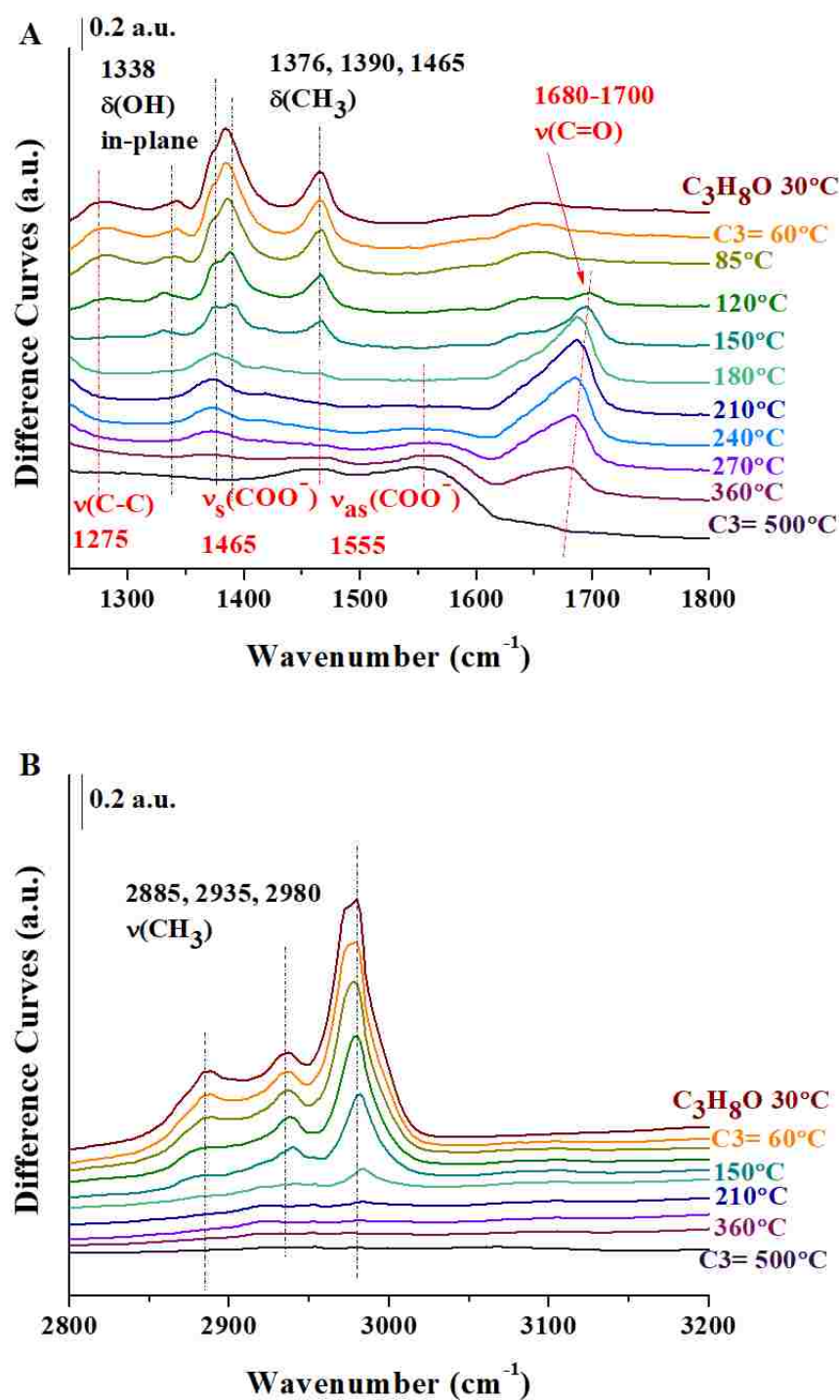
Figure S 7.3. *In situ* DRIFT spectra during iso-propanol adsorption at 30 °C and subsequent temperature programming at 10 °C/min under flowing propylene of the supported 20% MoO_x/Al_2O_3 catalyst. (A) 1250-1800 cm^{-1} and (B) 2800-3200 cm^{-1}.
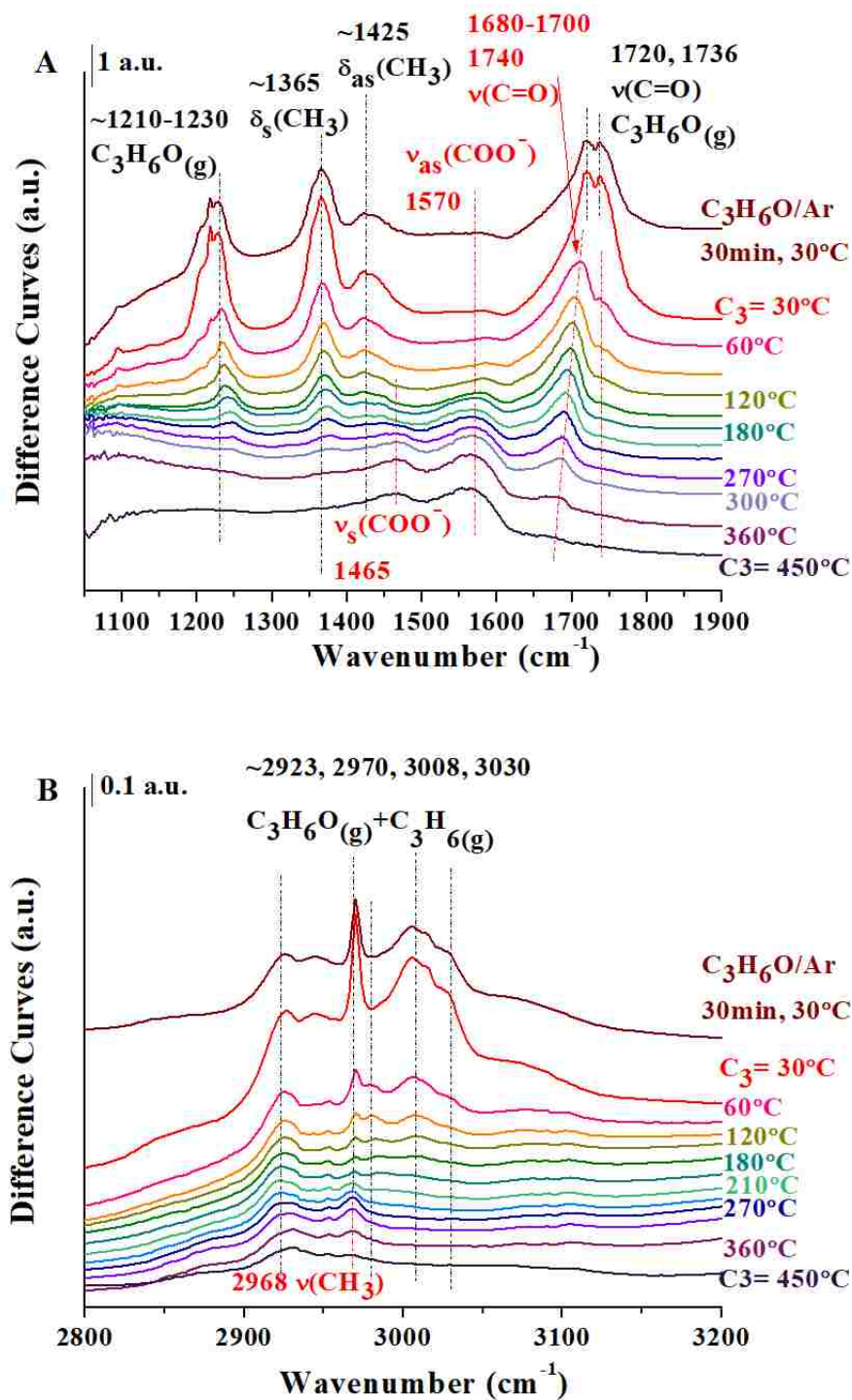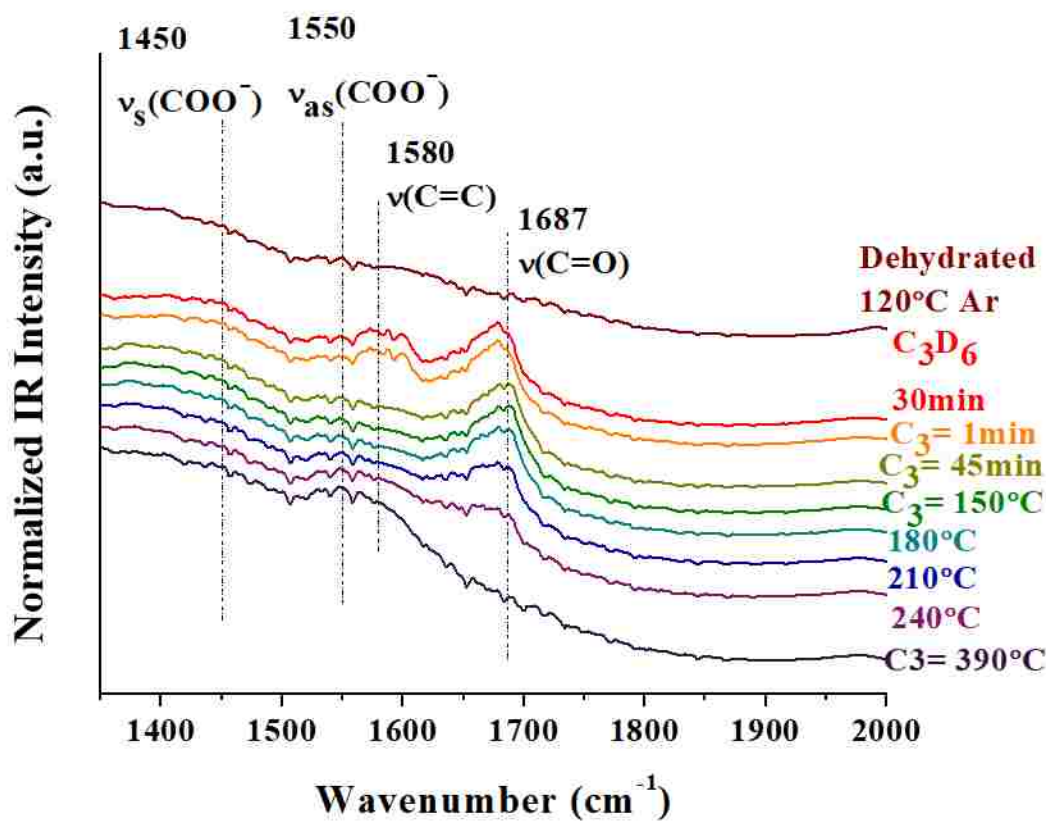
Figure S 7.4. *In situ* DRIFT spectra during C_3D_6-C_3H_6 isotope exchange at 120 °C and subsequent temperature programming at 10 °C/min under flowing propylene of the supported 20% MoO_x/Al_2O_3 catalyst (1350-2000 cm^{-1}).

Chapter 8 | Conclusions and Future Work

8.1   Ethylene Polymerization by Supported CrO_x/SiO_2 Catalysts

8.1.1   Summary and Conclusions

Critical review of the ethylene polymerization literature indicated that the nature of the surface CrO_x sites strongly depends on the environment to which the supported CrO_x/SiO_2 catalysts are exposed. Ambient conditions cause hydration of the surface CrO_x species. Several chromia species exist – CrO_4, Cr_2O_7, Cr_3O_{10}, and Cr_4O_{13} – and the extent of oligomerization increases with decreasing surface pH values at the point of zero charge. When the catalysts are dehydrated, only surface dioxo $(O=)_2CrO_2$ species are present on the surface of the silica support. Above the maximum dispersion limit, which depends on the Cr precursor, solvent, and surface properties of the SiO_2 support, crystalline Cr_2O_3 nanoparticles are present. Various reducing environments have been used to activate the supported CrO_x/SiO_2 catalysts. While activation with CO leads to Cr^{+2}, H_2 and C_2H_4 activation reduce the Cr^{+6} sites to Cr^{+3} sites. The literature review indicated the necessity for development of the active sites, surface intermediates, and structure-activity relationships for ethylene polymerization by the supported CrO_x/SiO_2 catalysts.

In situ and *operando* spectroscopy during activation with ethylene and ethylene polymerization was implemented to monitor the evolution of the supported CrO_x/SiO_2 catalyst. *In situ* Raman spectroscopy revealed the presence of one distinct, isolated surface chromia species, the tetrahedrally-coordinated dioxo $(O=)_2Cr^{+6}O_2$ site. C_2H_4- TPSR-MS demonstrated a two-step reduction process, $Cr^{+6} \rightarrow Cr^{+4} \rightarrow Cr^{+3}$, the former step being more facile than the latter. Upon activation with ethylene, *in situ* UV-vis and *operando* DRIFTS detected two distinct surface Cr^{+3} surface reaction intermediates: Cr^{+3}-

$(CH_2)_2CH=CH_2$ (PE oligomers forming nearer to the metal center) and Cr^{+3}-$CH=CH_2$ (vinyl center). Tracking the evolution of the surface intermediates demonstrated that while the concentration of the surface Cr^{+3}-$(CH_2)_2CH=CH_2$ structure saturates early in the ethylene polymerization reaction and may represent a spectator intermediate, evolution of the surface Cr^{+3}-$CH=CH_2$ surface species tracks the formation of the PE product, suggesting it to be the active reaction intermediate during ethylene polymerization by supported CrO_x/SiO_2 catalysts. Computational results indicate the possibility of the formation of Cr^{+3} active sites.

In situ and *operando* spectroscopy of the promoted $CrO_x/MO_x/SiO_2$ (M = Al, Ti, Zr) catalysts revealed the role of the promoter oxides in ethylene polymerization. The structure of the initial oxidized catalyst was analogous to that of the standard CrO_x/SiO_2 catalyst. Only the isolated dioxo $(O=)_2CrO_2$ surface chromia species is present in the Cr^{+6} oxidation state in tetrahedral coordination. *In situ* Raman spectroscopy showed that the CrO_x preferentially anchors to the promoter metal sites (M-O-Si), creating Cr-O-M-O-Si bridging bonds. The initial oxidized dioxo species are easily activated with ethylene. C_2H_4-TPSR-MS indicated a two-step reduction process for all the catalysts. All catalysts exhibited the same first reduction step ($Cr^{+6} \rightarrow Cr^{+4}$). However, while the Zr- and Al-promoted catalysts reduce to Cr^{+3} in the second step, the Ti-promoted catalyst reduced to a combination of Cr^{+2} and Cr^{+3}. The reduced sites were confirmed with *in situ* UV-vis spectroscopy during ethylene polymerization since deconvolution of the spectra for the Ti-promoted catalyst revealed the presence of a Cr^{+2} band. *Operando* DRIFTS revealed various distinct surface reaction intermediates that depended on the promoter oxide. Promotion with TiO_x yielded both Cr^{+3}-$(CH_2)_2CH=CH_2$ anchored to Cr-O-Si bonds

responsible for higher molecular weight polymer) and Cr^{+3}-CH=CH$_2$ sites anchored to the Cr-O-Ti-O-Si bonds responsible for the lower molecular weight polyethylene. Promotion by ZrO_x or AlO_x yields just one reactive intermediate (Cr^{+3}-CH=CH$_2$). Tracking the evolution of the surface reaction intermediates detected for the Zr- and Ti-promoted catalysts reveals that they correlate with the bulk PE production and the UV-vis Cr^{+3} sites, implying that these catalysts only produce active reaction intermediates. On the other hand, tracking the evolution of the Al-promoted catalyst revealed early saturation, and suggests that AlO_x is not a promoter for ethylene polymerization. TOF calculations revealed that the ZrO_x promotes by possessing the highest initial TOF value, while TiO_x promotes the creation of multiple active sites and deeper reduction, which slightly increases the initial TOF compared to the standard catalyst.

8.1.2 Future Work

Over the last several decades, ethylene polymerization has been a significant industrial reaction, and new uses for polyethylene are continuously developed. Promoted CrO_x/SiO$_2$ catalysts are already used in industry in the production of different types of polyethylene.

The type of polyethylene produced by each catalyst was not characterized in these studies. *In situ* ^{13}C MAS NMR spectroscopy would be able to characterize the type of polyethylene in even very small amounts during ethylene polymerization. Coupling this technique with the *in situ* and *operando* techniques would allow for determining the type and amount of polyethylene produced. Although the role of the promoters has been determined here, the complete reaction pathways have not yet been examined. Further computational studies are needed to determine the exact mechanism of ethylene polymerization by supported and promoted CrO_x/MO_x/SiO$_2$ catalysts. Recent studies in the

literature have suggested that the oxidation products remain in the coordination sphere. *In situ* DRIFTS and TPSR-MS during which the catalysts are exposed to HCHO/DCDO, HCCOOH, and CH_3COOH ethylene could provide more information about oxidation products formed during activation with ethylene and ethylene polymerization besides the CO_2 and H_2O observed in these studies.

Chromium is a hazardous and carcinogenic substance. The use of chromium has already been restricted in Europe for several years. These dangers mean that alternatives to chromium are needed and suggest a new path of research. This new knowledge of the structure-activity relationships for the supported CrO_x/SiO_2 catalysts presented here will allow for both the development of new materials for ethylene polymerization and the rational design and development of highly active catalysts tuned to the synthesis of the desired type of polyethylene.

8.2   Olefin Metathesis by Supported MoO_x/Al_2O_3 Catalysts

8.2.1   Summary and Conclusions

Review of the literature for olefin metathesis by heterogeneous supported MoO_x/Al_2O_3 catalysts determined that there is a lack of fundamental understanding primarily due to the absence of *in situ* and *operando* molecular spectroscopy studies.

In situ spectroscopy was used to develop the structure-reactivity of the heterogeneous supported MoO_x/Al_2O_3 catalysts. In the initial oxidized catalyst, several structures co-exist on the surface, dependent on the MoO_x surface coverage. The catalysts primarily consist of isolated dioxo MoO_4 surface sites at low coverage (<1 Mo atoms/nm^2), oligomeric mono-oxo $MoO_{5/6}$ surface species at intermediate coverage (1-4.6 Mo atoms/nm^2), and also crystalline MoO_3 nanoparticles above monolayer coverage (>4.6 Mo atoms/nm^2. The

271

isolated MoO_4 surface species anchored to basic alumina hydroxyls are quite stable and do not activate at mild propylene metathesis reaction conditions (~25-200 °C). However, the oligomeric $MoO_{5/6}$ surface species anchored to more acidic alumina hydroxyls easily activate during propylene metathesis at 25-200 °C. This demonstrates that the activation of the surface MoO_x species for propylene metathesis is strongly dependent on the anchoring surface hydroxyl site on the Al_2O_3 support. Crystalline MoO_3 nanoparticles are inactive for propylene metathesis, and their presence decreases the accessibility of propylene to the activated surface MoO_x species for metathesis. The catalytic active sites for propylene metathesis were established to the initial oligomeric mono-oxo $MoO_{5/6}$ surface species on the alumina support. The initial oligomeric mono-oxo $MoO_{5/6}$ surface species activate by removal of an oxo Mo=O and formation of $Mo=CH_2$ and $Mo=CHCH_3$ surface alkyls, thus, retaining the Mo^{+6} oxidation state.

In situ DRIFTS established the activation mechanism of the surface MoO_x sites for olefin metathesis. Overall, initial oligomeric mono-oxo $MoO_{5/6}$ surface species anchored to the acidic hydroxyl sites activate via removal of the oxo Mo=O bond and formation of $Mo=CH_2$ and $Mo=CHCH_3$ surface alkyls which retains the Mo^{+6} oxidation state. The activation mechanism proceeds first by protonation to form surface isopropoxide which oxidizes to acetone coordinated to the catalyst surface. The oxidation step causes reduction of the surface MoO_x from Mo^{+6} to Mo^{+4} via removal of oxygen from the Mo=O oxo bond. The acetone then de-coordinates from the catalyst surface and allows coordination of another propylene molecule via oxidative addition, re-oxidizing the molybdena sites back to Mo^{+6}. The active surface intermediates were determined to be $=CH_2$ and $=CHCH_3$ alkyl surface species. Further study is needed to determine if the activation mechanism for the

reverse direction (metathesis of ethylene and butene) is the same as that for propylene metathesis.

8.2.2 Future Work

There is a current global shortage of propylene, and the demand is expected to increase in the future. Olefin metathesis is one of the fastest-growing applications for on-purpose propylene production, which makes it a very industrially-relevant and significant reaction. Although the structure-reactivity, activation mechanism, and surface intermediates of the surface MoO_x sites for olefin metathesis have been elucidated, the literature review of heterogeneous MoO_x/Al_2O_3 catalysts for olefin metathesis revealed many more areas of improvement. Knowing the structure-reactivity relationships, the next step is to synthesize single-site catalysts. Recent studies of the supported ReO_x/Al_2O_3 catalysts for olefin metathesis nicely demonstrated that the basic alumina hydroxyls can be blocked by using an acidic metal oxide, such as TaO_x, leaving only active surface ReO_4 sites. This concept can be analogously applied to the MoO_x/Al_2O_3 catalysts to block the inactive isolated surface dioxo MoO_4 sites.

The single-site catalysts will allow the systematic determination of the number of active sites, surface kinetics, and reaction mechanism, which all still need to be determined to optimize olefin metathesis by supported MoO_x/Al_2O_3 catalysts (i.e. determination of optimal activation temperature and olefin partial pressure). The number of catalytic active sites has been proposed to be between 1-15%, and the discrepancies are due to inconsistencies in catalyst preparation and MoO_x coverage. Activation temperature and olefin partial pressure have been shown to affect the number of activated surface sites in recent studies of olefin metathesis by supported ReO_x/Al_2O_3 catalysts. Systematic study

with *in situ* and *operando* spectroscopy of consistently prepared catalysts using different activation temperatures and olefin partial pressures could finally determine the number of catalytic active sites and demonstrate the optimum activation temperature and olefin partial pressure.

The use of promoters or mixed silica-alumina supports has been suggested to improve the catalytic activity by increasing the number of sites, but the role of the promoters is still unknown. Elucidating the fundamental details of these promoted catalysts and the role of the promoters would allow for the rational design of improved catalysts for olefin metathesis.

The heterogeneous supported MoO_x/Al_2O_3 catalysts are widely used in industrial process, such as the Shell Higher Olefin Process, in which longer-chain olefins are produced (C_{11}-C_{14}). Extending these studies to longer-chain olefins will bridge the gap between this fundamental research and industrial application of the supported MoO_x/Al_2O_3 catalysts for olefin metathesis.

8.3   General Perspectives

Ethylene polymerization by supported CrO_x/SiO_2 catalysts and olefin metathesis by supported MoO_x/Al_2O_3 catalysts have been in existence since the 1950s-1960s and even today, are significant industrial reactions. Although extensively studied, the fundamental details of these two catalyst systems were mostly unknown. Despite the differences in the reactions, literature reviews of each catalyst system revealed that similar decades-old questions are debated, such as the structure of the activated catalysts, the surface intermediates, structure-activity relationships, and role of promoters. In both cases, the progress in the elucidation of the fundamental details has been hampered by an absence of

in situ and *operando* spectroscopic techniques that are capable of directly characterizing the catalyst surface during industrially-relevant reaction conditions. For both cases, a combination of *in situ* and *operando* spectroscopy techniques allowed for the determination of the structure of the activated catalyst and the surface intermediates that guided the development of structure-activity relationships. These structure-activity relationships will be able to guide the rational design of supported CrO_x/SiO_2 catalysts for ethylene polymerization and supported MoO_x/Al_2O_3 catalysts for olefin metathesis.

CURRICULUM VITAE

Anisha Chakrabarti

ADDRESS: 7 Asa Drive
            Sinclair Room 117
            Bethlehem, PA 18015
EMAIL: anc412@lehigh.edu
PHONE: (317) 525-2434
PLACE OF BIRTH: Indianapolis, IN
DATE OF BIRTH: October 31, 1989
PARENTS: Dr. Subir and Mrs. Tuhina Chakrabarti

EDUCATION

Lehigh University – Bethlehem, PA   2012 – December 2017
    Ph.D. Chemical Engineering
    Advisor: Professor Israel E. Wachs

Purdue University – West Lafayette, IN   May 2012
    Bachelor of Science in *Chemical Engineering*
    Specialization in *Energy and the Environment*
    Minor in *Economics*

RESEARCH EXPERIENCE

Graduate Research Assistant   2012 – Present
Lehigh University | Prof. Israel E. Wachs, Advisor

PROJECT 1: Olefin Metathesis by Supported MoO_x/Al_2O_3 Catalysts

- Synthesized supported MoO_x/Al_2O_3 catalysts via incipient wetness impregnation
- Identified and characterized the active species in olefin metathesis by supported MoO_x/Al_2O_3 catalysts to develop previously non-existent structure-activity relationships

PROJECT 2: Ethylene Polymerization by Supported CrO_x/SiO_2 Catalysts

- Synthesized supported and promoted $CrO_x/MO_x/SiO_2$ (M = Ti, Zr, Al) catalysts via incipient wetness impregnation
- Resolved ongoing controversy by identifying and characterizing the active surface intermediates for ethylene polymerization by supported CrO_x/SiO_2 catalysts
- Determined roles of ZrO_x, TiO_x, and AlO_x promoters

➢ Maintained and repaired characterization equipment including a Thermo FT-IR spectrometer and Agilent UV-Vis-NIR spectrometer

Undergraduate Research Assistant   2011 – 2012

Purdue University | Prof. Ronald P. Andres
Evaluated novel aerosol reactor for the synthesis of Au nanoparticle catalysts to use in the water-gas shift reaction

RESEARCH TECHNIQUES EMPLOYED

- ➤ **Raman** Spectroscopy – Infrared, Visible, and UV laser wavelengths, *in situ/operando*
- ➤ Infrared **(IR)** Spectroscopy – Diffuse Reflectance, Attenuated Total Reflection (ATR), *in situ/operando*
- ➤ **UV-Vis-NIR** Spectroscopy – Diffuse Reflectance, *in situ*
- ➤ **X-ray Absorption** Near Edge Structure/Extended X-ray Absorption Fine Structure **(XANES/EXAFS)** Spectroscopy – performed at Brookhaven National Laboratory X-ray Synchrotron, *in situ*
- ➤ Temperature Programmed Surface Reaction **(TPSR)** Spectroscopy with online Mass Spectrometry
- ➤ **BET Adsorption** – Determine catalytic surface area, *in situ*
- ➤ Atomic Absorption Spectroscopy

TEACHING EXPERIENCE

Teaching Assistant

Department of Chemical and Biomolecular Engineering	Spring 2014, 2015,
Lehigh University	2016
Mass Transfer (ChE 244)	

OTHER WORK EXPERIENCE

Systems Engineering Intern I	Summer 2011

Raytheon Technical Services Company, Indianapolis, IN
    V-22 team
- Helped to develop the Trainer Fault Insertion System (TFIS)

Systems Engineering Intern II	Summer 2012

    Hardware/Software Integration team (HSI)
- Learned Earned Value Management
- Tested and documented HSI performance

AWARDS AND HONORS

Overall Winner	2017
Catalysis Club of Philadelphia Student Poster Competition	
Chevron Scholars Award in Chemical Engineering	2017
ACS Catalysis Division Travel Award	2017
Fall ACS Meeting, Washington, D.C.	
ACS Catalysis Division Travel Award	2016
Fall ACS Meeting, Philadelphia	
Purdue Trustees Scholarship	
Four-year scholarship based on merit	2008 – 2012
National Merit Scholarship	2008 – 2012
Awarded to National Merit Finalists	

Purdue Honors Engineering Program and Learning Community   2008 – 2009

NON-TECHNICAL EXPERIENCE

➢ Maintained research group website   2015 – Present
➢ Proficient in Microsoft PowerPoint, Excel, Word, Publisher, Mathcad, OriginPro
➢ Knowledgeable in DOORS 9.3, MATLAB, C, Java, FORTRAN, HTML
➢ Excellent verbal and written communication, organizational, and interpersonal skills

LEADERSHIP POSITIONS & PROFESSIONAL AFFILIATIONS

ACS Member   2016 – Present
Webmaster   2014 – 2015
Lehigh University Chemical Engineering Graduate Student Association

PUBLICATIONS

1. **"Molecular Structure-Reactivity Relationships for Olefin Metathesis by Supported MoO_x/Al_2O_3 Catalysts,"** A. Chakrabarti and I.E. Wachs, *submitted to ACS Catalysis, under review.*

2. "**Role of Promoters in Ethylene Polymerization by Supported CrO_x/SiO_2 catalysts**," A. Chakrabarti, S. Luo, Z. Wu, and I.E. Wachs, *in preparation.*

3. "**A decade+ of *operando* molecular spectroscopy in catalysis**," A. Chakrabarti, M.E. Ford, D. Gregory, R. Hu, C.J. Keturakis, S. Lwin, Y. Tang, Z. Yang, M. Zhu, M.A. Bañares, I.E. Wachs, *Catalysis Today,* **2017**, *283, 27-53.*

4. "**Operando Molecular Spectroscopy during Ethylene Polymerization by Supported CrO_x/SiO_2 Catalysts: Active Sites, Reaction Intermediates, and Structure-Activity Relationship**," A. Chakrabarti, M. Gierada, J. Handzlik, I.E. Wachs, *Topics in Catalysis*, **2016**, 59, 725-739.

5. "**The Nature of Surface CrO_x Sites on SiO_2 in Different Environments**," A. Chakrabarti and I.E. Wachs, *Catalysis Letters,* **2015**, 145, 985-994.

ORAL PRESENTATIONS

1. "**Molecular Structure-Reactivity Relationships for Olefin Metathesis by Supported MoO_x/Al_2O_3 Catalysts,**" A. Chakrabarti and I.E. Wachs, October 2017, *The Catalysis Club of Philadelphia Meeting,* **Invited Student Lecture**

2. "**Molecular Structure-Reactivity Relationships for Olefin Metathesis by Supported MoOx/Al2O3 Catalysts,**" A. Chakrabarti and I.E. Wachs, August 2017, *254th ACS Meeting, Symposium on Mixed Metal Oxide Catalysis, Washington, D.C.*

3. **"The Role of Promoters in Ethylene Polymerization by Supported CrOx/MOx/SiO2 Catalysts**," A. Chakrabarti, S. Luo, Z. Wu, and I.E. Wachs,

August 2017, *254th ACS Meeting, Symposium on Mixed Metal Oxide Catalysis, Washington, D.C.*

4. "**The Role of Promoters for Ethylene Polymerization by Supported CrO$_x$/SiO$_2$ Catalysts**," A. Chakrabarti and I.E. Wachs, February 2017, *Graduate Student Symposium, Lehigh University, Bethlehem, PA*

5. "**Ethylene Polymerization by Supported CrO$_x$/SiO$_2$ Catalysts: Active Sites, Surface Intermediates, and Structure-Activity Relationship**," A. Chakrabarti and I.E. Wachs, August 2016, *American Chemical Society Meeting, Symposium in Honor of Israel E. Wachs: Celebrating Three Decades in Academia, Philadelphia, PA*, **Invited Talk**

6. "**The Role of Promoters for Ethylene Polymerization by Supported CrO$_x$/SiO$_2$ Catalysts**," A. Chakrabarti and I.E. Wachs, April 2016, *Graduate Student Symposium, Lehigh University, Bethlehem, PA*

7. "**Ethylene Polymerization by Supported CrO$_x$/SiO$_2$ Catalysts: Active Sites, Surface Intermediates, and Structure-Activity Relationship**," A. Chakrabarti and I.E. Wachs, February 2016, *The Catalysis Club of Philadelphia Meeting,* **Invited Student Lecture**

POSTER PRESENTATIONS

1. "**Molecular Structure-Reactivity Relationships for Olefin Metathesis by Supported MoO$_x$/Al$_2$O$_3$ Catalysts**," A. Chakrabarti and I.E. Wachs, November 2017, *The Catalysis Club of Philadelphia Student Poster Competition,* **Overall Winner**

2. **"Molecular Structure-Reactivity Relationships for Olefin Metathesis by Supported MoO$_x$/Al$_2$O$_3$ Catalysts**," A. Chakrabarti and I.E. Wachs, September 2017, *Graduate Student Symposium, Lehigh University, Bethlehem, PA*

3. "**Olefin Metathesis by Supported MoO$_x$/Al$_2$O$_3$ Catalysts**," A. Chakrabarti and I.E. Wachs, March 2017, *The Catalysis Society of Metropolitan New York Spring Symposium*

4. **"*Operando* Spectroscopy During Ethylene Polymerization by Supported CrO$_x$/SiO$_2$: Role of Promoters**," A. Chakrabarti and I.E. Wachs, November 2016, *The Catalysis Club of Philadelphia Student Poster Competition*

5. "**The Role of Promoters for Ethylene Polymerization by Supported CrO$_x$/SiO$_2$ Catalysts**," A. Chakrabarti and I.E. Wachs, June 2016, *Gordon Research Conference, New London, NH*

6. **"The Role of Promoters for Ethylene Polymerization by Supported CrO$_x$/SiO$_2$ Catalysts,"** A. Chakrabarti and I.E. Wachs, March 2016, *The Catalysis Society of Metropolitan New York Spring Symposium*

7. "**Ethylene Polymerization by Supported CrO$_x$/SiO$_2$ Catalysts: Active Sites, Surface Intermediates, and Structure-Activity Relationship**," A. Chakrabarti and I.E. Wachs, November 2015, *The Catalysis Club of Philadelphia Student Poster Competition*

8. "**An *In Situ* Molecular Spectroscopic Study of Ethylene Polymerization by Supported CrO$_x$/SiO$_2$ Catalysts**," A. Chakrabarti and I.E. Wachs, June 2015, *24th North American Catalysis Society Meeting, Pittsburgh*

9. "**Ethylene Polymerization by Supported CrO$_x$/SiO$_2$ Catalysts: Active Sites, Surface Intermediates, and Structure-Activity Relationship**," A. Chakrabarti and I.E. Wachs, March 2015, *The Catalysis Society of Metropolitan New York Spring Symposium*

10. "**An *In Situ* Molecular Spectroscopic Study of Ethylene Polymerization by Supported CrO$_x$/SiO$_2$ Catalysts**," A. Chakrabarti and I.E. Wachs, October 2014, *The Catalysis Club of Philadelphia Student Poster Competition*

11. "**An *In Situ* Molecular Spectroscopic Study of Ethylene Polymerization by Supported CrO$_x$/SiO$_2$ Catalysts**," A. Chakrabarti and I.E. Wachs, March 2014, *The Catalysis Society of Metropolitan New York Spring Symposium*

12. "***In Situ* Molecular Spectroscopy of Ethylene Polymerization by Supported CrO$_x$/SiO$_2$ Catalysts**," A. Chakrabarti and I. E. Wachs, October 2013, *The Catalysis Club of Philadelphia Student Poster Competition*